University of Wisconsin Milwaukee

UWM Digital Commons

December 2020

Design and Development of a 7 DOF Robot with Ergonomic Shoulder for Upper Limb Rehabilitation

Md Rasedul Islam
University of Wisconsin-Milwaukee

Follow this and additional works at: https://dc.uwm.edu/etd

Part of the Mechanical Engineering Commons

DESIGN AND DEVELOPMENT OF A 7 DOF ROBOT WITH ERGONOMIC

SHOULDER FOR UPPER LIMB REHABILITATION

by

Md Rasedul Islam

A Thesis Submitted in

Partial Fulfillment of the

Requirements for the Degree of

Doctor of Philosophy

in Engineering

at

The University of Wisconsin-Milwaukee

December 2020

ABSTRACT

DESIGN AND DEVELOPMENT OF A 7 DOF ROBOT WITH ERGONOMIC SHOULDER
FOR UPPER LIMB REHABILITATION

by

Md Rasedul Islam

The University of Wisconsin-Milwaukee, 2020
Under the Supervision of Professor Mohammad Habibur Rahman

With the increase of stroke patients, the number of upper limb dysfunction is increasing day by day. Robotic intervention in upper limb (UL) rehabilitation of post-stroke patients has gained much traction in recent years. Though many research groups have developed exoskeletons, existing exoskeletons have limitations in both hardware design and control approaches. In most cases, rehabilitative robotic devices have not considered the movement of the shoulder joint's center (center of glenohumeral joint); however, this movement leads to misalignment between human joints and robot joints, which is undesirable in any circumstances. To ensure better human-robot interaction (HRI), allowing mobility of shoulder joint's (glenohumeral joint) center of rotation without reducing the range of motion (ROM) remains a great challenge for UL exoskeleton researchers. Furthermore, being able to function as end-effector setup and exoskeleton setup (i.e., dual functionality) is a crucial need for exoskeletons to provide joint-based exercises and end-point exercises depending on the patient's condition, impairment level, and stage of rehabilitation. Moreover, interaction forces between user and robot have largely been ignored in passive rehabilitation. Force can also be used in performing active exercises. In this research, an

upper limb robotic exoskeleton has been designed and developed to provide better HRI, dual functionality, safe and effective, and patient-tailored therapy. The experimental results have shown its potential to be used with stroke-patients in a hospital setting.

TABLE OF CONTENTS

LIST OF FIGURES

LIST OF TABLES

LIST OF SYMBOLS

L_1	Distance between joint-1 origin and shoulder joint center of rotation in frontal mechanism, m
L_{11}	Distance between joint-1 origin and hinge joint in frontal mechanism, m
L_{12}	Distance between shoulder joint center of rotation and hinge joint in frontal mechanism, m
L_2	Distance between joint-2 origin and upper arm cuff point in sagittal mechanism, m
L_{21}	Distance between joint-2 origin and hinge joint in sagittal mechanism, m
L_{22}	Distance between upper arm cuff point and hinge joint in sagittal mechanism, m
a_{i-1}	Link length, m
α_{i-1}	Link twist, deg
d_i	Link offset, m
q_i	Joint variable, deg
$q \in \mathbb{R}^{7 \times 1}$	Vector of joint positions, rad
$q_d \in \mathbb{R}^{7 \times 1}$	Vector of desired (reference) joint positions, rad
$\dot{q} \in \mathbb{R}^{7 \times 1}$	Vector of joint velocity, rad/s
$\ddot{q} \in \mathbb{R}^{7 \times 1}$	Vector of joint acceleration, rad/s^2
$J(q) \in \mathbb{R}^{6 \times 7}$	Jacobian matrix
$J^{-1} \in \mathbb{R}^{6 \times 7}$	Inverse of Jacobian
$J^T \in \mathbb{R}^{7 \times 6}$	Transpose of Jacobian
$M(q) \in \mathbb{R}^{7 \times 7}$	Symmetric and positive diagonal inertia matrix, kg/m^2
$V(q, \dot{q}) \in \mathbb{R}^{7 \times 1}$	Torque due to centrifugal and coriolis term, Nm
$G(q) \in \mathbb{R}^{7 \times 1}$	Torque due to gravity term, Nm
$F(q, \dot{q}) \in \mathbb{R}^{7 \times 1}$	Torque due to coulomb friction, Nm
Fw_x	Wrist force in x8 axis

Fw_y	Wrist force in y8 axis
Fw_z	Wrist force in z8 axis
$F_w \in \mathbb{R}^{3\times1}$	Wrist forces, N
Fu_{x3}	Upper arm force along positive x3 axis
Fu_{-x3}	Upper arm force along negative x3 axis
Fu_{y3}	Upper arm force along y3 axis
$\dot{x}_d \in \mathbb{R}^{6\times1}$	Cartesian velocity vector of end-effector,
$\tau \in \mathbb{R}^{7\times1}$	Generalized torques vector, Nm
$\tau_{ua} \in \mathbb{R}^{7\times1}$	Vector of joint torques, calculated using upper arm forces, Nm
$\tau_{wa} \in \mathbb{R}^{7\times1}$	Vector of joint torques, calculated using wrist forces, Nm
δq	Joint space displacement, rad
$\lambda_1 \in \mathbb{R}^{7\times7}$	Diagonal weight matrix
$\lambda_2 \in \mathbb{R}^{7\times7}$	Diagonal weight matrix
DP	Diametral pitch
P_{d_1}	Pitch diameter of the driven gear, $inch$
P_{d_2}	Pitch diameter of the driver gear, $inch$
n_1	Rpm of the driven gear
n_2	Rpm of the driver gear
T_1	Number of teeth of the driven gear
T_2	Number of teeth of the driver gear
m_w	Velocity ratio of the matting gears

LIST OF ABREVIATIONS

AAN	Assist As Needed
AGMA	American Gear Manufacturers Association
CAGR	Compound Annual Growth Rate
CR	Center of Rotation
CTC	Computed Torque Control
DH	Denavit-Hartenberg
DOF	Degrees of Freedom
EERD	End-Effector type Robotic Device
ERD	Exoskeleton type robotic device
EMG	Electromyography signal
FPGA	Field-Programmable Gate Array
GH	Glenohumeral
GUI	Graphic User Interface
HRI	Human-Robot Interaction
ICR	Instantaneous Center of Rotation
NCMC	New Compound Model-Based Control
NSF	National Science Foundation
PID	Proportional Integral Derivative
PXI	PCI (Peripheral Component Interconnect) extensions for instrumentations
RD	Robotic Device
ROM	Range of Motion
UL	Upper Limb
ULD	Upper Limb Dysfunction
VR	Virtual Reality

ACKNOWLEDGEMENTS

Finally, yet importantly, Rasedul wishes to convey heartiest thanks to his lovely wife, Fatima Tabassum Tasin, for her enormous patience, sacrifice, support, and encouragement during this dissertation. She listened to Mr. Islam during stressful times and supported him until the stresses faded away. Mr. Islam feels lucky to have such a wonderful and compassionate wife during this endeavour.

INTRODUCTION

American heart association reports that approximately 785,000 individuals experienced a new or recurrent cerebral vascular accident (CVA) or stroke annually in the United States, among which the number of deaths estimated at 58000 (Benjamin et al., 2017; Benjamin et al., 2019). Stroke is a leading cause of serious long-term disability in the United States. The number of people living with stroke is projected to increase by 4 million by 2030 in the US (Heidenreich et al., 2011). Global scenario of stroke incidence and death are also similar to the US.

Hemiparesis/hemiplegia is the most common consequence of stroke, which leads to movement deficiency in the contralateral limbs to the brain's affected side. It causes the affected individual loss of arm motor function (Poli et al., 2013). As a result, many survivors following a stroke experience a disability like impaired upper limb function. Besides, the human upper limb's motor function can be lost due to sports injuries, trauma, occupational injuries, and spinal cord injuries (Dodson, 2008; Mehta, 2004; Reid, 1992). Moreover, physical disabilities such as full or partial loss of function in the shoulder, elbow, or wrist are common impairments in older adults. This impairment yields several impacts on domestic life, social life, and the country's economy. For instance, every year, the total cost from lost future productivity is $124.5 billion in the United States due to stroke (Mozaffarian et al., 2015).

It has well been proved that rehabilitation is the main method of promoting functional recovery in these individuals (Gresham et al., 1997). The conventional therapeutic approach requires a long commitment by both patient and therapist and/or somebody else –who helps the patient in doing rehabilitation. To rehabilitate post-stroke hemiparesis patients, the extensive task-

specific repetitive movement has been proved to be a safe and effective method to regain lost mobility in the upper limb; the upper limb rehabilitation requires incessant medical care and intensive training often requiring one-on-one physical interaction with the therapists (Poli et al., 2013).

Citing the constant growth of the upper limb (UL) dysfunction (ULD) and requiring long rehabilitation duration, robot-assisted therapy has already been begun contributing to UL rehabilitation. Robotic devices (RDs) have started being used to rehabilitate UL impairment since the early 1990s. Since then, plenty of research prototype ranging from end-effector type to exoskeleton has been developed, e.g., Inmotion, MARSE-7, CADEN-7, CABexo, CAREX-7, etc. (Krebs et al., 2007; LIU et al., 2016; Perry et al., 2007; Rahman et al., 2014; Xiao et al., 2017). Recent studies are corroborating that repetitive robot-assisted rehabilitation program significantly improves motor function in the upper limb (Amirabdollahian et al., 2007; Gandolfi et al., 2018; Janne et al., 2016; Kim et al., 2017; Lee et al., 2017; Sale et al., 2014; Yoo and Kim, 2015). For instance, Inmotion, one of the early rehabilitative robotic devices developed as MIT-MANUS in 1989, has been conducted clinical trials with thousands of patients so far and has shown it's a significant contribution in upper limb rehabilitation (Krebs et al., 2016).

To help patients with UL disability using robot-assisted therapy, research has been conducted substantially on different kinds of rehabilitation robots (e.g., end-effector type RDs and exoskeleton type RDs). Although plenty of exoskeletons have already been developed for upper limb rehabilitation, their use in a hospital setting with real patients is still limited. One of the major limitations of exoskeleton research is the shoulder girdle motion, which has largely been ignored in most existing exoskeletons design. The shoulder joint's center of rotation (CR) remained

stationary while such exoskeletons provide therapy. To provide shoulder girdle motion, the exoskeleton must realize the movement of shoulder joint CR (i.e., shoulder joint's instantaneous center of rotation-ICR). Although some exoskeletons, e.g., like ARMIN (Nef et al., 2009a; Nef et al., 2009b) and Harmony (Kim and Deshpande, 2015; Kim and Deshpande, 2017) have addressed mobility of shoulder joint CR; they have achieved it with a reduced range of motion (ROM) and complexity in design.

The exoskeleton is used for doing therapeutic exercises in joint space. However, in many cases (task-specific exercises, goal-oriented rehabilitation, game-based rehabilitation, spastic patients, and so on), patients need to do endpoint exercises (Pignolo, 2009), which involves Cartesian space control. In order to assist a user in doing exercises in Cartesian space, an inverse kinematic solution of the exoskeleton must be computed. To obtain an inverse kinematic solution of exoskeletons comprised of hybrid linkage (a combination of serial and parallel linkage) is difficult and remains an open problem as they involve the kinematic complexity of the serial-parallel mechanism.

As anthropometric parameters (e.g., limb segment, mass, limb's center of gravity, etc.) vary from patient to patient, the control approach for exoskeleton robot is expected to adopt those changes. Besides, the control approach should be able to provide passive as well as active exercises.

Being motivated by the above issues, firstly, this Ph.D. work aims to provide ergonomic shoulder movement in a wide range of motion in the proposed upper-limb rehab robot (7 DOFs) by allowing movement of shoulder joint's center of rotation (CR). As a step toward this goal, two custom-made parallel mechanisms (i.e., frontal and sagittal mechanisms) were incorporated in the

proposed exoskeleton robot to allow shoulder joint CR movement during abduction-adduction and flexion-extension. Thus, this robot becomes a hybrid manipulator, meaning it comprises of both serial and parallel linkage. Note that, *proposed exoskeleton robot* is meant to be worn on the lateral side of the human right arm. Secondly, this work has made the proposed robot have dual functionality that functions as an end-effector and exoskeleton type robot. To achieve this goal, an inverse kinematic solution was included in the proposed exoskeleton robot control approaches; thus, it performs end-point exercises as well. Thirdly, control approaches were applied in the proposed exoskeleton robot to perform a variety of upper limb rehabilitation exercises, including both passive and active exercises. As a step toward this goal, kinematic modeling, dynamic modeling, control approaches of the proposed exoskeleton robot (Islam et al., 2017) were done. Modified Denavit-Hartenberg (DH) notations (Denavit and Hartenberg, 1955) are used in kinematic modeling of the proposed robot. Iterative Newton-Euler dynamic formulation (Craig, 2017) is used for dynamic modeling of the proposed exoskeleton robot. The link length of the robot, masses of links, length of different segments of the upper limb, segment masses, and inertia have been estimated based on the anthropometric data of typical adults (Winter, 2009). The rest of the chapters of this dissertation is organized as follows.

Chapter 1: Literature Review

The first chapter is an inclusion of discussion of previous research works done and critical overview of the fields of development of therapeutic robotic devices, including both end-effector type and exoskeleton type. In addition, methods adopted to control such robots are presented.

Chapter 2: Upper Limb Rehabilitation Robot (proposed exoskeleton robot)

This chapter presents details of two parallel mechanisms for shoulder joint ICR, their development, motion support part of the *proposed exoskeleton robot*, actuators, sensors, and electrical and electronics instrumentation. It also presents major design choices and why those choices are included in this research.

Chapter 3: Kinematics and Dynamics

This chapter describes the development of the proposed exoskeleton robot's forward kinematics, inverse kinematic, and dynamic model. It includes the kinematics of two parallel mechanism for realizing shoulder joint's center of rotation. It also includes modified Denavit-Hartenberg parameters used to develop the kinematic model and the iterative Newton-Euler formulation used in dynamic modeling.

Chapter 4: Control and Simulation

The fourth chapter depicts the structure of the different control techniques (Computed torque control and New compound model-based control) used in the simulation to maneuver the proposed exoskeleton robot to follow a reference trajectory. This chapter also presents simulation results to validate the proposed exoskeleton robot model developed in Chapter-3 and shows performance evaluation of the control methods, as mentioned above. At the end of the chapter, simulation results are presented to validate the inverse kinematic solution using Jacobian described in Chapter-3.

Chapter 5: Virtual Reality Rehabilitation

The fifth chapter of this thesis depicts the development of Virtual Reality based rehabilitation for the exoskeleton system developed in this research.

Chapter 6: Experimental Results

This chapter presents the experimental results of a variety of passive and active exercises for upper limb rehabilitation. The exercises include both individual and simultaneous joint movement. This chapter also discusses the results in detail and gives some specific comments on the results.

Conclusions and future recommendations

Finally, in this section, the research outcomes of this thesis are summarized, and recommendations for future work are suggested.

CHAPTER-1   LITERATURE REVIEW

Section-1, Section-2, and Section-3 of this chapter describe rehabilitation, neuroplasticity, and neuro-rehabilitation, respectively. Types of rehabilitation exercises are discussed in Section-4. Section-5 reviews robotic devices developed for upper limb rehabilitation, followed by Section-6 that outlines hardware limitations in existing rehab devices. The control approaches used in the rehabilitative robot are discussed in Section-7, whereas Section-8 outlines the control limitations. Section-9 of this chapter presents customer discovery and the market size of the rehabilitation robot. The specific objectives and contribution of this Ph.D. work are stated in Section-10 and section-11, respectively.

1.1   Rehabilitation:

According to the World Health Organization, the term 'rehabilitation' is defined as "a set of interventions designed to optimize functioning and reduce disability in individuals with health conditions in interaction with their environment." (WHO, 2020)

In a similar fashion, 'upper limb rehabilitation' can be defined as a set of interventions designed to regain or relearn lost mobility and reduce disability in the upper limb to improve quality of life by enabling an individual to perform a wide variety of daily activities.

Upper limb rehabilitation is highly patient-centered, meaning that each individual's interventions and approach depend on the patient's condition, severity, and type of impairment. There are many different settings for upper limb rehabilitation. It can be done in inpatient, or in outpatient hospital settings, or in community settings such as an individual's home. The

physiotherapists, occupational therapists, recreational therapists, orthotists, and physical medicine and rehabilitation doctors constitute the workforce for upper limb rehabilitation.

1.2 Neuroplasticity and its ten principles:

With the advancement of neuroscience, researchers are now eager more than ever to develop rehabilitation programs based on principles of neuroplasticity to drive functionally distorted and damaged brains in corrective directions (Nahum et al., 2013). Therefore, to develop therapeutic approaches for effective upper limb rehabilitation of post-stroke individuals, understanding neuroplasticity and its principles are helpful. Neuroplasticity is the ability of the brain to modify, change and adapt new connections of neurons (nerve cells) and their behavior in the brain circuitry in response to experience (i.e., new information, sensory stimulation, development, damage, or dysfunction) (Voss et al., 2017). This change, adaption and/or modification would bring change to both sensory and motor function. Because of neuroplasticity, the damaged brain learns lost behavior in response to rehabilitation (Nahum et al., 2013). These principles may be considered while developing a therapeutic tool for upper limb rehabilitation.

Kleim and Jones (2008) outlined ten neuroplasticity principles by discussing various learning and relearning models to improve rehabilitation efforts and optimize functional outcomes. Those principles are stated below with examples regarding upper limb impairment following stroke.

1. **Use It or Lose It:** *"Neural circuits not actively engaged in task performance for an extended period of time begin to degrade."*

An example of this can be seen in a recovering stroke patient with a paralyzed arm who has to relearn how to move the arm. The impaired arm remains unused over a period of time. This lack of use results in the degradation of neural circuits responsible for arm movements. Therefore, when the patient tries to use that arm, it can take additional time and trials to regenerate the neural circuits as they have been inactive.

2. **"Use It and Improve It:** *"Training that drives a specific brain function can lead to enhancement of that function."*

An example of this can be highlighted from the previous discussion of the stroke patient who has lost mobility in his arm might find it challenging to move that part of the body and avoid using it. Only by systematic and frequent exercising movements in that arm can improve its abilities.

3. **Specificity:** *"The nature of the training experience dictates the nature of the plasticity."*

From a rehabilitation standpoint, specificity highlights the importance of tailoring an exercise to produce a result in specific circuitry to promote functional recovery. For example, exercises or activities involving elbow movement can be utilized to promote functional recovery in the elbow.

4. **Repetition Matters:** *"Induction of plasticity requires sufficient repetition."*

It is very hard to tell or predict the actual number of repetitions a patient would require to regain lost mobility. This prediction remains a challenge for all the stakeholders (e.g., therapist, insurance agents, and patient). However, it is safe to say that repetition is

crucial to generate movement in an inactive part of the body. A stroke patient with an impaired limb may require an abundance of practice to regain muscle functions. To ensure adequate repetitions, therapeutic exercises may be designed so that it combines as many kinds of movement as possible. For example, diagonal reaching exercises include movement from the shoulder, elbow, and wrist.

5. **Intensity Matters:** *"Induction of plasticity requires sufficient intensity."*

The concept of intensity follows the concept of repetition. Research shows that upper limb rehabilitation of stroke patients often requires task-specific intensive rehabilitation (Poli et al., 2013).

6. **Time Matters:** *"Different forms of plasticity occur at different times during recovery."*

A significant amount of recovery for motor function usually takes place in the first three months following stroke (Kwakkel et al., 2006; Langhorne et al., 2011; Wade et al., 1983). This is because the brain really wants to recover after an injury. If the recovery process is initiated sooner by beginning rehabilitation, then there is less chance of dysfunctional behavior to occur.

7. **Salience Matters:** *"The training experience must be sufficiently salient to induce plasticity."*

A patient's emotions can influence the frequency, strength, etc., of the training. As their brain is already acquiring new information, it is important for therapists to know and

provide accurate motivational information to them so that it helps to remember their memory circuits of specific skills with time.

8. **Age Matters:** *"Training-induced plasticity occurs more readily in younger brains."*

   Age also plays a role in neuroplasticity. A younger brain is more flexible and adjustable to change than an older brain, making it important for therapists to acknowledge while administering treatment.

9. **Transference or Generalization:** *"Plasticity in response to one training experience can enhance the acquisition of similar behaviors."*

   During training, therapists need to convert a general training exercise to correlate with real-life activities to facilitate their endeavors. For instance, the hand's 2D movement in the frontal plane can be associated with wiping a board or a table.

10. **Interference:** *"Plasticity in response to one training experience can impede the acquisition of similar behaviors."*

    Delayed neurological treatment can cause patients to use other ways to compensate for their lack of skills, which may not be the correct way. Unlearning their earlier behavior can help further the treatments.

1.3 Principles of post-stroke neurorehabilitation:

Based on existing literature and evidence from clinical studies, Maier et al. (2019) identified 15 motor learning principles. These principles aim to find therapeutic intervention to promote and optimize functional recovery in stroke patients' impaired limbs.

Principle-1: Massed Practice/repeated practice

Massed practice (or repeated practice) is basically training of a skill continuously with very little or no breaks in between (Schmidt et al., 2019). In rehabilitation, researchers refer the term repetitive practice to the use of an affected limb in a constant fashion to speed up performance and recovery (Kwakkel, 2009; Kwakkel et al., 2015; Taub et al., 1999). Research has shown that massed practice led to faster acquisition of lost motor function (Poli et al., 2013; Shea and Morgan, 1979).

Principle-2: Spaced Practice

This principle suggests that training should be designed such that there is sufficient time for rest between sessions. In doing so, humans can retain knowledge more effectively and provide a better performance output (Cepeda et al., 2006). It is also essential to keep a balance of massed practice and spaced practice as extended breaks could reduce learning and development (Savion-Lemieux and Penhune, 2005).

Principle-3: Dosage

Dosage can be defined as the number of hours spent in rehabilitation (Schmidt et al., 2019). This can be characterized by the duration and frequency of rehabilitation sessions (Basso and Lang, 2017; Kwakkel, 2009). Effective rehabilitation depends on the frequency and duration of the training. A person who has suffered a stroke cannot immediately start with intense training as it may not affect the motor skills then (Dromerick et al., 2009; Kwakkel, 2009). Hence it is necessary to determine when high-intensity training can be applied. Research suggests that increasing the dosage of training therapy can improve

performance, stimulate structural plastic change and mobility (Boissoneault et al., 2020; Daly and Ruff, 2007; Lohse et al., 2014).

Principle-4: Task-Specific Practice

As each task requires a specific set of skills and motor functions, shaping of internal sensorimotor representation depends on the condition of exercises or training performed in rehabilitation (Schmidt et al., 2019). If training conditions is designed similar to a person's day to day activities such as pick and place, lifting a bag, opening a door, and other such conditions, the sensorimotor accumulates these task-specific data which the patient can utilize in the real world (Bayona et al., 2005; Blennerhassett and Dite, 2004; Narayan Arya et al., 2012; Poli et al., 2013). Thus, creating task-specific training can ease and improve a patient's chance of relearning lost mobility.

Principle-5: Goal-oriented practice

A goal (e.g., pick an object) can be achieved through a variety of functional movements. This principle lets the patient explores the way to achieve a given goal without emphasizing just arm movement training. For instance, if the goal is to move a ball, a movement-specific exercise would use only moving the ball from a particular side (e.g., moving forward). But in a goal-oriented practice, the target would be the movement of the limb, which could be done by moving the ball to the left, right, or back. Consequently, this results in higher motor learning performance and adds variations of skills. In rehabilitation, goal-oriented exercises yield higher activity in the sensorimotor area, a better reaching performance, and a better motor learning performance (Nathan et al., 2012; Pereira et al., 2017; Wisneski and Johnson, 2007; Wu et al., 2000).

Principle-6: Variable Practice

Variable practice can be defined as the variation of exercises and their performing sequence in a rehab session. This principle has proved to be successful in enhancing motor performance (Park et al., 2016).

Principle-7: Increasing difficulty

Functional task difficulty is defined as the level of difficulty of performing an exercise (Schmidt et al., 2019). Increasing difficulty in tasks can enhance and broaden the patient's motor performance and increase retention (Guadagnoli and Lee, 2004). The ideal challenge of functional task difficulty is to ensure a balance between difficulty level and performance. Designing difficulty levels catering to the patient's needs leads to better results.

Principle-8: Multisensory Stimulation

The brain can perceive and process multiple senses and functions at the same time. Our sensory information is correlated to one another (Knill and Pouget, 2004). For instance, our sense of touch can help us to picture the object. Therefore, using multisensory stimulation can enhance greater accuracy for recognizing the link between the sensory and motor cortex. In upper limb rehabilitation, a patient's performance during a therapy session can be translated into virtual reality or a game. This way, the patient see how therapy is going on.

Principle-9: Rhythmic Cueing

Rhythmic movements can stimulate activity in the motor network areas and cerebellum. For example, if a patient is trained a dance step to a song the next time that song is played, the motor movements can anticipate those particular movement patterns as the

brain synchronizes these movements. Using such rhythmic cues increases motor activity and creates patterns for future cues.

Principle-10: Explicit feedback

For training to be effective explicit feedback (e.g., verbal, real-time visual, terminal, augmented) plays an important role in upper limb rehabilitation. For example, if a patient is asked to flex his/her elbow to 90°, real-time feedback, in this case, would be displaying the flex angle to the patient.

Principle-11: Implicit feedback

In rehabilitation, implicit feedback can be presented in the form of descriptions, demonstrations, or video demonstrations. The basic concept of implicit feedback is to give feedback based on performance without any expectation of a specific outcome. For instance, in a game-based method where the target is to move the ball forward. The patient could use his impaired arm to move the ball an inch forward rather than all the way. The feedback displayed would be regarding the patient's performance rather than the quantifiable result.

Principle-12: Modulate Effector Selection

In the initial stages after a stroke, it becomes difficult for the patient to use the impaired limb due to pain/weakness. Hence, the patient increases the use of the functioning limb. This can affect the loss of neuro functions in the paretic limb (Taub et al., 2006). Many therapies use constraints on the unaffected limb to increase the use of the impaired limb. Other methods include encouraging the use of the paretic arm through bilateral arm training or devices.

Principle-13: Action Observation/Embodied Practice

Action observation can be defined as mirroring an action performed by another individual. Research shows that humans performed a task better when they observed it being done by somebody else (Mulder, 2007). Movement observation activates the primary motor cortex, which helps facilitate the movements and motor system. Likewise, mirror therapy helps increase functional connectivity, which stimulates movements in the paretic limb by visual representation.

Principle-14: Motor Imagery/Mental Practice

Motor imagery and mental practice rely on the ability to imagine the movements in a paretic limb (Schmidt et al., 2019). This is useful for patients with severely impaired limbs as it helps them picture the movements without explicitly acting on them (Di Rienzo et al., 2016; Mulder, 2007). Motor imagery is deemed mirror therapy and has similar effects on the premotor areas, somatosensory cortex, and subcortical areas.

Principle-15: Social Interaction

Social interaction can influence a patient's desire to perform if he feels confident doing ADL. If the patient feels like he can do tasks without depending on another person, it will influence him to achieve more.

1.4 Types of upper-limb rehabilitation:

In the rehabilitation of upper-limb dysfunction, therapy, or exercises are chosen based on the patient's condition, type, and severity of impairment. There are three types of exercises that are commonly included in upper limb rehabilitation.

1.4.1 Passive rehabilitation therapy:

In passive rehabilitation, a therapist or therapeutic device carries the patient's limb and mobilizes it to perform the given exercise. This kind of rehabilitation does not require any effort from the patient; hence it is suitable for patients with very little or no mobility. The goal of passive rehabilitation therapy is to increase the range of motion. An example of passive exercise might be seen in stroke patients' rehabilitation, where a therapist provides repeated elbow flexion-extension motion to the patients.

1.4.2 Active-assist rehabilitation therapy:

When some mobility is restored, the therapist or therapeutic device must allow the patient's effort in performing exercises. In active-assist/active rehabilitation, exercises or training are completed by the combined effort of the patient and therapist/therapeutic device. An example of this sort of exercise would be 'point to point reach,' where a therapeutic device helps a patient accomplishes a given exercise. This kind of rehabilitation is helpful for increasing strength.

1.4.3 Resistive rehabilitation therapy:

In active-resist rehabilitation, the therapist/rehab device compensates the gravity and offers resistance while a patient is asked to do given exercise. Thus, there is no contribution from a therapist/device. An example of such exercise would be stretching the elbow against a resistive band. In robot-aided rehabilitation, such resistance is provided by applying resistive torques at robot joints. To increase the subject's strength, this kind of rehabilitation therapy is used.

1.5 Robotic devices in upper limb rehabilitation:

The history of robotics tells us that robots were meant to be used in industrial applications that associate repetitive, precision, tedious, heavy, and risky works. The repetitive nature,

tediousness, precision, explicit feedback, intensity, and tailored-difficulty of physical rehabilitation have encouraged researchers to develop robots to be used in rehabilitation. The use of robotic devices (RDs) in upper limb rehabilitation is seen to have started in the early1990s (Hogan et al., 1992; Kommu S S, 2007) (Kommu S S, 2007). This opened the opportunity for people with upper extremity impairment to provoke neuroplasticity by robot-aided rehabilitation. Robotic devices have the capability of being used in providing therapy for a long period of time irrespective of skills and fatigue compared to manual therapy (Teasell and Kalra, 2004). This emphasizes the incorporation of such devices into human upper limb rehabilitation. Robotic devices can also work in multi degrees of freedom with virtual reality interfaces and provide therapy ranging from passive to active rehabilitation. This leverage over traditional therapy could increase the efficiency as well as effectiveness of therapists by alleviating the labor-intensive aspects of physical rehabilitation of post stroke patients (Lum et al., 2002). To provide rehabilitation therapy to the individuals with upper-limb impairment, research on therapeutic robotics has enormously been carried out (Accogli et al., 2017; Bhagat et al., 2016; Crea et al., 2016; Cui et al., 2017; Fazekas et al., 2007; Frisoli et al., 2009; Gopura et al., 2009; Hesse et al., 2003; J Reinkensmeyer et al., 2000; Kiguchi and Hayashi, 2012; Krebs et al., 2016; Krebs et al., 2007; LIU et al., 2016; Nef et al., 2009a; Nef et al., 2009b; Otten et al., 2015; Perry et al., 2007; Pignolo et al., 2012; Rahman et al., 2014; Toth et al., 2005; Xiao et al., 2017). Depending on the way robotic device's kinematic chain maps on to the upper limb's joint, they can be classified into two main groups as end-effector type and exoskeleton type robot.

1.5.1 End-effector type robotic devices

Figure 1.1 Inmotion Arm (Krebs et al., 2007)

In an End-effector type robotic device (EERD), the patient's limb is attached to the device's end-effector, which is the robot's last link. These kinds of devices cannot map the robot's joint motion to the corresponding human anatomical joint motion. EERDs' joint does not correspond to human anatomical joints, unlikely to mimic the anatomical movements. However, EERDs are very suitable to provide endpoint exercises in rehabilitation. Besides, these devices are simple in structure, lightweight, and require a simple control method. One of the early robotic devices of its kind is MIT-MANUS (Hogan et al., 1992), a research prototype of InMotion Arm™ (Interactive Motion Technologies, Inc., MA, USA). It is a robotic arm with two active DOFs and was used to rehabilitate the shoulder and elbow. The later version of Inmotion has been extended for wrist and hand rehabilitation (Krebs et al., 2007; Masia et al., 2007). The device was used for performance-based training that focuses on improving the patient's range of motion (ROM), strength, movement speeds, and movement smoothness.

Mirror Image Movement Enabler (MIME) robotic device has been built to provide bilateral, unilateral, and combined bilateral and unilateral neurorehabilitation for shoulder and elbow

(Burgar, 2000; Burgar et al., 2011; Lum et al., 2006; Lum et al., 2002). In unilateral mode, only the impaired limb was moved with the assistance of the robot, leaving the unimpaired limb idle. In bilateral mode, subjects were asked to move both unimpaired limb and impaired limb with assistance from the robot for either limb. Combined bilateral and unilateral therapy has been claimed to have advantages over conventional therapy in chronic stroke neurorehabilitation (Lum et al., 2006).
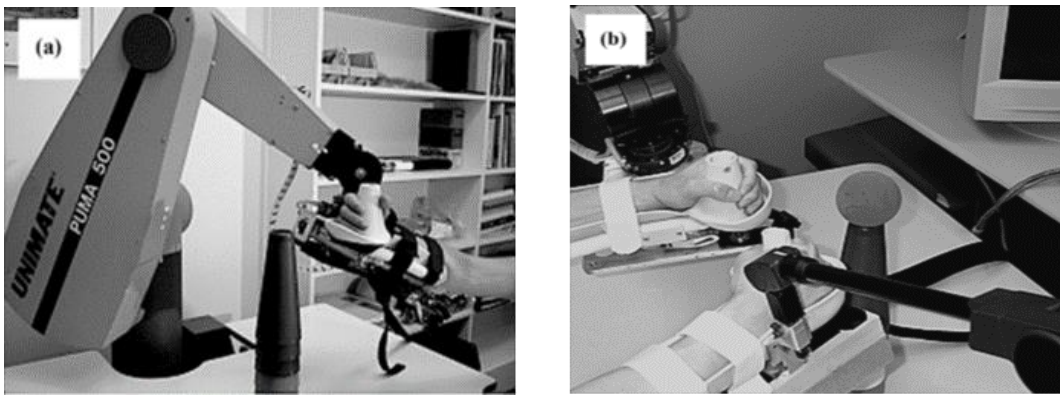
Figure 1.2 MIME platform in (a) unilateral and (b) bilateral movements set up (Lum et al., 2006)

One DOF Bi-Manu-track, being able to do exercises involving the motion of forearm pronation-supination and wrist flexion-extension, has also been designed to provide bilateral therapy during human upper limb rehabilitation (Hesse et al., 2003). Researchers from Robotics Research Centre (at Nanyang Technological University, Singapore) developed a planar robotic device, based on cabled differential transmission, that applied haptic channels (i.e., stiffness channel and complainant channel) in the rehabilitation of upper extremity dysfunction (Campolo et al., 2014). E2Rebot, an ergonomic planar robotic platform for upper-limb neuromotor disability,

also used virtual rehabilitation therapies by implementing a force-based impedance control method (Fraile et al., 2016).
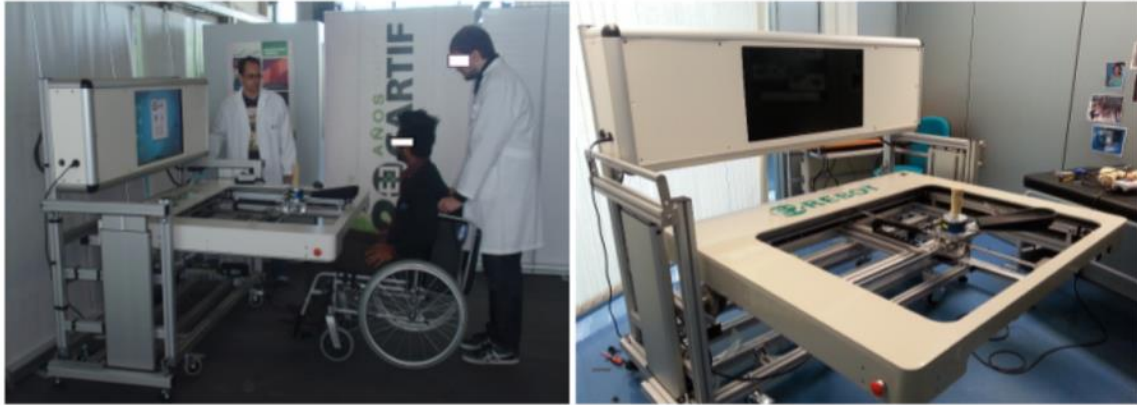
Figure 1.3 E2Rebot platform (Fraile et al., 2016)

Robotic arms that are typically meant for industrial application has gained much interest in robot-aided rehabilitation. Such an example is MAAT-Multimodal interfaces to improve therApeutic outcomes in robot-Assisted rehabiliTation. A research group at Università Campus Bio-Medico di Roma, Rome, Italy, developed this robotic platform that incorporated 7 DOF Kuka LWR III robotic arm for upper-limb rehabilitation (Badesa et al., 2014). This robot-aided rehabilitation is a bio-cooperative system, which takes into account both physiological and biomechanical measures.
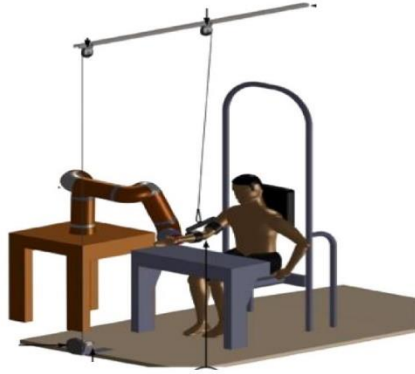
Figure 1.4 MAAT system (Badesa et al., 2014)

There are many more EERDs that have been built for human upper limb rehabilitation. Those devices have been summarized in Table 1. The first column in the table mentions the device's name or researchers who developed it, whereas the second column describes types. Here, robotic devices are categorized based on three criteria. Firstly, they are organized based on the type of actuation, which could be electrical, pneumatic, or hydraulic actuation. Secondly, devices are further categorized into either bilateral or unilateral based on the kind of training mode, provided that unilateral mode involves the only movement of the affected limb while bilateral mode requires the simultaneous movement of both affected and unaffected limb in a similar fashion. The third category is based on the device's portability, given that if the device is attached to a fixed/stationary frame. This kind of device can be mounted on (i) a mobile base, (b) a desk, and/or (c)a wheelchair. The degrees of freedom are shown in the third column, whereas the fourth column depicts the upper limb's scope of movement. The fifth column lists the control approach that was used in the device. The sixth column mentions the mode of therapy (i.e., active or passive). The last column in the table shows the clinical trial/test of that device.

Abbreviations used in the table:

Types: e = electric actuation, p = pneumatic actuation, h=hydraulic actuation, U=Unilateral, B= Bilateral, G = Grounded-Exoskeleton's base is fixed to a location, Ug=Ungrounded - base is movable.

Movements: A/A= Abduction/Adduction, F/E= Flexion/Extension, R= Internal/External rotation, P/S= Pronation/Supination, R/U=Radial/Ulnar deviation, NDA=Not defined by basic anatomical movement.

Control approach: FC=Force control, FF=Force Feedback control, FFC=Force Forward control, PC=Position control, PD=Proportional Derivative control, PID= Proportional Integral Derivative control, CTC=Computed Torque control, IC=Impedance control, AC=Admittance control, EMG= Electromyography (EMG) based control, SMC= Sliding mode control, SME= Sliding mode control with exponential reaching law, PCM =Pulse code modulation scheme, VRC=Virtual reality based control, RC= Robust Control

Clinical test: The number in the bracket term in the last column shows the number of patients who participated in the clinical trial.

Table 1: End-effector type rehabilitative robotic devices

Name/developer	Type	Active DOF	Scope of movements	Control approach	Modes of therapy	Clinical Test
Bi-Manu-Track (Hesse et al., 2003)	e, B, G	1	Forearm P/S, Wrist F/E	IC	Passive assist, active assist and resist	Yes (12)
(Colombo et al., 2007)	e, U, G	1	Wrist F/E	AC	Active assist	Yes (8)

Name/developer	Type	Active DOF	Scope of movements	Control approach	Modes of therapy	Clinical Test
(Hu et al., 2009)	e, U, G	1	Wrist F/E	EMG	Active assist	Yes (15)
(Freeman et al., 2009)	e, U, G	2	Planar movement of the forearm	IC	Active assist	No
BFIAMT (Chang et al., 2007)	e, B, G	2	Axial movement of the forearm	PC	Active assist Passive assist	Yes (20)
H-man (Campolo et al., 2014; Hussain et al., 2016; Hussain et al., 2015)	e, U, G	2	Planar movement of the forearm	FC, IC	Active assist Passive assist	No
ARM Guide (J Reinkensmeyer et al., 2000)	e, U, G	3	Axial, elevation, and yaw of the forearm	-----------	Active assist Passive assist resist	Yes (19)
NeReBot (Rosati et al., 2007; Stefano et al., 2014)	e, U, G	3	Spatial movement of shoulder and elbow	PID	Active assist Passive assist	Yes (24)
InMotion WRIST (Krebs et al., 2007)	e, U, G	3	Forearm P/S, Wrist F/E Wrist R/U	IC	Active assist Passive assist resist	Yes (36)
(Takaiwa and Noritsugu, 2009; Takaiwa and Noritsugu, 2010)	p, U, G	3	Forearm P/S, Wrist F/E Wrist R/U	IC EMG	Active assist	No
MIME (Burgar et al., 2011; Lum et al., 2006; Lum et al., 2002)	e, B, G	6	Shoulder Elbow (NDA)	------------	Active assist Passive assist resist	Yes (57)

Name/developer	Type	Active DOF	Scope of movements	Control approach	Modes of therapy	Clinical Test
Gentle/S, (Amirabdollahian et al., 2007; Coote et al., 2008)	e, U, G	6	Shoulder Elbow Forearm (NDA)	------------	Active assist Passive assist resist	Yes (31)
MAAT (Badesa et al., 2014; Badesa et al., 2012; Papaleo et al., 2013)	e, U, G	7	Shoulder Elbow Forearm (NDA)	------------	Active assist Passive assist	No
(Umemura et al., 2009)	H, U, G	7	Shoulder A/A, F/E, R Elbow F/E Forearm P/S, Wrist F/E Wrist R/U	------------	Active assist	No
REHAROB (Toth et al., 2005)	e, U, G	12	Shoulder Elbow (NDA)	---------	Active assist	Yes (8)

1.5.2   Exoskeleton type robotic devices

Exoskeleton type robotic devices (ERDs) cannot provide end-point exercises like their counterpart does. On the other hand, they can deliver individual joint movement of an upper limb and also mimic the whole arm motion (if degrees of freedom is at least 7). As a result, these devices can generate and control individual joint torque. Besides, this kind of device has better guidance and a broad range of motion. It appears from previous literature that ERDs have started being enriched in the mid-2000s. ARMin-III (successor of ARMIn and ARMin-II), developed at ETH Zurich, Switzerland, has been one of the early robotic exoskeletons with high degrees of freedom for upper extremity rehabilitation (Nef et al., 2009b). The very first version ARMin (Nef et al.,

2007a) was designed with four DOFs intended to provide rehabilitation in the human shoulder (giving mobility for shoulder abduction-adduction, flexion-extension, and internal-external rotation) and elbow (flexion-extension).

Figure 1.5 Subject seated wearing ARMin (left, (Nef et al., 2007b)) and ARMin-II (right, (Mihelj et al., 2007))

Figure 1.6 Subject seated wearing ARMin-III (Nef and Riener, 2008)

Then seven DOFs ARMin-II was developed with five adjustable length segments to provide better patient cooperative rehabilitation. Unlike ARMin, the shoulder axis of rotation is not fixed in ARMin-II, allowing passive elevation/depression and protraction/retraction of glenohumeral

joint during shoulder vertical flexion-extension (Mihelj et al., 2007). ARMin-II also has included

ergonomic shoulder actuation to provide as much natural movement as it could for shoulder

rehabilitation (Nef et al., 2009b). The advancement of ARMin rehabilitative exoskeleton had gone

through several stages of development, and now it is commercially available (known as

ArmeoPower developed by Hocoma AG, Volketswil, Switzerland) to be used for human upper

extremity rehabilitation in a clinical setting in hospitals.
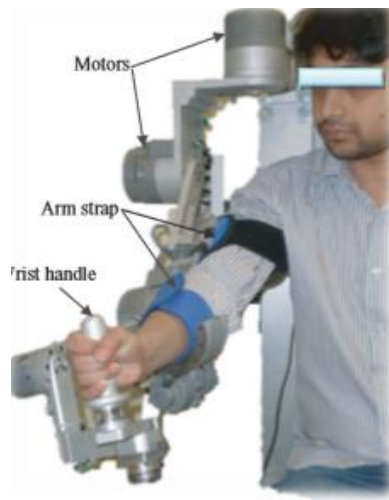
Figure 1.7 Subject wearing ETS-MARSE (Rahman et al., 2014)

In ETS-MARSE, a 7 DOF upper limb exoskeleton for the whole arm, a novel power

transmission mechanism was used for assisting shoulder internal-external rotation and forearm

pronation supination (Rahman et al., 2012; Rahman et al., 2014). Since it is somewhat difficult to

fit a shaft along the axis of rotation of the above cases (axis of humerus and radius), the developer

of ETS-MARSE used an anti-backlash spur gear meshed with open type semicircular gear and

bearing assembly. Unlike ARMin-III, it lacked allowing passive elevation/depression and

protraction/retraction of glenohumeral joint during shoulder movement. Unlike ARMin-III, it

lacked allowing passive elevation/depression and protraction/retraction of glenohumeral joint during shoulder movement.

Harmony, a recent robotic exoskeleton, has been developed intending to enable subject doing bilateral arm training. This system comprises of dual-arm with a four-bar linkage, which makes it capable of providing naturalistic shoulder movement. Unlike ARMin-III (where shifting of shoulder center of rotation was considered only for vertical flexion-extension), Harmony used a four-bar linkage mechanism to move the shoulder's center of rotation during either shoulder abduction-adduction and vertical flexion-extension, which made it more anatomical like (Kim and Deshpande, 2017). The range of motion of the robot differs based on the way it's other joints are configured. For instance, the ROM of shoulder abduction increased when it was performed simultaneously with external shoulder rotation.
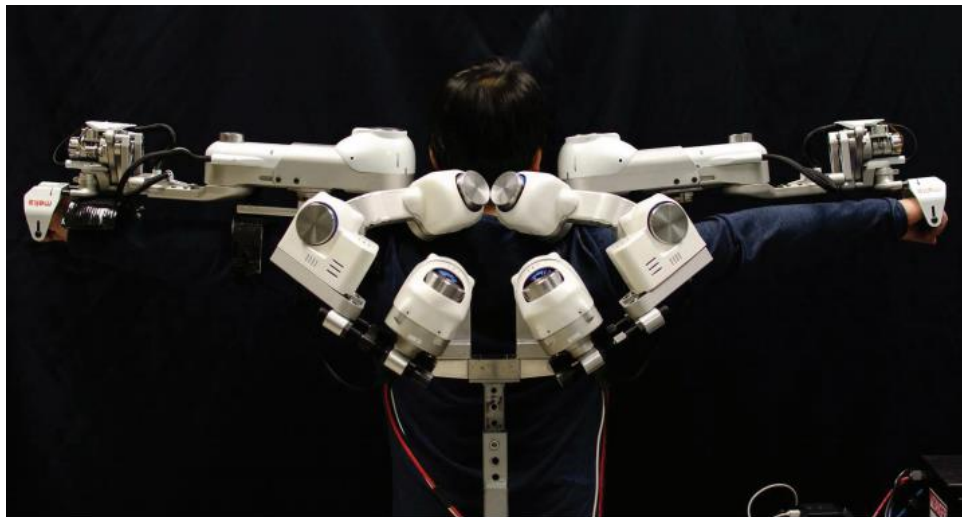
Figure 1.8 Subject wearing Harmony bimanual robot (Kim and Deshpande, 2017)

CAREX-7, a cable-driven whole arm exoskeleton, is another recently developed exoskeleton meant for dexterous motion training or assistance of the whole arm (Cui et al., 2017). Such an exoskeleton is advantageous in being lightweight. All the actuators are mounted away

from exoskeleton body segments and give more assurance of alignment of exoskeleton segments with corresponding human segments over the range of motion to ensure safe and effective transfer of forces and torques. To provide assistance as needed, a novel wrench (force and torque) field controller was applied to regulate necessary forces and torques to follow the given trajectory. Quadratic programming is applied to optimize cable tensions (Cui et al., 2017). Although the robot has provided the benefit of long-range transmission of force and power, the cable can easily stretch and slip, leading to produce different joint movement than desired.
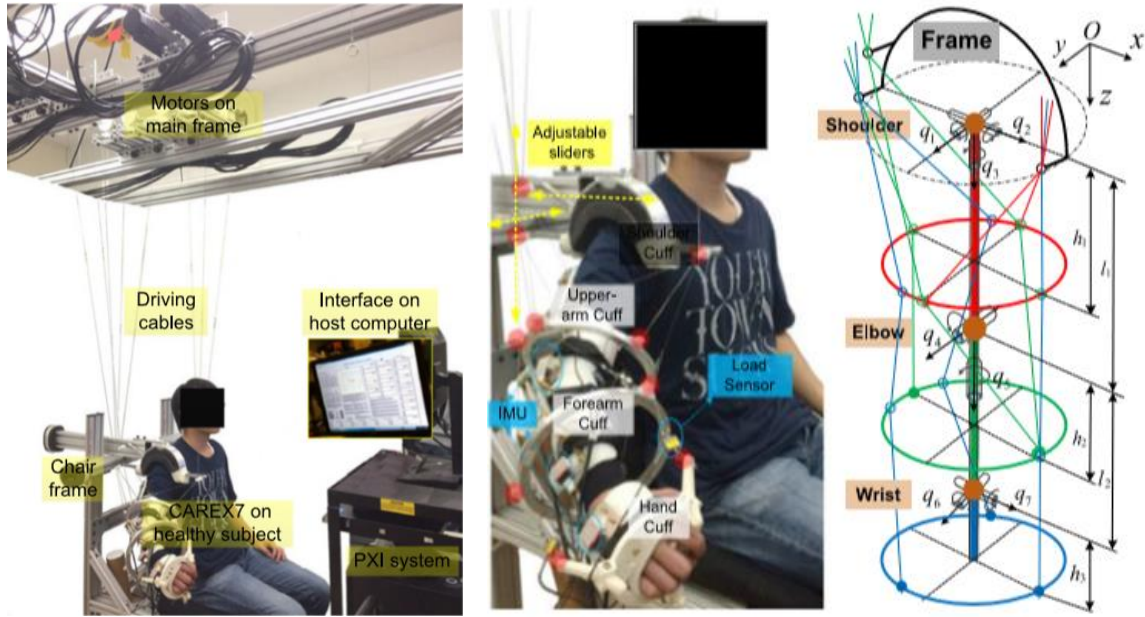
Figure 1.9 Subject wearing cable-driven CAREX-7 (Cui et al., 2017)

A 7-DOF cable-driven upper limb exoskeleton, namely CABXLexo-7 was developed at Harbin Institute of Technology (HIT), China & Hefei University of Technology (HFUT), China as a joint effort in 2017 (Xiao et al., 2017; Xiao et al., 2018). In CABXLexo-7, three epicyclic gear train structures were included for the upper arm, forearm, and palm. The intent of using such a structure was to replace the 'cable-driven parallel mechanism with flexible links', which is hard to

be controlled for ROM. Besides, in order to create a lightweight exoskeleton robot capable of providing all 7 DOF, the development team put all the actuators on the stationary board and transmitted power through a cable-conduit system using two types of cable-driven differential mechanisms and utilized a tension device to work with the cable slag problem. This device's limitations are (a) this robot does not consider the movement of the center of rotation of the human shoulder. (b) this system does not realize upper arm internal-external rotation (c) The gear train would generate backlash, which may disrupt the smooth transmission of motion.
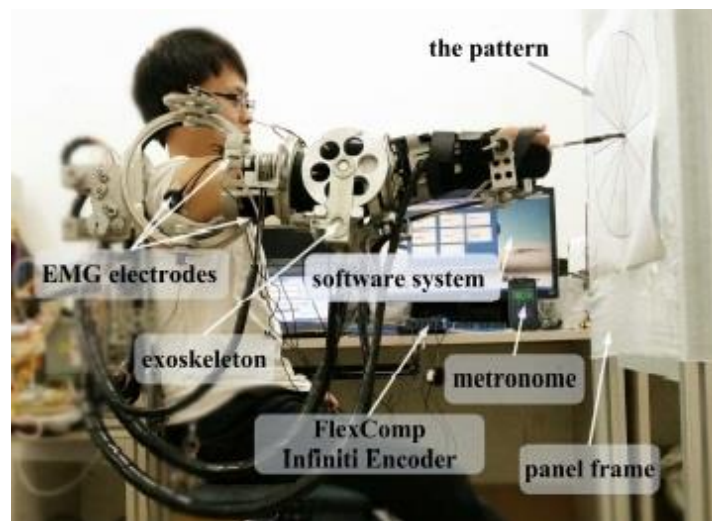
Figure 1.10 CABXLexo (Xiao et al., 2017; Xiao et al., 2018)

In MAHI Exo II, a 4 DOF exoskeleton built for elbow and wrist rehabilitation, researchers also used cable drive transmission to increase power to weight ratio (Fitle et al., 2015; French et al., 2014). However, the cable-driven transmission is appeared to have stretch and slip in the cable.
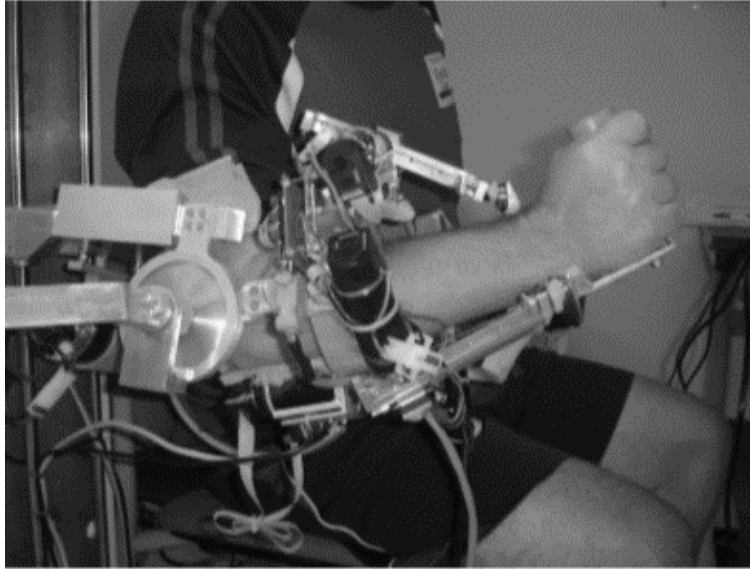
Figure 1.11 Subject wearing MAHI Exo II

Figure 1.12 Subject wearing Rehab-Arm (LIU et al., 2016)

One research group at Shanghai Jiao Tong University, China, came up with an idea of using two actuators for forearm (pronation-supination) and wrist motion (flexion-extension and radial-ulnar deviation) support part instead of three actuators (LIU et al., 2016). In their 7 DOF exoskeleton, namely Rehab-Arm, they basically used one motor to actuate forearm motion and one motor to actuate wrist motion. The initial position (at 0°) of the forearm actuator has made the

wrist actuator able to do flexion-extension. The wrist radial-ulnar deviation can only be performed when the forearm motor shaft is positioned at 90º. This design would not be able to do exercises that involve the simultaneous movement of both the forearm and wrist. In addition, there is complexity in control as wrist motion depends on forearm actuators.

There are many more exoskeleton type devices that have been built for human upper limb rehabilitation. Some of them are summarized in Table 2.

Abbreviations used in the table:

Types: e = electric actuation, p = pneumatic actuation, h=hydraulic actuation, U=Unilateral, B= Bilateral, G = Grounded-Exoskeleton's base is fixed to a location, Ug=Ungrounded - base is movable

Movements: A/A= Abduction/Adduction, F/E= Flexion/Extension, R= Internal/External rotation, P/S= Pronation/Supination, R/U=Radial/Ulnar deviation, NDA=Not defined by basic anatomical movement

Control approach: FC=Force control, FF=Force Feedback control, FFC=Force Forward control, PC=Position control, PD=Proportional Derivative control, PID= Proportional Integral Derivative control, CTC=Computed Torque control, IC=Impedance control, AC=Admittance control, EMG= Electromyography (EMG) based control, SMC= Sliding mode control, SME= Sliding mode control with exponential reaching law, PCM =Pulse code modulation scheme, VRC=Virtual reality based control, RC= Robust Control

Clinical test: The number in the bracket term in the last column shows the number of patients who participated in the clinical trial.

Table 2: Exoskeletons developed for human upper limb rehabilitation

Name/developer	Type	Active DOF	Scope of movements	Control approach	Modes of therapy	Clinical Test
(Kung et al., 2007)	e, U, G	1	Forearm P/S	FC	Active assist Passive assist	No
(Song et al., 2007)	e, U, G	1	Wrist F/E	PID,EMG	Active assist	Yes (5)
(Pylatiuk et al., 2009)	h, U, Ug	1	Elbow F/E	EMG	Active assist	No
(Kiguchi et al., 2003)	e, U, G	1	Elbow F/E	EMG	Active assist	No
(Cheng et al., 2004)	e, U, G	1	Elbow F/E	EMG	Active assist	Yes (5)
(Beigzadeh et al., 2015)	e, U, G	1	Elbow F/E	EMG	Active assist	No
(Jarrett and McDaid, 2017)	e, U, G	1	Elbow F/E	PD, SMC	Active assist	No
ASSIST (Sasaki et al., 2005)	p, U, Ug	1	Wrist F/E	EMG	Active assist	No
(Papadopoulos, 2007)	e, U, Ug	2	Shoulder A/A Shoulder F/E	-----------	Active assist	No
(Rosen et al., 2001)	e, U, G	2	Shoulder F/E Elbow F/E	EMG	Active assist	No
(Triwiyanto et al., 2016)	e, B, G	2	Shoulder F/E Elbow F/E	EMG	Active assist	No
(Kiguchi et al., 2008)	e, U, Ug	3	Shoulder A/A Shoulder F/E Elbow F/E	EMG	Active assist	No

Name/developer	Type	Active DOF	Scope of movements	Control approach	Modes of therapy	Clinical Test
CRAMER (Spencer et al., 2008)	p, U, g	3	Forearm P/S, Wrist F/E Wrist R/U	PCM	Active assist	No
WOTAS (Rocon et al., 2007; Ruiz et al., 2009)	e, U, Ug	3	Elbow F/E Forearm P/S, Wrist F/E	IC	resist	Yes (10)
(Rosales et al., 2015)	e, U, Ug	3	Shoulder A/A Shoulder F/E Shoulder R	-----------	Active assist Passive assist	No
(Mahdavian et al., 2015)	e, U, G	3	Shoulder F/E, A/A, Elbow F/E	IC	Passive assist	No
(Sharma and Ordonez, 2016)	e, U, G	3	Shoulder F/E, Elbow F/E Forearm P/S,	PID	Passive assist	No
ULEL (Madani et al., 2017)	e, U, G	3	Shoulder F/E, Elbow F/E Wrist F/E	EMG	Passive assist	No
ExoRob (Rahman et al., 2010)	e, U, G	4	Elbow F/E Forearm P/S, Wrist F/E Wrist R/U	PID, CTC, SMC	Passive assist	No
ARMin-I (Nef et al., 2007a; Nef et al., 2007b)	e, U, G	4	Shoulder A/A, F/E, R Elbow F/E	PD, CTC, IC	Active assist Passive assist	Yes (8)
ABLE (Garrec et al., 2008)	e, U, G	4	Shoulder A/A, F/E, R Elbow F/E	FF	Active assist Passive assist	No
BONES (Klein et al., 2010)	p, U, G	4	Shoulder A/A,F/E, R Elbow F/E	PC,FC	Active assist	No

Name/developer	Type	Active DOF	Scope of movements	Control approach	Modes of therapy	Clinical Test
(Sutapun and Sangveraphunsiri, 2015)	p, U, G	4	Shoulder A/A,F/E, R Elbow F/E	IC	Active assist	No
RUPERT (Balasubramanian et al., 2008; Sugar et al., 2007)	p, U, Ug	4	Shoulder F/E Elbow F/E Forearm P/S, Wrist F/E	FFC	Active assist Passive assist	Yes (10)
Dampace, (Stienen et al., 2009)	h, U, G	4	Shoulder A/A, F/E, R Elbow F/E	PC, CTC	Passive assist	No
Brackbill (Brackbill et al., 2009)	e, U, G	4	Shoulder A/A, F/E, R Elbow F/E	PD, CTC	Active assist Passive assist	No
(Garrido et al., 2016)	e, U, G	4	Shoulder A/A, F/E, R Elbow F/E Forearm P/S, Wrist F/E Wrist R/U	AC	Active assist Passive assist	No
ALEx (Pirondini et al., 2014; Stroppa et al., 2017)	e, U, G	4	Shoulder A/A, F/E, R Elbow F/E	EMG	Active assist Passive assist	Yes (1)
LIMPACT (Otten et al., 2015)	h, U, G	4	Shoulder A/A, F/E, I/R Elbow F/E	CTC, IC	Passive assist	No
NEMS (Accogli et al., 2017; Crea et al., 2016)	e, U, G	4	Shoulder A/A, F/E, I/R Elbow F/E	PID	Passive assist	No
(Li et al., 2017)	e, U, G	4	Shoulder A/A, F/E Elbow F/E Forearm P/S	EMG	Passive assist	No

Name/developer	Type	Active DOF	Scope of movements	Control approach	Modes of therapy	Clinical Test
(Piña-Martínez et al., 2017)	e, U, G	4	Shoulder A/A, F/E, R Elbow F/E	-----------	Passive assist	No
MAHI Exo II (Fitle et al., 2015; French et al., 2014)	e, U, Ug	4	Elbow F/E Forearm P/S Wrist F/E Wrist R/U (NDA)	IC, AC	Active assist Passive assist	No
L-EXOS (Frisoli et al., 2009)	e, U, G	5	Shoulder A/A, F/E, R Elbow F/E Forearm P/S	IC	Active assist Passive assist	Yes (6)
MULOS (Johnson et al., 2001)	e, U, Ug	5	Shoulder A/A, F/E, R Elbow F/E Forearm P/S	PID	Active assist Passive assist	No
MARSE-5 (Rahman et al., 2012)	e, U, G	5	Shoulder A/A, F/E, R Elbow F/E Forearm P/S	SMC	Active assist Passive assist	No
MGA (Carignan et al., 2007)	e, U, G	5	Shoulder A/A, F/E, R Elbow F/E Forearm P/S	IC, AC	Active assist Passive assist	No
T-WREX (Sanchez et al., 2004)	p, U, G	5	Shoulder A/A, F/E, R Elbow F/E Finger Grasp	-------------	Active assist Passive assist	Yes (51)
RUPERT IV (Balasubramanian and He, 2012)	p, U, Ug	5	Shoulder A/A, F /E, R Elbow F/E Forearm P/S Wrist F/E	FFC	Active assist Passive assist	Yes (6)

Name/developer	Type	Active DOF	Scope of movements	Control approach	Modes of therapy	Clinical Test
MAHI (Gupta and Malley, 2006)	e, U, Ug	5	Elbow F/E Forearm P/S Wrist F/E Wrist R/U (NDA)	IC, AC	Active assist Passive assist	No
(Mushage et al., 2017)	e, U, Ug	5	Shoulder A/A, F/E, R Elbow F/E Wrist F/E	SMC	Active assist Passive assist	No
(Kang and Wang, 2015)	e, B, U, G	5	Shoulder A/A, R Elbow F/E Forearm P/S Wrist F/E	RRC	Passive assist	No
ARAMIS (Pignolo et al., 2012)	e,B,G	6	Shoulder A/A, F/E, R Elbow F/E Forearm P/S wrist F/E	------------	Active assist Passive assist	Yes (14)
ARMin-III (Guidali et al., 2011; Nef et al., 2009a; Nef et al., 2009b)	e, U, G	6	Shoulder A/A, F/E, R Elbow F/E Forearm P/S, wrist F/E	PD, CTC, IC	Active assist Passive assist	No
(Chen et al., 2015)	e, U, G	6	Shoulder A/A, F/E Elbow F/E Forearm P/S, Wrist F/E Wrist R/U	------------	Passive assist	No
CABexo (Xiao et al., 2017)	e, U, G	6	Shoulder A/A, F/E Elbow F/E Forearm P/S, Wrist F/E Wrist R/U	------------	Passive assist	No

Name/developer	Type	Active DOF	Scope of movements	Control approach	Modes of therapy	Clinical Test
6-REXOS (Gunasekara et al., 2015)	e, U, G	4	Elbow F/E Forearm P/S, Wrist F/E Wrist R/U	------------	Passive assist	No
CADEN-7 (Perry et al., 2007)	e, B, G	7	Shoulder A/A, F/E, R Elbow F/E Forearm P/S, Wrist F/E Wrist R/U	PID, EMG	Active assist Passive assist	No
MARSE-7 (Rahman et al., 2014; Rahman et al., 2013)	e, U, G	7	Shoulder A/A, F/E, R Elbow F/E Forearm P/S, Wrist F/E Wrist R/U	PID, CTC, EMG, SMC, SME	Active assist Passive assist	No
SRE (Tsagarakis and Caldwell, 2003)	p, U, G	7	Shoulder A/A, F/E, R Elbow F/E Forearm P/S, Wrist F/E Wrist R/U	PID, IC	Active assist Passive assist	No
SUEFUL-7 (Gopura et al., 2009)	e, U, G	7	Shoulder A/A, F/E, R Elbow F/E Forearm P/S, Wrist F/E Wrist R/U	EMG, FC	Active assist Passive assist	No
Rehab-Arm (LIU et al., 2016)	h, U, G	7	Shoulder A/A, F/E, R Elbow F/E Forearm P/S, Wrist F/E Wrist R/U	PID	Active assist	No

Name/developer	Type	Active DOF	Scope of movements	Control approach	Modes of therapy	Clinical Test
CAREX-7 (Cui et al., 2017)	e, U, G	7	Shoulder A/A, F/E, I/R Elbow F/E Forearm P/S, Wrist F/E Wrist R/U	CTC, PID	Passive assist, Active assist	No
(Kim and Kim, 2017)	e, U, G	7	Shoulder A/A, F/E, I/R Elbow F/E Forearm P/S, Wrist F/E Wrist R/U	------------	Passive assist, Active assist	No

Although plenty of rehabilitative robotic devices have been developed, existing RDs have not fully restored upper limb functionality due to their design limitations in both hardware and control approaches.

1.6 Hardware limitations in existing robotic rehabilitative devices

Research on rehabilitative robotic devices is still a growing field and demands novel approaches to solve key limitations in hardware design (e.g., human-machine interface, dual functionality, etc.). Our literature review reveals that there are some key limitations in existing exoskeletons, which are discussed in the following sub-sections.

1.6.1 Movement of shoulder joint's center of rotation (CR)

To perform exercises during rehabilitation, forces and torques generated in exoskeleton joints must successfully be transferred in human joints to provide better human-robot interaction.

This transfer does not happen suitably if exoskeleton joints are not aligned with human joints. Besides, misalignment might reach exoskeleton's wearer pain and/or discomfort during rehabilitation (Gopura et al., 2016; Schiele and Helm, 2006; Siciliano et al., 2009). Therefore, to provide better compliance and a successful transfer of forces and torques, exoskeleton joints need to be aligned with corresponding human joints. The human shoulder complex is the most biomechanically complex joint. It has many articulations that lead to three general motions, vertical flexion-extension, abduction-adduction, and internal-external rotation (Schenkman and Rugo de Cartaya, 1987). The center of rotation (CR) of the shoulder joint does not remain fixed during shoulder movements and has two additional movements, which are elevation-depression in the frontal plane and protraction and retraction in the sagittal plane as shown in (Bai et al., 2017; Halder et al., 2000). In literature, there found many exoskeletons where the shoulder joint is simplified and modeled as a 3 DOFs ball-and-socket joint by ignoring motion of CR joint (Chen et al., 2014; LIU et al., 2016; Madani et al., 2017; Mahdavian et al., 2015; Perry et al., 2007; Rahman et al., 2014; Stroppa et al., 2017; Tang et al., 2014). However, some exoskeletons have considered this matter in their kinematic structure (Gopura et al., 2016; Kiguchi et al., 2003; Kiguchi et al., 2008; Kim and Deshpande, 2017; Nef et al., 2009b). These adjustments have come with the tradeoff of reduced ROM and complex design. Table 3 shows an example of such exoskeletons and finds what shortcomings they have in addressing additional movement in the shoulder.

Table 3: State of the art of the exoskeleton robots that have taken mobility of shoulder joint's CR into consideration

Exoskeleton/ Researcher	Brief Description	DOFs	Shoulder ROM	Limitations / Remarks
Mobile Exoskeleton Robot (Kiguchi et al., 2008)	This exoskeleton was developed at Saga University in Japan. It included a center of rotation mechanism using linear bushing to compensate shoulder protraction/retraction and horizontal translation in the frontal plane. No active DOF was used to address additional shoulder movements. This mechanism was later adopted in SUEFUL-7 exoskeleton (Gopura et al., 2009; Kiguchi and Hayashi, 2012).	3	Abduction/Adduction: 90°/0° Flexion/Extension: 90°/0° Internal/External rotation: Not available	It cannot realize shoulder depression/elevation during any shoulder movement. Besides, it cannot produce internal-external rotation.
ARMIN-III (Nef et al., 2009b)	Developed at ETH Zurich in late 2000, this was one of the early exoskeleton developed for human upper limb rehabilitation. The shoulder motion support part included two passive joints to allow additional movement in the shoulder during abduction-adduction and flexion-extension. In addition, this	6	Abduction/Adduction: 135°/45° Flexion/Extension: 135°/45° Internal/External rotation: 90°/90°	The ROM is lower than the corresponding natural ROM for the human upper limb.

	exoskeleton was clinically tested with stroke patients.			
Harmony (Kim and Deshpande, 2015; Kim and Deshpande, 2017)	This dual arm exoskeleton was developed at The University of Texas at Austin. It included a parallelogram mechanism at the shoulder articulation and was able to maneuver over variable ROM based on inter-Joint configuration.	5	Abduction/Adduction: 135°/45° Flexion/Extension: 135°/45° Internal/External rotation: 90°/90°	ROM varies depending on the inter-joint configuration. For example, maximum abduction (172º) angle can be achieved only when the shoulder joint's external rotation reaches 62º. Otherwise, abduction could not go beyond 118º
Christensen (Bai et al., 2017; Christensen and Bai, 2017)	Developed at Alborg University, Denmark, this exoskeleton was designed with a spherical mechanism that included passive double parallelogram linkage in the shoulder motion support part. The spherical mechanism, along with a parallelogram linkage was responsible for allowing passive movement of the Glenohumeral joint's center. To actuate the spherical mechanism, it used two actuators that limits	4	Abduction/Adduction: 170°/10° Flexion/Extension: 170°/60° Internal/External rotation: 30°/60°	Relatively lower internal and external rotation than corresponding human natural ROM.

	internal and external rotation.			
CLEVER ARM (Zeiaee et al., 2017)	This design was proposed with five DOFs at the shoulder to articulate three general motions as well as assure mobility of Shoulder joint ICR. Of five DOFs, two DOFs (a revolute joint and a prismatic joint) were used to allow movement of ICR in the frontal plane. The remaining DOF was intended to realize elbow flexion-extension. Two passive DOF were included in the design to deliver wrist motions. The links and axis were placed in a way to avoid the singularity.	6	Abduction/Adduction: 180°/0° Flexion/Extension: 180°/0° Internal/External rotation is obtained with arm elevation and horizontal abduction.	Active DOFs are used to realize shoulder joint ICR. This design allows ICR's movement in the frontal plane.

In this research, a 7 DOF robot has been designed and developed that allows mobility of shoulder joint for increased range of motion.

1.6.2   Dual functionality

Considering the design, an exoskeleton type robot is certainly advantageous over an end-effector type robot in providing motion to individual joints and being able to mimic the whole arm motion (if the robot has at least seven DOF for all seven joints of the human upper limb). However, exoskeleton robots are not very suitable for providing end-point exercises that many patients are

expected to do in upper limb rehabilitation. Also, exoskeleton robots cannot provide therapy to the patients having upper limb spasticity, which is observed approximately among one-third of the stroke survivors (Jiang et al., 2015; Kwakkel et al., 2003), and more than 80% among the patients who suffer from a spinal cord injury (Adams and Hicks, 2005). In upper limb rehabilitation, therapists frequently encounter patients with rotated shoulder, flexed elbow, pronated forearm, flexed wrist, etc., as shown in Figure 1.13.

Figure 1.13 Upper Limb Spasticity (a) Rotated Shoulder, (b) Flexed Elbow and flexed wrist, (c) Pronated forearm, (d) Wrist Flexing

In such a case, existing exoskeleton robots (Fitle et al., 2015; Kim and Deshpande, 2017; LIU et al., 2016; Nef et al., 2009b; Rahman et al., 2013; Xiao et al., 2017) have not been able to accommodate patients while end-effector type robots can accommodate those patients. Therefore, as an individual role, exoskeleton and end-effector type robots have apparent limitations in serving a wide variety of patients with different degrees of upper limb impairments and providing different types of therapeutic exercises. This could be overcome by making a single robot that will have both exoskeleton and end-effector type functionality. This way, it is possible to have a larger domain of patient inclusion and facilitate rehabilitation to patients with spasticity. Therefore, this research provided dual functionality in the proposed exoskeleton robot exoskeleton by allowing it to function as an end-effector type robot.

1.6.3   Other limitations

There are other limitations in the hardware design of robotic devices. Some exoskeleton robots have been built with fewer degrees of freedom that are unable to use in full arm rehabilitation (Accogli et al., 2017; Balasubramanian et al., 2008; Crea et al., 2016; Frisoli et al., 2009; Gunasekara et al., 2015; Otten et al., 2015; Sharma and Ordonez, 2016). Some systems did not include a mechanism for moving the instantaneous center of rotation (ICR) of the shoulder glenohumeral joint during shoulder range of motion (LIU et al., 2016; Perry et al., 2007; Rahman et al., 2013; Stroppa et al., 2017). The joint misalignment between the human-robot interface can lead to high torques as well as interaction forces. Some robotic systems are bulky and complex in structure (Klein et al., 2010; Perry et al., 2007; Stienen et al., 2009).

The proposed exoskeleton robot has considered existing hardware limitations, and it has been designed based on the natural range of motion of the human arm. It has short don/doff times, safe in operation, able to compensate for gravity.

1.7   Control approaches used in rehabilitative devices

The motion control of upper limb rehabilitative robots is a crucial element in upper limb rehabilitation. The control requirements and objectives of a therapeutic robot are different from traditional industrial and field robots. One of the major causes is the involvement of human-robot interaction as a disturbance to the controllers could reach damage to the wearer. In addition, the dynamics of a rehabilitation robot is non-linear in nature as it comprises of many links, joint, actuators, and sensors. The centrifugal and Coriolis forces and friction at joints cause non-linearity to appear in the robot's manipulator dynamics. This requires a non-linear control strategy, which is somewhat difficult and complex. The effectiveness of robot-aided upper extremity rehabilitation

depends on the controlled movement of provided therapeutic exercise. The rehabilitation paradigm could vary with the time elapsed after getting impairment, level of spasticity, and level of mobility loss. This dependence necessitates a robot having different control strategies rather than stick to a single approach. Depending on the way rehabilitation therapy is given, the control algorithm to recover motor function can be grouped: passive rehabilitation, assist as needed (AAN), challenge-based exercise, patient triggered rehabilitation, and adaptive control. The latter three fall into the category of assistive controllers.

A patient with impaired upper limb needs passive rehabilitation in which the patient seems to have very low or no movement of his/her limb at all. In such a case, the patient embodying robot is given exercise in the form of trajectory. The robot would produce the required torque to take the patient's limb to follow a given exercise/trajectory with no contribution from the patient. Most robotic devices developed over the past years can provide passive rehabilitation (Crea et al., 2016; Jarrett and McDaid, 2017; Krebs et al., 2007; Rahman et al., 2014; Sutapun and Sangveraphunsiri, 2015). In the passive mode of rehabilitation, both linear and non-linear control approaches have been used. Some researchers used linear proportional derivative (PD) controller (Brackbill et al., 2009; Jarrett and McDaid, 2017; Nef et al., 2007b), which has limitations of having some steady-state error. While other researchers used the proportional integral derivative (PID) control approach in which an integral term was added in the controller to compensates for steady-state error during the robot-aided therapy (Crea et al., 2016; LIU et al., 2016; Rahman et al., 2010; Sharma and Ordonez, 2016). Researchers also used non-linear control method; e.g., computed torque control (Nef et al., 2007b; Otten et al., 2015; Rahman et al., 2014), impedance control

(Carignan et al., 2007; Frisoli et al., 2009; Gupta and Malley, 2006; Mahdavian et al., 2015), and admittance control (Carignan et al., 2007; Fitle et al., 2015; Garrido et al., 2016).

For the assist-as-needed control algorithm, the patient is supposed to have some mobility, and the robot allows patients to move their impaired limb actively. When patients deviate from doing the task (e.g., grasping, reaching, etc.) the way they are supposed to do, robots start helping patients to do the given task the right way. The initiation of assistance may be carried out by sensing the patient' s force, the torque produced by the patient, arm position, arm's velocity threshold, elapsed time, muscle activity from electromyography signal. A simple assist-as-needed algorithm uses 'Feedback position control' based on a predefined boundary channel (Virtual channel). In this control approach, the patient's arm moves along a boundary channel, and a feedback-position control ensures the patient's whereabouts in the channel. This approach resembles maintaining the position of a limb by attaching a spring to the boundary channel. In MIT-MANUS, the assist-as-needed technique based on a threshold velocity that initiated assistance was used (Hogan and I Krebs, 2004; Krebs et al., 2007). In CAREX-7, a novel wrench filed controller based on the assist-as-needed paradigm was used to regulate the necessary force and torque required to maneuver it dexterously during a therapy session (Cui et al., 2017). Two-level of control have been implemented in the CAREX-7, where high-level control does force and torque generation by computing reference cable tensions, and low-level control is being used for actuators to follow reference tension trajectories. Here assistance parameter is set manually by the therapist based on the motor ability of the patient. The tracking results of cable tension of CAREX-7 shows some overshoot, which has always been undesirable in upper extremity rehabilitation. Moreover, some researchers used surface electromyography (EMG) to assess patient's

47

contribution and intention during rehabilitation (Li et al., 2017; Madani et al., 2017; Perry et al., 2007; Stroppa et al., 2017; Triwiyanto et al., 2016). However, proper estimation of EMG signals is difficult though. Instead, many researchers chose to apply force-based controllers in their devices where patients need to generate enough force to initiate getting assistance to accomplish a specific exercise (Frisoli et al., 2009; Lum et al., 2006; Lum et al., 2002).

Unlike assist-as-needed, challenge-based exercise offers some resistance or challenge to the patient while they are doing exercises (Rocon et al., 2007; Ruiz et al., 2009).

Patient-triggered rehabilitation refers to where assistance is initiated only when the patient has achieved a threshold force or velocity. A disadvantage of this genre is that patient remains passive for the rest of the exercise once assistance is triggered.

All the control algorithm discussed above do not adapt control parameters. On the contrary, an adaptive control strategy does modification of control parameters based on online estimation system parameters. For example, such a method is used to modify control parameters based on an online estimation of dynamic parameters as those vary from patient to patient.

Razzaghian et al. (2015) proposed a sliding mode fuzzy adaption control technique for the upper limb exoskeleton. Tang et al. (2014) used a back-propagation neural network based on EMG to follow the desired trajectory, whereas Kiguchi et al. (2008) and Kiguchi et al. (2012) used a neuro-fuzzy adaption controller based on EMG signals. Neural networks and fuzzy logic control require heavy computation, though. Besides, various non-linear hybrid control techniques, e.g., sliding mode with exponential reaching law, sliding mode backstepping, etc., have been developed

to control robotic devices for rehabilitation (Brahim et al., 2016; Islam et al., 2020a; Rahman et al., 2013).

1.8 Control limitations in existing robotic rehabilitative devices

Though enormous researches have been done, control strategies for upper limb rehabilitation robots are still evolving to deliver good tracking performance and safe rehabilitation.

1.8.1 Interactive force monitoring in passive rehabilitation:

The force exerted by the subject on the robot has mostly been ignored in passive rehabilitation by existing devices. However, monitoring of interactive forces between subject and robot is essential for safety as well as better human-robot interface. For a stiff limb, it is crucial to understand the forces between limb and robot. Besides, these forces may be considered in control design. In the *proposed exoskeleton robot*, forces exerted at the wrist, and upper arm are continuously monitored.

1.8.2 Use of upper arm forces in active exercises:

Existing exoskeletons consider only wrist forces in active exercises and force-based control (Brahmi et al., 2018; Hou and Kiguchi, 2018; Kim and Deshpande, 2017). However, interaction forces during shoulder movement primarily come from the upper arm than the wrist. Therefore, interactive forces from both the upper arm and wrist should be taken into account in the controller design. In the *proposed exoskeleton robot*, both upper arm and wrist interaction forces were considered in the active exercises.

1.9 Customer discovery:

In addition to the literature review, this research was also motivated by customer discovery through the NSF I-Corps program (Rahman, 2018a; Rahman, 2018b). The customers feedback helped set the design consideration.

1.9.1 Individuals interviewed:

We have conducted 100+ interviews with different customer segments to explore (a) the customer pains/needs; (b) a minimum viable solution to address customer needs; and (c) the market opportunity and trends. The customer segments interviewed was

- Stroke survivors,
- Occupational therapists (OTs),
- Recreational therapists (RTs),
- Physiotherapists (PTs),
- Clinicians,
- Caregivers, family members, assistive technology professionals (ATPs), and
- Insurance providers

1.9.2 Initial hypotheses tested:

The following hypotheses were tested during the interviews.

a) Use of an exoskeleton in upper limb rehabilitation (i) will increase mobility and independence of the Individuals with upper extremity dysfunction, (ii) reduce rehabilitation cost;

b) Insurance providers are willing to pay for this device if therapists suggest this device to patients for faster rehab;

c) Therapists/clinicians are eager to suggest a device of such type (our type) because a device of this kind provides a wide variety of recommended rehab exercises;

d) Individuals with upper extremity dysfunction would love to have a rehabilitation device able to help them do rehabilitation exercise;

e) Since individuals with upper extremity dysfunctions require intensive therapeutic exercises in the early stage of impairments, a therapeutic device of this type will be an essential addition both at the inpatient/outpatient clinics and at home;

f) Patients prefer game-based exercise during rehabilitation;

g) Insurance providers are willing to pay for this device as it lowers the insurance providers' overall cost of paying caregivers for the length of the disability period of individuals with upper extremity dysfunction.

We validated/invalidated our hypotheses through this customer discovery process, and notable comments from key interviewees are listed in Section 1.9.5.

1.9.3 Potential customer segments:

The potential customer segments that were identified throughout this customer discovery process are:

a) Individuals with Upper Extremity Dysfunction are our potential customer/end-users;

b) Inpatient and Outpatient care units

1.9.4   The key findings:

Our key findings/takeaways from customer discovery are:

a) Patients' unaffordability (cost of rehabilitation therapy) increases early dropout from rehabilitation;

b) Occupational therapists (OTs) are the key stakeholders who can suggest anything suitable for the rehabilitation;

c) Insurance companies pay for a rehab/assistive device that is suggested and justified by the OTs;

d) OTs below 35 years of age are interested in adopting new technology in rehab;

e) Individuals with upper limb dysfunction are much more interested in rehab devices than in assistive devices because they think such devices increase their recovery chances;

f)   A therapeutic device needs to be customizable;

g) In robot-aided rehabilitation, patients prefer game-based rehabilitation, where a patient can see their performance. They said it motivates them.

h)   Individuals with upper limb dysfunction are our potential customer/end-users;

i) OTs and ATPs are the key recommenders;

j) Individuals with upper limb dysfunction are in urgent need of self-care, rehabilitation exercise, and mobility assistance (key societal needs).

The above findings have thus motivated us to research and develop an MVP (prototype) of a 7 DOF robotic exoskeleton with an ergonomic shoulder to (i) provide upper limb rehabilitation exercises; (ii) improve upper limb range of motion, mobility, and strength;

1.9.5   Notable comments from the interviews

During the customer discovery, we have got following notable comments

- *"I would have been in a better position if I had more rehab session covered by insurance" — Jon G., Stroke Survivor*

- *"Home exercises intensify the rehabilitation process and need the help of family members or caregivers in many cases"—Jessica S. OT, Froedtert Hospital*

- *The most challenging part about rehab is expenses because only 24 therapy sessions are covered in a year"—Pamela S., Spinal Cord Injury Patient*

1.9.6   Rehabilitation exoskeleton market size:

The global market size of the exoskeleton is anticipated to reach USD 4.2 billion by 2027, expanding at a compound annual growth rate (CAGR) of 26.3% over the forecast period, according to a new report by Grand View Research, Inc (Healthcare Robot market size , 2020b). According to this report, in 2019, North America dominated the market with a value of USD 297.8 million. The driving factors include 'increasing investments in robotics,' 'increasing stroke patients,' and favorable reimbursement policies.

The industry growth report "Healthcare Robot Market Size, Growth, Potential, Price Trends, Competitive Market Share & Forecast, 2016 – 2024" by Global Market Insights, Inc. states that Healthcare Robot Market size is poised to reach USD 950 million by 2024 (Industry analysis for Exosketon Market, 2020a). The rehabilitation robot market share was over 40% of the global industry size in 2015 and is expected to reach USD 400 million by 2024. The use of rehabilitation robots has made it possible to safely implement efficient exercises and reduce the time spent on

supervision by the therapist. These products are used as a therapeutic tool and can accommodate a significant number of patients under a single therapist's supervision.

1.10 Specific research aims/Objectives

This research aims to develop a rehabilitation robot system that includes motor learning principles described in Section 1.3 to provide upper limb rehabilitation (objectives) to stroke survivors. The research conducted under this Ph.D. work has addressed three specific research aims as listed below.

1. **Aim-1:** Engineer a 7 DOFs upper limb exoskeleton robot incorporating an ergonomic shoulder joint allowing mobility of shoulder joint's center of rotation (CR). The specific research tasks include (a) design, (b) modeling, (c) fabrication, and (d) electrical, electronic, and sensor instrumentation.

2. **Aim-2:** Provide dual functionality to the proposed exoskeleton robot to provide joint-based and end-point (Cartesian coordinates) exercises.

3. **Aim-3:** Implement a non-linear control algorithm to maneuver the developed exoskeleton robot to deliver passive and active rehabilitation therapy.

1.11 Contribution

As a step toward the research Aim-1, a 7 DOF exoskeleton robot with two custom-made parallel mechanisms (i.e., frontal and sagittal mechanisms) was designed to allow the shoulder joint's center of rotation movement during abduction-adduction and flexion.

1. As a step toward the research Aim-1, a 7 DOF exoskeleton robot with two custom-made parallel mechanisms (i.e., frontal and sagittal mechanisms) was designed to allow the shoulder joint's center of rotation movement during abduction-adduction and flexion.

2. As a step toward the research Aim-2, an inverse kinematic solution of the proposed exoskeleton robot was derived. This inverse kinematic solution was used in the control of the exoskeleton in Cartesian space.

3. As a step toward Aim-3, an error-driven and model-based non-linear control law was designed and implemented to control the developed exoskeleton robot to perform passive exercises. To perform exoskeleton-aided active exercises, force-based control was designed and implemented.

CHAPTER-2   THE PROPOSED EXOSKELETON ROBOT

In this chapter, Section-1 describes the general design requirement of an upper limb rehabilitation robot. Section 2 through 5 depicts design consideration, steps in development, hardware development, actuators, and reducer selection of the proposed exoskeleton robot, respectively. The ergonomic shoulder motion support of the proposed robot is discussed in Section-6. Section 7 and 8 describes the elbow and wrist part of the proposed robot. The mass and inertia properties are presented in Section-9. This chapter ends with Section-10, where electrical and electronic design is discussed.

2.1   General design requirements

A rehabilitative robot's design requirements largely depend on the range of motion and limb segment to where it will be attached to. The complex joint articulation of the human upper limb makes the design of exoskeleton robots difficult. The human upper limb is mainly composed of seven degrees of freedom (DOFs). The *proposed exoskeleton robot* will assist upper limb movement at the shoulder, elbow, forearm, and wrist joints. The motions assisted by the proposed exoskeleton are listed below.

- Shoulder (2 DOFs): abduction-adduction, flexion-extension;
- The upper arm (1 DOF): internal-external rotation;
- Elbow (1 DOF): flexion-extension;
- Forearm (1 DOF): pronation-supination;
- Wrist (2 DOFs): flexion-extension; radial-ulnar deviation;

Following are critical design criteria, which should be considered while designing a rehabilitation robot.

a) Safety:

Since upper limb robots have close interactions with wearers, safety is paramount. Human-robot interaction (HRI) must be designed so as to ensure safe operation. For robots' safe running, an HRI should include safety measures in mechanical, electronic, and control design. Mechanically, safety is ensured by placing physical stoppers in the robot's structure to prevent it from going beyond the chosen ROM; safety can also be ensured by designing links and robot parts in a way so that adjacent links act as physical stoppers in extremes. Electronically, by setting current and voltage limits in motors, robot joints can be refrained from going beyond permissible ROM. In control design, saturation can be set for torque, force, velocity, and position to ensure the wearer's safety if the robot malfunctions. When it comes to the design requirement of rehabilitation robots, safety comes first since these sorts of robots are in direct interaction with patients. Safety is imperative during the robot's operation. Therefore, adequate safety features should be implemented in hardware (e.g., mechanical stopper, design of link compliance with ROM) and control (e.g., limits for a range of motion and velocity).

b) Degrees of Freedom (DOFs):

The design of an upper limb exoskeleton robot should mimic the human upper limb's joint movement and range of motion. Therefore, the exoskeleton's degrees of freedom must provide a corresponding upper-limb joint movement and natural range of motion. The human upper limb's joint articulations can be simplified and modeled with at least seven

active revolute DOFs that include 3 DOF at the shoulder glenohumeral (GH) joint, 1 DOF at the elbow joint, 1 DOF at the forearm, and 2 DOF at the wrist joint. The shoulder GH joint can be modeled as a ball and socket joint as the surface of the joint is nearly spherical (Gams and Lenarcic, 2006; Holzbaur et al., 2005; Moeslund et al., 2005; Soslowsky et al., 1992). The GH joint, which connects the shoulder girdle and upper arm, is not fixed, and additional sliding (prismatic) DOFs (Dvir and Berme, 1978). Often researchers consider GH joint as the center of the shoulder and term it as a shoulder joint. The elbow joint connecting the upper arm and forearm is modeled as a hinge joint (Gray and Clemente, 1985). The mechanical function of the wrist can be obtained by a revolute joint with two DOF (Lenar et al., 2006; Soslowsky et al., 1992). Following are motions associated with shoulder, elbow, forearm, and wrist.

Motion associated with shoulder joint:

- Abduction-adduction (Figure 2.1)
- Vertical flexion-extension (Figure 2.2)
- Internal-external rotation (Figure 2.3)

Motion associated with elbow joint and forearm:

- Elbow flexion-extension (Figure 2.5)
- Forearm pronation-supination (Figure 2.6)

Motion associated with wrist joint:

- Flexion-extension (Figure 2.7)
- Radial-ulnar deviation (Figure 2.8)

The shoulder joint, horizontal flexion-extension, can be obtained in the form of a combination of vertical flexion-extension and abduction-adduction, as shown in Figure 2.4. All the figures have been drawn using Poser 11.1, developed by Smith micro software, Inc (Aliso Viejo, CA, USA).
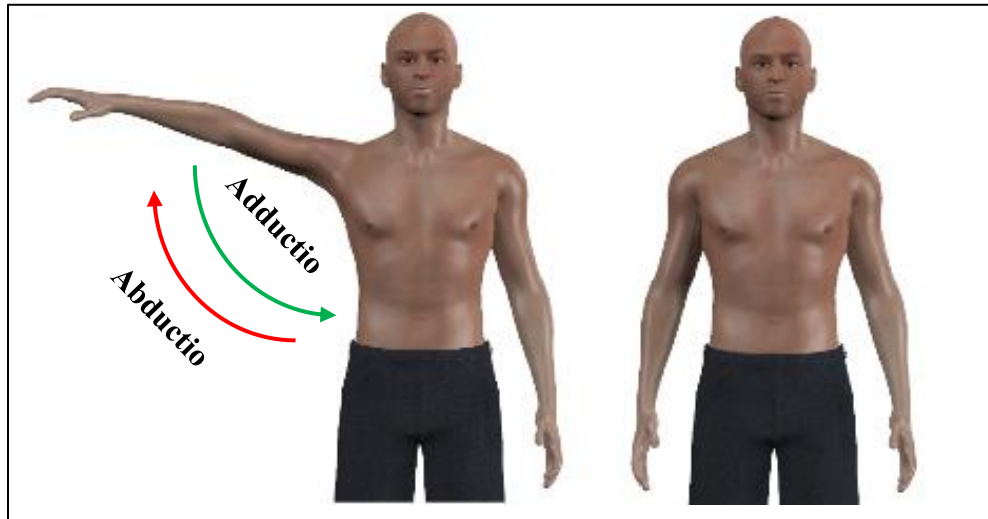
Figure 2.1 Shoulder joint, abduction-adduction
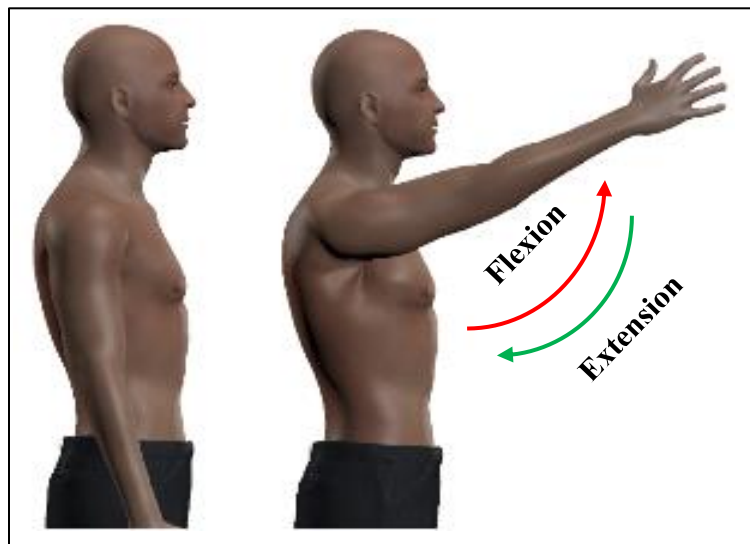
Figure 2.2 Shoulder joint, vertical flexion-extension
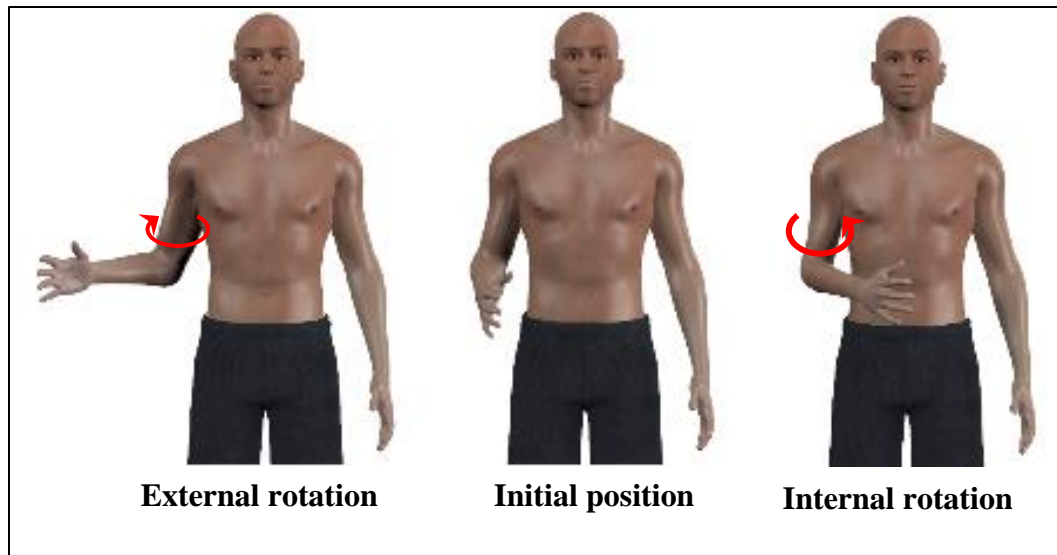
Figure 2.3 Shoulder joint, upper arm internal-external rotation
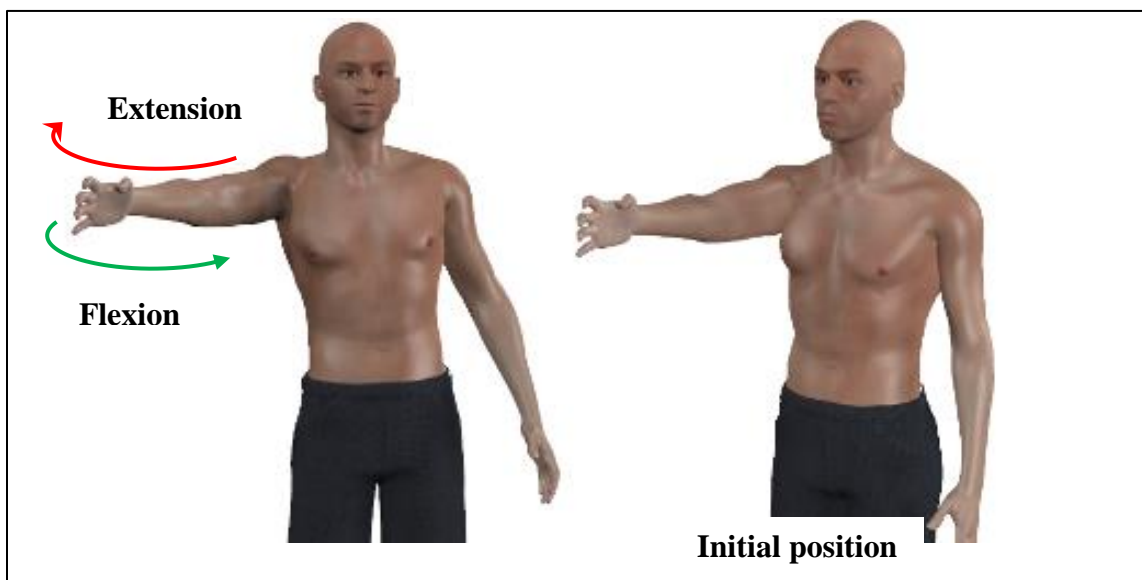
Figure 2.4 Shoulder joint, Horizontal flexion-extension
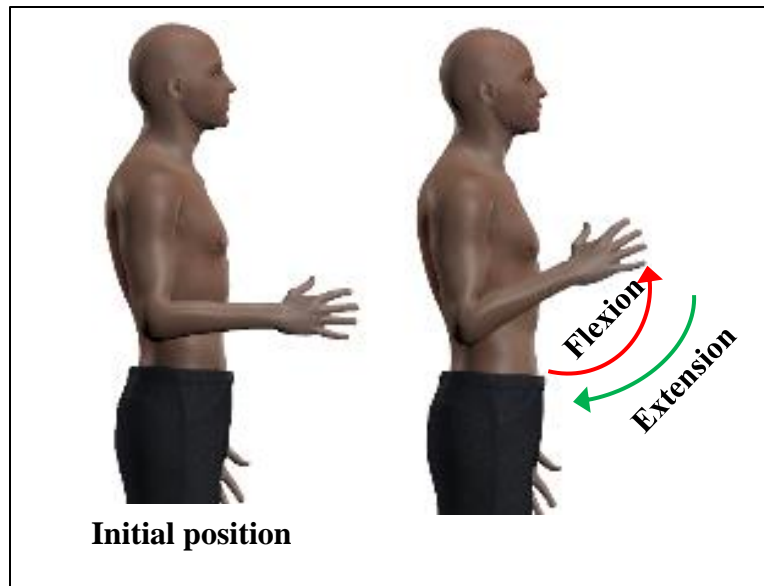
Figure 2.5 Elbow joint, flexion-extension
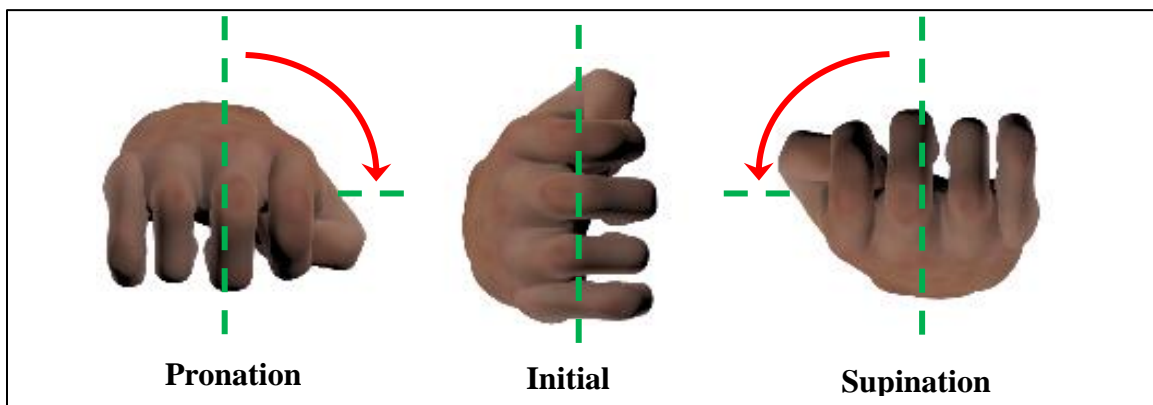
Figure 2.6 Forearm pronation-supination
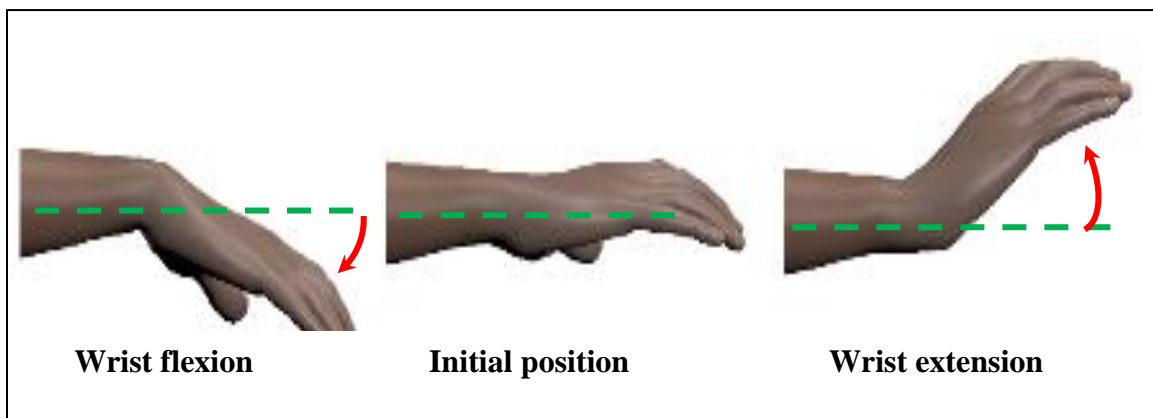
Figure 2.7 Wrist flexion-extension
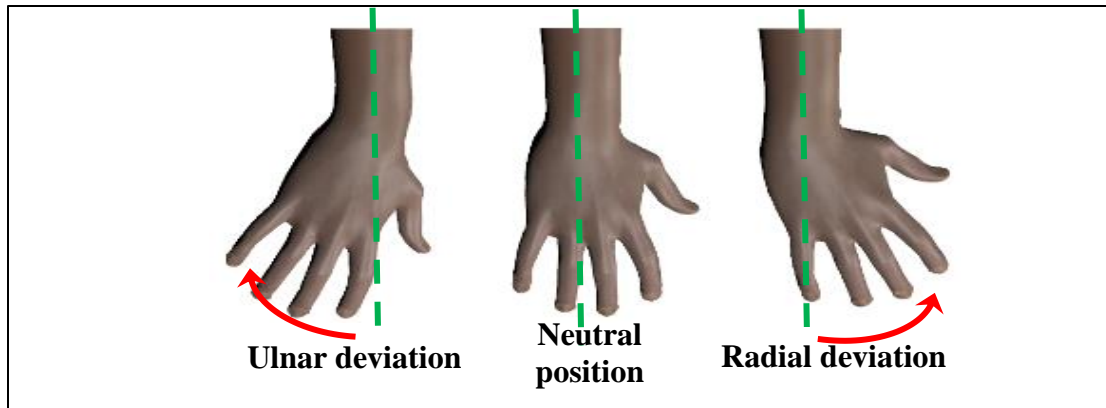
Figure 2.8 Wrist radial-ulnar deviation

c) Range of Motion:

Once degrees of freedom is established, the next design requirement focuses on how much motion it would allow for each degree of freedom during maneuvering, eventually leading to the robot's workspace. The robot should be designed to have an extensive range of motion compliant with upper limb anatomy (Tsagarakis and Caldwell, 2003). Table 4 shows the typical range of motion for the human upper limb from three different sources.

d) Functionality:

Functionality is seen to have been a crucial factor in rehabilitation robots. As far as functionality is concerned, Exoskeleton type devices have advantages over end-effector-type devices, as they have complete control over a patient's individual joint movement and applied torque, better guidance of motion, relatively larger range of motion (ROM), and better quantitative feedback. However, there are cases where end-point exercises are recommended, which exoskeleton type robots cannot do. Besides, it is difficult for a patient with a spastic limb to wear an exoskeleton; in many cases, impossible. Keeping these issues in mind, it is recommended to have dual functionality in a single device.

Table 4: Range of Motion of Human Upper Limb

Limb Segment	Kinds of Motion	Source 1 (Hamilton et al., 2012)	Source 2 (Range of Joint Motion Evaluation Chart (2014))
Shoulder	Abduction	180º	150
	Adduction	50º	30
	Vertical flexion	180º	150
	Vertical extension	50º	50
	Internal rotation	90º	-
	External rotation	90º	-
Elbow and Forearm	Flexion	145º	150
	Extension	0º	0
	Pronation	80º	80
	Supination	80º	80
Wrist	Flexion	60º	60
	Extension	60º	60
	Radial deviation	20º	20
	Ulnar deviation	30º	30

e) Light Weight with Low Mass/Inertia:

As long as weight is concerned, the hardware design of a robot should be done such that

mass is kept at a minimum (Tsagarakis and Caldwell, 2003). Choosing the material to

fabricate hardware should require great attention as it significantly contributes to the robot's weight. Besides, actuators and reducers are responsible for increasing weight. The proper selection of those is necessary to reduce the weight. High power to weight ratio actuators is always desirable in rehabilitation robots.

f) Easy and Quick don/doff:

The don/doff of a rehabilitative device should always be easy to make setting up the device comfortable for both patient and therapist. A complex don/doff might make the therapist/clinician demotivated to use the device. Also, the don/doff should be quick to reduce setup and removal time in the rehab session.

g) Comfort of Wearing:

Since patients would wear the robot the entire time during the rehab session, which ranges from a half an hour to 2 hours, any kind of discomfort is unexpected. A human-robot interaction needs to ensure the patient's comfort. Exoskeleton joints correspond to human joints, and as such, there are reactive forces and torques between exoskeleton joints and human joints. The weight of the exoskeleton contributes to producing reactive forces and torques in the human joint. Therefore, the lesser the weight, the more comfortable is the robot for the wearer. When it comes to wearing the robot, an open-type structure (e.g., CADEN-7 (Perry et al., 2007), ARMIN (Nef et al., 2009b), SUEFUL-7 (Gopura et al., 2009), MARSE-7 (Rahman et al., 2014) is always preferred in rehabilitative robot design. An open-type structure is advantageous because of easy don/doff, comfortable fitting, and better compliance. In addition, it is expected that the rehab robots are connected to their wearer with flexible straps/links in between.

h) Gravity Compensation:

The load due to gravity should always be compensated. While the device remains static, the weight of the mechanical structure should be compensated in the sense that the wearer should not feel any extra load to the arm (Vaca Benitez et al., 2013). When the exoskeleton is in operation, in addition to static compensation, gravity force should be compensated in the control approach to avoid the appearance of any extra load.

i) Accurate Force Feedback:

The proper motion control of rehabilitation robots largely depends on getting accurate force feedback (Tsagarakis and Caldwell, 2003). To assist patients as needed (with the assistive device), patient participation in the given exercise is monumental. A patient can be troubled in doing exercises due to inaccurate and delayed force feedback from the exoskeleton/therapeutic device.

2.2 Design consideration for the proposed exoskeleton robot

The proposed exoskeleton robot has addressed the design, as mentioned in Section 2.1.

a) Safety:

The links of the proposed exoskeleton robot have been designed in a way that they act as an inherent physical stopper for chosen Range of Motion (ROM). In Graphic User Interface, a user-specific safe zone of ROM depending on the subject's requirement can be set at each session. An emergency switch has been placed to shut down the device in case of any malfunction. Besides, the ROM threshold, velocity threshold, and torque threshold have been included in the LabVIEW based program control interface.

b) Degrees of Freedom:

To provide a full arm rehabilitation, the proposed exoskeleton is composed of 7 (3-2-2) active DOFs. 3-DOF shoulder articulations (abduction-adduction, vertical flexion-extension, and internal-external rotation) are obtained by three revolute joints. In addition, two passive DOFs at the shoulder allow shoulder protraction/retraction and rotation in the frontal plane that allows shoulder elevation/depression with horizontal translation. For 1-DOF elbow articulation, the proposed exoskeleton robot has a revolute joint. To realize forearm pronation-supination, a revolute joint is used. The 2 DOF wrist articulations are realized with 2 revolute joints.

c) Range of Motion:

A large workspace allows designing a rehabilitation protocol with a variety of exercises. The suitable range of motions for the proposed exoskeleton robot was chosen based on existing literature (Gates et al., 2015; Hamilton et al., 2012; Kim et al., 2011; Namdari et al., 2012; Van Cott and Kinkade, 1972). A comparison of the selected range of motion of the proposed exoskeleton robot with other contemporary robotic devices is shown in following Table 5.

d) Functionality:

Considering the different stages of mobility recovery and patient's specificity, *the proposed exoskeleton robot* has been developed to serve dual functionality in the sense that it is functioning as an exoskeleton and end-effector type robot. As an exoskeleton role, it has control over individual joint movement, while, as an end-effector role, the proposed exoskeleton robot would assist patients in doing end-point exercises. The conceptual sketch is shown in Figure 2.9.

66

Table 5: Comparison of range of motion of proposed exoskeleton robot with existing robots

Limb Segment	Joint No	Kinds of Motion		(Cui et al., 2017)	(Rahman et al., 2013)
			Proposed Exoskeleton Robot	**CAREX-7**	**MARSE-7**
Shoulder	Joint-1	Abduction	90°	60°	140°
		Adduction	0°	25°	0°
	Joint-2	Vertical flexion	180°	70°	140°
		Vertical extension	0°	25°	0°
	Joint-3	Internal rotation	90°	40°	85°
		External rotation	90°	40°	75°
Elbow and Forearm	Joint-4	Flexion	135°	60°	120°
		Extension	0°	0°	0°
	Joint-5	Pronation	90°	50°	85°
		Supination	90°	35°	85°
Wrist	Joint-6	Flexion	60°	30°	60°
		Extension	50°	45°	50°
	Joint-7	Radial deviation	20°	20°	20°
		Ulnar deviation	30°	30°	25°
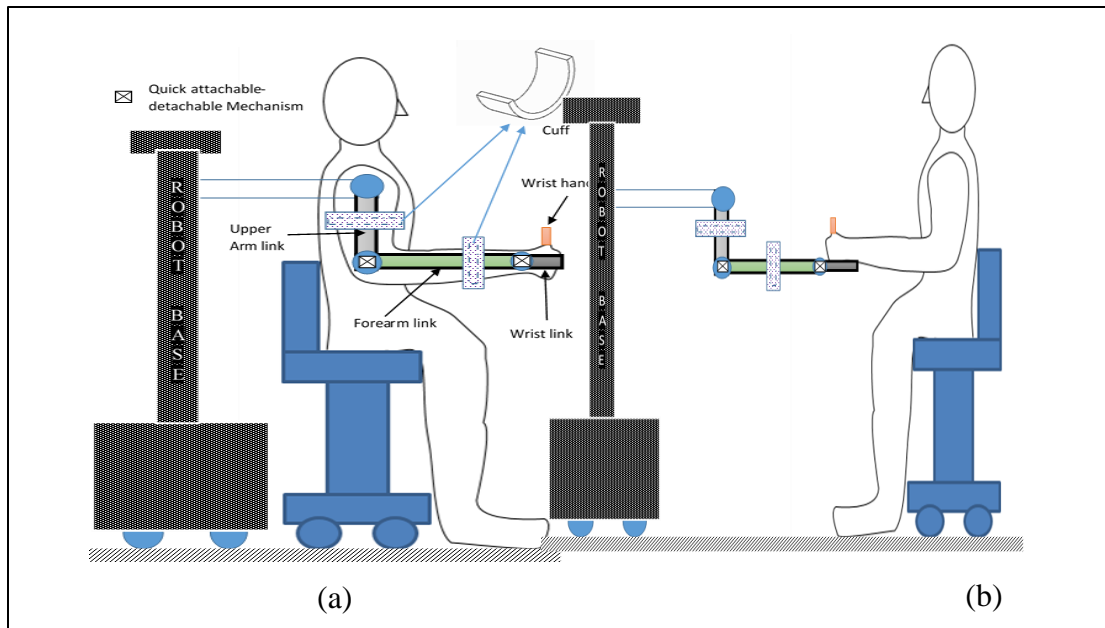
Figure 2.9 Conceptual sketch of proposed exoskeleton robot, functioning as (a) exoskeleton and (b) end-effector type robot

e) Easy and Quick don/doff:

The subject wears the proposed exoskeleton robot by attaching the right arm to the robot's upper arm and forearm cuffs by using flexible straps. The cuffs are semicircular and open type. As mentioned earlier, these open type cuffs facilitate easy don/doff. The adjustable links for the upper arm, forearm, and wrist have been designed and made to fit the wearer easily and quickly. These links include the rack and screw mechanism on it to fit a wide range of the user.

f) Comfort of Wearing:

The proposed exoskeleton robot is worn using flexible straps to make sure comfort. Moreover, mobility of the shoulder joint's center of rotation has also provided better alignment and ergonomic movement by allowing passive shoulder protraction-retraction and elevation-depression.

g) Gravity Compensation:

The *proposed exoskeleton robot* has been designed to gets balanced with or without the wearer at its home condition. In addition, real-time gravity force has been compensated in the control approach to cancel out ill effects caused by gravity.

h) Accurate Force Feedback:

To get the force exerted by the patients (wearer) as feedback, in this research, we used three-button type force sensors (Model TAS606, HT Sensor technology) at the upper arm cuff and a 3-axis force sensor (GPB160-50N, GALOCE) to get forces in all three Cartesian axes.

2.3 Development of proposed exoskeleton robot

The development of the *proposed exoskeleton robot* involves steps shown in Figure 2.10. Details about kinematic and dynamic modeling are discussed in Chapter-3. The control and simulation are discussed in Chapter-4. In this chapter, hardware design and fabrication are discussed.
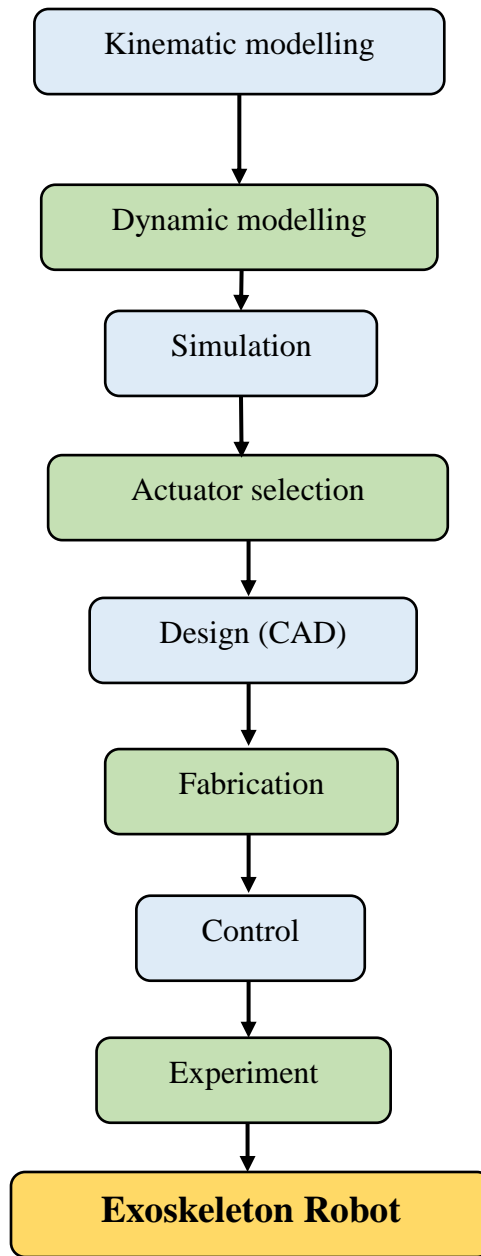
Figure 2.10 General layout of development of proposed exoskeleton robot

2.4 Hardware development of the proposed exoskeleton robot:

To develop the proposed exoskeleton robot, the following steps were carried out.

- The very first step in the development of the *proposed exoskeleton robot*'s Hardware was

    to study the anatomy and biomechanics of the human upper limb to find the safe range of

motion for the proposed exoskeleton robot (Halder et al., 2000; Hamilton et al., 2012; Van Cott and Kinkade, 1972).

- Anthropometric parameters (e.g., arm length, arm segment's weight, and segment inertia) of the upper limb were studied to obtain the *proposed exoskeleton robot's* link parameters. Besides, they have been used in the simulation to choose actuators (Winter, 2009).

- With the selected range of motion and length of the various segments, mechanical components were designed, and a complete CAD model of the proposed exoskeleton robot (shown in Figure 2.11) was developed in PTC Creo (Needham, Massachusetts, USA. This model provided the center of gravity and inertia properties of the *proposed exoskeleton robot's* segments.

- The CAM of mechanical components were designed in Fusion 360 (Autodesk Inc., San Rafael, CA, USA).

- A CNC milling, centering, and drilling operations were used to fabricate the proposed exoskeleton robot's components.

- The *proposed exoskeleton robot* was made ready to function (see Figure 2.12) with all the components fabricated and assembled with the required screw and fasteners.

Throughout the next sub-sections, motion support parts of the *proposed exoskeleton robot*, actuator selection, and a CAD model of the *proposed exoskeleton robot*, fabrication of the *proposed exoskeleton robot* parts are presented. Note that the *proposed exoskeleton robot* is comprised of three major hardware parts, namely, shoulder motion support part or shoulder module, elbow and forearm motion support part or elbow module, and wrist motion support part or wrist module.

71
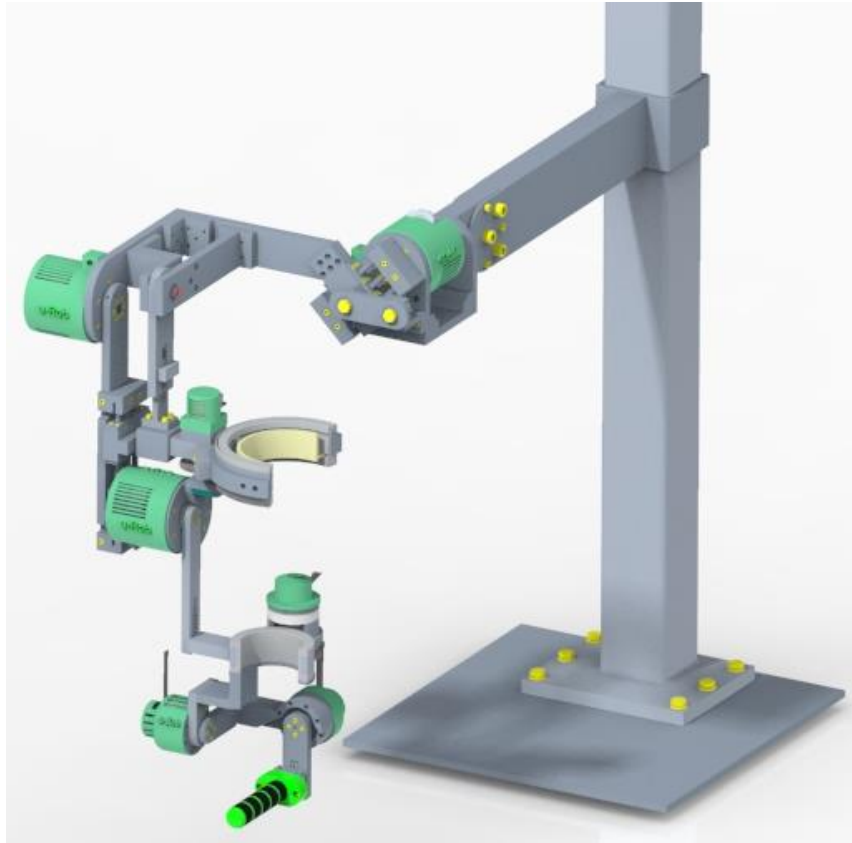
Figure 2.11 Rendered CAD model of the proposed exoskeleton robot
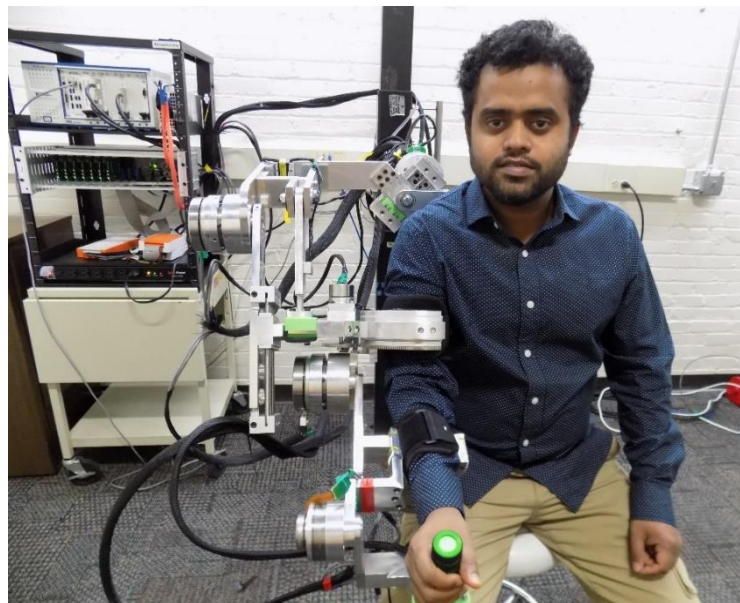
Figure 2.12 Subject wearing proposed exoskeleton

2.5 Actuators and reducer selection

Based on the simulation result of the *proposed exoskeleton robot* – which is presented in chapter-4, actuators for all seven joints have been selected. In this research, all the actuators are brushless DC motors. Maxon EC90 flat 90W (PN 323772) motor is used in joint-1, 2, and 4. Maxon EC45 flat 70W (PN 397172) motor was used for joint-3. To actuate joint 5, 6, and 7, Maxon EC45 flat 70W (PN 339281) was used. The selected motors with nominal torque are shown in Table 6. All motors' specification is given in ANNEX I, ANNEX II, and ANNEX II.

Table 6: Motors/actuators selected to be used in proposed exoskeleton robot

Joint No.	Application domain	Maxon Motor with Hall sensors (Input Voltage 24V for all motors)		Nominal torque (*when coupled with reducer*)
		Model	Part Number	
Joint-1	Shoulder abduction-adduction	EC 90 flat Ø90 mm, brushless, 90 Watt	323772	44.4 Nm
Joint-2	Shoulder vertical flexion-extension	EC 90 flat Ø90 mm, brushless, 90 Watt	323772	44.4 Nm
Joint-3	Shoulder internal-external rotation	EC 45 flat Ø42.8 mm, brushless, 70 Watt	397172	12.8 Nm
Joint-4	Elbow flexion-extension	EC 90 flat Ø90 mm, brushless, 90 Watt	323772	44.4 Nm
Joint-5	Forearm pronation-supination	EC 45 flat Ø42.9 mm, brushless, 30 Watt	339281	5.5 Nm
Joint-6	Wrist ulnar-radial deviation	EC 45 flat Ø42.9 mm, brushless, 30 Watt	339281	5.5 Nm
Joint-7	Wrist flexion-extension	EC 45 flat Ø42.9 mm, brushless, 30 Watt	339281	5.5 Nm

To reduce the motor speeds, harmonic reducers (strain wave gears) were used. Because of being advantageous over traditional gears, this kind of reducer has been increasing over the past

several years. The reason for selecting harmonic reducer in the proposed exoskeleton robot is to provide zero-backlash motion. In the proposed exoskeleton robot, harmonic reducers from two companies have been used. Joint1,2,3 and 4 have used harmonic reducers from Harmonic Drive LLC, US Headquarter, Dunham Ridge, MA. Whereas Joint 5,6 and 7 have used reducers from Leaderdrive, Suzhou, China. Table 7 shows harmonic reducers used for all joints in the proposed exoskeleton robot and their rated L10, average, repeated, and Momentary peak torque. The specification of reducers are given in ANNEX IV, and ANNEX V.

Table 7: Specification of harmonic reducers

Joint No.	Reducer (Harmonic Drive)	Rated L10 (90% life) /Average/Repeated Peak/ Momentary Peak Torque (Nm)
Joint-1	CSF-17-100-2UH	24/39/54/108
Joint-2	CSF-17-100-2UH	24/39/54/108
Joint-3	CSF-11-100-2XH-F	5/8.9/11/25
Joint-4	CSF-17-100-2UH	24/39/54/108
Joint-5	LHSG-14-C-I	9.6/13.5/34/66
Joint-6	LHSG-14-C-I	9.6/13.5/34/66
Joint-7	LHSG-14-C-I	9.6/13.5/34/66

2.6 **Ergonomic shoulder motion support part** (Islam et al., 2020b; Islam et al., 2020c):

To design shoulder motion support part, anatomical planes of the human body shown in Figure 2.13 and upper limb anatomy were studied. According to human upper limb anatomy, there are three general motions (i.e., shoulder abduction-adduction in the frontal plane, shoulder vertical or horizontal flexion-extension in the sagittal plane, and internal-external rotation in the transverse plane) in the shoulder. These three movements are also known as glenohumeral (GH) articulations.

The intersecting point of axes of these three motions is often known as the center of the GH joint (also known as shoulder joint Instantaneous Center of Rotation (ICR)). In addition to these three general motions, there are two other motions (i.e., elevation-depression and protraction-retraction) in the frontal plane and sagittal plane of the human body while realizing shoulder abduction-adduction and flexion-extension accordingly; the conventional ball and socket joint cannot provide movement to the shoulder joint's center of rotation. In such a case, the shoulder joint's Instantaneous Center of Rotation (ICR) is no longer being able to realize additional movement in the frontal and sagittal plane.
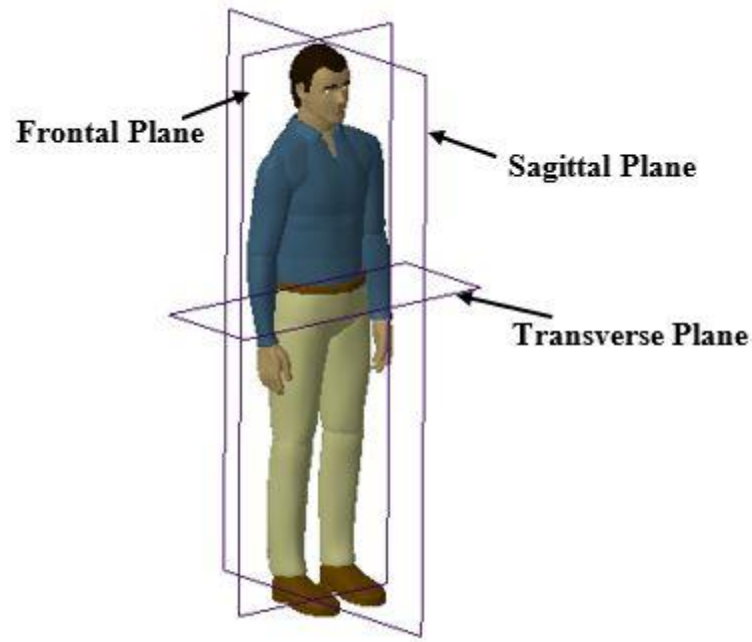
Figure 2.13 Anatomical planes of the human body

To realize additional movements in the frontal and sagittal plane during shoulder rehabilitation, the shoulder motion support part in the *proposed exoskeleton robot* part has been designed as shown in Figure 2.14 using a hybrid approach by incorporating both parallel and serial mechanisms. Two parallel mechanisms, namely frontal and sagittal mechanisms, as shown in

Figure 2.15 and Figure 2.22, were used in the design of the proposed ergonomic shoulder motion support part. Combinedly, these mechanisms will allow mobility of the shoulder joint's instantaneous center of rotation by providing movement in the frontal and sagittal plane, respectively. There were altogether three actuated (active) DOFs and two passively actuated DOFs used in the ergonomic shoulder motion support part. All the actuated DOFs are revolute joint and responsible for doing abduction-adduction (joint-1), vertical flexion-extension (joint-2), and internal-external rotation (joint-3), whereas two passive DOFs are responsible for moving shoulder joint ICR (passive joint-1) during abduction-adduction and doing protraction-retraction (passive joint-2) during vertical flexion-extension. Note that the intersection of Joint-1, Joint-2, and Joint-3 locates shoulder joint instantaneous center of rotation in the *proposed exoskeleton robot*.
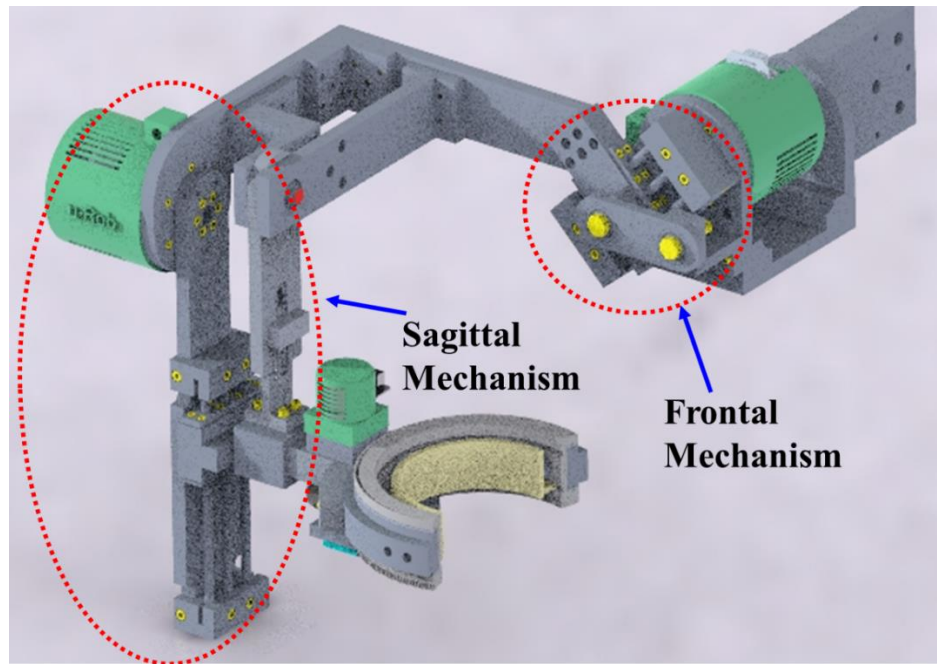
Figure 2.14 Ergonomic shoulder motion support part of the proposed exoskeleton robot

Figure 2.15 Schematic of link-slider mechanism for joint-2 (Frontal mechanism)

2.6.1 Frontal mechanism:

It is known from the literature that while doing abduction-adduction, shoulder joint instantaneous center of rotation (often termed as the center of the glenohumeral joint) does not remain fixed. Rather it moves in the frontal plane (i.e., a combined motion of depression/elevation and horizontal translation) as shown in Figure 2.16.

In this research, we developed a novel link-slider mechanism to address this issue, which allows shoulder joint instantaneous center of rotation to travel in the frontal plane when joint-1 rotates. It consists of a slider, a circular free ended shaft (link-1A), a rectangular both end hinged link (link-1B), as shown in Figure 2.17. One end of link-1A is connected to joint-1, thereby gets through the same rotation as joint-1 does. Link-1A carries the slider, which can translate along the longitudinal axis of Link-1A depending on the rotation of joint-1. The slider has link-1B mounted on it through a revolute joint. The point where link-1B is connected on the slider is termed as

Shoulder Joint ICR. Since the right end of Link-1B is hinged, it constrains the slider's translation along with link-1A.
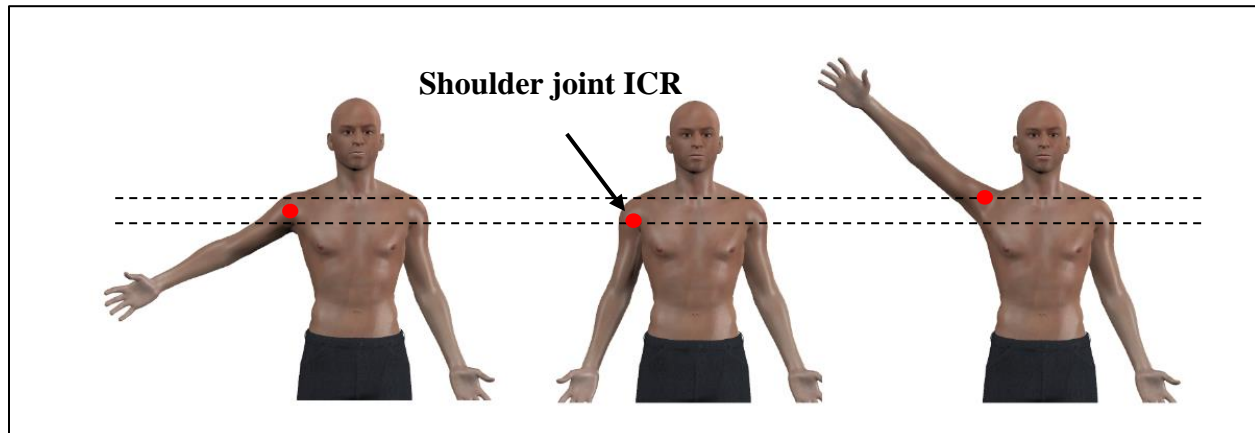
Figure 2.16 Location of shoulder joint instantaneous center of rotation during abduction-adduction
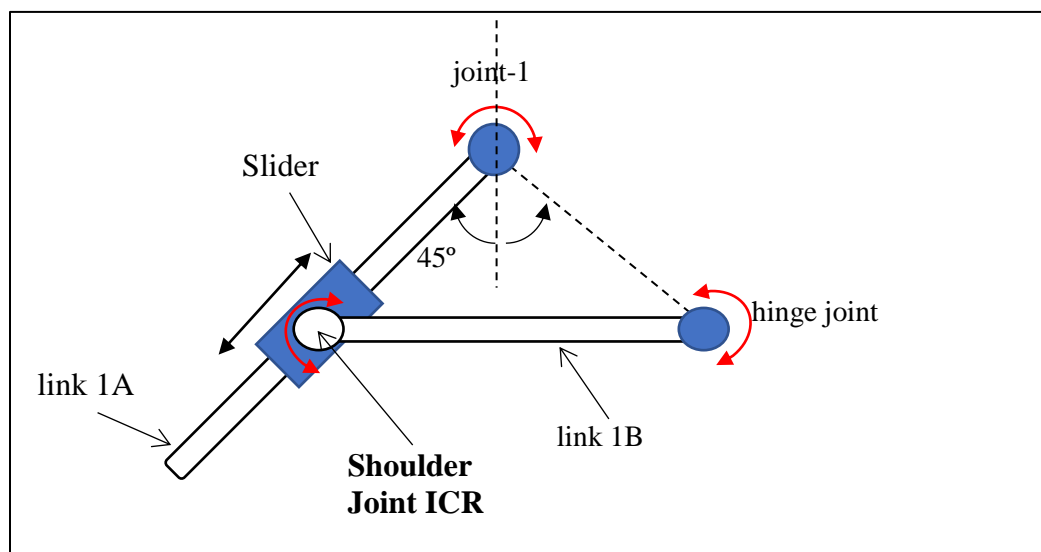
Figure 2.17 Schematic of link-slider mechanism for joint-1 (frontal mechanism)
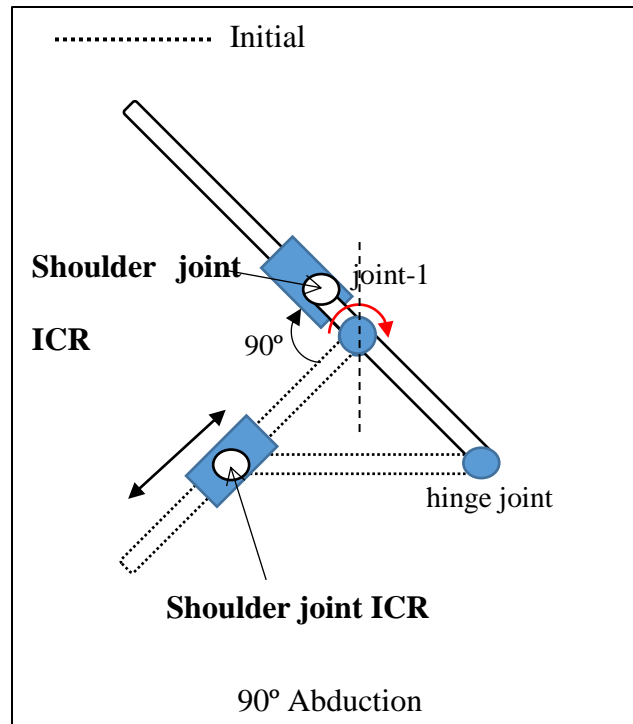
Figure 2.18 Location of shoulder joint's instantaneous center of rotation for abduction

As link-1A has the same sense of rotation as joint-1, it rotates clockwise when joint-1 gets through the clockwise rotation. This clockwise rotation makes the slider to translate towards joint-1 origin due to the constraining motion of the slider by the link-1B. Though link-1A is going through the same rotation as joint-1, however, link-1B is going through approximately half of the joint-1 rotation. Thus, a circular path is followed by shoulder joint ICR during 90° abduction, as shown in Figure 2.18. The radius of the path can be specified by choosing the length of link-1B. Figure 2.18 shows the typical displacement of shoulder joint instantaneous center of rotation of ergonomic shoulder motion support part that could be achieved by using the frontal mechanism. For example, from Figure 2.18, it is clearly seen that for shoulder abduction of 90°, shoulder joint instantaneous center of rotation (ICR) is displaced by a vertical and horizontal translation.

Placement of slider, link-1A, and link-1B:

In the frontal mechanism, the amount of passive movement of shoulder joint ICR depends on the placement of the slider, link-1A, and link-1B. For example, if link-1A is placed at 0° angle offset initially, shoulder joint ICR will be displaced by a vertical distance (only elevation) for 180° abduction. However, shoulder joint ICR is supposed to have a horizontal displacement as well. Again, if link-1A is placed at 90° angle offset initially, the frontal mechanism gets shoulder joint ICR to have only horizontal displacement for 180° abduction. The suitable angular position to place link-1A is at an angle offset of 45° from the vertical axis of joint 1, as shown in Figure 2.19. This placement allows both elevation/depression and horizontal translation for all configurations of shoulder abduction.
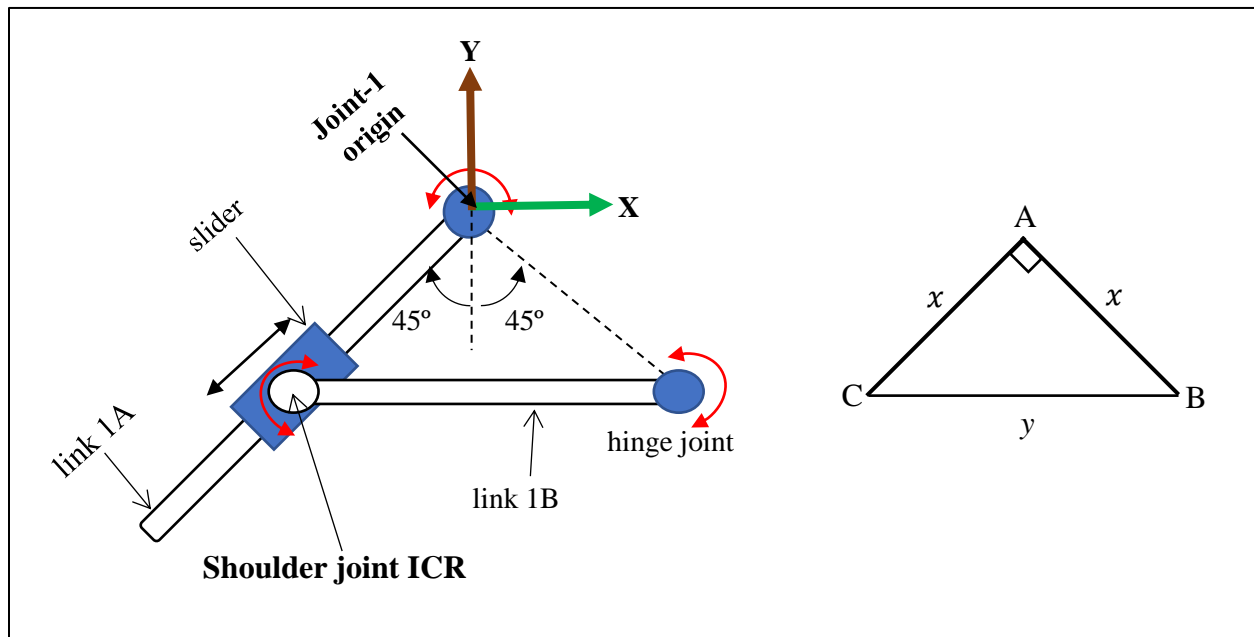
Figure 2.19 initial configuration of link-slider, forming an isosceles right-angle triangle

The slider's placement determines the maximum amount of distance shoulder joint instantaneous center of rotation is going to be displaced by. The length of link-1B gives us

80

the distance at which the primary slider should be placed from the joint-1 origin. If shoulder joint ICR (point C), the right end of link-1B (point B), and joint-1 origin (point A) are connected by straight lines among each other, those lines make a triangle ABC as shown in Figure 2.19. As link-1A is placed initially at 45° angle offset, this triangle is an isosceles right-angled triangle. x, y and x be the length of sides AB, BC and AC respectively, from trainable ABC,

$$AC^2 + AB^2 = BC^2$$

$$\Rightarrow x^2 + x^2 = y^2$$

$$\Rightarrow x = \frac{1}{\sqrt{2}}y \approx 0.707y$$

Note that, y is the length of link 1B, where x is the distance between joint-1 origin and hinge joint.

The distance at which the slider can be placed is $\frac{1}{\sqrt{2}}y$ away from the joint-1 origin, while link-1B should be mounted horizontally. The past literature reveals that the arc radius of shoulder ICR travel has an approximate range of 50~80 mm (Crabolu et al., 2017; Halder et al., 2000; Kim and Deshpande, 2017; Soltani-Zarrin et al., 2017). In this research, y has been chosen 70 mm to allow ergonomic shoulder motion support part to have a maximum 50 mm elevation and 50 mm rightward (inward) horizontal displacement of shoulder joint's Instantaneous Center of Rotation (ICR) during 90° abduction.

Validation of Frontal Mechanism:

To validate the functionality, a model of the developed mechanism was created in a multibody dynamics simulation software called ADAMS (Newport Beach, CA, USA). Simulations were carried out to see the location of shoulder joint ICR for full (0° to 90°) abduction, which used 0° to 90° rotation of joint-1. Note that, in ADAMS, y length was chosen as 60 mm. The ADAMS simulation result is shown in Figure 2.20-Figure 2.21. Figure 2.20 shows the location of shoulder joint ICR for different abduction angle, whereas Figure 2.21 presents the variation of link-1B angle with respect to the abduction angle. From these figures, it is seen that the simulation results corroborate the functionality which frontal mechanism is aimed for.
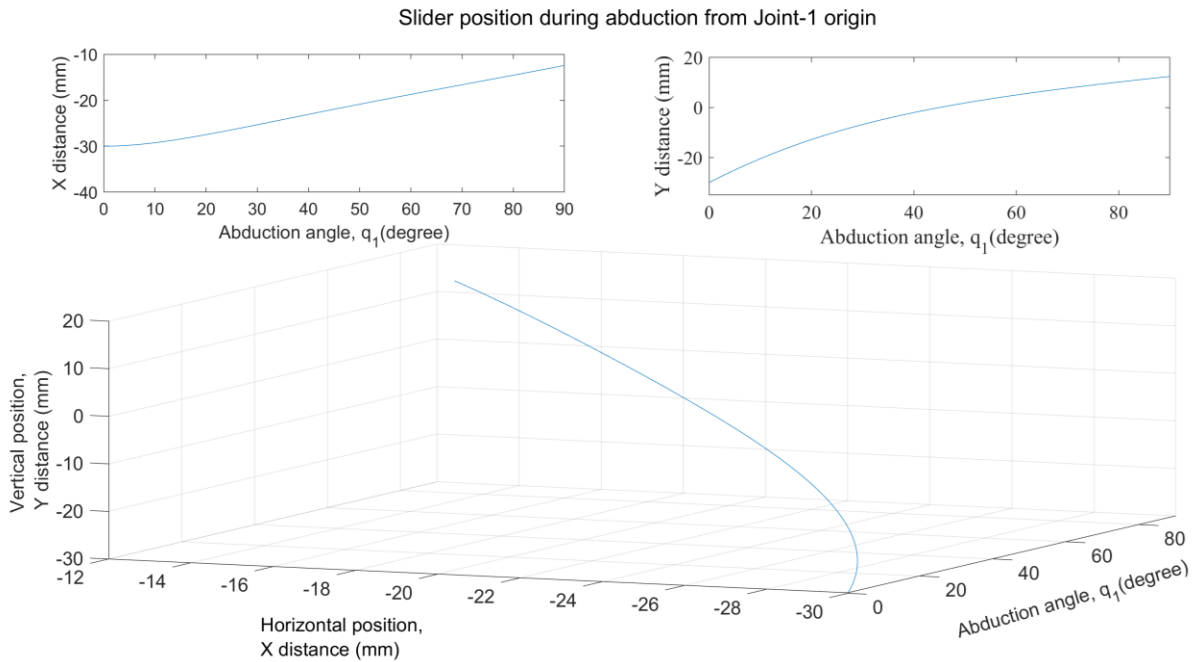
Figure 2.20 Shoulder joint instantaneous center of rotation position during abduction-adduction, measured from the joint-1 origin
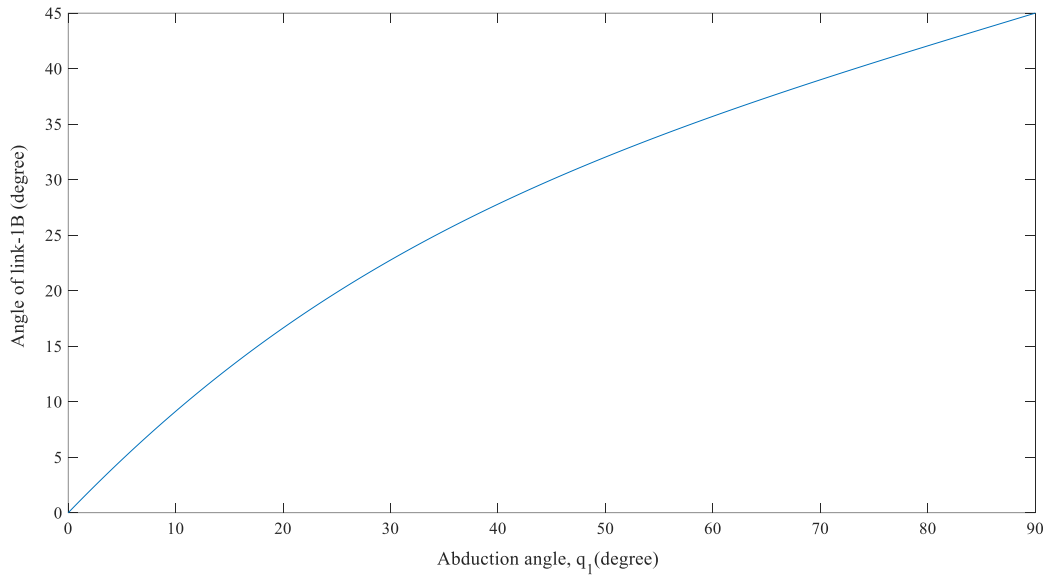
Figure 2.21 Relation between the angle of link-1B and abduction angle

2.6.2 Sagittal mechanism:
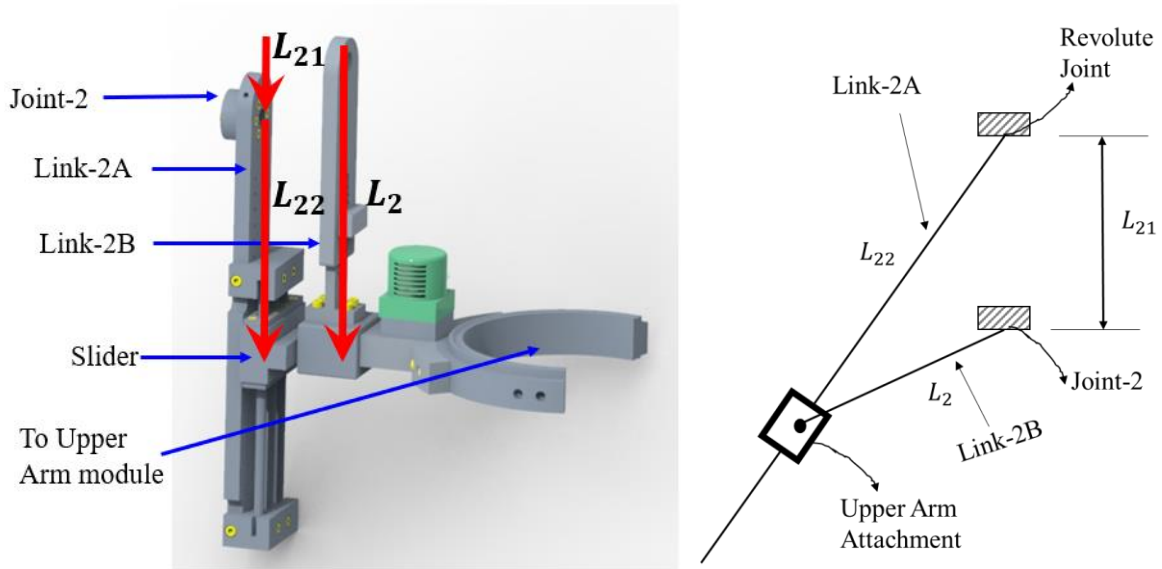
Figure 2.22 Schematic of link-slider mechanism for joint-2 (Sagittal mechanism)

This mechanism compensates relative movement caused by shoulder protraction-retraction between the human shoulder and the proposed exoskeleton robot during vertical flexion-extension. It consists of a free end link (link-2A), both end hinged links (link-2B), and a slider, as shown in

83

Figure 2.22. The proximal end of link-2A is connected to the actuator's shaft of joint-2, thereby gets through the same rotation as joint-2 does. The distal end of link-2A remains free. The slider, which can translate along the longitudinal axis of link-2A depending on the rotation of joint-2, is placed on link-2A. The slider is also connected to link-2B as well as the upper arm module through a custom-made coupler to maintain the proposed exoskeleton robot's serial chain for its rest of the part. The proximal end of link-2B is connected to a rigid plate by a hinge joint, whereas the distal is connected to the slider and upper arm motion support part. The link-2B has been designed with two individual links that have rack and slot. This rack and slot in link-2B allow it to accommodate different wearer sizes to the proposed exoskeleton robot by varying its length to a suitable position. Anyway, since link-2A and link-2B is hinged at different locations, the slider translates along the link-2A with the rotation of joint-2. This translation compensates the shoulder protraction/retraction by allowing relative movement between the proposed exoskeleton robot and its wearer. The sagittal and frontal mechanism is similar; therefore, presenting validation of it is redundant.

2.6.3 Fabrication of frontal mechanism:

Figure 2.23 shows the parts used in the fabrication of the frontal mechanism and its exploded view. All the parts except standard elements (e.g., bearings, bushing, stainless steel shaft) are machined out of aluminum 6061. To provide linear motion, three standard (LM8LUU Linear bushing) sliders (part 3) and three 8mm stainless steel shaft (part 2) were used, as shown in Figure 2.23. Note that, three sets of sliders were used to prevent rotation of the slider around the axis of the shaft. The shafts have made fit into the slider bore, whereas sliders have been inserted into the bores of slider retainers (part 8). To prevent horizontal translations of slider itself, two preregular plates (part 4)

have been fastened by M4 screws (part 5) at both ends of the slider retainer (part 8). Note that, slider retainer also connects the joint2 assembly. To hold the shaft, two block parts (part 11) with appropriate groove and slot have been fabricated. These blocks have been mounted on the plate (part 9) attached joint-1. The link-1A (part 1) that contains two standard ball bearing (6200Z 10mm x 30mm x 9mm double Sealed Ball Bearing). These bearings are pressed fit and provide bearing support at two M10 screws. The left end of the link-1A (part 1) has connected shoulder joint CR on part 8 and hinged at the right end.
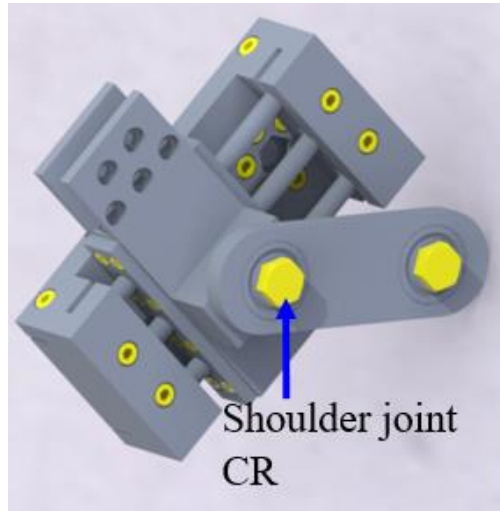
Parts:

1	Link-1A
2	Link-1B
3	Slider
4	Slider stoppers
5	$M3 \times 0.5$ screw
6	$10 \times 30 \times 9$ mm Ball Bearing
7	$M10 \times 1.5$ screw
8	Slider retainers
9	Joint-1 plate
10	$M5 \times 0.8$ screw
11	Link-1B retainers
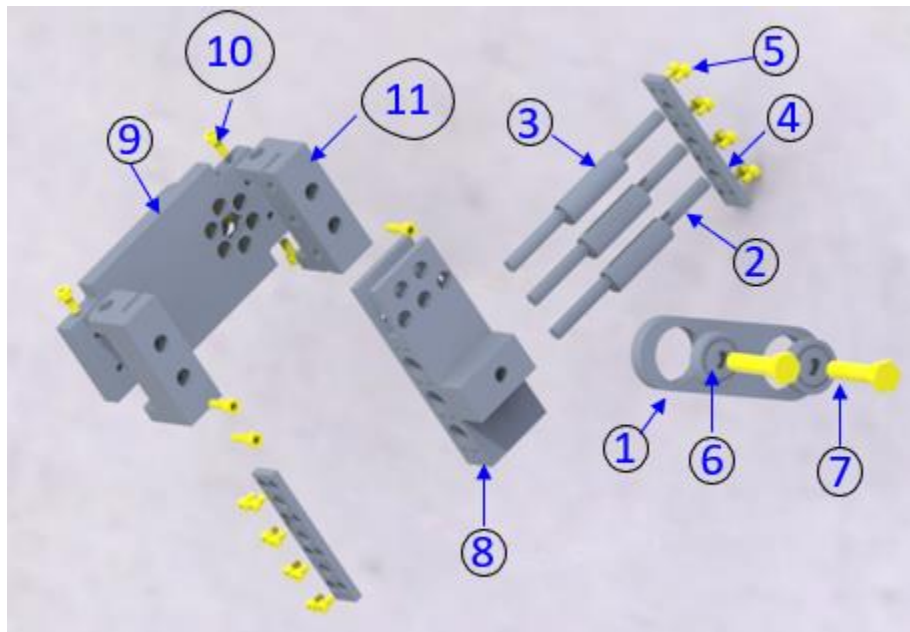
Figure 2.23 Exploded view of the frontal mechanism

2.6.4 Fabrication of sagittal mechanism:

Figure 2.24 shows an exploded view of the parts used in the sagittal mechanism. All the parts except standard elements (e.g., bearings, bushing, stainless steel shafts) are machined out of aluminum 6061. To provide linear motion along the shaft axis, three standard (LM8LUU Linear bushing) sliders (part 3) and three 8mm stainless steel shaft (part 6) have been used as shown in

Figure 2.24. The purpose of using three sliders is to prevent rotation of the slider retainer about the shaft axis. The link-2A (part 1) houses the shaft retainer (part 8). The sliders (part 3) have been inserted into the slider retainer (part 7) that eventually provides the linear motion along the shaft axis. In order to make a connection between link-2B (part 2), slider retainer (part 7), and upper arm module, a 3D printed part (part 9) has been used. The adjustability of link 2B can be done by an aluminum machine part (part 11) that can be placed at the desired slot.

Parts:

1	Link-2A
2	Link-2B
3	Slider
4	Slider stopper
5	$M3 \times 0.5$ screw
6	SS shaft
7	Slider retainer
8	Shaft stopper
9	Connector for 8 and Link 2B
10	$M6 \times 1$ screw
11	Adjustable connector
12	To Upper Arm Module
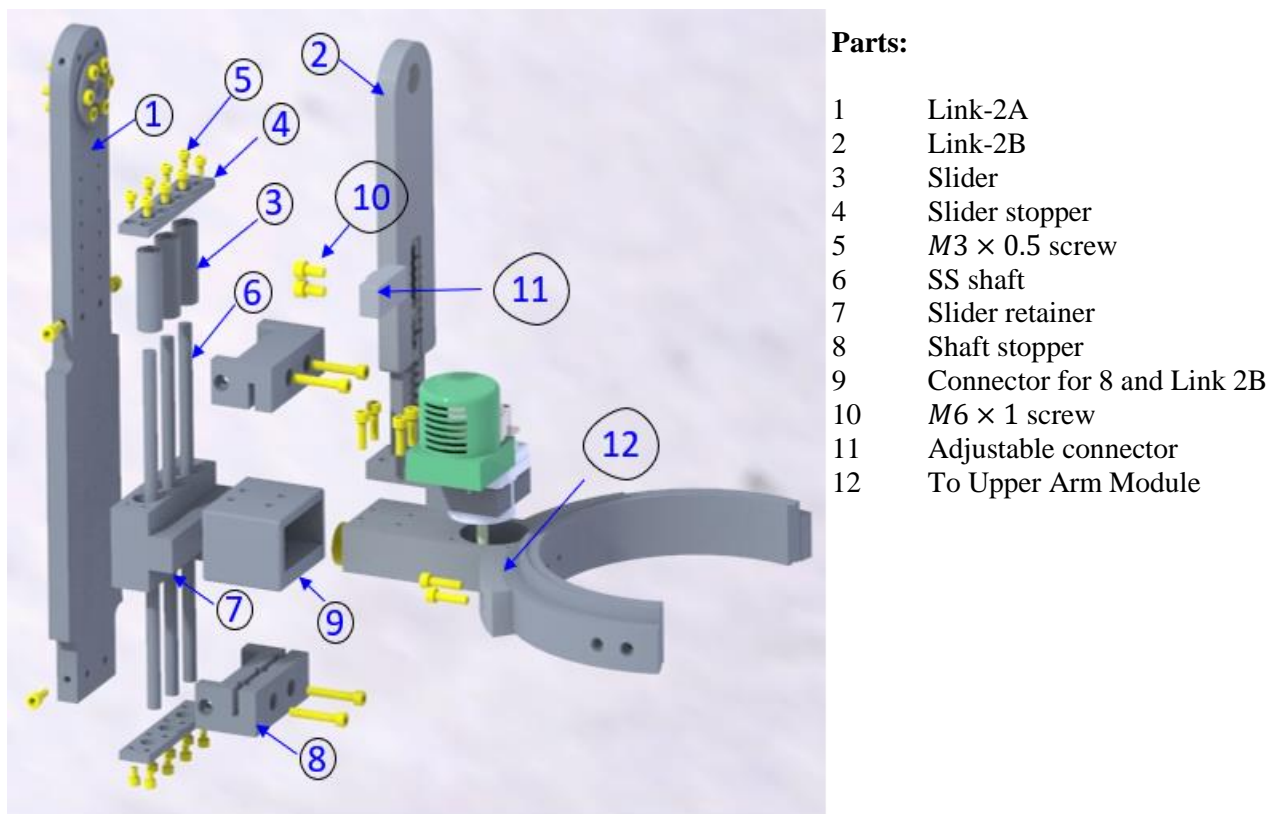
Figure 2.24 Exploded view of the sagittal mechanism

2.6.5 Sensored upper arm cuff

Figure 2.25 shows the sensored cuff assembly for the upper arm. In order to have a rotation in the upper arm, as shown in Figure 2.25, the outer cuff remains stationary where the inner cuff rotates. The reduction of actuator-3 speed was made in two stages. First, motor speed was reduced

using harmonic reducer (CSF-11-100-2XH-F, Harmonic Drive LLC, US Headquarter, Dunham Ridge, MA). After that, speed is further reduced using a standard anti-backlash spur gear. Finally, the motion has been transmitted to the semi-circular ring (spur). This gear is fastened to the inner cuff. Thus, the inner cuff has obtained the rotation to realize upper arm internal-external movement.
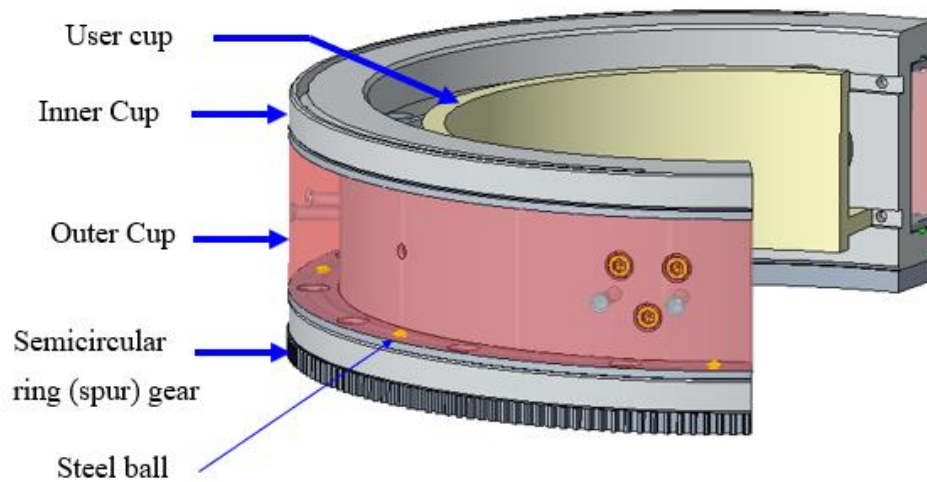
Figure 2.25 Upper arm sensored cuff assembly.

Parts:

1	Inner Cup
2	Force Sensors
3	$M3 \times 0.5$ screw
4	Semi-circular ring gear
5	3D Printed cup
6	$M3 \times 0.5$ counter sunk screw
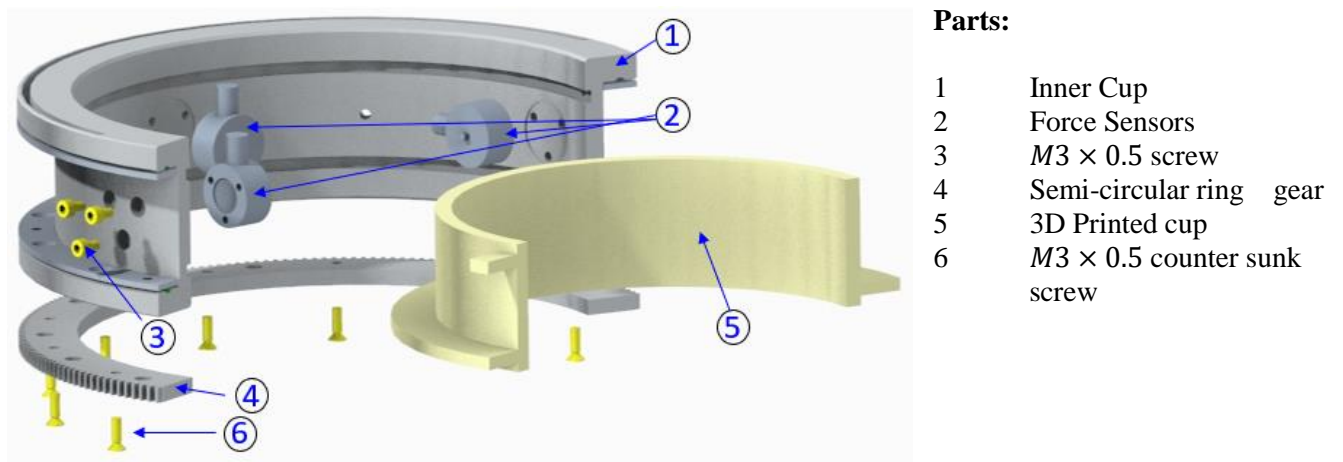
Figure 2.26 Exploded view of upper arm sensored cuff assembly

To measure the upper arm force, three button-type force sensors (part 2) have been mounted on the inner cuff (part 1), as shown in Figure 2.26. The sensors have been fastened by three M3 screws (part 3) that were spaced at 120°. The user cuff (part 5) has been placed inside the rectangular groove of the inner cuff (part 1). Two ball plungers mounted on the inner cuff (part 1) maintain the initial tension of the user cuff on the force sensors. To get the upper arm rotation, the inner cuff has housed custom-made a semi-circular spur gear (part 4). This gear has meshed with anti-backlash spur gear (Model LFS-D6-80, Nordex, Inc, Brookfield, CT) that transfers output motion from the joint-3 actuator. The bearing action between the inner cuff and outer cuff (coming from joint-2) is provided by a bearing sleeve. The bearing action in the sleeve is achieved by steel balls, which are placed inside the circular guide. Thus, bearing action is provided during the relative movement of the inner and outer cuff.

The inner cuff has been machined in both lathe and computer numerical control (CNC) mill; aluminum 6061 hollow round bar has been used in the fabrication. The user cuff has been 3d printed, hence can be easily made for different size of the user. The semi-circular spur gear has been machined out of stainless steel.

2.6.6   Design of semi-circular ring (spur gear) for upper arm cuff assembly:

Since, the human upper arm is rotated about the axis of the arm. Hence, there is no direct way to put an actuator on this axis to realize upper arm internal-external rotation. Spur gears are used to transfer motion between two parallel shafts. Therefore, in the proposed exoskeleton robot, we have placed the joint-3 actuator at an offset from the upper arm axis. Then, using a standard anti-backlash gear and a custom-designed spur gear, upper arm internal-external rotation is provided. The design of the spur gear here is crucial to provide the desired reduction. In the design

of the gear, we followed AGMA recommendations and Shigley's mechanical engineering design (Budynas. and Nisbett, 2015).

- The actuator-3 is going to be reduced to a nominal speed of 48.6 rpm with the help of a harmonic reducer (CSF-11-100-2XH-F) from Harmonic Drive LLC.
- The outside diameter of the inner cuff is 195 mm [7.6771 inch].

Gear 1 is the larger gear (semicircular gear, Driven), having outside dia equal to the outside diameter of the inner cuff.

$$P_{d1} = 7.6141$$

Diametral Pitch $DP = 32$ (**Chosen**)

$$n_1 = 34 \, rpm \, (200 \, deg/sec)$$

In the mesh, Gear 2 is the Anti-Backlash spur (Input gear, Driver).

$$P_{d2} = 2.5$$

$$T_2 = 80$$

Diametral Pitch $DP = 32$

Pressure Angle $20°$

The relation between two gears in terms of Pitch diameter and speed,

$$\frac{P_{d1}}{P_{d2}} = \frac{n_2}{n_1}$$

$$\Rightarrow n_2 = \left(\frac{P_{d1}}{P_{d2}}\right) n_1$$

$$\Rightarrow n_2 = \left(\frac{7.6141}{2.5}\right) 34 = 103.55 \approx 104 \, rpm$$

The relation between two gears in terms of Pitch diameter and number of teeth,

$$\frac{P_{d1}}{P_{d2}} = \frac{T_1}{T_2}$$

$$=> T_1 = \left(\frac{P_{d1}}{P_{d2}}\right) T_2$$

$$=> \boldsymbol{T_1} = \left(\frac{7.6141}{2.5}\right) 80 = 243.6512 \approx \boldsymbol{244}$$

Alternatively, $T_1 = DP \times P_{d1} = 32 \times 7.6141 = 243.6512 \approx \boldsymbol{244}$

Velocity ratio:

$$m_w = \frac{T_1}{T_2} = \frac{244}{80} = 3.05$$

Based on the above design, the specification of both gears are summarized in the table below.

Specification	Semi-circular spur gear	Anti-Backlash spur gear
Pressure angle	20°	20°
Diametral Pitch	32	32
Pitch diameter	7.61 in [193.4 mm]	2.5 in [25.4 mm]
No of teeth	244	80
Speed	34 rpm (200 deg/sec)	104 rpm
Outside Diameter	7.68 in [195 mm]	2.563 in [27 mm]
Bore	6.32 in [160.6 mm]	1/4 in [6.35 mm]

Note that gears were assumed as rigid; therefore, strength analysis was not presented.

2.7 Elbow and forearm motion support part:

The elbow & forearm motion support part is responsible for realizing flexion-extension at the elbow and pronation-supination at the forearm. The elbow flexion-extension is achieved through actuator-4 assembly, which consists of motor, harmonic reducer, output adapter. The

output of the actuator-4 assembly is fastened to the forearm link, as shown in Figure 2.27. The

forearm link houses the forearm cuff assembly, which is discussed in the next sub-section.
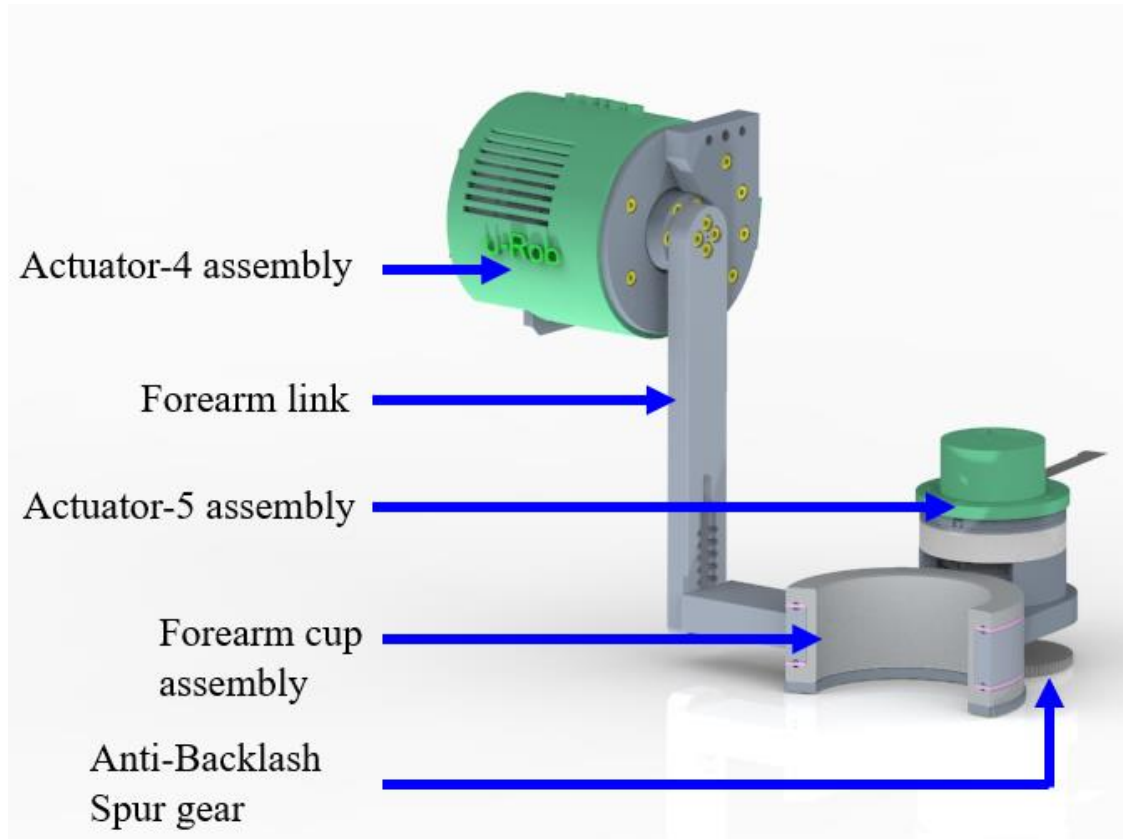
Figure 2.27 Elbow and forearm motion support part

Parts:
1 Outer Cup
2 Inner Cup
3 Sleeve
4,7 $M3 \times 0.5$ screw
5 Ball
6 Semi-circular ring gear
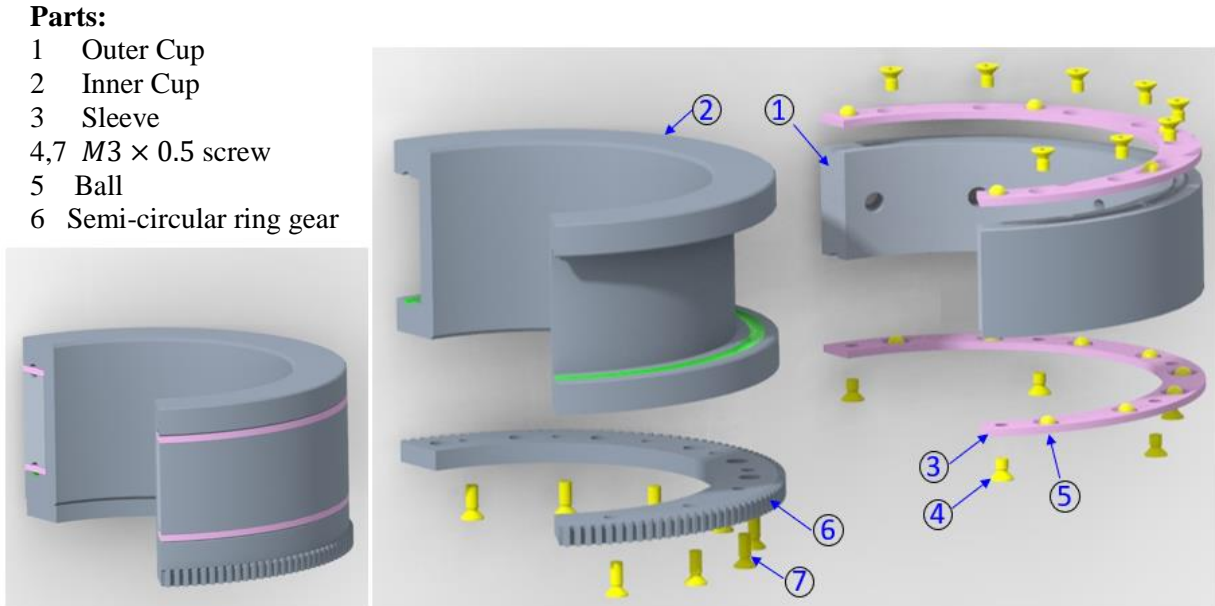
Figure 2.28 Forearm cuff assembly and its exploded view

2.7.1 Forearm cuff assembly

Figure 2.28 shows the forearm cuff assembly and its exploded view. As shown in Figure

2.28, the design of the forearm cuff consists of an outer cuff (stationary; part 1), inner cuff (rotary;

part 2), sleeve, balls, a custom made semicircular ring (spur) gear (part 6). The outer cuff is

connected to the forearm link and realizes motion from the elbow joint (joint-4). Inner cuff realizes

motion for pronation-supination by the motion of actuator-5. Therefore, bearing motion should be

provided between the inner cuff and outer cuff. This bearing action has been achieved by making

a sleeve that houses steel balls. During pronation-supination, these balls travel along the circular

groove on the outer and inner cuff. Sleeves have been fastened to the outer cuff by counter-sunk

flat-headed $M3 \times 0.5$ screws (part 4). To get the motion from actuator-5, a semicircular ring gear

(part 6) has been fastened to the bottom of the inner cuff by counter-sunk flat-headed $M3 \times 0.5$

93

screws (part 7) This ring gear has been meshed to the anti-backlash spur gear, which has been attached to the output shaft of actuator-5.

2.7.2 Design of semi-circular ring (spur gear) for forearm cuff assembly:

Since the axis of rotation of the human forearm is located along the forearm. Hence, there is no direct way to put an actuator on this axis to realize forearm pronation-supination. Spur gears are used to transfer motion between two parallel shafts. Therefore, in the proposed exoskeleton robot, we have placed the joint-5 actuator at an offset from the forearm axis. Then, using a standard anti-backlash gear and a custom-designed open type spur gear, forearm pronation-supination is provided. The design of the spur gear (e.g., number of teeth) here is crucial to provide the desired reduction. In the design of the gear, we followed AGMA recommendations and Shigley's mechanical engineering design (Budynas. and Nisbett, 2015).

- The actuator-5 is going to be reduced to a nominal speed 34 rpm with the help of a harmonic reducer (LHSG-14-C-I) from Leaderdrive, Suzhou, China.
- Outside diameter of the inner cuff is 115 mm [4.53 inch].

Gear 1 is the larger gear (ring gear), having an outside dia equal to the outer cuff.

$$P_{d1} = 4.4646 \ inch \ [113.4 \ mm]$$

$$n_1 = 34 \ rpm \ (200 \ deg/sec)$$

Gear 2 is the smaller gear (Input gear, Driver).

$$P_{d2} = 2.5 \ inch \ [63.5 \ mm]$$

$$T_2 = 80$$

Diametral Pitch $DP = 32$

Pressure Angle $20°$

The relation between two gears in terms of Pitch diameter and speed,

$$\frac{P_{d1}}{P_{d2}} = \frac{n_2}{n_1}$$

$$=> \; n_2 = \left(\frac{P_{d1}}{P_{d2}}\right) n_1$$

$$=> \; \boldsymbol{n_2} = \left(\frac{4.4646}{2.5}\right) 34 = 60.718 \approx \boldsymbol{61 \; rpm}$$

The relation between two gears in terms of Pitch diameter and number of teeth,

$$\frac{P_{d1}}{P_{d2}} = \frac{T_1}{T_2}$$

$$=> \; T_1 = \left(\frac{P_{d1}}{P_{d2}}\right) T_2$$

$$=> \; \boldsymbol{T_1} = \left(\frac{4.4646}{2.5}\right) 80 = 142.86 \approx \boldsymbol{143}$$

Alternatively, $T_1 = DP \times P_{d1} = 32 \times 4.4646 = 142.86 \approx \boldsymbol{143}$

Velocity ratio:

$$m_w = \frac{T_1}{T_2} = \frac{143}{80} = 1.79$$

Based on the above design, the specification of both gears are summarized below.

Specification	Semi-circular spur gear	Anti-Backlash spur gear
Pressure angle	20°	20°
Diametral Pitch	32	32
Pitch diameter	4.46 in [113.4 mm]	2.5 in [25.4 mm]
No of teeth	143	80
Speed	34 rpm (200 deg/sec)	104 rpm
Outside Diameter	4.53 in [115 mm]	2.563 in [27 mm]
Bore	3.35 in [85 mm]	1/4 in [6.35 mm]

Note that, gears were assumed as rigid, therefore, strength analysis was not presented.

2.7.3 Fabrication of forearm motion support part:

In the fabrication of the forearm motion support part, aluminum (aluminum 6061) was used for the forearm link, outer cuff, and inner cuff. Both lathe and CNC milling were used in the fabrication. The machining operations included facing, 2D adaptive clearing, contouring, groove cutting, turning, drilling, and chamfering. The custom-made semi-circular ring (spur) gear has been fabricated out of stainless steel (stainless steel 304). The sleeves in the forearm cuff assembly were 3D printed using 1.75mm PLA filament. The balls used in the forearm cuff assembly are standard 4mm stainless steel balls.

2.8 Wrist motion support part:
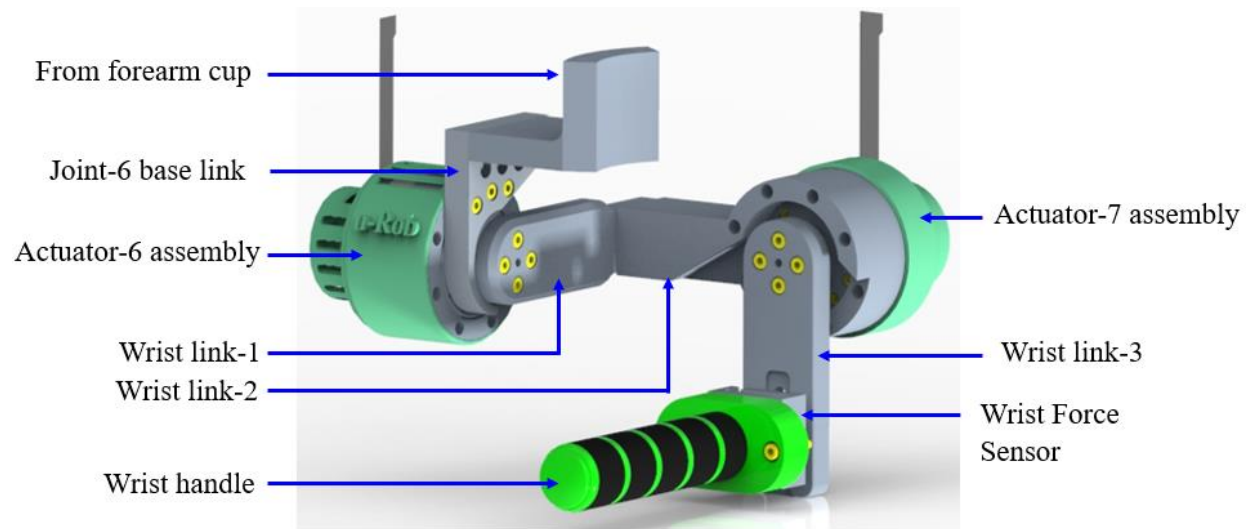
Figure 2.29 wrist motion support part of the proposed exoskeleton robot

The wrist motion support part of the proposed exoskeleton robot consists of two revolute joints to provide wrist radial-ulnar deviation and flexion-extension. Moreover, a force sensor has been placed at the wrist handle to sense three cartesian forces exerted by the user. As shown in Figure 2.29, the actuator assembly for joint-6 was mounted on the joint-6 base link; the base link was rigidly connected to the output of the forearm cuff. The output of actuator-6 is then fastened to one of the wrist link-1. Note that the base link was designed so that it acts as a physical stopper for wrist link-1. The other end of wrist link-1 is rigidly fastened to wrist link-2, which housed the actuator assembly for joint-7. The output of actuator-7 is connected to wrist link-3 with a force sensor in between.

2.8.1 Integration of the wrist force sensor
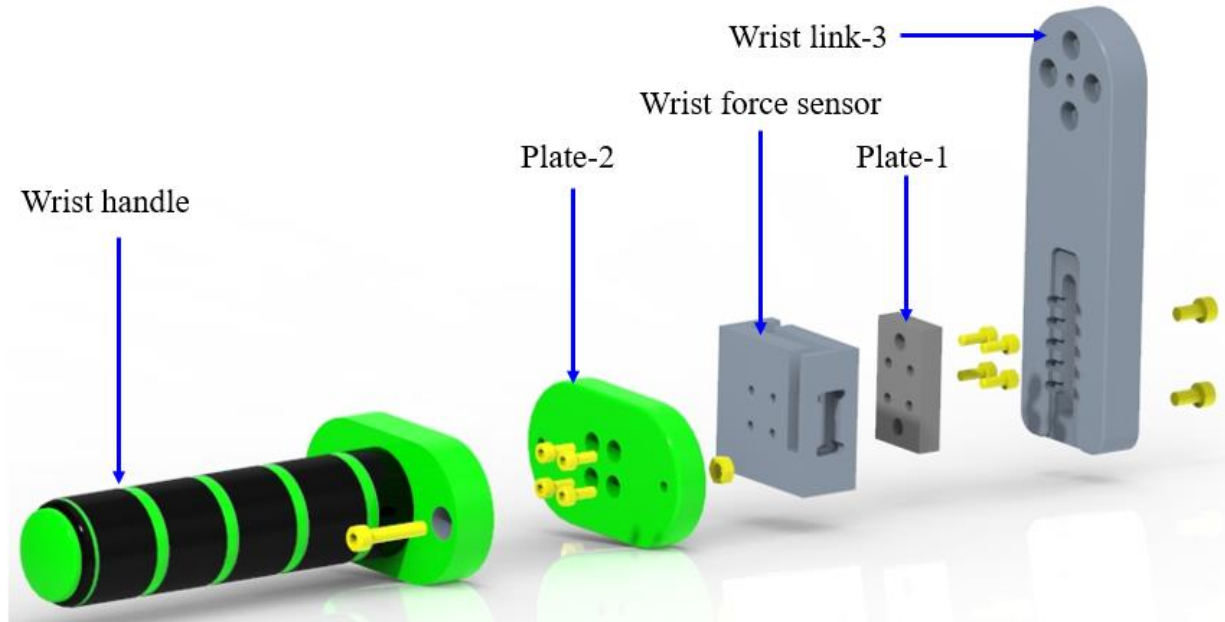
Figure 2.30 Exploded view of the integration of the wrist force sensor in the proposed exoskeleton robot

To integrate the wrist force sensor, first, plate-1, as shown in Figure 2.30, has been mounted on wrist link-3 by two M6 screws. Then, the force sensor has been sandwiched between plate-1 and plate-2. After that, the wrist handle has been fastened to plate-2. Thus, force applied by the user at the wrist handle is transmitted to the sensor.

2.8.2 Fabrication of wrist motion support part:

In the fabrication of the wrist motion support part, aluminum was used for the fabrication of joint-6 base link, wrist link-1, wrist link-2, wrist link-3, and plate-1. Computer-Aided Manufacturing (CAM) of these parts has been designed in AutoCAD Fusion 360 and machined in CNC. The operations done in milling included facing, 2D adaptive clearing, contouring, drilling, and chamfering. The wrist handle and plate-2 have been 3D printed.

2.9 Mass and inertia properties of the proposed exoskeleton robot:

The mass and mass-moment of inertia about the center of gravity (CG) for the segments of the proposed exoskeleton robot were determined in the CAD environment in PTC Creo. Mass properties were also validated by checking the mass of the real parts of the proposed exoskeleton robot. The segment has been determined according to the movement. For instance, the first segment is every element situated after joint-1 actuator output and before joint-2 actuator output. Details CAD diagram and properties are also included in the **ANNEX IX-XV.**

Table 8: Mass inertia properties of the proposed exoskeleton system

Segment	Segment length (mm)	Segment weight (kg)	Centre of gravity CG (mm)			Moment of Inertia I at CG (kg.mm²) (10^3)		
			CG_X	CG_Y	CG_Z	Ixx	Iyy	Izz
Segment-1 (joint-1 to joint-2)	231.4	4.93	-6.65	-221.5	-63.6	118.5	31.5	94.4
Segment-2 (joint-2 to joint-3)	183.5 ± 50	1.12	-8.95	-10.95	17.3	47.2	25.7	24.3
Segment-3 (joint-3 to joint-4)	82.04	3.35	-10.9	13.87	-27.7	40.06	14.09	32.94
Segment-4 (joint-4 to joint-5)	163.5 ± 40	1.24	-57.6	-142.3	40.6	4.27	4.64	3.74
Segment-5 (joint-5 to joint-6)	132.775	1.34	-18.2	83.2	-48.6	9.45	5.12	7.68
Segment-6 (joint-6 to joint-7)	92.76	1.08	-0.55	-92.26	33.8	4.54	2.93	2.24
Segment-7 (joint-7 to wrist handle)	47	0.22	23.8	0.00	-80.9	0.00683	0.036	0.037

2.10 Electrical and electronic design, and instrumentation

The electrical and electronic configuration for the proposed exoskeleton robot robotic rehabilitative system is depicted in Figure 2.31. Basically, a Host PC a PXI Real-Time Target are the main elements of the electrical & electronic configuration of the proposed exoskeleton robot. The Real-Time target consists of a NI PXIe-8135 real-time controller (Industrial PC) with two PXI

Reconfigurable IO (i.e., PXIe 6738 and PXIe 6254) cards with an embedded FPGA housed in a

PXIe-1078 chassis, a mainboard, seven motor driver cards, and actuators.
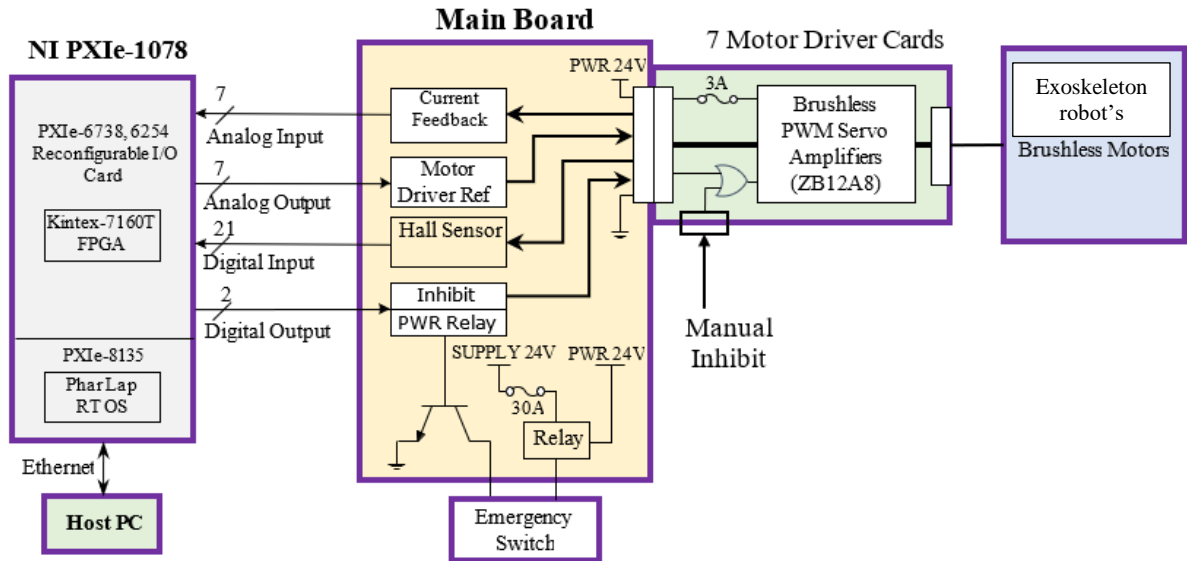
Figure 2.31 Electrical and electronic configuration of the proposed exoskeleton robot

2.10.1 PXI real-time target

The PXI Real-Time Target consists of a National Instruments PXIe-8135 Real-Time

Controller and two PXIe-76738, 6254 Reconfigurable IO cards housed in a PXIe-1078 chassis.

The standard I/O module runs Phar Lap real-time OS provided by National Instruments and

executes the real-time portions of the LabVIEW code. It is connected to the back panel of the

PXIe-1078 Chassis through National Instrument's PXI Express. The module communicates with

the Host PC via one of the two Gigabit Ethernet connectors. The PXIe-6738 and PXIe-6254

reconfigurable IO Device with 8 Analog Inputs (±10V 16bit SAR ADCs), 8 Analog Outputs (±10V

16bit ER2R DACs), and 48 Digital I/O (3.3v LVTTL/LVCMOS Compatible) pins arranged across

two connectors. The PXIe-6738 includes a Kinetix-7 FPGA processor that executes at a default

clock speed of 40MHz and communicates with the RT OS by DMA through the PXI Express bus. The FPGA unit reads and keeps track of joint positions by reading hall sensor pulses through digital inputs in a 100µs cycle. It also reads the current feedback from the motor drivers through analog inputs, applies a second-order filter before passing it to the controller running in RT OS. And finally, it gets the current signal from the controller in RT OS and executes a PI controller running at 50 µs frequency before outputting it through analog output pins.

Table 9: Specification of PXIe 8135 Controller and I/O module

Specification of PXIe 8135 Controller	
Processor	Intel Core i7-3610QE processor
Clock speed	3.3 GHz
RAM	4GB dual-channel DDR3
Specification of I/O module	
Display Port	2
RS-232 Port	1
USB 2 Port	4
USB 3 Port	2
Connectors	Two Gigabit ethernet
Controller	a PCI-based GPIB controller

2.10.2 Mainboard

In the proposed exoskeleton robot's electronic configuration, the mainboard, as shown in Figure 2.31, portrays the role of a connection hub for all motor drivers and control units and is powered by a 24V 42A switch mode DC power supply. The analog and digital signals of the proposed exoskeleton robot motors, relays, and power switch are routed either from or to the

motherboard. To give an example, it routes the hall sensor pulses to digital inputs of PXIe-6378

For instance, it routes the current feedback of the motor drivers to the PXIe-6378 I/O. The board, as shown, was designed to have slots for seven motor driver cards. Note that as a safety feature, an emergency stop switch was installed with the board to cut off the power in case of an emergency. In addition, a 30A quick blow fuse was also used to protect the whole system from short circuits.

2.10.3 Motor driver cards

Several identical slide-in cards carrying motor driver units are used for each motor in the proposed exoskeleton robot rehabilitative system. Zilvertron-ZB12A8 type PWM servo amplifiers, industrial standard units for driving brushless DC motors at high switching frequency (33 kHz) (spec: reference voltage: ± 15 VDC; analog output: ± 10 VDC; maximum continuous current: ± 6 A) are used in proposed exoskeleton robot. Each motor driver has 3A slow blow fuses installed for extended safety. The cards contain circuitry to connect the motor driver's current reference and feedback signals to the PXI Real-Time Target as well as motor phases and hall sensor feedback signals to the motor through the motherboard. The cards also include circuitry to enable the motor driver unit's inhibit state depending on individual physical switches or inhibit signal from the motherboard.

2.10.4 The host PC

The host PC, as depicted in the schematic (Figure 2.31), is used for user interface purposes. Ethernet was used for the connection between the host PC and the PXI Real-Time Target. The host PC runs a non-real-time portion of the LabVIEW code and communicates to the Real-Time Target partially via Network Published Variables and via File Transfer Protocol (FTP). The FTP was

mainly used to save the data of the experiment conducted. Note that, host PC is also connected to the augmented feedback PC (Game PC) via network switch; the game PC provides the environment to the user's performance during exercises. The host PC has a Graphical User Interface. One can command set the proposed exoskeleton robot's home position and initial position, activate and deactivate the joint motor. It also let's operator select a control from the available control approach, trajectory, type of rehab (i.e., passive or active), send data for augmented feedback, etc. The input via the user interface in the Host PC is sent to the PXI Real-Time Target, and after completion of each trajectory run, the data recorded in the PXI Real-Time Target is sent back to the Host PC via FTP for storage.

CHAPTER-3   KINEMATICS AND DYNAMICS

Section-1 of this chapter describes the kinematics of the proposed exoskeleton robot. The inverse kinematics and singularity analysis of the proposed exoskeleton robot is discussed in Section 2 and Section 3, respectively. Section-4 describes the dynamics, whereas Section-5 describes the Jacobian of the proposed exoskeleton robot.

3.1   Kinematics

The kinematic parameters (position, velocity, and acceleration) of robotic manipulators can be determined by analytical or geometric approaches. The analytical approach involves the vector formation of kinematic parameters and their vector operation, leading to obtain the kinematic model. However, in the case of a serial manipulator, robotic researchers have extensively been interested in using modified Denavit-Hartenberg parameters (Denavit and Hartenberg, 1955) due to their simplicity and ease to use in applications (e.g., developing forward kinematics, inverse kinematics, Jacobians, dynamic model, etc.). Since the *proposed exoskeleton robot* is composed of both serial linkage and parallel mechanisms, combined approach was applied to find the kinematics. The analytical approach was used to find the kinematics of parallel mechanisms discussed in sub-section 2.6.1 and 2.6.2 (i.e., frontal and sagittal mechanism). For the serial link parts of the proposed exoskeleton robot, the modified Denavit-Hartenberg convention was applied to get the proposed exoskeleton robot's kinematic model. Note that the kinematic model of the proposed exoskeleton robot has been developed on the basis of anatomy and biomechanics of the human upper limb.

3.1.1 Kinematics of frontal mechanism:
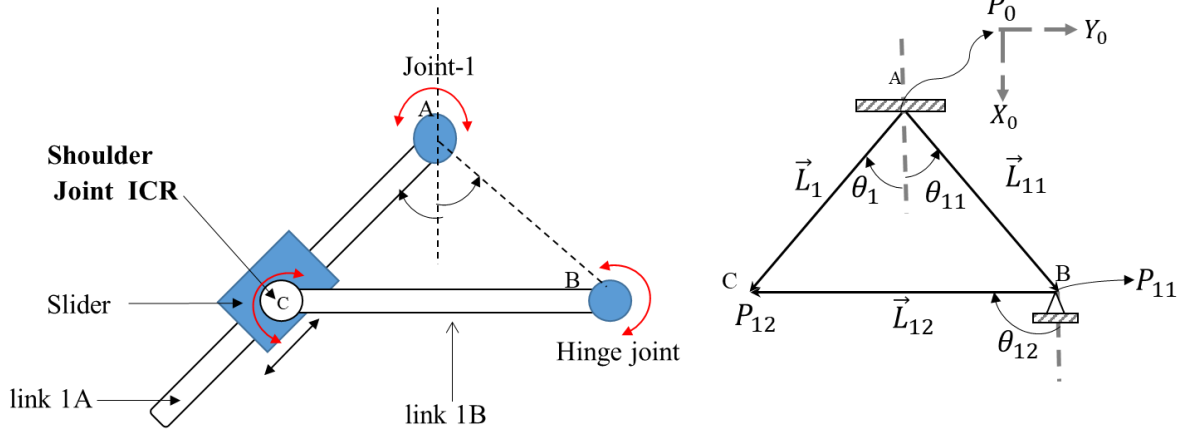
Figure 3.1 Vector formation of links in the frontal mechanism

To obtain the forward kinematics of the frontal mechanism (see Figure 3.1), the following vectors, namely $\vec{L}_1$, $\vec{L}_{11}$ and $\vec{L}_{12}$ were formed, as shown in Figure 3.1. Using these vectors, the following closed-loop equation (Eq 3.1) was formed.

$$\vec{L}_1 = \vec{L}_{11} + \vec{L}_{12}$$

$$\begin{bmatrix} L_1 \cos\theta_1 \\ L_1 \sin\theta_1 \end{bmatrix} = \begin{bmatrix} L_{11} \cos\theta_{11} \\ L_{11} \sin\theta_{11} \end{bmatrix} + \begin{bmatrix} L_{12} \cos\theta_{12} \\ L_{12} \sin\theta_{12} \end{bmatrix} \tag{3.1}$$

The equation (3.1) is a function of θ_1 where L_{11}, θ_{11} and L_{12} are known values that depend on the geometry of the function. With these values, the unknowns L_1 and θ_{12} can be found.

Rearranging above equation (Eq 3.1), we obtain

$$\begin{bmatrix} L_1 \cos\theta_1 \\ L_1 \sin\theta_1 \end{bmatrix} - \begin{bmatrix} L_{11} \cos\theta_{11} \\ L_{11} \sin\theta_{11} \end{bmatrix} = \begin{bmatrix} L_{12} \cos\theta_{12} \\ L_{12} \sin\theta_{12} \end{bmatrix} \tag{3.2}$$

105

Squaring both components of the above equation (Eq 3.2) and then adding, we have

$$\Rightarrow L_1^2 \cos^2\theta_1 + L_1^2 \sin^2\theta_1 + L_{11}^2 \cos^2\theta_{11} + L_{11}^2 \sin^2\theta_{11} - 2L_1L_{11} \cos\theta_1 \cos\theta_{11}$$

$$- 2L_1L_{11} \sin\theta_1 \sin\theta_{11} = L_{12}^2 \cos^2\theta_{12} + L_{12}^2 \sin^2\theta_{12}$$

$$\Rightarrow L_1^2 + L_{11}^2 - 2L_1L_{11}(\cos\theta_1 \cos\theta_{11} + \sin\theta_1 \sin\theta_{11}) = L_{12}^2$$

$$\Rightarrow L_1^2 - 2L_1L_{11} \cos(\theta_1 - \theta_{11}) + (L_{11}^2 - L_{12}^2) = 0$$

$$\Rightarrow L_1 = \frac{2L_{11} \cos(\theta_1 - \theta_{11})}{2} \pm \frac{\sqrt{4L_{11}^2 \cos^2(\theta_1 - \theta_{11}) - 4(L_{11}^2 - L_{12}^2)}}{2}$$

$$\Rightarrow L_1 = L_{11} \cos(\theta_1 - \theta_{11}) \pm \sqrt{L_{11}^2 \cos^2(\theta_1 - \theta_{11}) - (L_{11}^2 - L_{12}^2)}$$

$$\Rightarrow L_1 = L_{11} \cos(\theta_1 - \theta_{11}) \pm \sqrt{L_{11}^2 \cos^2(\theta_1 - \theta_{11}) - L_{11}^2 + L_{12}^2}$$

$$L_1 = L_{11} \cos(\theta_1 - \theta_{11}) + \sqrt{L_{11}^2 \cos^2(\theta_1 - \theta_{11}) - L_{11}^2 + L_{12}^2} \qquad (3.3)$$

Equation (3.3) provides the location of the slider, which is the instantaneous center of the shoulder joint.

To obtain the solution for θ_{12}, Sine component of equation (3.2) is divided by the Cosine component as follows.

$$\tan\theta_{12} = \frac{L_1 \sin\theta_1 - L_{11} \sin\theta_{11}}{L_1 \cos\theta_1 - L_{11} \cos\theta_{11}}$$

$$\theta_{12} = \arctan\left(\frac{L_1 \sin\theta_1 - L_{11} \sin\theta_{11}}{L_1 \cos\theta_1 - L_{11} \cos\theta_{11}}\right) \tag{3.4}$$

Equation (3.3) and (3.4) solves forward kinematics of frontal mechanism.

3.1.2   Kinematics of sagittal mechanism:
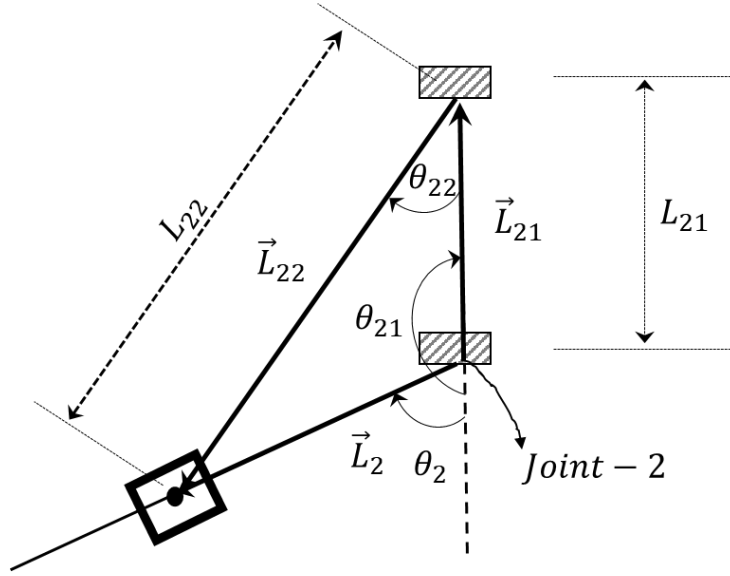
Figure 3.2 Vector formation of links in the sagittal mechanism

To obtain the forward kinematics of sagittal mechanism, the following vectors, namely $\vec{L}_2$, $\vec{L}_{21}$ and $\vec{L}_{22}$ were formed, as shown in Figure 3.2 and Figure 2.22. Using these vectors, the following closed-loop equation was formed (Eq 3.5).

$$\vec{L}_{22} = \vec{L}_2 - \vec{L}_{21}$$

$$\begin{bmatrix} L_{22} \cos\theta_{12} \\ L_{22} \sin\theta_{12} \end{bmatrix} = \begin{bmatrix} L_2 \cos\theta_2 \\ L_2 \sin\theta_2 \end{bmatrix} - \begin{bmatrix} L_{21} \cos\theta_{21} \\ L_{21} \sin\theta_{21} \end{bmatrix} \tag{3.5}$$

The equation (3.5) is a function of θ_2 where L_{21}, θ_{21} and L_{22} are known values that depend on the geometry of the function. With these values, the unknowns L_2 and θ_{22} can be found.

107

Squaring both components of the above equation (Eq 3.5) and then adding, we have

$$\Rightarrow L_{22}^2 \cos^2 \theta_{22} + L_{22}^2 \sin^2 \theta_{22}$$

$$= L_2^2 \cos^2 \theta_2 + L_2^2 \sin^2 \theta_2 + L_{21}^2 \cos^2 \theta_{21} + L_{21}^2 \sin^2 \theta_{21} - 2L_2 L_{21} \cos \theta_2 \cos \theta_{21}$$

$$- 2L_2 L_{21} \sin \theta_2 \sin \theta_{21}$$

$$\Rightarrow L_2^2 + L_{21}^2 - 2L_2 L_{21}(\cos \theta_2 \cos \theta_{21} + \sin \theta_2 \sin \theta_{21}) = L_{22}^2$$

$$\Rightarrow L_2^2 - 2L_2 L_{21} \cos(\theta_2 - \theta_{21}) + (L_{21}^2 - L_{22}^2) = 0$$

$$\Rightarrow L_2 = \frac{2L_{21} \cos(\theta_2 - \theta_{21})}{2} \pm \frac{\sqrt{4L_{21}^2 \cos^2(\theta_2 - \theta_{21}) - 4(L_{21}^2 - L_{22}^2)}}{2}$$

$$\Rightarrow L_2 = L_{21} \cos(\theta_2 - \theta_{21}) \pm \sqrt{L_{21}^2 \cos^2(\theta_2 - \theta_{21}) - (L_{21}^2 - L_{22}^2)}$$

$$\Rightarrow L_2 = L_{21} \cos(\theta_2 - \theta_{21}) + \sqrt{L_{21}^2 \cos^2(\theta_2 - \theta_{21}) - L_{21}^2 + L_{22}^2}$$

$$L_2 = L_{21} \cos(\theta_2 - \theta_{21}) + \sqrt{L_{21}^2 \cos^2(\theta_2 - \theta_{21}) - L_{21}^2 + L_{22}^2} \qquad (3.6)$$

Equation (3.6) provides the location of upper arm attachment.

To obtain the solution for θ_{22}, Sine component of equation (3.5) is divided by its Cosine component as follows.

$$\tan \theta_{22} = \frac{L_2 \sin \theta_2 - L_{21} \sin \theta_{21}}{L_2 \cos \theta_2 - L_{21} \cos \theta_{21}}$$

$$\theta_{22} = \arctan \left(\frac{L_2 \sin \theta_2 - L_{21} \sin \theta_{21}}{L_2 \cos \theta_2 - L_{21} \cos \theta_{21}} \right) \qquad (3.7)$$

Equation (3.6) and (3.7) solves forward kinematics of sagittal mechanism.

3.1.3 Coordinate frame assignment
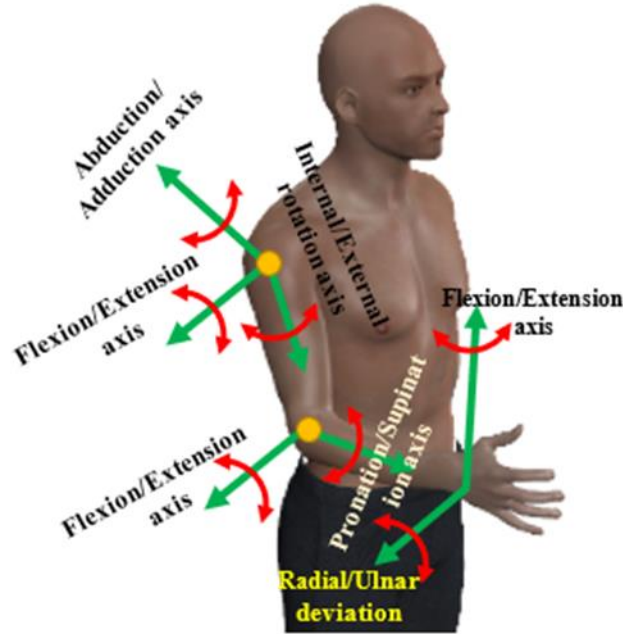
Figure 3.3 Human arm's joint axes of rotation

To assign coordinate frames, human arm's joint axes of rotation should be identified first. Figure 3.3 shows the human arm's joint axes of rotation. Frame assignment to manipulator links could be done in many ways. In the proposed exoskeleton robot, the link-frame assignment convention for modified Denavit-Hartenberg (Denavit and Hartenberg, 1955) method has been followed. Required steps of frame assignment are given as follows:

- assume each joint motion is generated from one DOF revolute joint

- determine the axes of rotation and denote each axis as $Z_0, \ldots \ldots, Z_n$

- locate the origin of each link-frame (O_i) where the common perpendicular line between the successive joint axes (i.e., Z_{i-1} and Z_i) intersects. If the joint axes are not parallel, locate the link-frame origin at the point of intersection between the axes

- locate the X_i axis (at link frame origin O_i) as pointing along the common normal line between the axes Z_{i-1} and Z_i. If the joint axes intersect, establish X_i in a direction normal to the plane containing both axes (Z_{i-1} and Z_i)

- establish the Y_i axis through the origin O_i to complete a right-hand coordinate system.
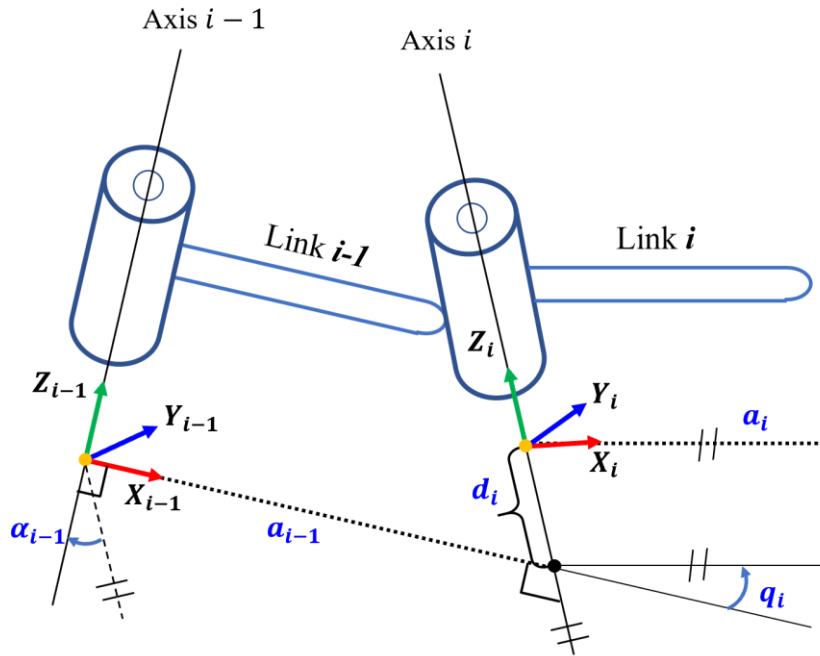
Figure 3.4 Coordinate frame assignment, adapted from (Craig, 2017)

3.1.4 DH Parameters

Any serial robotic manipulator can be described by four parameters (two parameters for describing a link and the other two for describing its relation to a neighboring link) if we assign the co-ordinate frames as described above.

To obtain the DH parameters, co-ordinate frames (i.e., the link-frames which map between the successive axes of rotation) are assumed to have coincided with the joint axes of rotation and have the same order, i.e., frame {1} coincides with joint 1, frame {2} with joint 2, and so on. Note that,

base frame {0} have been placed away back at a distance of L_0 from the shoulder, while and end-effector frame/last frame {8} is placed at an offset of L_7 from the joint-7.
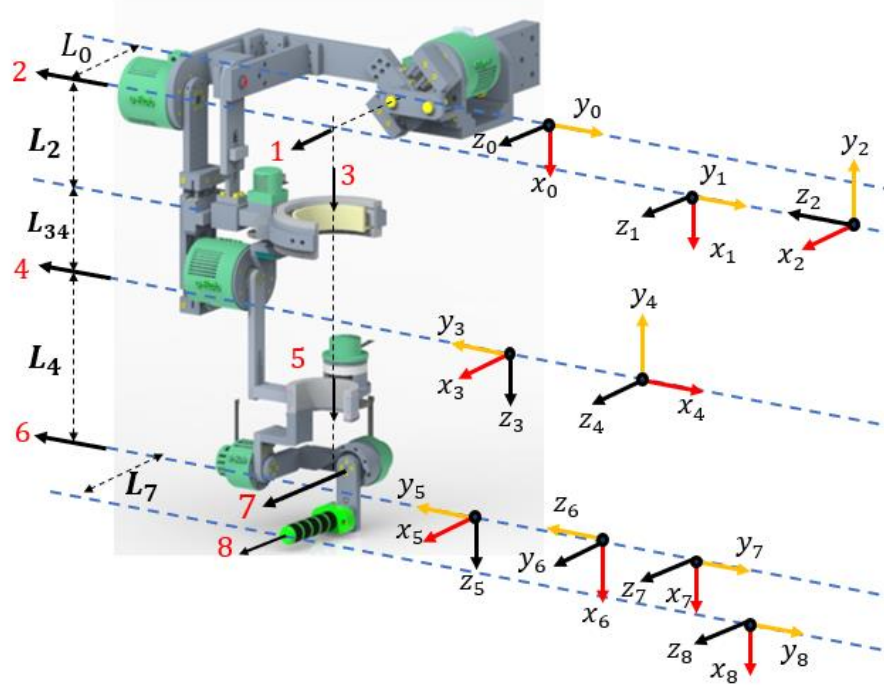
Figure 3.5 Link frame attachments to the proposed exoskeleton robot

As shown in Figure 3.5, the joint axes of rotation of the *proposed exoskeleton robot* corresponding to that of the human upper limb are indicated by black arrowheads. In this model, the shoulder joint is constituted by collectively joint-1, 2, and 3 where joint-1 represents shoulder abduction-adduction, joint-2 matches for shoulder vertical flexion-extension, and joint-3 corresponds to shoulder internal-external rotation. Note that the shoulder joint, which is the origin of joint-1, joint-2, and joint-3 is located L_0 distance away front from base and L_1 distance away from joint-1 actuator's origin. The upper arm cuff is placed at the distance of L_2. The elbow joint is located at a distance L_{34} away from upper arm cuff, eventually placing the elbow joint is located at a distance $L_2 + L_{34}$ (length of humerus) away from the shoulder joint. The joint-4 and joint-5

corresponds to the flexion-extension of the elbow pronation-supination of the forearm, respectively. As depicted in Figure 3.5, joints 6 and 7 intersect at the wrist joint, at a distance L_4 (length of radius) from the elbow joint, where joint 6 corresponds to radial-ulnar deviation, and joint 7 to flexion-extension. The last frame/end-effector frame is located at a distance of L_7 away from wrist joint. The last frame does not correspond to any joint since it is non actuated and has no joint variable.

The modified DH parameters corresponding to the placement of the link frames (as shown in Figure 3.5) are summarized in Table 10. These DH parameters have been used to obtain the homogeneous transformation matrix, which essentially represents the positions and orientations of one frame with respect to another frame. In this research, the position and orientation of the end-effector frame were obtained with respect to the fixed (base) frame.

Table 10: Modified Denavit-Hartenberg parameters for proposed exoskeleton robot

Joint (i)	α_{i-1} (Link twist)	d_i (Link offset)	a_{i-1} (Link length)	q_i (Joint variable)
1	0	0	L_0	q_1
2	$\pi/2$	0	0	$q_2 + \pi/2$
3	$\pi/2$	$L_2 + L_{34}$	0	q_3
4	$-\pi/2$	0	0	q_4
5	$\pi/2$	L_4	0	q_5
6	$-\pi/2$	0	0	$q_6 - \pi/2$
7	$-\pi/2$	0	0	q_7
8	0	0	L_7	0

Using the modified DH Parameters, homogenous transformation matrix between two successive frame $\{i\}$ and frame $\{i-1\}$ (Craig, 2017) was obtained using the following equation (Eq 3.8).

$$^{i-1}_iT = \begin{bmatrix} ^{i-1}_iR^{3\times3} & ^{i-1}_iP^{3\times1} \\ 0^{1\times3} & 1 \end{bmatrix} \tag{3.8}$$

where, $^{i-1}_iR$ is the rotation matrix that describes the frame $\{i\}$ relative to frame $\{i-1\}$ and can be expressed as:

$$^{i-1}_iR = \begin{bmatrix} \cos q_i & -\sin q_i & 0 \\ \sin q_i \cos \alpha_{i-1} & \cos q_i \cos \alpha_{i-1} & -\sin \alpha_{i-1} \\ \sin q_i \sin \alpha_{i-1} & \cos q_i \sin \alpha_{i-1} & \cos \alpha_{i-1} \end{bmatrix} \tag{3.9}$$

and, $^{i-1}_iP$ is the vector that locates the origin of the frame $\{i\}$ relative to frame $\{i-1\}$ and can be expressed as:

$$^{i-1}_iP = \begin{bmatrix} a_{i-1} \\ -s\,\alpha_{i-1}\,d_i \\ c\,\alpha_{i-1}\,d_i \end{bmatrix} \tag{3.10}$$

Because of two parallel mechanisms, homogenous transformation for frame $\{1\}$ and frame $\{2\}$ were obtained using hybrid approach (Lakhal et al., 2016). Transformation for rest frames can be obtained using the modified DH convention.

Frame $\{1\}$:

Using equation (3.8) through (3.10), the following transformation can be obtained.

$$(^0_1T)_{DH} = \begin{bmatrix} \cos q_1 & -\sin q_1 & 0 & 0 \\ \sin q_1 & \cos q_1 & 0 & 0 \\ 0 & 0 & 1 & L_0 \\ 0 & 0 & 0 & 1 \end{bmatrix}$$

113

However, as mentioned earlier, the slider in the frontal mechanism described in section 2.6.1 is placed initially at 45°. This initial placement gives the frame {1} a rotation of 45°, which caused offsets in the x and y position. So, with modified DH convention and kinematics of frontal mechanism, the homogenous transformation between frame {1} and frame {0} is obtained as follows.

$$
{}^0_1T = \begin{bmatrix} \cos\left(q_1 + \dfrac{\pi}{4}\right) & -\sin\left(q_1 + \dfrac{\pi}{4}\right) & 0 & L_1\cos\left(q_1 + \dfrac{\pi}{4}\right) \\ \sin\left(q_1 + \dfrac{\pi}{4}\right) & \cos\left(q_1 + \dfrac{\pi}{4}\right) & 0 & -L_1\sin\left(q_1 + \dfrac{\pi}{4}\right) \\ 0 & 0 & 1 & L_0 \\ 0 & 0 & 0 & 1 \end{bmatrix}
$$

Frame {2}:

Using equation (3.8) through (3.10), following transformation can be obtained.

$$
({}^1_2T)_{DH} = \begin{bmatrix} \cos\left(q_2 + \dfrac{\pi}{2}\right) & -\sin\left(q_2 + \dfrac{\pi}{2}\right) & 0 & 0 \\ 0 & 0 & -1 & 0 \\ \sin\left(q_2 + \dfrac{\pi}{2}\right) & \cos\left(q_2 + \dfrac{\pi}{2}\right) & 0 & 0 \\ 0 & 0 & 0 & 1 \end{bmatrix}
$$

Though frame {1} is rotated initially at 45°, frame {2} remains aligned with upper arm. Therefore, this initial rotation of frame {1} should be adjusted in the homogenous transformation of frame {2} by pre-multiplying following matrix.

$$
({}^1_2T)_{adjust} = \begin{bmatrix} \cos\left(2q_1 + \dfrac{\pi}{4}\right) & \sin\left(2q_1 + \dfrac{\pi}{4}\right) & 0 & 0 \\ -\sin\left(2q_1 + \dfrac{\pi}{4}\right) & \cos\left(2q_1 + \dfrac{\pi}{4}\right) & 0 & 0 \\ 0 & 0 & 1 & 0 \\ 0 & 0 & 0 & 1 \end{bmatrix}
$$

$$\tfrac{1}{2}T = (\tfrac{1}{2}T)_{DH} * (\tfrac{1}{2}T)_{adjust}$$

$$\tfrac{1}{2}T = \begin{bmatrix} \cos\left(2q_1 + \frac{\pi}{4}\right)\cos\left(q_2 + \frac{\pi}{2}\right) & -\cos\left(2q_1 + \frac{\pi}{4}\right)\sin\left(2q_1 + \frac{\pi}{4}\right) & -\sin\left(2q_1 + \frac{\pi}{4}\right) & 0 \\ -\sin\left(2q_1 + \frac{\pi}{4}\right)\cos\left(q_2 + \frac{\pi}{2}\right) & \sin\left(2q_1 + \frac{\pi}{4}\right)\sin\left(q_2 + \frac{\pi}{2}\right) & -\cos\left(2q_1 + \frac{\pi}{4}\right) & 0 \\ \sin\left(q_2 + \frac{\pi}{2}\right) & \cos\left(q_2 + \frac{\pi}{2}\right) & 0 & 0 \\ 0 & 0 & 0 & 1 \end{bmatrix}$$

The homogenous transformation matrices for the rest frames were found by applying modified DH convention as they involve only serial links. Using equation (3.8) through (3.10), the following transformation matrices were obtained.

$$\tfrac{2}{3}T = \begin{bmatrix} \cos q_3 & -\sin q_3 & 0 & 0 \\ 0 & 0 & -1 & -(L_2 + L_{34}) \\ \sin q_3 & \cos q_3 & 0 & 0 \\ 0 & 0 & 0 & 1 \end{bmatrix}$$

$$\tfrac{3}{4}T = \begin{bmatrix} \cos q_4 & -\sin q_4 & 0 & 0 \\ 0 & 0 & 1 & 0 \\ -\sin q_4 & -\cos q_4 & 0 & 0 \\ 0 & 0 & 0 & 1 \end{bmatrix}$$

$$\tfrac{4}{5}T = \begin{bmatrix} \cos q_5 & -\sin q_5 & 0 & 0 \\ 0 & 0 & -1 & -L_4 \\ \sin q_5 & \cos q_5 & 0 & 0 \\ 0 & 0 & 0 & 1 \end{bmatrix}$$

$$\tfrac{5}{6}T = \begin{bmatrix} \cos\left(q_6 - \frac{\pi}{2}\right) & -\sin\left(q_6 - \frac{\pi}{2}\right) & 0 & 0 \\ 0 & 0 & -1 & 0 \\ -\sin\left(q_6 - \frac{\pi}{2}\right) & -\cos\left(q_6 - \frac{\pi}{2}\right) & 0 & 0 \\ 0 & 0 & 0 & 1 \end{bmatrix}$$

$$\underset{7}{6}T = \begin{bmatrix} \cos q_7 & -\sin q_7 & 0 & 0 \\ 0 & 0 & -1 & 0 \\ \sin q_7 & \cos q_7 & 0 & 0 \\ 0 & 0 & 0 & 1 \end{bmatrix}$$

$$\underset{8}{7}T = \begin{bmatrix} 1 & 0 & 0 & L_7 \\ 0 & 1 & 0 & 0 \\ 0 & 0 & 1 & 0 \\ 0 & 0 & 0 & 1 \end{bmatrix}$$

The homogenous transformation matrix that represents frame {8} with respect to frame {0} can be obtained by multiplying individual transformation matrices.

$$\underset{8}{0}T = [\underset{1}{0}T \cdot \underset{2}{1}T \underset{3}{2}T \cdot \underset{4}{3}T \cdot \underset{5}{4}T \cdot \underset{6}{5}T \cdot \underset{7}{6}T \underset{8}{7}T] = \begin{bmatrix} r11 & r12 & r13 & Px \\ r21 & r22 & r23 & Py \\ r31 & r32 & r33 & Pz \\ 0 & 0 & 0 & 1 \end{bmatrix} \qquad (3.11)$$

The equation obtained from this transformation matrix is known as forward kinematics equations. With the joint variable of each joint ($q_1, q_2, q_3, q_4, q_5, q_6$ and q_7), using this forward kinematics equations, the position and orientation of frames were determined with respect to the reference (base) frame.

3.2 Inverse kinematics

There are two approaches, namely analytical and geometrical approach, to get the inverse kinematic solution. The complexity arises with the increase of degrees of freedom. Again, the inverse kinematics solution for a manipulator is computationally costly compared to direct kinematics. To find a closed-form solution is hard as non-linear equations often appear in the Cartesian positions. There is a probability of getting multiple solutions. An inverse kinematics problem for a redundant manipulator is much more complex since it gives multiple solutions. On the other hand, for a manipulator having a square Jacobian, joint velocities can be found using inverse Jacobian from the following relation (Craig, 2017):

$$\dot{q} = J^{-1}(q)v \qquad (3.12)$$

Where $J(q)$ is $n \times n$ Jacobian matrix, $\dot{q}$ is $n \times 1$ joint rate vector, and v is 6×1 Cartesian velocity vector. Therefore, inverse kinematic solutions can be obtained easily by simply integrating the joint velocities.

The *proposed 7DOF exoskeleton robot* is a redundant manipulator; therefore, it is not possible to find closed-form solutions. Moreover, its Jacobian is not square (6×1), therefore we are not able to directly use Equation (3.12) to find joint positions. As an alternative approach, the inverse kinematic solution of the *proposed exoskeleton robot* was obtained by using the pseudo-inverse of Jacobian matrix $J(q)$ (Siciliano et al., 2009). For a redundant manipulator, the Equation (3.12) can be reformulated as

$$\dot{q} = J_{pseudo-inverse}(q)v \qquad (3.13)$$

where $J_{pseudo-inverse}$ is the pseudo inverse generalized, and can be expressed as:

$$J_{pseudo-inverse} = J^{T}(q)(J(q)J^{T}(q))^{-1} \qquad (3.14)$$

3.3 Singularity analysis:

The mechanical singularity is another issue that appears in robots when two joint axes of a robot are aligned with each other. In that case, one DOF is lost, and it requires infinite torque to move the robot joint away from this position. A similar situation can be observed in our exoskeleton robot's case, when the axes of rotation of the exoskeleton's shoulder internal-external rotation and forearm pronation-supination motions are aligned with each other. Some research groups introduced elbow joint misalignment to get rid of singularity, limited to mimic the

kinematics of the human upper limb (Malosio et al., 2011). The human upper limb has a natural singularity, and it does not create trouble to move the limb from its singular position. Unlike the human upper limb, actuators in the exoskeleton require infinite torque to move its joint from the singular position. Some researchers didn't consider the issue because it is not common to encounter a singular position in providing rehabilitation exercises (Carignan et al., 2007; Perry et al., 2007). But an exoskeleton robot ideally should avoid the singularity. There are two areas where effort can be given to solve the issue. Researchers can address this issue in designing the exoskeleton's structure or in the control strategy to make the exoskeleton avoid singular configuration during operation.

The proposed exoskeleton robot will be in a singular position when it is extended; the axis of rotation (Z-axis of) joint-2, and/or joint-4, and/or joint-6 become aligned with each other ($q_2 = 0°,\ and/or\ q_4 = 0°,\ and/or\ q_6 = 90°$.). Singularity is not problematic when joint-space based control algorithms are applied to control a robot as those algorithms do not require a Jacobian matrix or inversion of a Jacobian matrix. However, singularity does matter for Cartesian based control approaches where an inverse Jacobian matrix of the robot are used for its inverse kinematics solution. Since the *proposed exoskeleton robot* is meant to be used in rehabilitation, to replicate these types of trajectories as a rehabilitative exercise, e.g., to follow a square trajectory over the surface of a table, joints 2, 4, and 6 are usually far away from the singular configuration of the *proposed exoskeleton robot* model. Note that anatomically rotation of joint-6 is limited to +20° to -25°. Moreover, as a safety measure when using Cartesian based control, a singularity could be easily avoided by limiting the position of joint-2 and joint-4 (say, $q_2, q_4 \geq 10°$).

3.4 Dynamics:

The studies of dynamics discuss the manipulator motion, and the forces/torques that cause that motion. Among the various methods found in literature, the iterative Newton-Euler formulation and the Lagrangian formulation are widely used to develop the dynamic model of a manipulator. Note that for a 6DoFs manipulator, the Newton-Euler approach is 100 times (computationally) more efficient compared to the Lagrangian approach. This has motivated us to use the iterative Newton-Euler method to formulate the dynamics of the proposed exoskeleton robot. This method involves outward iterations to compute velocities and accelerations to be used in inward iterations. Then it does inward iterations to compute forces and torques. A brief overview of this particular method is given below (Craig, 2017).

Iterative Newton-Euler Formulation:

In this approach, the manipulator's joint torque is computed iteratively using Newton's and Euler's equations. For a rigid body manipulator, Newton's and Euler's equations can be expressed as follows:

Newton's Equation:

For a force *'F'* acting on the center of a rigid body having mass *'m'*, that causes mass moving at an acceleration of $\dot{v}_c$. In such a case, Newton's equation of motion will be as follows

$$F = m\dot{v}_c \tag{3.15}$$

Euler's Equation:

For a moment, *'N'* acting on rigid body of having mass inertia tensor c_I at its center of mass, that causes the motion of a rigid body with angular velocity and acceleration, ω *and* $\dot{\omega}$ accordingly. Euler's equation will be as follows

$$N = c_I \dot{\omega} + \omega \times c_I \omega$$ (3.16)

The algorithm to compute joint torques (τ_i) as well as to derive the dynamic model of a manipulator includes the following steps:

- Outward iterations:

  Step 1: compute the link velocities (angular) and accelerations (linear and angular) iteratively from link 1 out to link *n*.

  Step 2: compute the inertial force and torque (acting at the center of mass) of each link using Newton-Euler equations.

- Inward iterations:

  Step 3: compute forces and torques of interaction and joint recursively from link *n* back to link 1. Complete derivation of Newton-Euler formulation can be found in (Craig, 2017).

The generic dynamic equation of a rigid body manipulator derived from the Newton-Euler formulation is as follows:

$$\tau = M(q)\ddot{q} + V(q, \dot{q}) + G(q)$$ (3.17)

Where $M(q)$ is the $n \times n$ mass matrix of the manipulator, $V(q, \dot{q})$ is a $n \times 1$ dimension vector composed of centrifugal and Coriolis terms, and $G(q)$ is a $n \times 1$ vector of gravity terms. Introducing friction to the model, the dynamic equation becomes:

$$\tau = M(q)\ddot{q} + V(q, \dot{q}) + G(q) + F(q, \dot{q}) \qquad (3.18)$$

where $F(q, \dot{q})$ $n \times 1$ vector of nonlinear Coulomb friction and can be expressed by the following relation.

$$F(q, \dot{q}) = c.\,sgn(\dot{q}) \qquad (3.19)$$

Identification of the Developed E*xoskeleton* R*obot* Parameters:

The dynamic equations for the proposed exoskeleton robot have been developed in MATLAB (The MathWorks, USA). Then mass, centrifugal & Coriolis terms, and gravity terms $(M(q), V(q, \dot{q}), and\ G(q))$ were computed (symbolically) from developed dynamic equations and stored in separate MATLAB functions. To verify and validate the MATLAB outputs, the same computation was performed using the Robotics Toolbox for MATLAB, developed by Peter Corke (Gresham et al., 1997). In addition, static torques from MATLAB output were checked for different configurations of the proposed exoskeleton robot. Note that both approaches gave identical results. For the proposed exoskeleton robot as depicted in Figure 3.3, the center of mass (in meter) of each link can be identified as:

$$1_{P_{C_1}} = \begin{bmatrix} -0.0223 \\ 0.1511 \\ -0.1624 \end{bmatrix} \quad 2_{P_{C_2}} = \begin{bmatrix} -0.0348 \\ -0.1554 \\ 0.1818 \end{bmatrix} \quad 3_{P_{C_3}} = \begin{bmatrix} -0.0014 \\ 0.1462 \\ -0.0215 \end{bmatrix}$$

$$\begin{aligned}^{4}P_{C_4} = \begin{bmatrix} -0.0576 \\ -0.1423 \\ 0.0406 \end{bmatrix} \quad ^{5}P_{C_5} = \begin{bmatrix} -0.0182 \\ 0.0833 \\ -0.0483 \end{bmatrix}\end{aligned}$$

$$\begin{aligned}^{6}P_{C_6} = \begin{bmatrix} -0.0555 \\ -0.0926 \\ 0.0381 \end{bmatrix} \quad ^{7}P_{C_7} = \begin{bmatrix} 0.0238 \\ 0 \\ -0.0809 \end{bmatrix}\end{aligned}$$

3.5 Jacobians:

Jacobian is basically a mapping between variables. In robotics, joints' velocities of a manipulator can be transformed into Cartesian velocities of its end-effector (Craig, 2017), given that Jacobian is computed at the end-effector frame. For example, the Cartesian velocities of an end-effector with respect to the base frame can be obtained by the following equation.

$$^{0}V = {^{0}J_{(q)}}\dot{q} \tag{3.20}$$

For an n DOFs robot, Jacobian is a $6 \times n$ matrix, $\dot{q}$ is $n \times 1$ vector, and ^{0}V is a 6×1 vector. This 6×1 Cartesian velocity vector consists of 3×1 linear velocity vector (v) and 3×1 rotational velocity vector (ω). The linear velocity vector is comprised of velocities along three Cartesian axes, whereas rotational velocity vector contains angular velocities around three Cartesian axes.

$$^{0}V = \begin{bmatrix} {^{0}v} \\ {^{0}\omega} \end{bmatrix} \tag{3.21}$$

The Jacobian of the *proposed exoskeleton robot* was computed in MATLAB (The MathWorks, USA). In Jacobian, the number of rows equals the number of DOFs in the Cartesian space being considered. While the number of columns in a Jacobian is equal to the DOFs of the manipulator.

CHAPTER-4   CONTROL AND SIMULATION

In this chapter, the simulation of the proposed exoskeleton robot using Computed Torque Control is presented to see the torque requirements of actuators. Section 4.1 presents the formulation of Computed Torque Control, whereas Section 4.2 presents the simulation result. Besides, Section 4.3 presents the simulation results using a new compound control (model-based). This chapter also focuses on Cartesian space control (simulation results are presented in Section 4.5), which is suitable for end-point (Cartesian coordinates) exercises. The simulations were done to evaluate the trajectory (representing rehabilitation exercises) tracking performance of the controller.

4.1   Computed torque control

The term 'computed torque control' (CTC), also known as inverse dynamic control, is one of the controllers that has been widely adapted for several applications in the field of robotics. In the CTC, the control command is obtained using model dynamics. The global stability of CTC can be ensured by assuming that the dynamic model of the system (robot) is known. However, obtaining an accurate dynamic model of a nonlinear system (such as a robot manipulator) is difficult. In reality, some degree of mismatch between the model adopted for the control and the real system exists. To solve this issue, CTC is often extended and modified. The formulation of CTC for the proposed exoskeleton robot is following (Craig, 2017):

In chapter-3, the dynamic equation of the proposed exoskeleton robot was developed. From equation (3.18), we have

$$\tau = M(q)\ddot{q} + V(q,\dot{q}) + G(q) + F(q,\dot{q}) \tag{3.18}$$

where

$q \in \mathbb{R}^{7 \times 1}$ is the vector of joint variables of the proposed exoskeleton robot,

$\dot{q} \in \mathbb{R}^{7 \times 1}$ is the vector of joint velocity,

$\ddot{q} \in \mathbb{R}^{7 \times 1}$ is the vector of joint velocity,

$M(q) \in \mathbb{R}^{7 \times 7}$ is the inertia matrix,

$V(q,\dot{q}) \in \mathbb{R}^{7 \times 1}$ is the vector of centrifugal and Coriolis terms,

$G(q) \in \mathbb{R}^{7 \times 1}$ is the gravity vector,

$F(q,\dot{q}) \in \mathbb{R}^{7 \times 1}$ is the friction vector using nonlinear Coulomb friction model,

$\tau \in \mathbb{R}^{7 \times 1}$ is the torque vector.

The problem of controlling such a complicated system can be handled by partitioning control law into two portions; a model-based portion of the control and a servo portion, which runs on the basis of error between reference trajectory and actual trajectory.

The model-based portion of the control is

$$\tau = \alpha \acute{\tau} + \beta \tag{4.1}$$

Where α and β are chosen as follows.

$\alpha = M(q)$

$$\beta = V(q, \dot{q}) + G(q) + F(q, \dot{q})$$

The servo portion of the control laws is:

$$\acute{t} = \ddot{q}_d + K_v \dot{E} + K_p E \tag{4.2}$$

Where,

K_v and K_p are diagonal positive definite matrices. Error 'E' is defined as the difference between reference (desired) trajectory and actual (measured) trajectory.

$$E = q_d - q \tag{4.3}$$

Combining equations (3.18), (4.1), (4.2), and (4.3), we have

$$\tau = \alpha \acute{t} + \beta$$

$$=> M(q)\ddot{q} + V(q, \dot{q}) + G(q) + F(q, \dot{q})$$

$$= M(q)\left[\ddot{q}_d + K_v(\dot{q}_d - \dot{q}) + K_p(q_d - q)\right] + V(q, \dot{q}) + G(q) + F(q, \dot{q})$$

$$=> M(q)\ddot{q} = M(q)\left[\ddot{q}_d + K_v(\dot{q}_d - \dot{q}) + K_p(q_d - q)\right]$$

$$=> \ddot{q} = \ddot{q}_d + K_v(\dot{q}_d - \dot{q}) + K_p(q_d - q)$$

Where, $\ddot{q}_d$ and $\dot{q}$ are reference joint acceleration and velocity vector.

$$\ddot{q}_d - \ddot{q} + K_v(\dot{q}_d - \dot{q}) + K_p(q_d - q) = 0 \tag{4.4}$$

The equation (4.4) can be written as

$$\ddot{E} + K_v \dot{E} + K_p E = 0 \tag{4.5}$$

The stability of this control depends on the proper choice of matrices K_v and K_p.
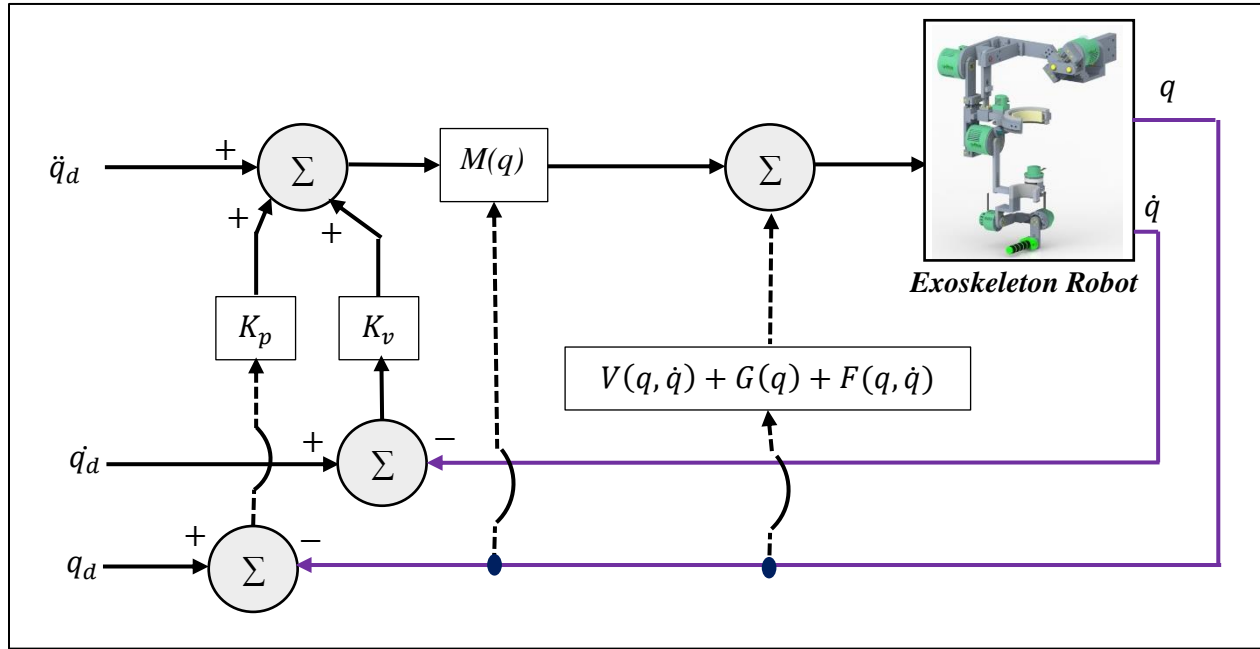
Figure 4.1 Schematic diagram of computed torque control method

4.2 Simulation result with CTC

The proposed exoskeleton robot is meant to be used for a typical adult. The upper limb anthropometric parameter (arm's length, arm segment's weight, segment inertia.) were estimated to generate simulation results (Winter, 2009). Details of upper limb anthropometric parameters are shown in ANNEX VI-VIII. The simulation was carried out considering standard rehabilitation therapy protocol (Physical Therapy Standards of Care and Protocol, 2020; FlintRehab, 2020; WebMD, 2020) and for subjects with different mass and height. Therapy exercises were transformed into a predefined trajectory that the robot is supposed to follow. In every simulation

126

result, the topmost graph is angle vs. time plot, the graph below the topmost graph is error vs. time plot, followed by velocity vs. time pot, and Torque vs. time plot. In the angle and velocity plot, the solid red line stands for desired (reference) trajectory, whereas the blue line stands for the simulated result (trajectory from the simulation of the proposed exoskeleton robot).

4.2.1   Simulation result-1
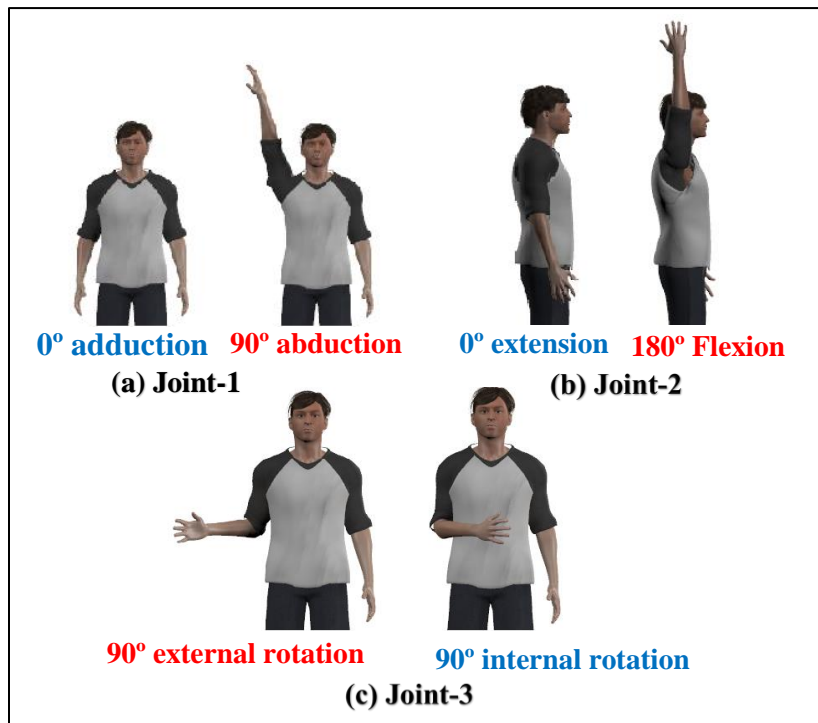
Figure 4.2 Shoulder joints' full range of ROM
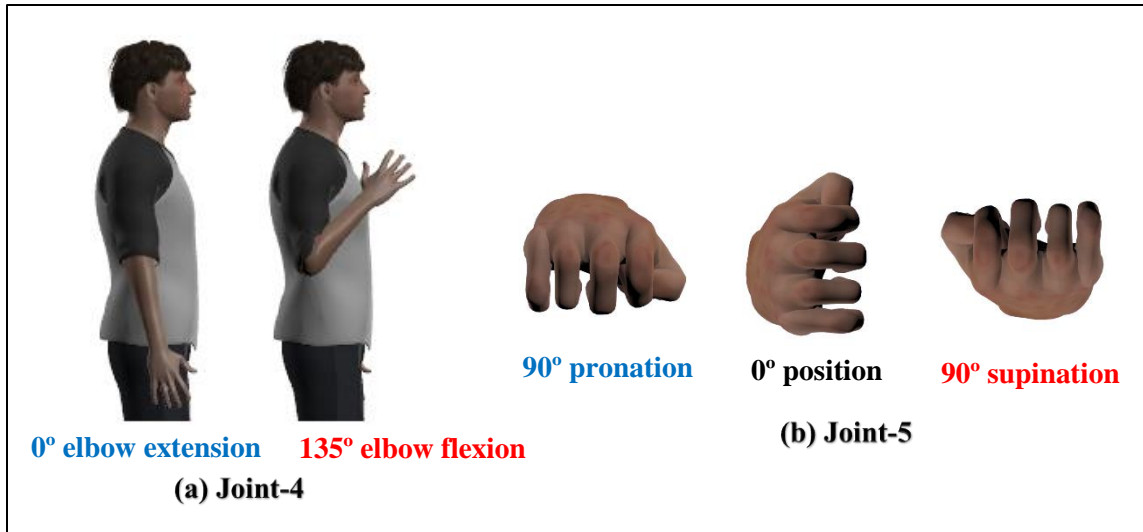
Figure 4.3 Elbow and forearm joints' full range of ROM
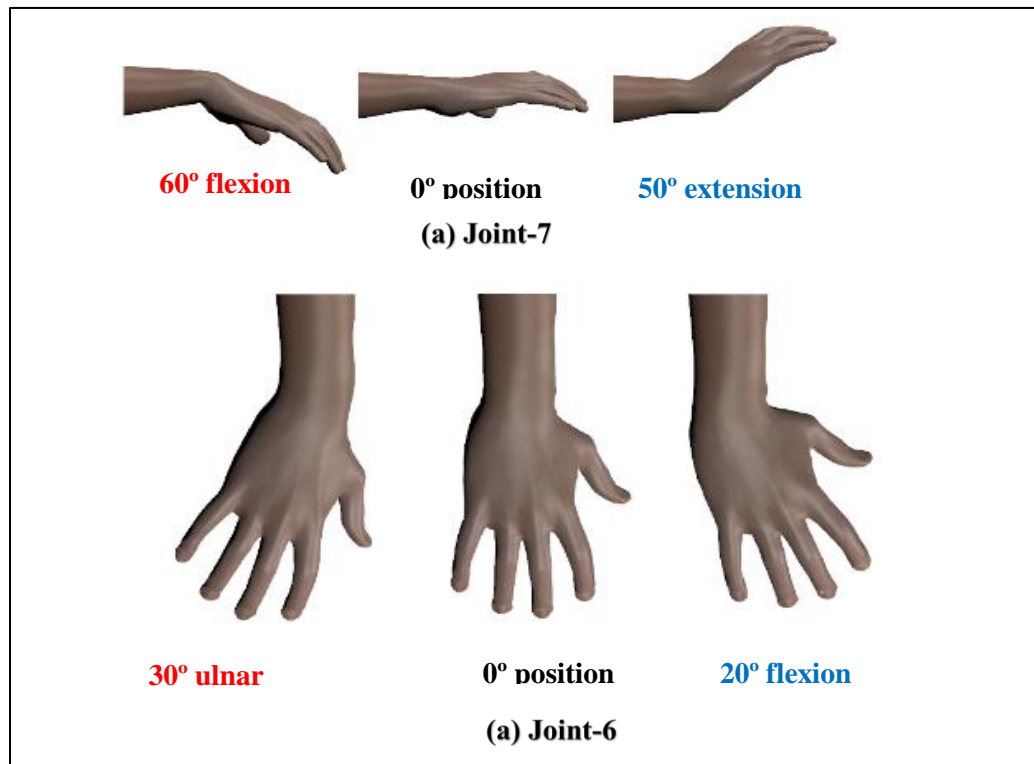
Figure 4.4 Wrist joints' full range of ROM

At first, the simulation was conducted for a trajectory that involved the individual joint movement of a subject (Weight: 75 kg, Height: 173 cm) while the subject remained passive. The

movement was carried out from the lower limit to the upper limit of ROM of the proposed

exoskeleton robot. Schematics are shown in Figure 4.2 through Figure 4.4. Every joint were moved

from their allowed minimum ROM to maximum ROM. For example, shoulder abduction (joint-1)

was carried out up to 90° from 0º and then returns back to 0°(adduction). Similarly, shoulder

vertical flexion was done to 180° from 0º and then extended back to 0°. Similarly, exercises of

other joints were carried out for their respective lower and upper limit of ROM. Finally, the

exercise ends with wrist flexion to 60° from 0º wrist position and extension to 50°.
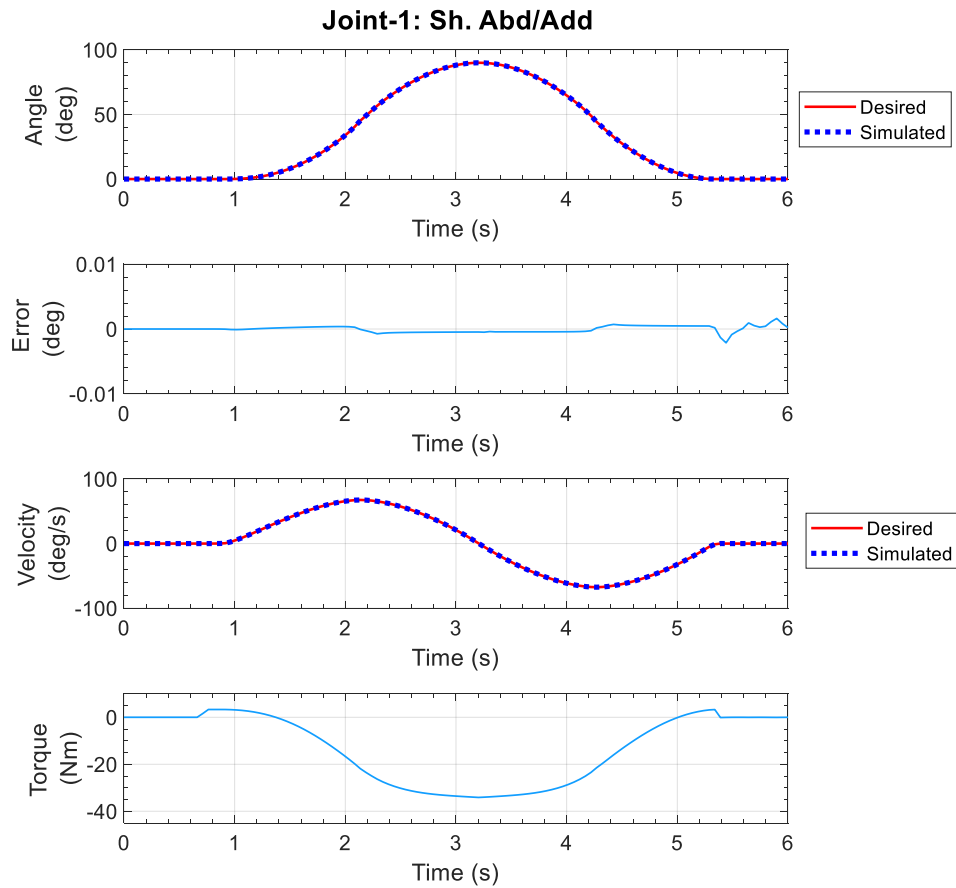
Figure 4.5 Simulation result of shoulder abduction-adduction.

Here, the cubic polynomial approach was used to generate the desired trajectories (Craig,

2017). The simulation result is shown in Figure 4.5 through Figure 4.11. These figures contain

plots of position tracking, the error between desired trajectory and measured trajectory, velocity tracking, torque as a function of time. In the trajectory tracking plot, the solid red line and blue dotted line stand for the desired and simulated trajectory, respectively. From Figure 4.5- Figure 4.11, it is seen that the desired and simulated trajectory are overlapped (maximum error found is 0.025°; which happened for wrist flexion-extension), which proves the controller's performance. Note that, measured velocity and desired velocity are also overlapped in simulation results.
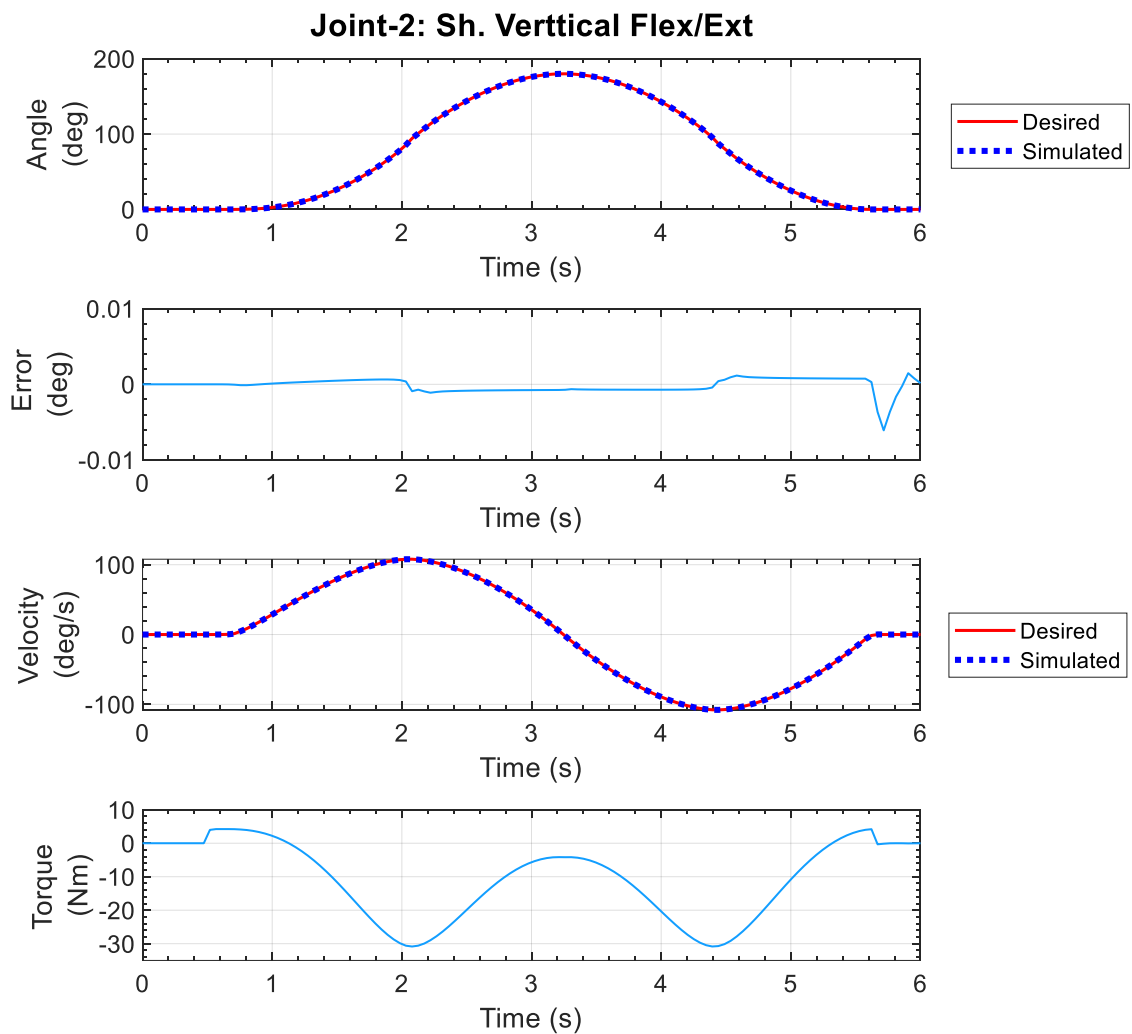
Figure 4.6 Simulation result of vertical flexion-extension
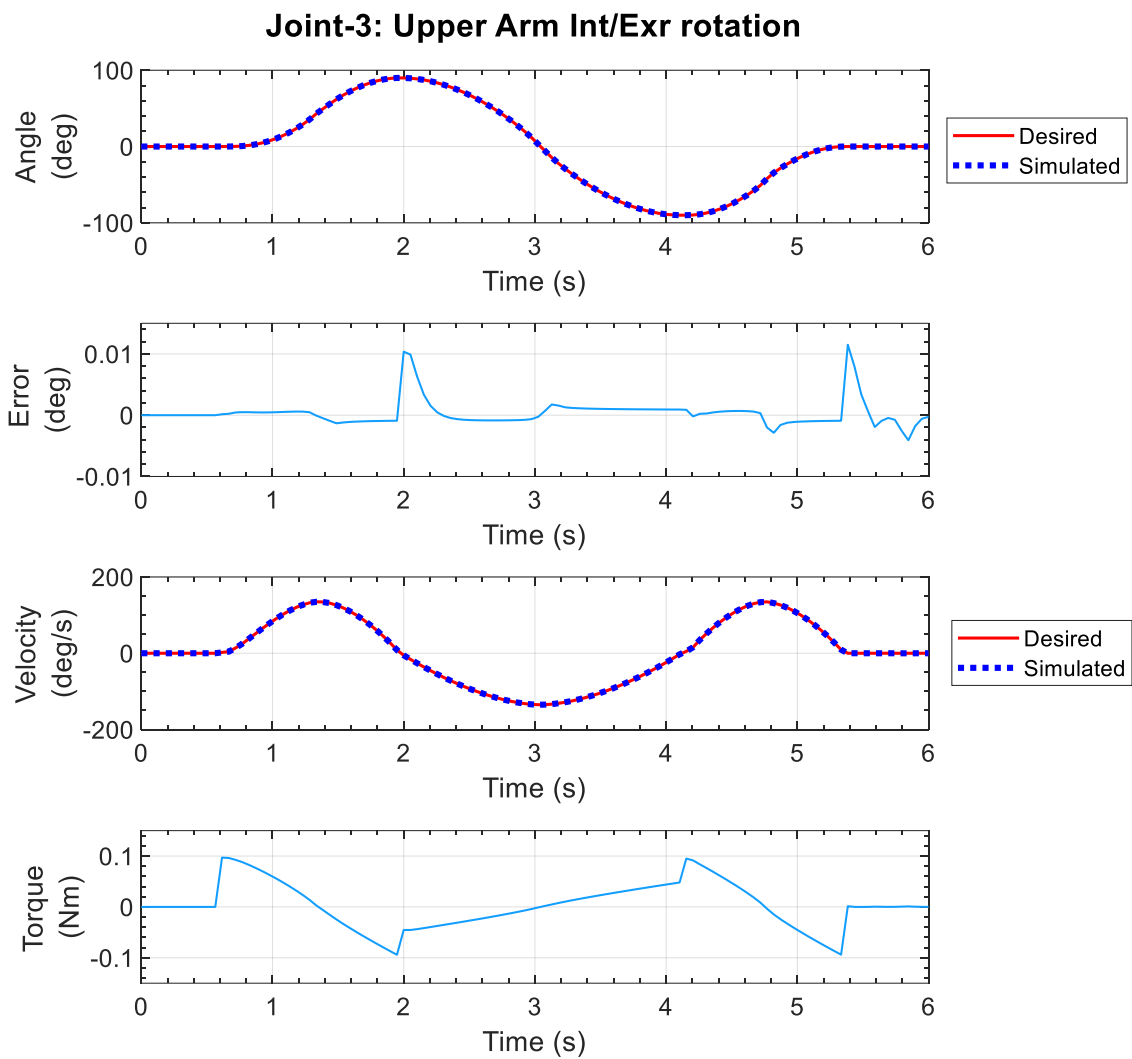
Figure 4.7 Simulation result of upper arm internal-external rotation
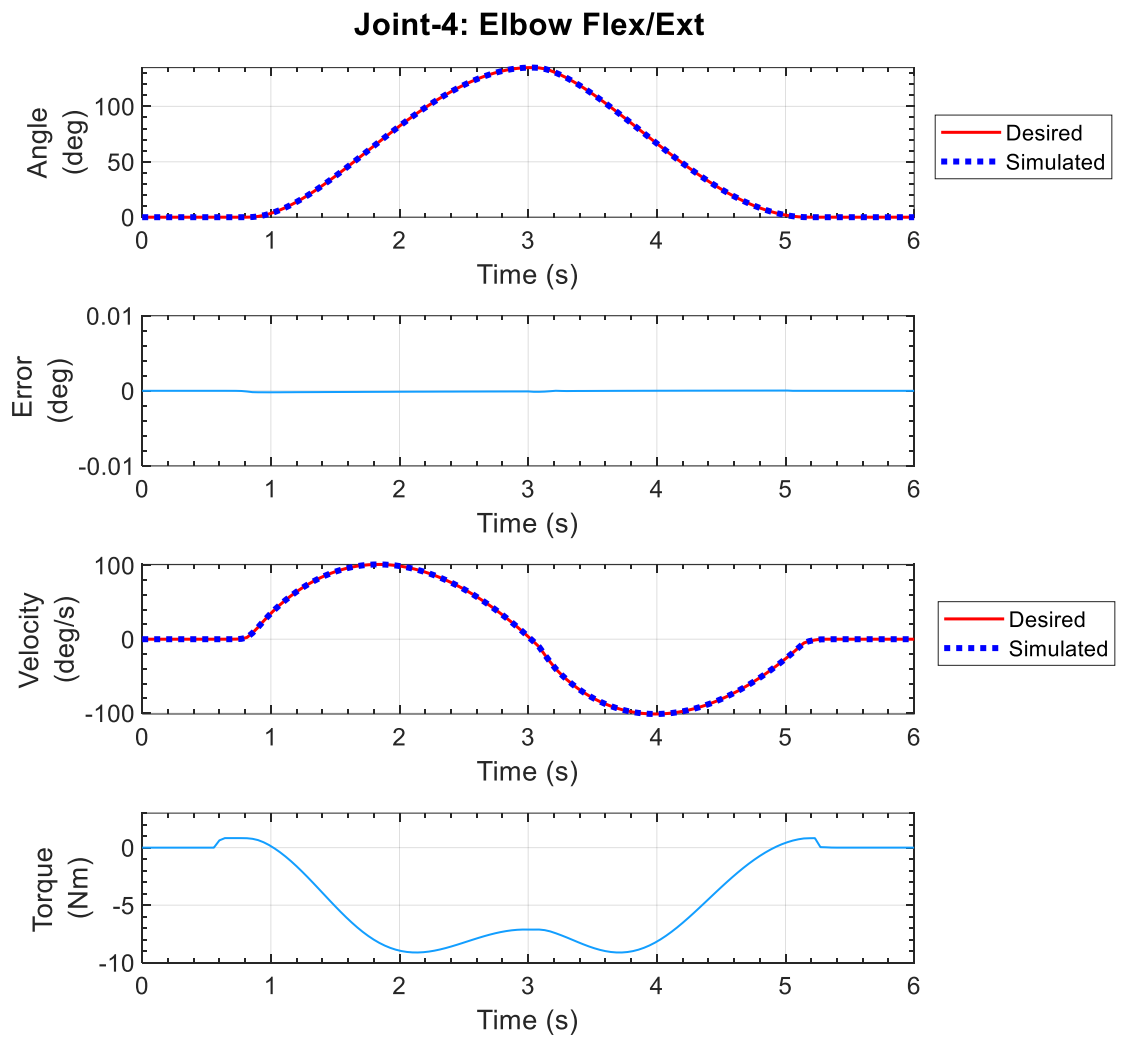
Figure 4.8 Simulation result of elbow flexion-extension
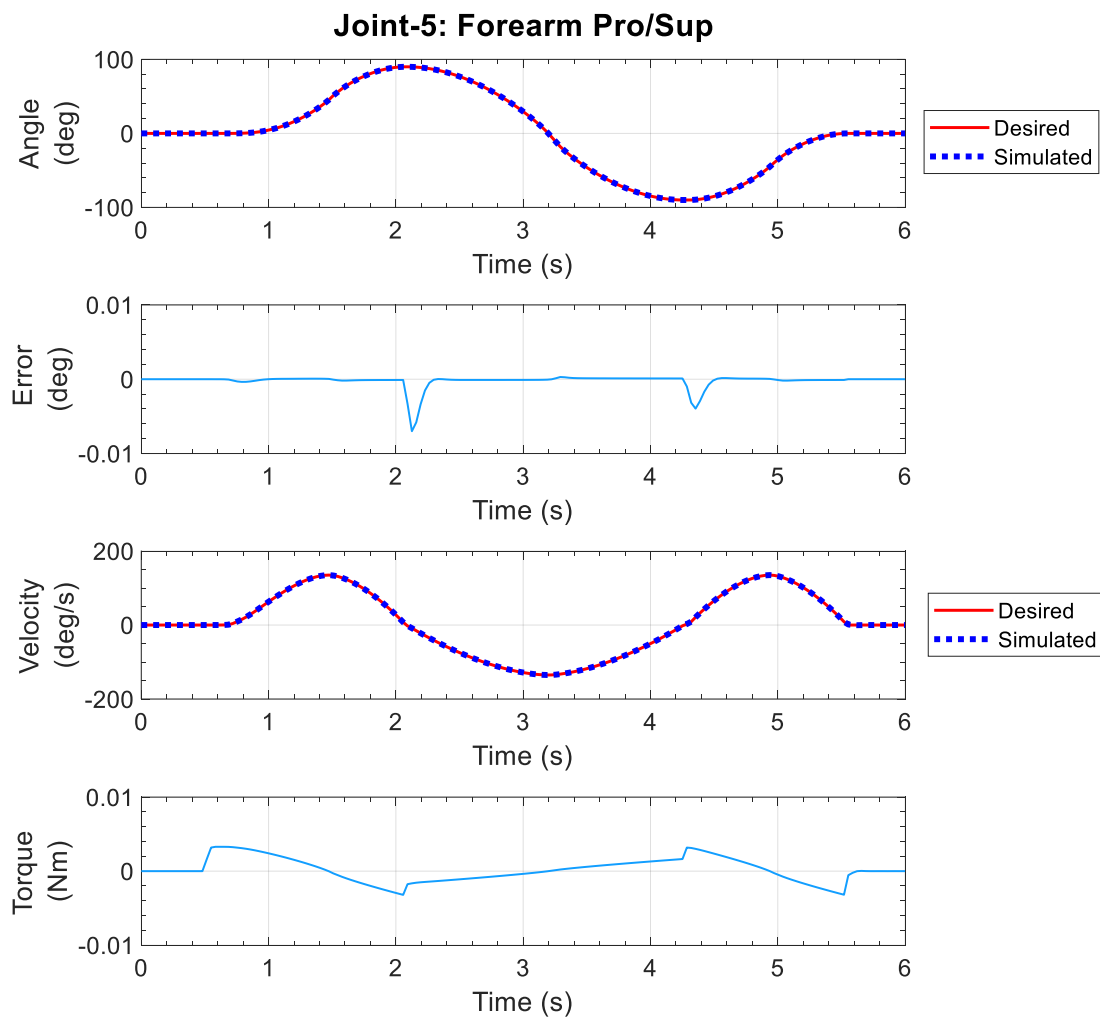
Figure 4.9 Simulation result of forearm pronation-supination
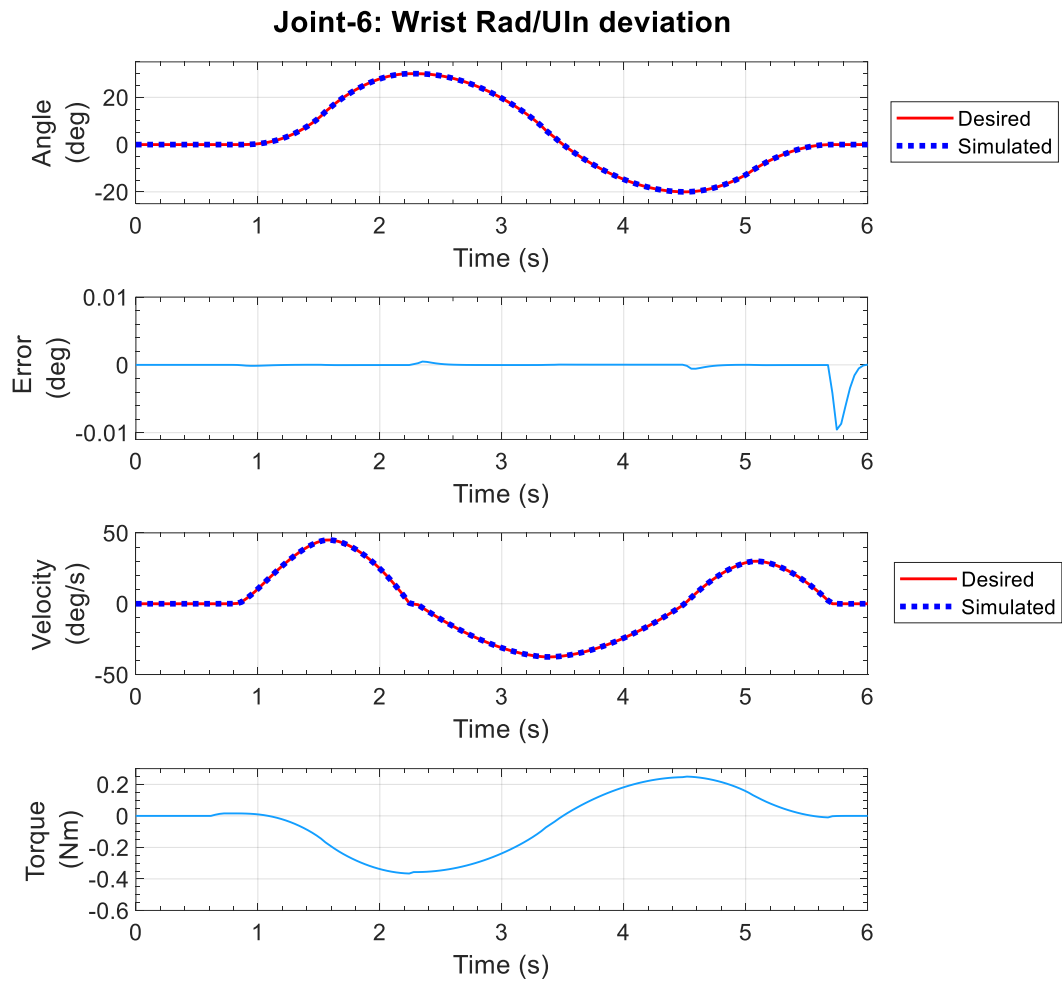
Figure 4.10 Simulation result of wrist radial-ulnar deviation
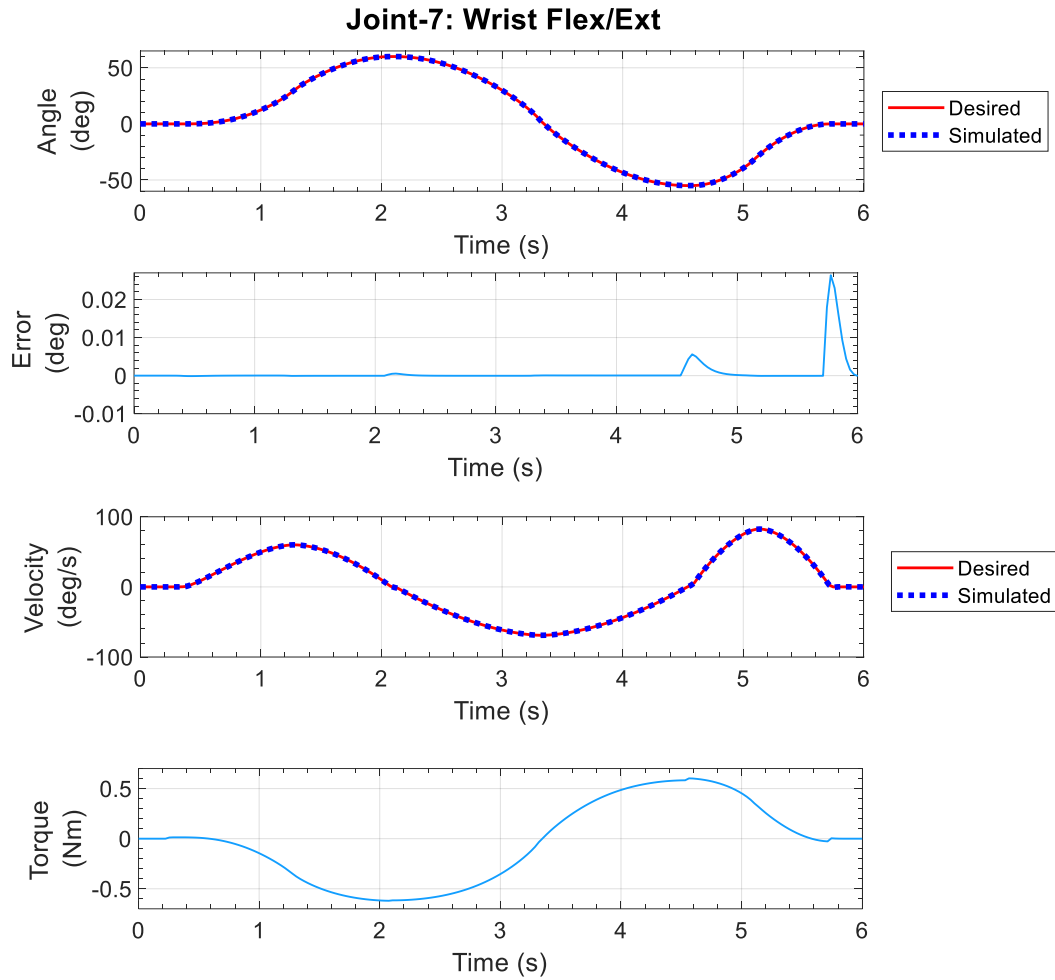
Figure 4.11 Simulation result of wrist flexion-extension

4.2.2   Simulation result-2

In this attempt, a simulation was run for exercise that involves simultaneous movement of all joints

except the joint-7 (wrist flexion-extension). This exercise replicates diagonal reaching movement

as shown in Figure 4.12 that starts moving from an initial position (all joints are in 0º while the

elbow is at 90º position) to the reaching position (abduction 45º, vertical flexion 25º, external

rotation 30º, elbow flexion 10º, forearm pronation 45º and wrist ulnar deviation 15º), and then

return to the initial position. The exercises are repeated three times, as shown in Figure 4.13 through Figure 4.15.
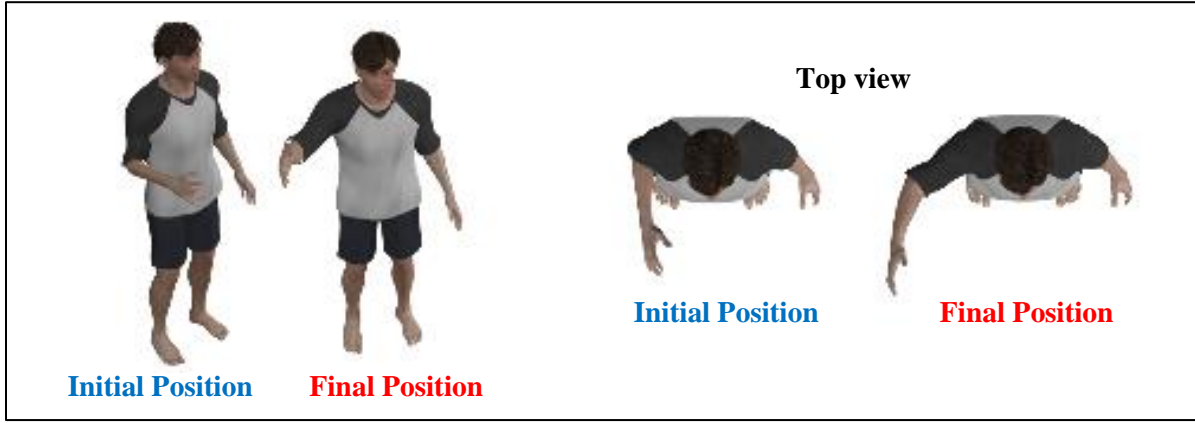
Figure 4.12 Schematic of diagonal reaching movement

It can be seen from from Figure 4.13 through Figure 4.15 , the desired trajectory and the desired velocity are overlapped on the measured (simulated) trajectory and velocity, respectively, which corroborate the robustness of the controller.
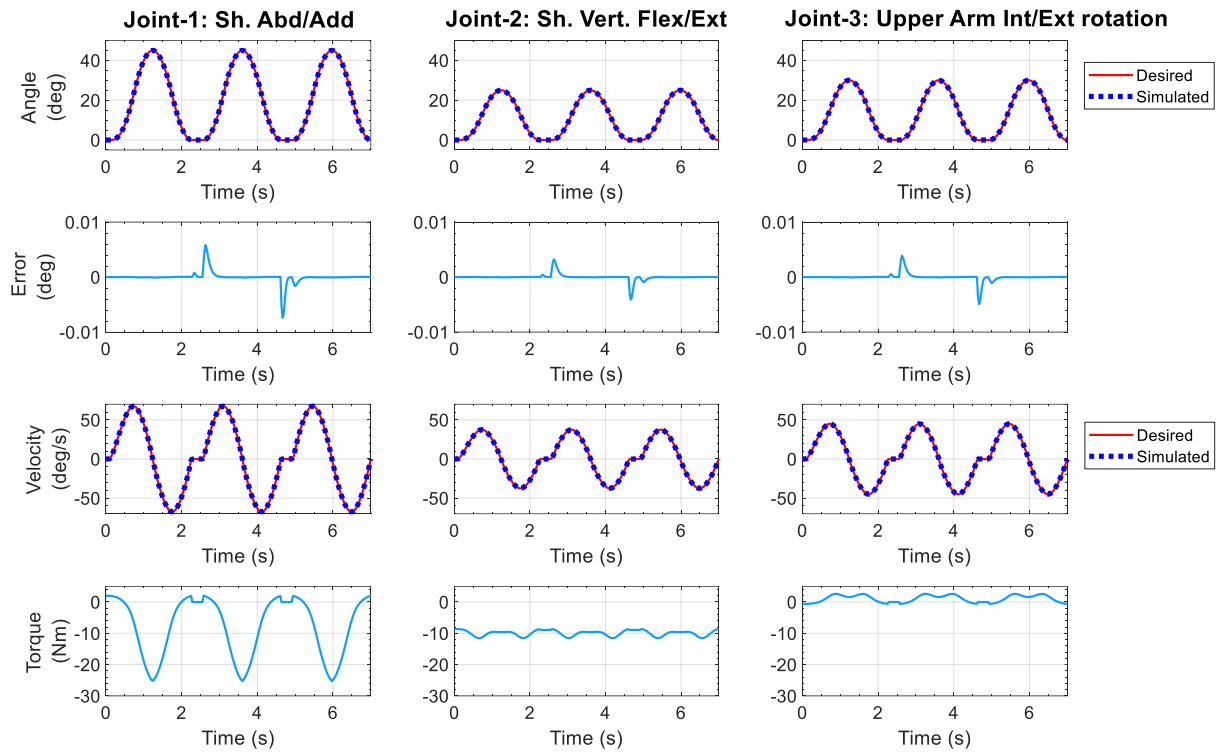
Figure 4.13 Plot of shoulder joints for simultaneous movement exercise
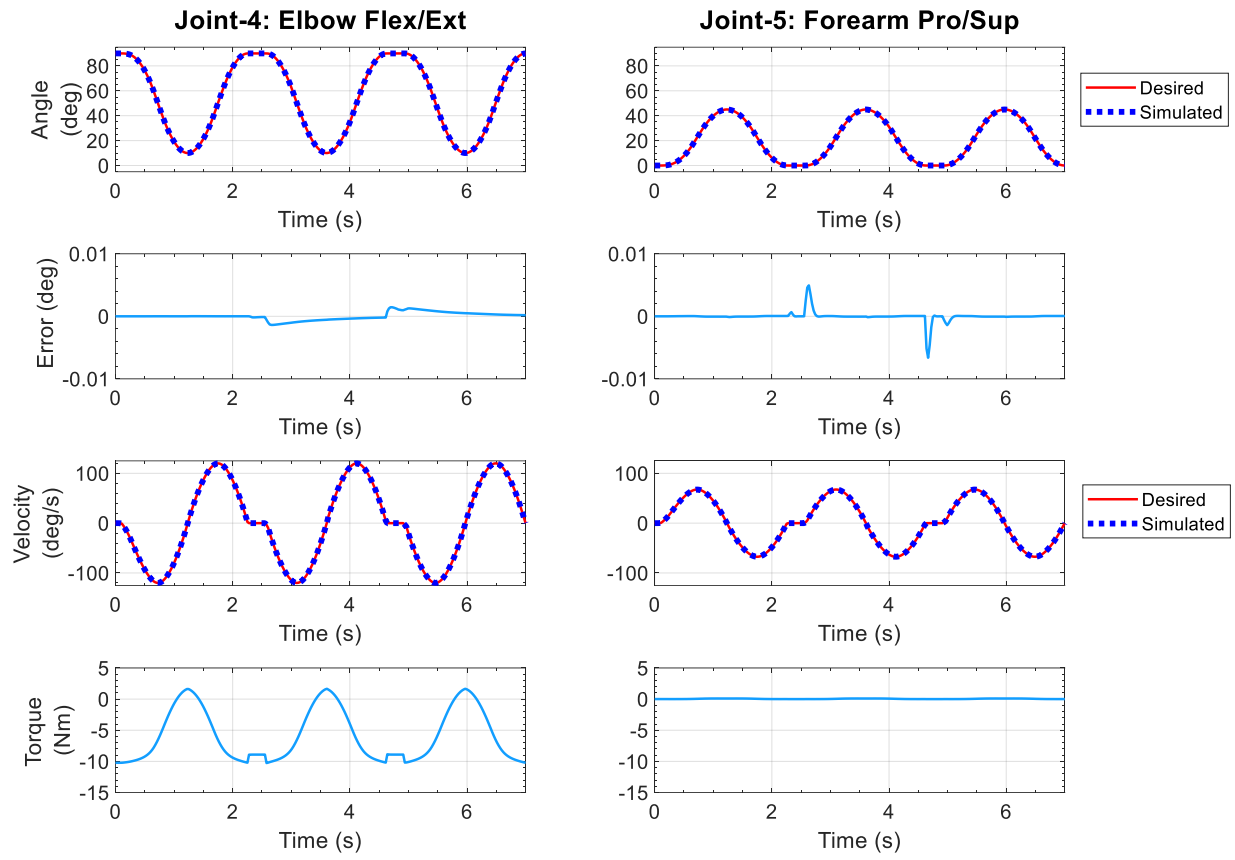
Figure 4.14 Plot of elbow joints for simultaneous movement exercise
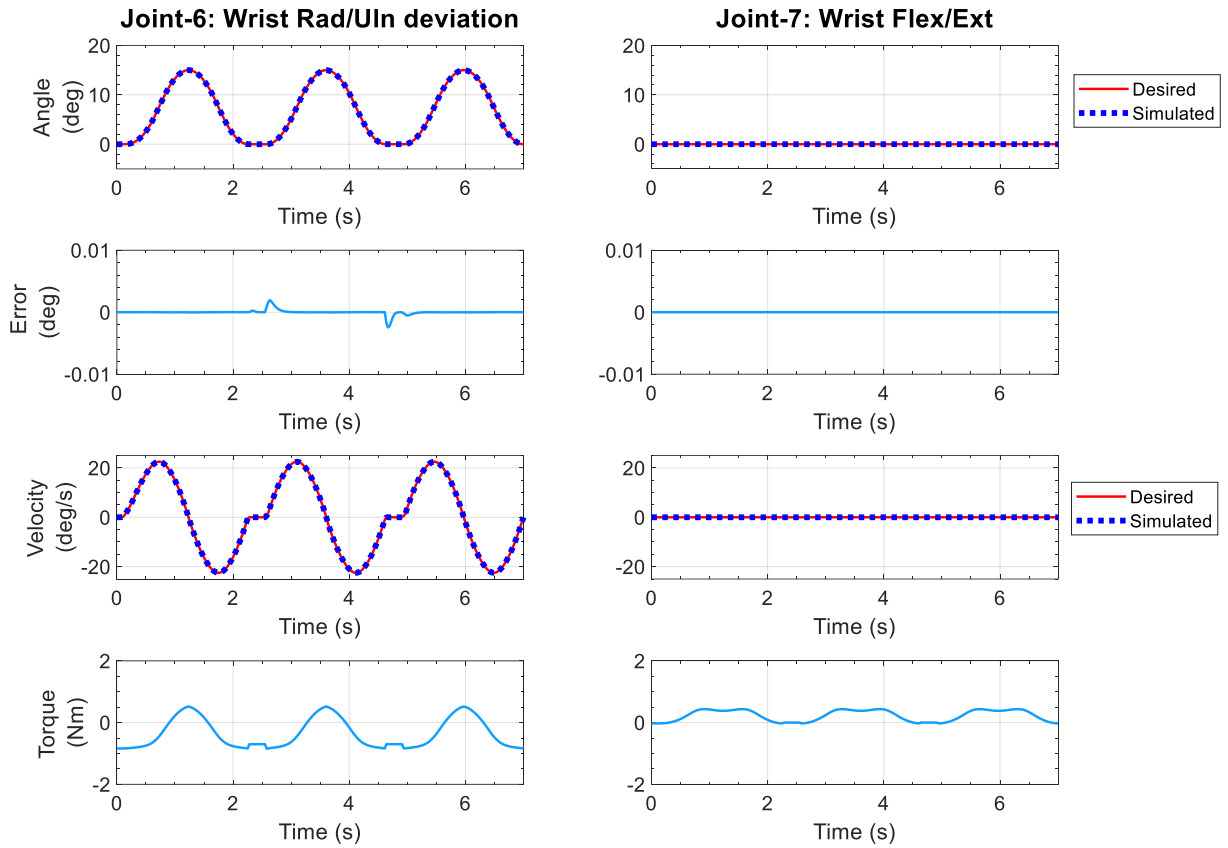
Figure 4.15 Plot of wrist joints for simultaneous movement exercise

4.2.3 Simulation result-3

Exercise-1 Co-operative movement of upper arm and elbow:

In this exercise, a cooperative movement of elbow and shoulder joints were performed where the elbow joint (joint-4) is expected to flex from its initial position up to an angle of 90∘, and finally, maintain that position against the gravity while the subject is supposed to do repetitive shoulder joint internal-external rotation. The schematic is shown in Figure 4.16. The simulation results are shown in Figure 4.17. The controller performance is very good as reference trajectories are overlapped with measured (simulated) trajectories with an error less than 0.01°.
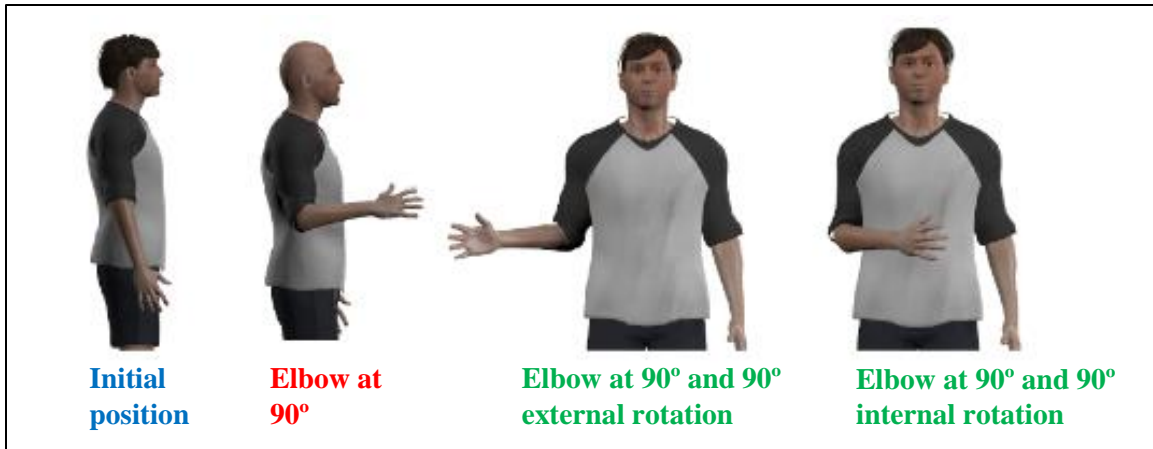
Figure 4.16 Schematic of cooperative exercise of the elbow and upper arm rotation
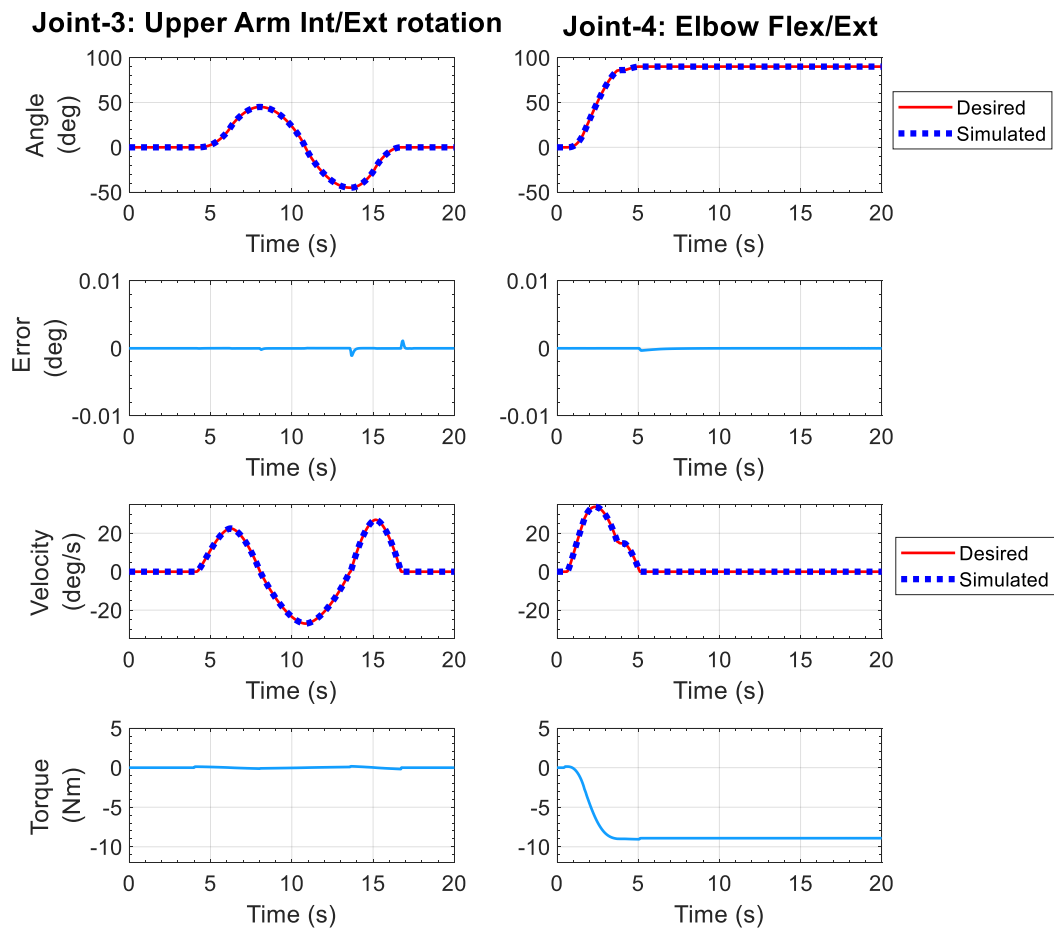
Figure 4.17 Simulation result for exercise-1

Exercise-2 Reaching Exercise:

This diagonal reaching exercise comprises elbow and shoulder joint movement. As shown in Figure 4.18, the exercise is initiated with elbow flexion, where joint-4 is expected to flex from its initial position (0°) up to an angle of $90\circ$. After that, the shoulder joint is abducted from 0° to 45° and adducted back to 0° at the end of the exercise. Also, it can be seen from the figure the shoulder is vertically flexed from 0° to 45° and extended back to 0° at the end of the exercise. During the movement of the shoulder, the elbow is extended to zero and goes back to 0°. Once the shoulder movement is done, in the end, the elbow is extended back to zero. The simulation results are shown in Figure 4.19. The very small error (0.002°) between reference and measured trajectory makes them overlapped, which indicates the good performance of the controller.
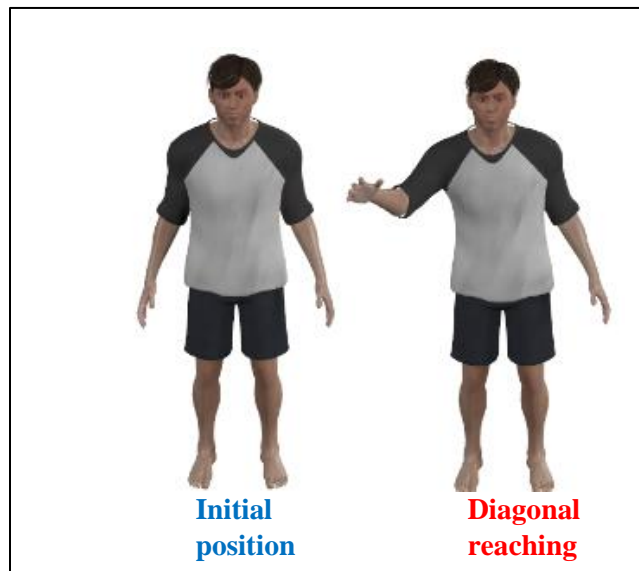
Figure 4.18 Schematic of reaching exercise
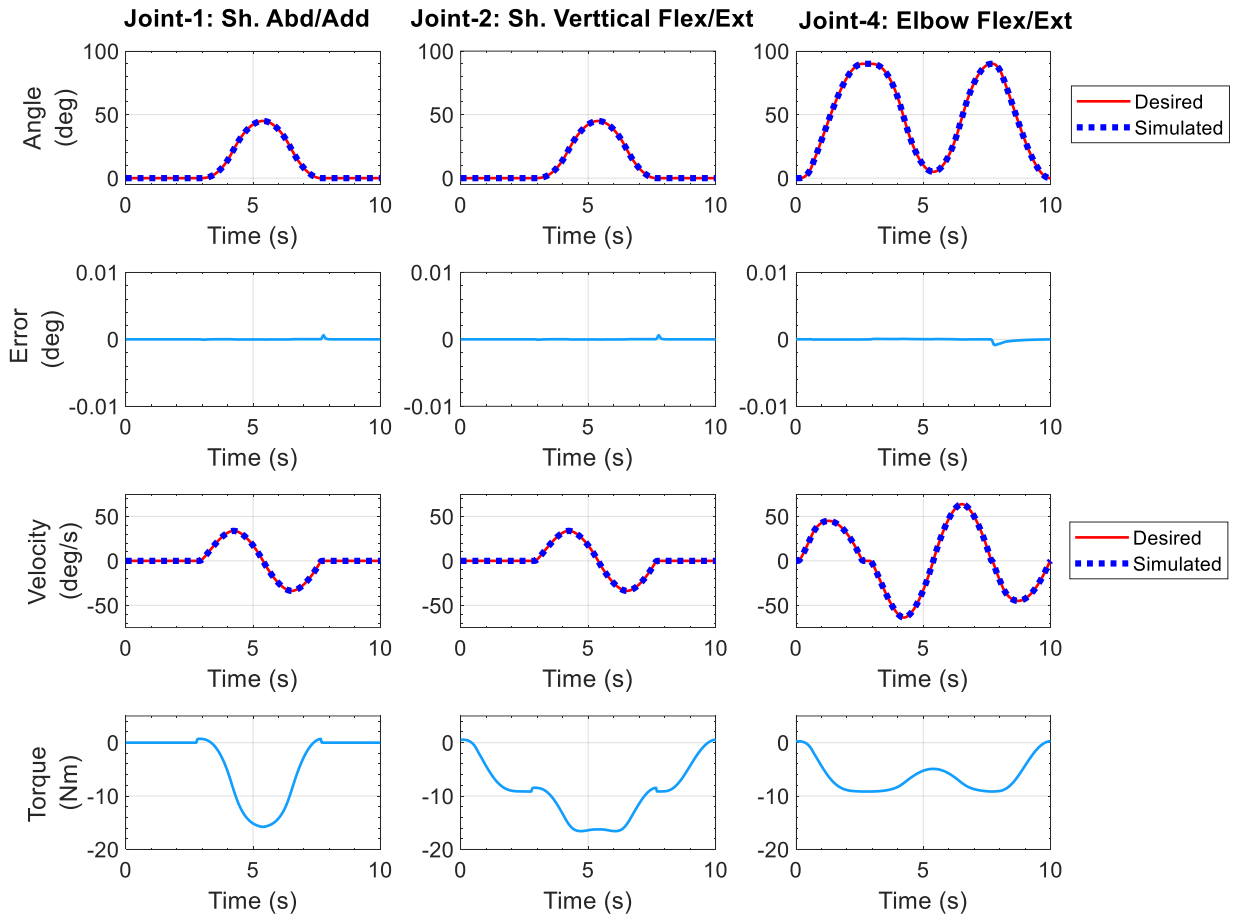
Figure 4.19 Simulation result for exercise-2 (diagonal reaching with Joint-1, 2, and 4)

Exercise-3 Forward reaching Exercise:

This cooperative forward reaching exercise involves movement of the shoulder and elbow joint. The exercise initiates with the elbow flexed at 90º (joint-4) is expected to extend to the position (5º). At the same time, the shoulder is vertically flexed from 0º to 75º and extended back to 0º at the end of the exercise. The simulation result is shown in Figure 4.20**.** The controller performance is very good as reference trajectories are overlapped with measured trajectories with 0.01º error

142
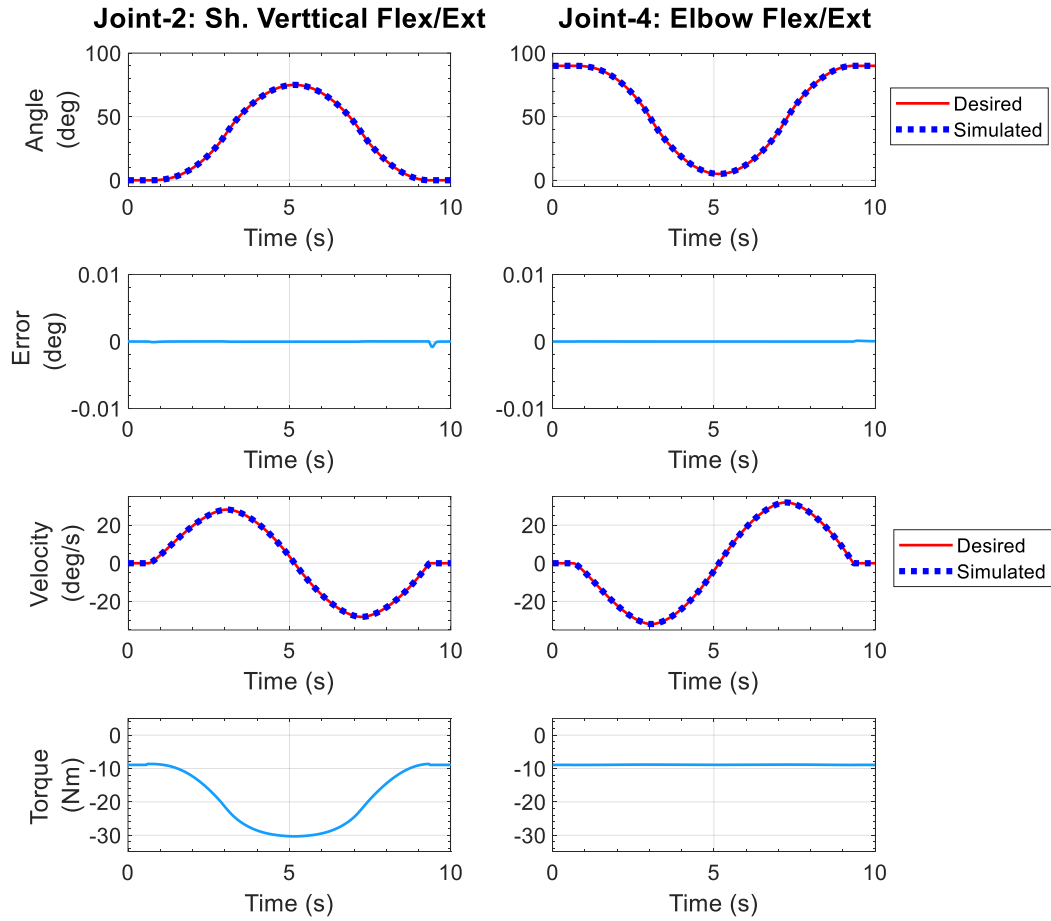
Figure 4.20 Simulation result for exercise-3 (Forward reaching)

Exercise-4 Elbow and forearm movement:

This cooperative movement of elbow and forearm joint, where the exercise initiates with elbow flexion where joint-4 is expected to flex from its initial position (0°) up to an angle 90∘, maintains that position against gravity certain specific time, and finally returned to initial position. In addition, the subject is supposed to do repetitive forearm pronation and supination. The simulation results are shown in Figure 4.21. The minimal error (0.01°) between reference and measured trajectory makes the trajectories overlapped, which indicates the excellent performance of the controller.

143
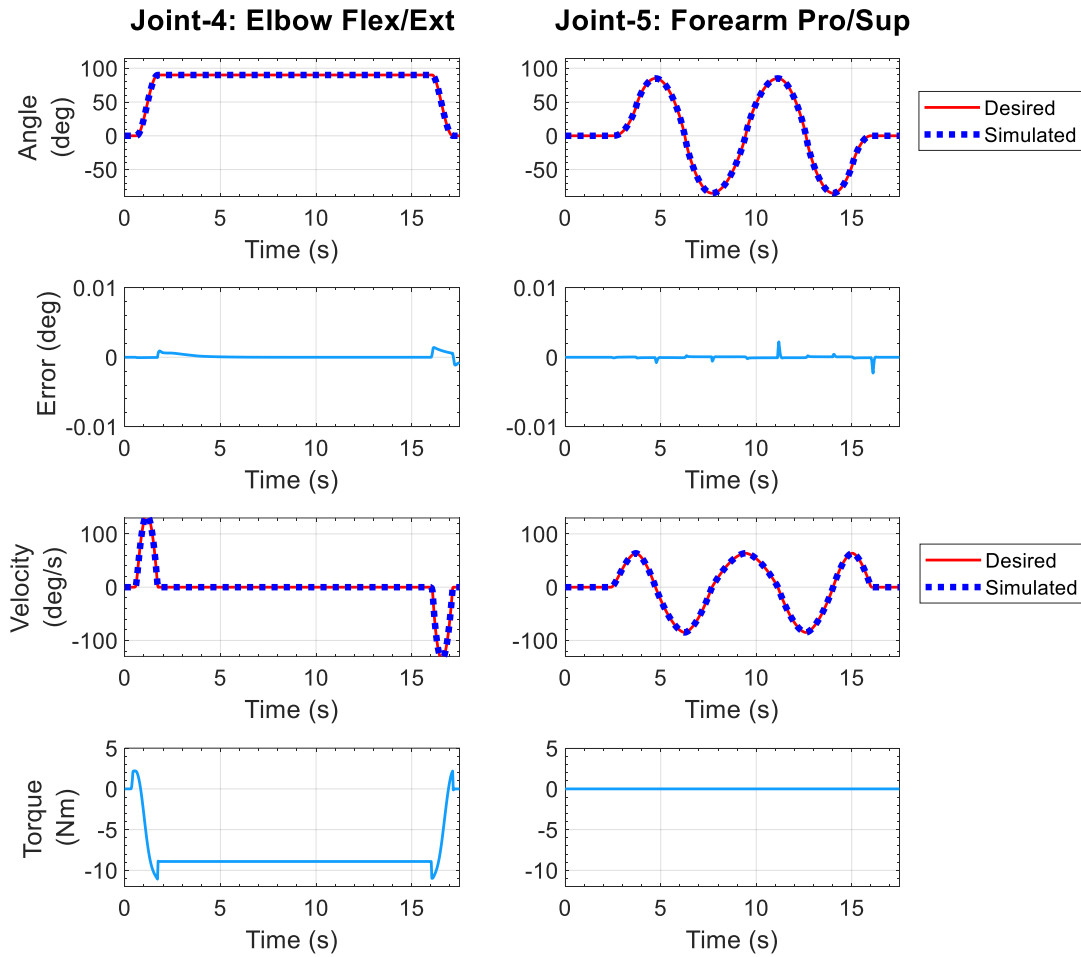
Figure 4.21 Simulation result for exercise-5

Exercise-6 cooperative exercise of wrist radial-ulnar deviation and flexion-extension:

This cooperative movement of elbow and wrist, where joint-6 was rotated to 15º (ulnar deviation) and joint-7 was rotated to 20º (extension). After that, joint-6 travels to -15º (radial deviation), and joint-7 travels to 30º (flexion). In the end, both joints returned to their initial position. The simulation results are shown in Figure 4.22. The very small error (less than 0.01º) between reference and simulated trajectory makes them overlapped, which indicates the excellent performance of the controller.
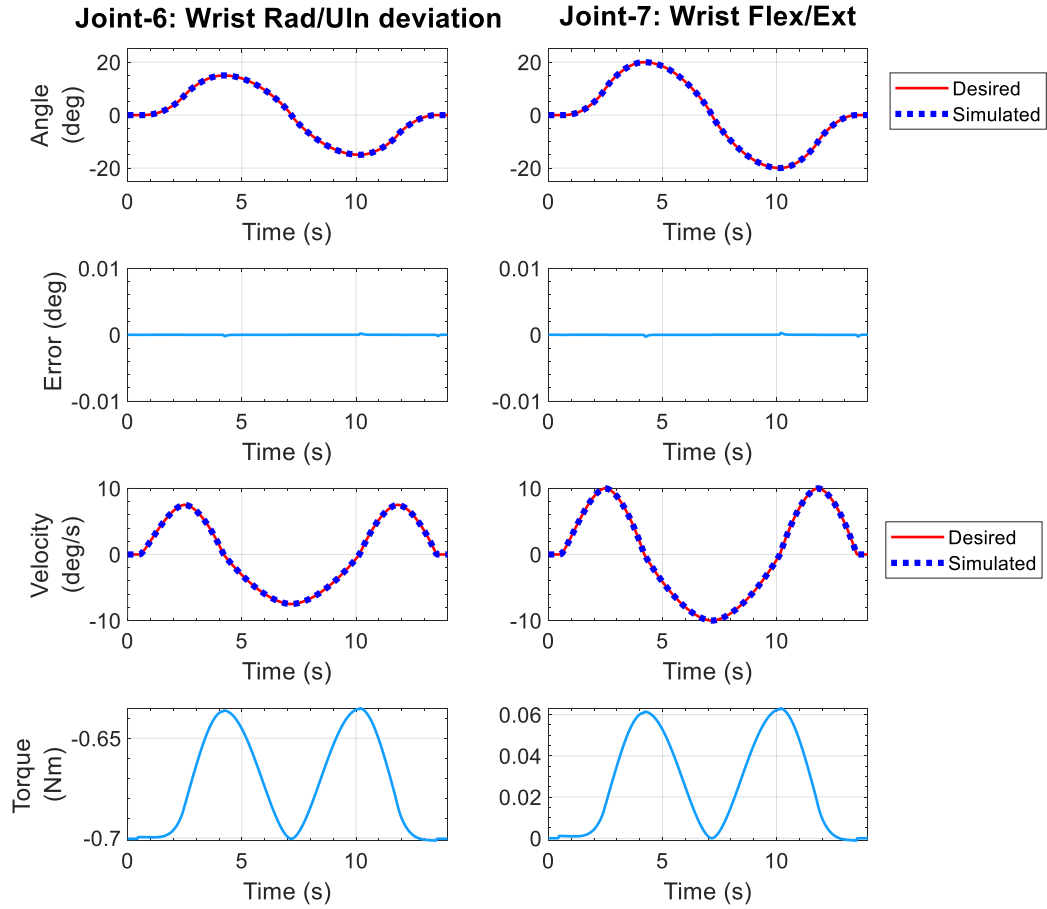
Figure 4.22 Simulation result for exercise-6

4.3 New compound model-based control (NCMC)

As a rehabilitative device, the proposed exoskeleton robot requires a control approach that ensures safe and effective maneuvering. Since anthropometric parameters (arm's length, arm segment's weight, segment inertia) vary from patient to patient, a model-based controller does not ensure safe and stable maneuvering. Besides, the interactive forces between the wearer (subject) and the proposed exoskeleton robot should be considered in the control approach. Existing exoskeletons have largely ignored the interaction force in passive rehabilitation. Therefore, to take the parameter variation and the interaction forces into the control approach, the error-driven

portion of control law and force estimation were included in addition to the model-driven portion. The goal here is to provide a basis to the proposed exoskeleton robot (which was given by the model-driven portion), and then any error occurred due to model uncertainty and variation of the anthropometric parameter is for the error-driven portion law to be taken care of. Thus, to control the motion of the proposed exoskeleton robot, a hybrid approach (based on model-driven computed torque, error-driven proportional derivative torque, and Jacobian based torque) was used. The overall control law, model-driven, and error-driven portions were given below.

Error driven portion of control law: $- K_p e - K_v \dot{e}$

Model driven portion of control law: $M\ddot{q}_d + C\dot{q}_d + G + F$

Ineteration force : $J^T(q, \dot{q})\, F_w$

Modified model driven portion: $M\ddot{q}_d + C\dot{q}_d + G + F - J^T(q)\, F_w$

The overall control law:

$$\tau = -K_p e - K_v \dot{e} + M\ddot{q}_d + C\dot{q}_d + G + F - J^T(q)\, F_w \qquad (4.6)$$

Where,

M is a positive definite inertia matrix

$q_d \in \mathbb{R}^{7\times1}$ is the desired joint position vector

$\dot{q}_d \in \mathbb{R}^{7\times1}$ is the desired joint velocity vector

$\ddot{q}_d \in \mathbb{R}^{7\times1}$ is the desired joint acceleration vector

$e = q - q_d$

$\dot{e} = \dot{q} - \dot{q}_d$

$\ddot{e} = \ddot{q} - \ddot{q}_d$

$J^T \in \mathbb{R}^{7\times6}$ is the Jacobian of end-effector expressed in end-effector frame

$F_w \in \mathbb{R}^{3\times1}$ is the Cartesian forces between user and the developed exoskeleton robot at the wrist

$K_p \in \mathbb{R}^{7\times7}$ is the positive definite diagonal proportional gain matrix

$K_v \in \mathbb{R}^{7\times7}$ the positive definite diagonal derivative gain matrix

Proof of Lyapunov stability:

From equation (4.6),

$$\ddot{q} = M^{-1}(\tau - C\dot{q} - G - F + J^T(q)\,F_w)$$

Setting, Lyapunov function, V

$$V = \frac{1}{2}e^T K_p e + \frac{1}{2}\dot{e}^T M \dot{e}$$

$$\frac{dV}{dt} = \dot{V} = \frac{1}{2}\dot{e}^T K_p e + \frac{1}{2}e^T K_p \dot{e} + \frac{1}{2}\ddot{e}^T M \dot{e} + \frac{1}{2}\dot{e}^T M \ddot{e} + \frac{1}{2}\dot{e}^T \dot{M} \dot{e}$$

Since, $M, K_p\ and\ K_v\ are\ symmetrix$ matrices, following equality, hold true.

$$\dot{e}^T K_p e = e^T K_p \dot{e} \qquad \ddot{e}^T M \dot{e} = \dot{e}^T M \ddot{e}$$

Thus,

$$\dot{V} = e^T K_p \dot{e} + \dot{e}^T M \ddot{e} + \frac{1}{2}\dot{e}^T \dot{M} \dot{e}$$

$$\dot{V} = e^T K_p \dot{e} + \dot{e}^T M(\ddot{q} - \ddot{q}_d) + \frac{1}{2}\dot{e}^T \dot{M} \dot{e}$$

$$\dot{V} = e^T K_p \dot{e} + \dot{e}^T M\ (M^{-1}(\tau - C\dot{q} - G - F + \ J^T(q)\,F_w) - \ddot{q}_d) + \frac{1}{2}\dot{e}^T \dot{M} \dot{e}$$

$$\dot{V} = e^T K_p \dot{e} + \dot{e}^T (\tau - C\dot{q} - G - F + J^T(q)\,F_w - M\ddot{q}_d) + \frac{1}{2}\dot{e}^T \dot{M} \dot{e}$$

$$\dot{V} = e^T K_p \dot{e} + \dot{e}^T (\tau - C\dot{q} - G - F + \ J^T(q)\,F_w - M\ddot{q}_d) + \frac{1}{2}\dot{e}^T \dot{M} \dot{e}$$

$$\dot{V} = e^T K_p \dot{e} + \dot{e}^T (\tau - C\dot{q} - G - F + J^T(q) F_w - M\ddot{q}_d) + \frac{1}{2}\dot{e}^T \dot{M}\dot{e} - \dot{e}^T C\dot{e}$$

$$\dot{V} = e^T K_p \dot{e} + \dot{e}^T (\tau - C\dot{q} - G - F + J^T(q) F_w - M\ddot{q}_d) + \frac{1}{2}\dot{e}^T (\dot{M} - 2C)\dot{e}$$

Lemma: If $M(q)$ is a $n \times n$ inertia matrix and $C(q, \dot{q})$ is a $n \times 1$ Coriolis and centrifugal vector, then they satisfy following (Li et al., 2015)

$$\dot{e}^T [\dot{M}(q) - 2C(q, \dot{q})]\dot{e} = 0, \quad \forall x, q, \dot{q} \ are \ 7 \times 1 \ vectors$$

$$\dot{V} = e^T K_p \dot{e} + \dot{e}^T (\tau - C\dot{q} - G - F + J^T(q) F_w - M\ddot{q}_d)$$

Choosing $\tau = -K_p e - K_v \dot{e} + M\ddot{q}_d + C\dot{q}_d + G + F - J^T(q) F_w$

$$\dot{V} = -\dot{e}^T K_v \dot{e}$$

$$\dot{V} = -\dot{e}^T K_v \dot{e}$$

$$\dot{V} \leq 0$$

Thus, the stability of the designed controller is guaranteed.

4.4 Simulation with NCMC:

To see the performance of New Compound Model-Based Control, simulations were performed. It is always required to see the simulation result before applying a new controller to a device. Simulations were carried out for many exercises. However, it seems redundant to present all those. Therefore, results are presented here for only three exercises.
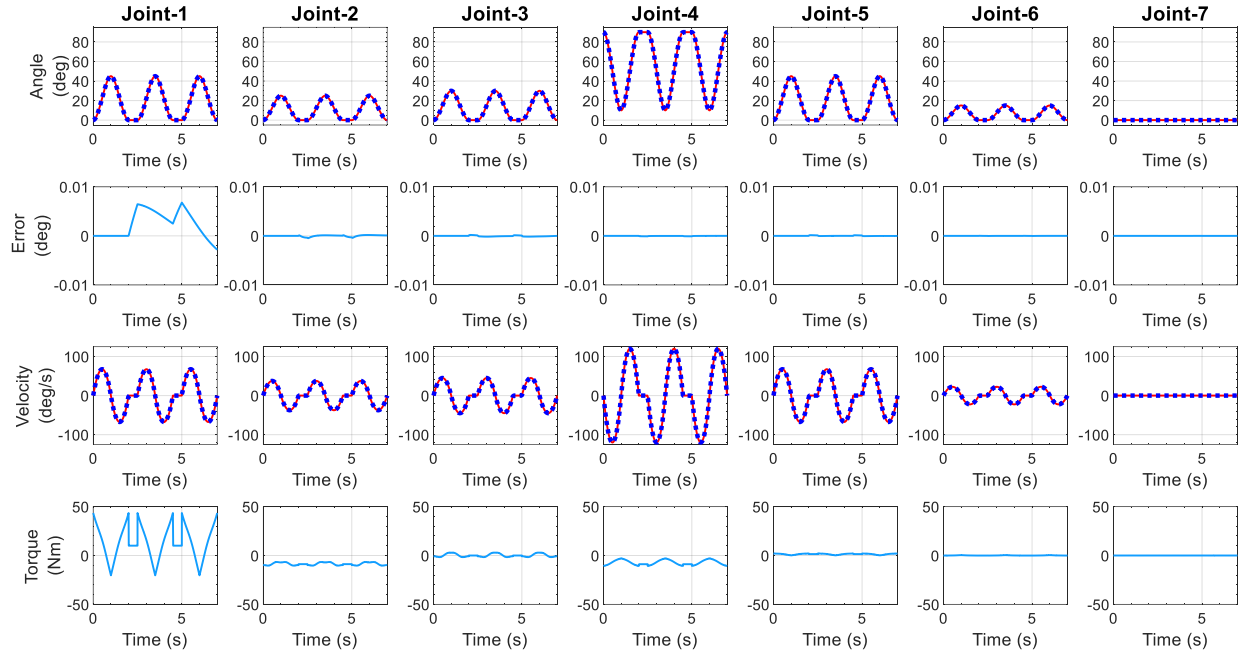
Figure 4.23 Simulation result of simultaneous joint movement exercise with NCMC control

First, the simulation was run for exercise that involves simultaneous movement of all joints except the joint-7 (wrist flexion-extension). This exercise replicates diagonal reaching movement as shown in Figure 4.23. that starts moving from an initial position (all joints are in 0º while the elbow is at 90º position) to the reaching position (abduction 45º, vertical flexion 25º, external rotation 30º, elbow flexion 10º, forearm pronation 45º and wrist ulnar deviation 15º), and then return to the initial position. The exercise is repeated three times, as shown in Figure 4.23.

Second, as the shoulder and elbow cover most of the upper limb workspace, an exercise of diagonal reaching was simulated. This exercise involves 45º shoulder abduction-adduction, 45º shoulder vertical flexion-extension, and 90º elbow flexion-extension. The simulation result is shown in Figure 4.24. It is seen from the simulation result that the position error remains below 0.01º, which shows the effectiveness of the controller.
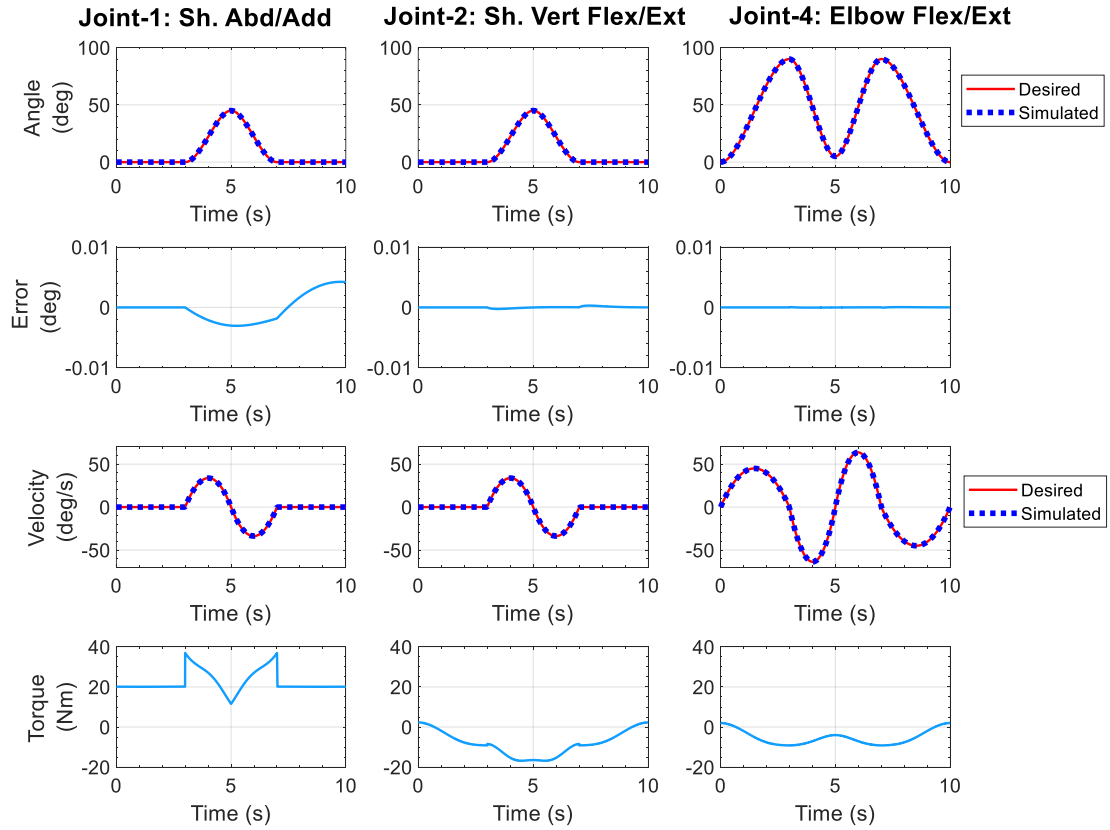
Figure 4.24 Diagonal reaching with NCMC control

The third exercise involves elbow and wrist movement. This exercise was initiated with the elbow being flexed to 45º from zero position. At this position, the elbow maintains gravity for the subsequent wrist motion. The wrist was flexed to 50º and extended to 55º at the end of the exercises. Once again, the position is negligible.
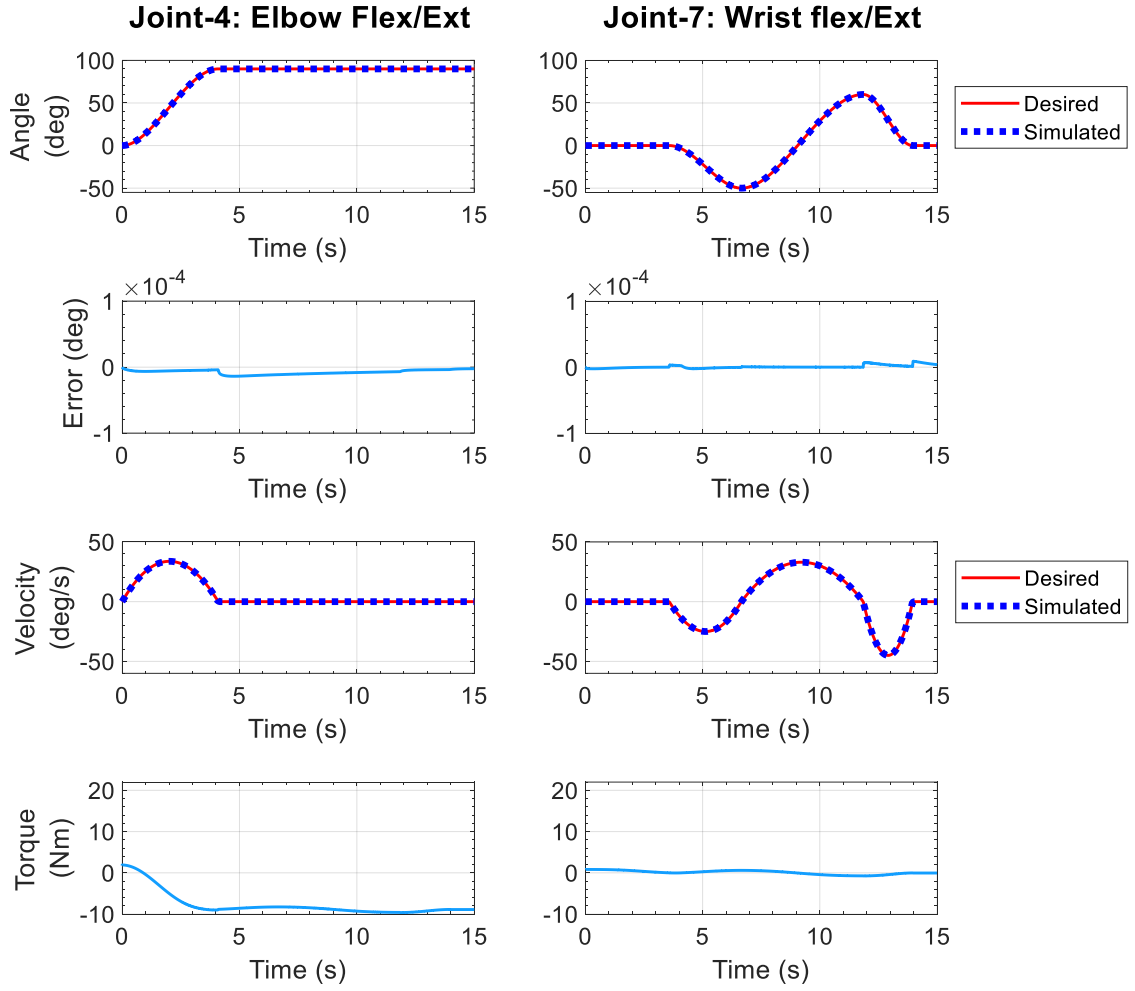
Figure 4.25 Cooperative exercise of elbow and wrist with NCMC control

4.5   Inverse kinematic simulation:

The Jacobian of the proposed exoskeleton robot has been developed according to subsection 3.5 described in chapter-3. The Jacobian (J) of end-effector velocity was developed and expressed in the base frame {0}. MATLAB has been used for the computation of the Jacobian matrix. Basically, an inverse kinematic solution using Jacobian was found for the given cartesian trajectories using equations (3.20) and (3.21) as follows.

$$q = \int \dot{q} \ dt = \int (J^{-1} \dot{x}_d) \ dt$$

Where,

$q \in \mathbb{R}^{7\times1}$ is the vector of joint positions

$\dot{q} \in \mathbb{R}^{7\times1}$ is the vector of joint velocities

$J^{-1} \in \mathbb{R}^{7\times1}$ is the inverse of Jacobian matrix expressed in the robot base

$\dot{x}_d \in \mathbb{R}^{6\times1}$ is the velocity vector of end-effector expressed in robot's base frame

The schematic is shown in Figure 4.26.
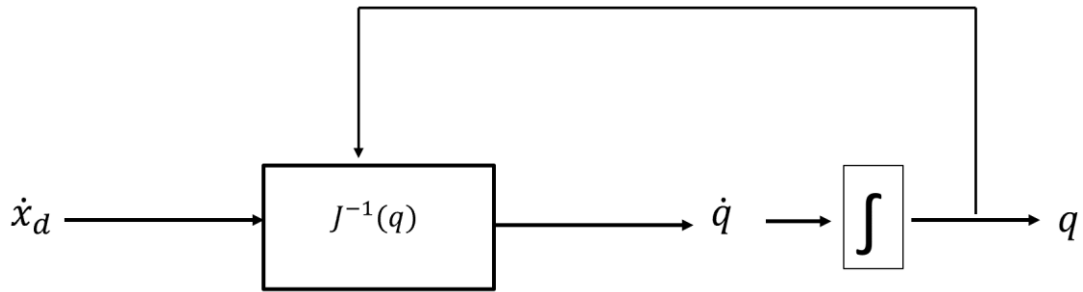
Figure 4.26 Schematic of Inverse Kinematics using Jacobian

The simulation was done for straight lines, squares, and 3D reaching trajectories. The purpose of the simulation was to singularity free solution.

4.5.1 A straight line in the sagittal plane:

In this simulation, as shown in Figure 4.27, the reference position of the proposed exoskeleton robot is parallel to the x-axis, which remains in the sagittal plane (YZ- plane in this case). Cubic polynomial was used to generate the trajectories. The orientation of the end-effector was used to find angular velocities around three cartesian axes. The simulation result is shown in Figure 4.27. In the result, the solid red line stands for the reference position of the end-effector, and the blue dotted line stands for the position computed using inverse Jacobian. From Figure 4.27,

it is seen that reference and computed position is almost overlapped except for at the end. Besides, the end-effector approaches near to the singular solution.
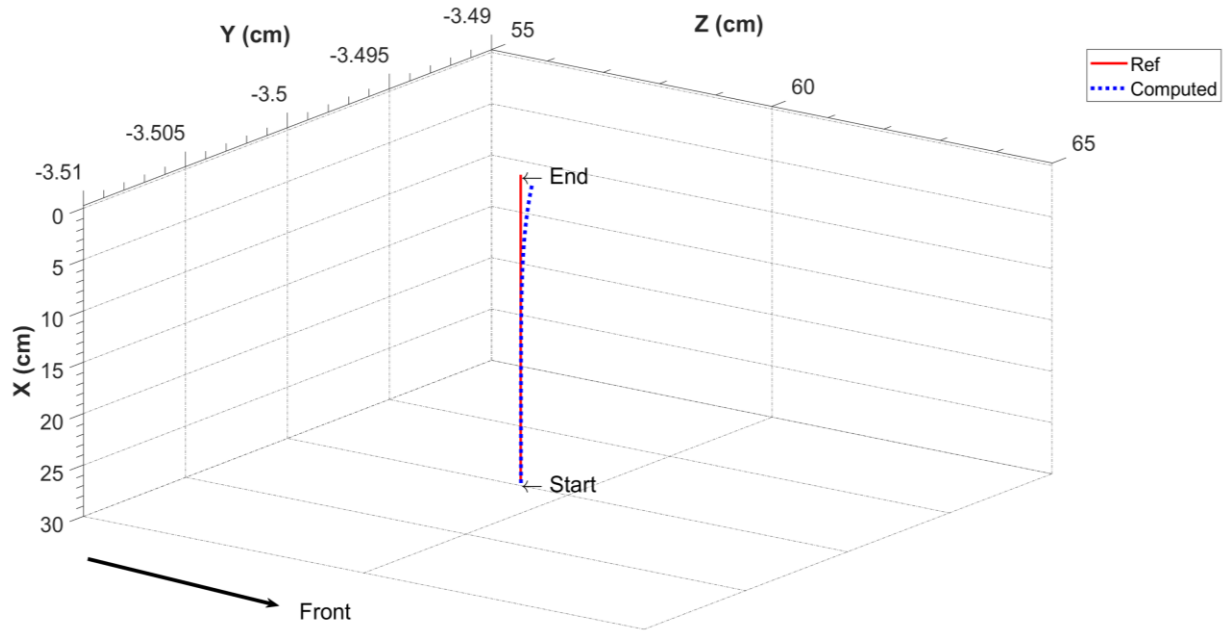
Figure 4.27 Simulation of a straight line in the sagittal plane

4.5.2   A straight line in the frontal plane:

In this simulation, as shown in Figure 4.27, the reference position of the proposed exoskeleton robot was parallel to z-axis, which remains in the frontal plane (XY- plane in this case). From the simulation result, it is seen that the computed position deviates from reference as it approaches towards the workspace boundary of the proposed exoskeleton robot.
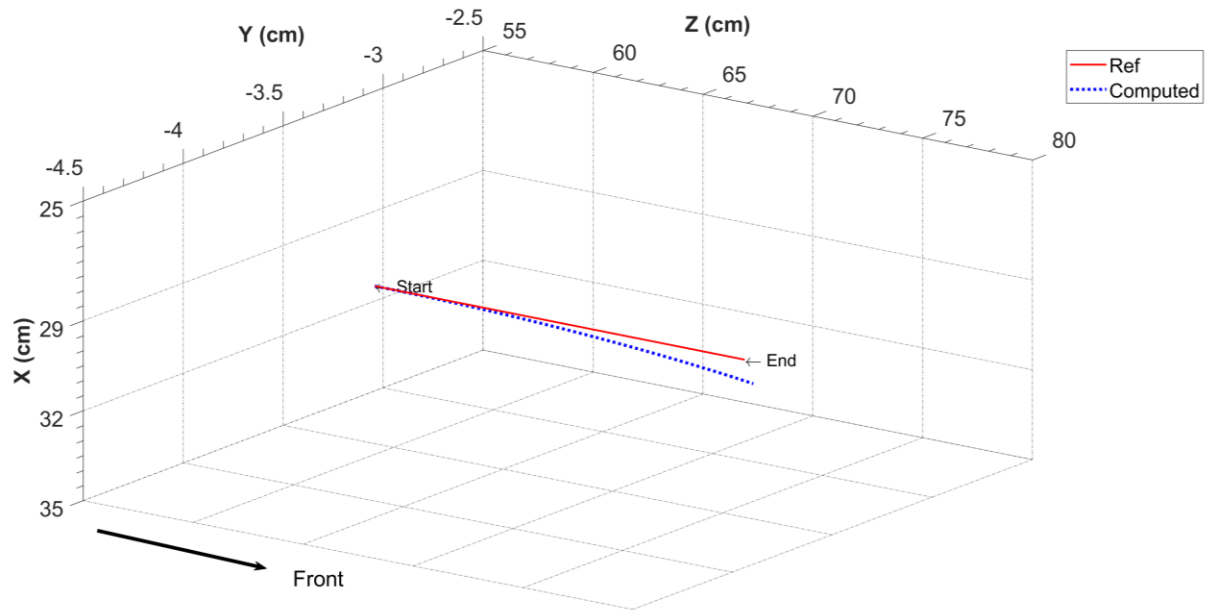
Figure 4.28 Simulation of a straight line in the sagittal plane

4.5.3 Square trajectory

In this simulation, the reference position is a square on the YZ Plane, as shown in Figure 4.29. The end-effector follows the reference position in a clockwise direction. From the simulation result, it is seen that the Jacobian of the proposed robot is able to generate an inverse kinematic solution for the given reference positions.
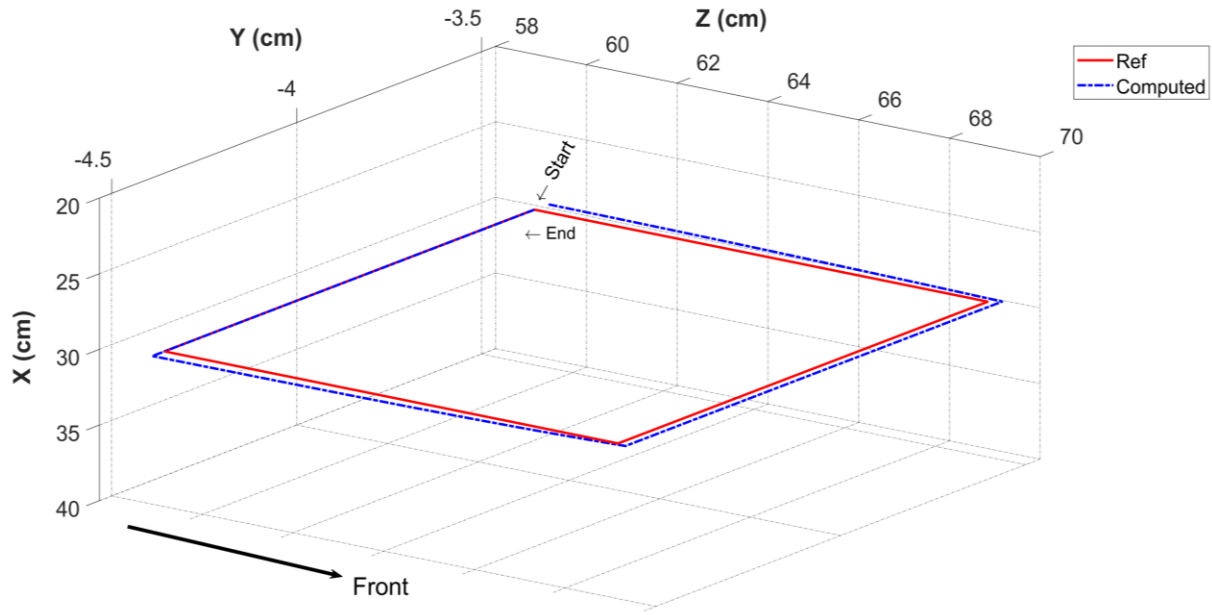
Figure 4.29 Square trajectory

4.6 Conclusion

In this chapter, simulations were carried out with individual joint movement, simultaneous joint movement, and different cooperative exercises. The simulations were also conducted for a new proposed controller. The trajectory tracking graph from each simulation shows the good performance of the controller. Moreover, simulation of inverse kinematics based on Jacobian was performed to see the usefulness of Jacobian.

CHAPTER-5   VIRTUAL REALITY REHABILITATION

Section-1 of this chapter describes virtual reality, whereas section-2 presents the detailed development of virtual reality-based rehabilitation for the developed exoskeleton system. Section-3 describes the virtual reality designed for rehabilitation with the developed exoskeleton system.

5.1   Virtual reality:

Virtual Reality is designed for the user to interact with a simulated "real" environment via computer hardware and software (Holden, 2005). In virtual Reality-based rehabilitation, the user gets visual feedback and interact with virtual environments. The visual feedback may be presented on a flat screen, projector, or any other display.

5.2   Motivation:

Virtual Reality (VR) based rehabilitation has been promising in stroke rehabilitation. It may be advantageous as it offers several neuro-rehabilitation principles (e.g., goal-oriented task and feedback). These principles have already shown to be useful in neuro-rehabilitation (Langhorne et al., 2011; Laver et al., 2017; Shin et al., 2016)(Langhorne 2011; Veerbeek 2014). Previous studies clearly show promising results of Virtual Reality being used in upper limb rehabilitation. In this research, the VR based rehabilitation system was developed for our exoskeleton robot system to offer goal-oriented rehabilitation, explicit feedback, and implicit feedback.

5.3   Virtual reality in the rehabilitation with developed exoskeleton robot:

In this project, the subject's hand position (end-effector position) is linked to a sphere in Virtual Reality (VR). Therefore, when a subject moves his/her hand while performing a rehabilitation exercise, the sphere moves in VR display. Besides, the subject's hand position is

displayed in real-time on the Graphical User Interface (GUI) in Unity3D. A scene for elbow exercise is shown in Figure 5.1, whereas Figure 5.2 shows the experimental setup for VR based rehabilitation with the developed exoskeleton system.

Figure 5.1 Virtual reality scene for the developed exoskeleton system
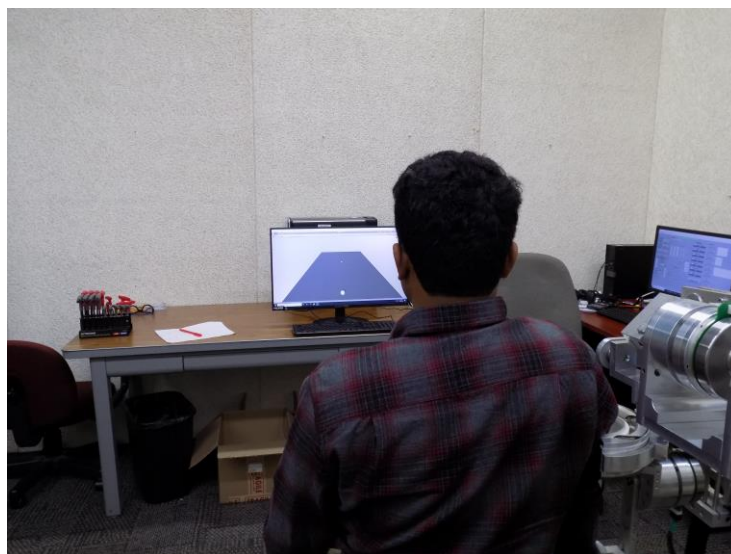
Figure 5.2 Experimental set up for VR based rehabilitation with the developed exoskeleton system

157

5.3.1 Platform – Unity3D:

The VR in the current research was developed in the Unity3D platform (Unity Technologies Inc, San Francisco, USA). Though it's a game development software, it has been extensively used in virtual reality (Kucera et al., 2018; Nguyen and Dang, 2017; Wang et al., 2010). The operating system for unity 3D includes Windows and Mac OSX. The game object, data acquisition and processing, and GUI can be done using any of the three programming (scripting) languages: JavaScript, C#, and Boo (a dialect of python). Generally, scripting is considered as a slow method, but in Unity3D, scripts are compiled to native code and run nearly as fast as C++. In this research, C# was used to get and transform the game object (sphere).

5.3.2 Framework:

Two layers of framework, namely data layer and presentation layer, was used in VR development.

Data layer: it includes data generated while performing rehabilitation exercises (i.e., end-effector position and joint position).

Presentation layer: it is mainly used to show objects in a graphical user interface and real-time data.

5.3.3 VR interface for the developed exoskeleton system:

The developed VR system is depicted in Figure 5.3. The end-effector position of the robot from LabVIEW was sent to the remote host PC using UDP (User Datagram Protocol) communication protocol. For three positions (x , y, and z position of end-effector with respect to base), three dedicated ports were used. The Unity3D on the remote host PC used a C# script to

read those positions. Using another C# script and the data, the position of the game object (i.e., the sphere) was transformed into the unity interface (see Figure 5.1). A timer was set to show elapsed time during rehabilitation. Besides, a C# script was made to render the trail of the sphere. The static game objects were used to display floor, start, goal/target to reach, and so on. The processing in Unity3D Figure 5.4
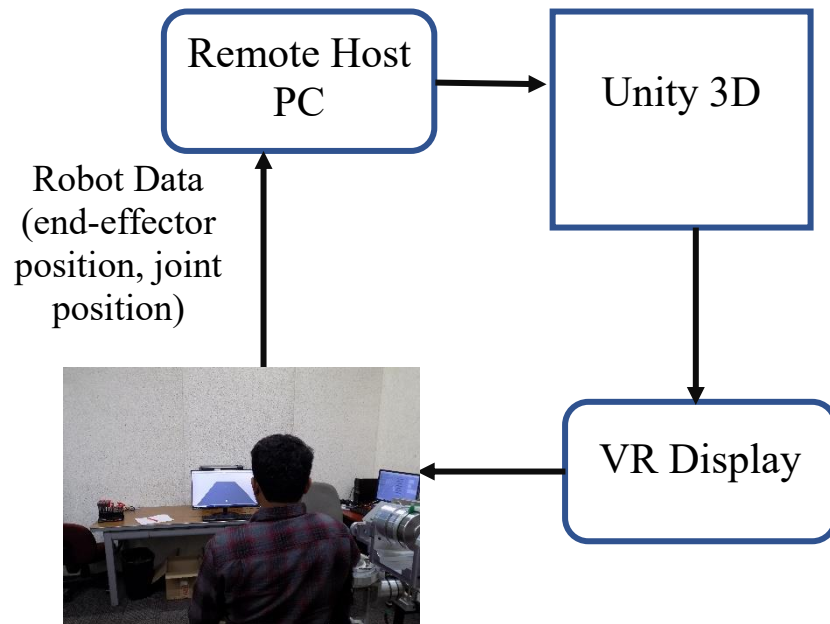
Figure 5.3 Schematic of VR developed for the developed exoskeleton system
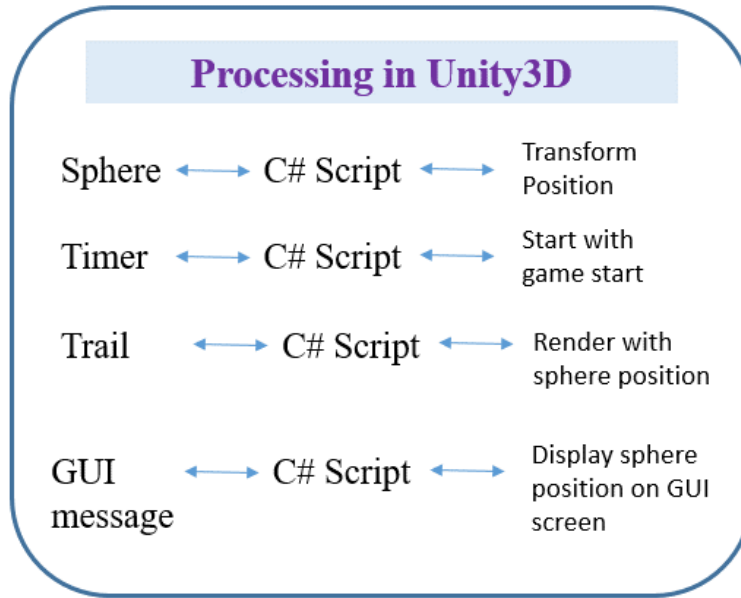
Figure 5.4 Work done in Unity3D for the VR of our exoskeleton robot

5.3.4 VR for different exercises:

VR was developed for both passive and active exercises. For example, VR interface is developed for passive elbow rehabilitation, where the subject can see the sphere moves with the elbow flexion-extension. The end-effector's position and elbow joint angle is also displayed in the GUI. VR was made for other passive rehabilitation exercises as well. For example, a cartesian exercise where the developed exoskeleton robot moves in a transverse (horizontal) plane is shown in Figure 5.5.

Figure 5.6 shows VR interface of an active exercise, where the subject is asked to reach the goal in the YZ plane.

Another example of an active exercise is to move the elbow from a start position to a goal shown in Figure 5.7. There are more game scenes developed in this research to provide VR for other exercises such as reaching a goal in the frontal plane.

Figure 5.5 VR for a cartesian exercise in the horizontal plane.
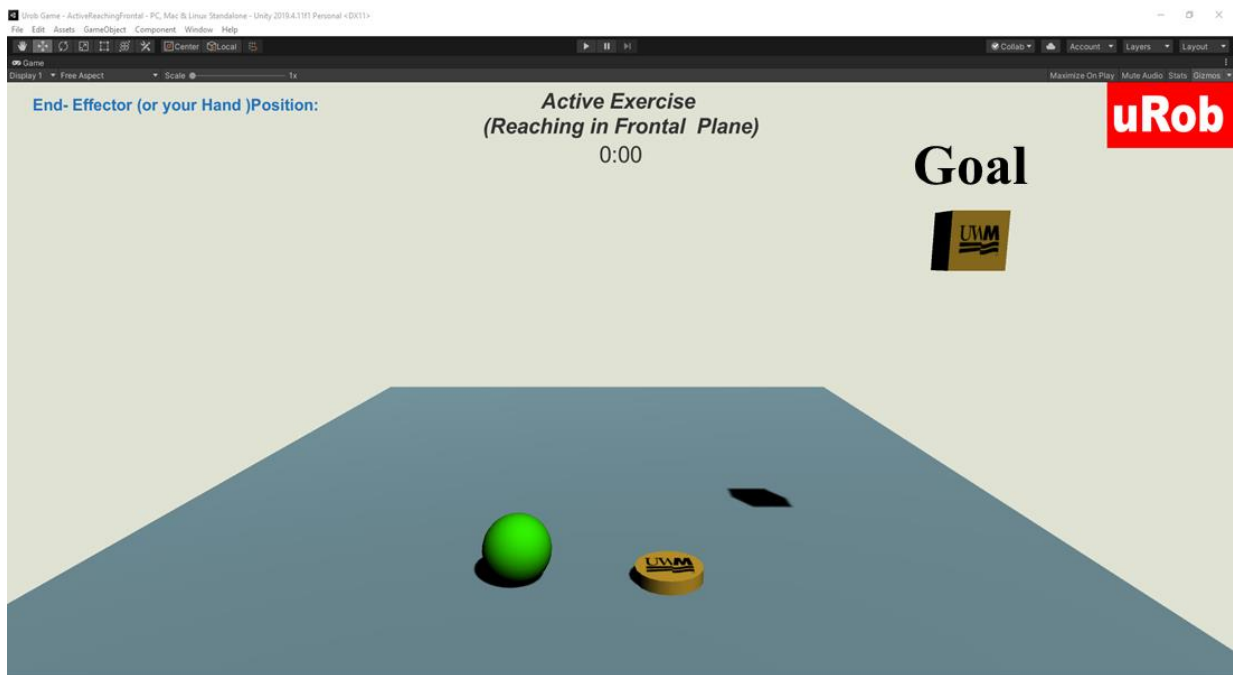
Figure 5.6 VR Reaching a goal in the YZ plane
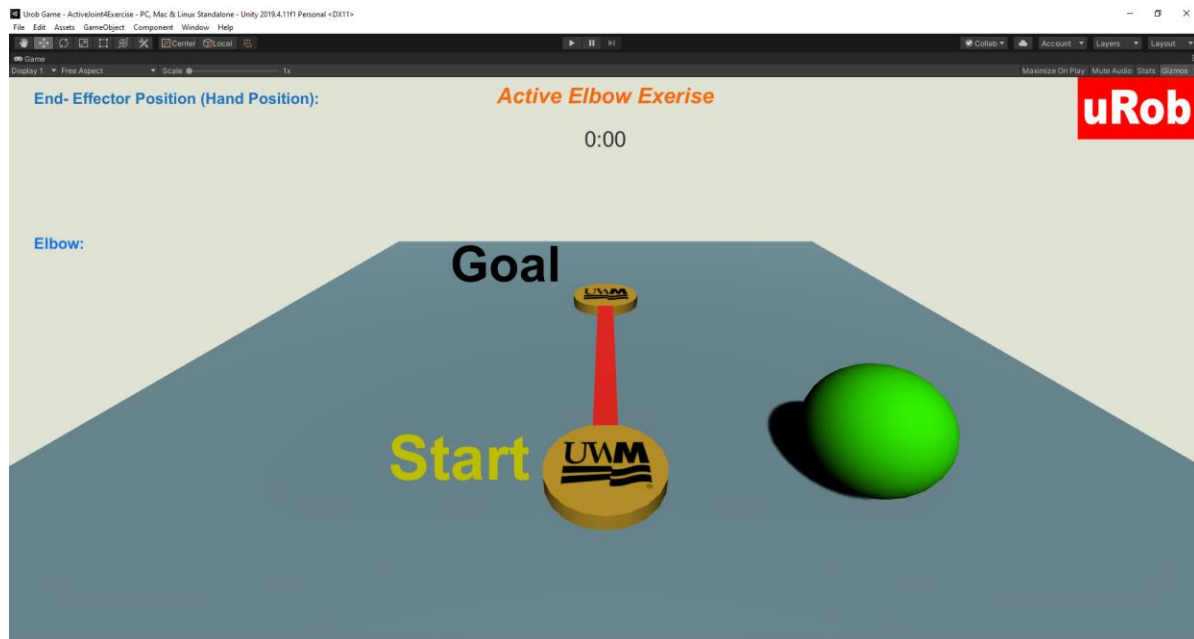
Figure 5.7 VR for active elbow exercises, where subject is asked to reach a goal in the frontal plane

CHAPTER-6   EXPERIMENTAL RESULTS

This chapter presents the experimental results with our developed exoskeleton robot and the proposed controller to provide upper limb rehabilitation therapy. Experiments were conducted with five healthy participants. Figure 6.1 shows the type of exercises used in the experiments. The experiments were conducted with a linear Proportional Integral Derivative (PID) control, and a non-linear model-based control named New Compound Model-based Control (NCMC). Performance comparison of the proposed NCMC and PID is presented in Section 6.7. Besides, to validate the use of force values in active exercises, experiments were conducted to see corresponding muscle activity (i.e., Electromyography signals) of biceps and triceps. Results from these experiments are presented in Section-8.

6.1   Exercises with the developed exoskeleton robot

Depending on the severity of upper limb impairment and rehabilitation stages, different rehabilitation exercises are used in rehabilitation programs. In this research, the developed exoskeleton robot was used to provide similar rehabilitation exercises, including passive and active rehabilitation therapies. Note that passive movement therapies are useful for ROM improvement, whereas active therapies are carried out to increase limb's strength. Figure 6.1 shows the types of rehabilitation exercises that were considered in our experiments; it also shows the corresponding *'Principles of Neuro-Rehabilitation'* that can be fulfilled by the proposed exercises.

The experiment was conducted with healthy five healthy subjects (age: 28 ± 3 years, weight: 165 $\pm$ 30 lbs, height: 5 ft 5 inch $\pm$ 5 inch). The UWM Institutional Review Board approved the study

(**IRB#:**19.064; **Study title:** Experiment of the human natural range of motion with developed robotic device for upper limb rehabilitation.
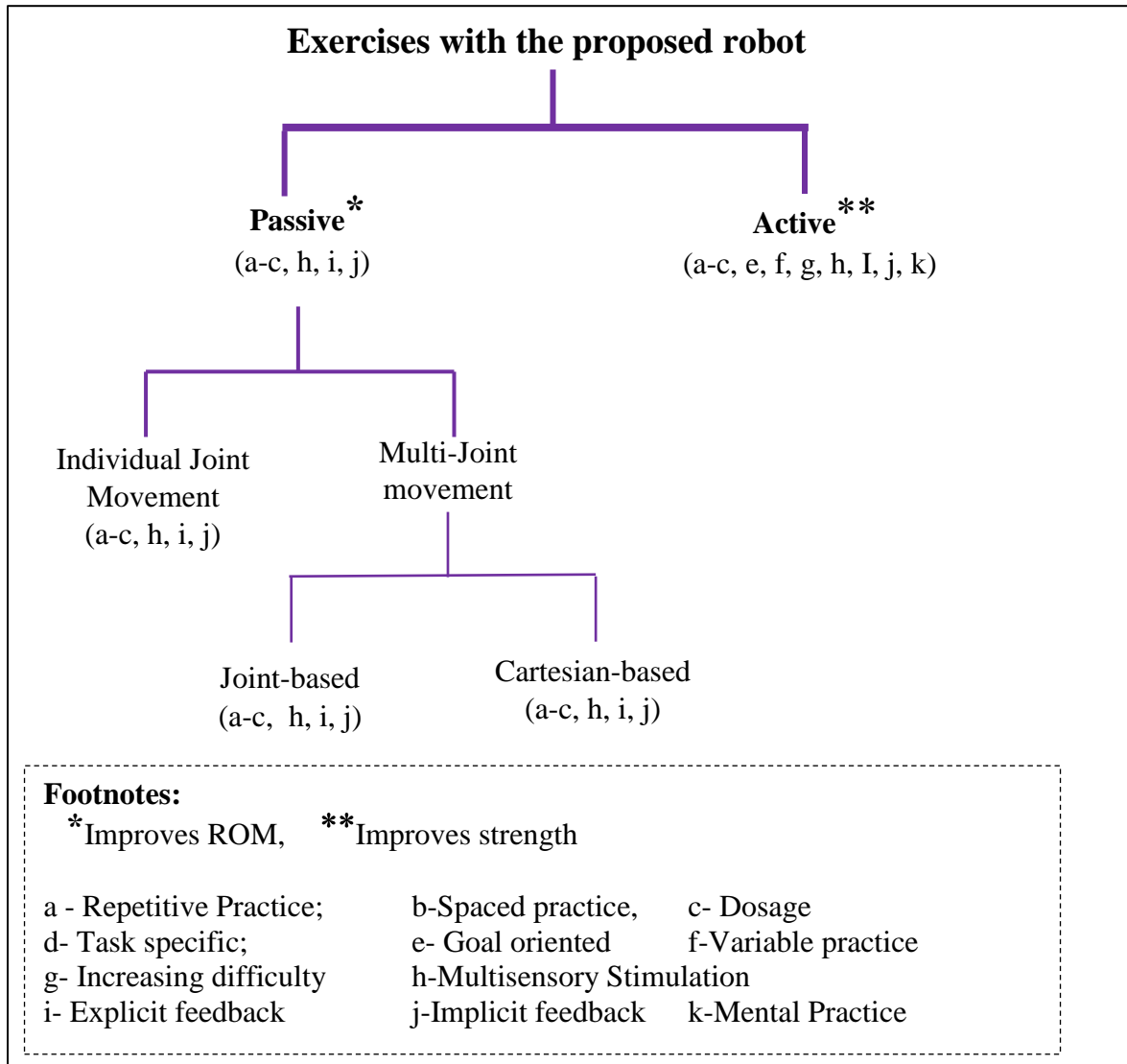
Figure 6.1 Exercises with the Exoskeleton robot

6.2 Principles of neuro-rehabilitation followed by the proposed exoskeleton robot

As the proposed exoskeleton robot is meant to rehabilitate post-stroke mobility impairment, this research considers the following neuro-rehabilitation principles (Maier et al., 2019).

- **Repetitive practice** - the proposed robot can perform the exercises repetitively.

- **Spaced practice -** It can do the spaced practice.

- **Dosage** – It can perform therapy for the given duration and frequency.

- **Goal-oriented practice-** The virtual reality developed for the proposed robot enables it to do goal-oriented exercises.

- **Variable practice –** Active exercises with the proposed robot allow the user to do the variable practice.

- **Increasing difficulty** – The difficulty level can be adjusted in the proposed exoskeleton robot by changing the amplification of user input forces.

- **Multi-sensory stimulation** –Virtual reality displays the performance to the user.

- **Explicit feedback** – Explicit feedback such as hand/end-effector position is incorporated in the virtual reality.

- **Implicit feedback** – It is obtained in terms of performance shown in (game) virtual reality

- **Mental Practice –** This principle can be followed by showing previously recorded games and session videos to the user.

6.3 Experimental setup and control implementation:

Figure 6.2 illustrates the experimental setup of the developed exoskeleton robot system. All joint motors are equipped with hall sensors. The hall sensors data were used to measure the position of the robot joints. The sampling frequency for reading hall sensor data was 100µs.
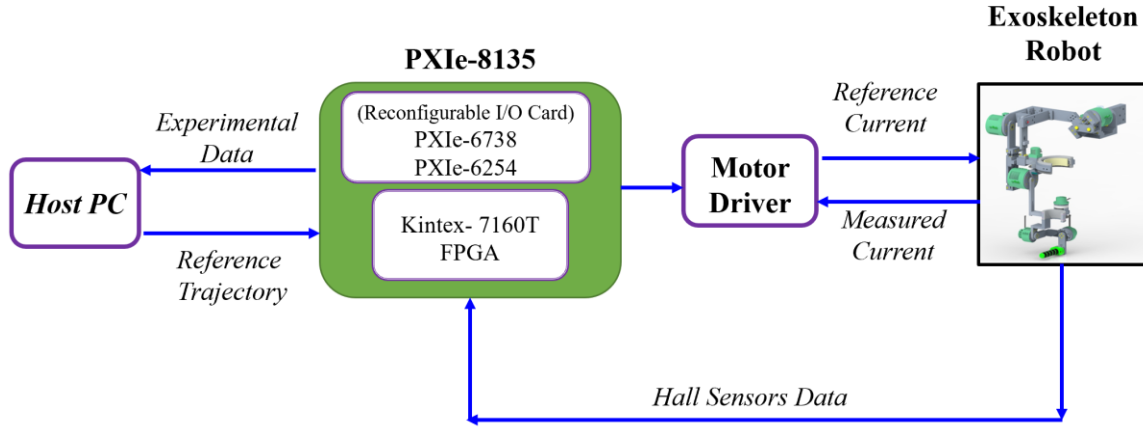
Figure 6.2 Experimental setup of the developed exoskeleton robot system

6.4 Passive rehabilitation with the proposed exoskeleton robot

The passive rehabilitation exercise carried out in the experiments were adapted from the recommended library of exercises from the standard rehabilitation therapy protocol (FlintRehab, 2020; WebMD, 2020). The exercises were converted to a pre-defined trajectory for the robot to follow. The experiments were conducted for both individual joint and multi-joint movements. To demonstrate the experimental results, plots of joint position vs. time, error between the reference and actual position, velocity vs. time, and torque vs. time are presented. Also, force sensors data from one 3-axis force sensor instrumented at the wrist joint and three one axis force sensors instrumented with upper arm cuff are plotted. The red dotted line stands for reference (desired) value in the position and velocity tracking, whereas the solid blue line stands for the actual value. Note that the experiments presented in Sections 6.4.1 to 6.4.4 were performed with the proposed NCMC.

6.4.1 Experimental results for individual joint movements:

Experiments were conducted for all the individual joint movement of the upper limb. These kinds of exercises involve the movement of the particular joint of the robot.

166

Shoulder Abduction-Adduction exercise:
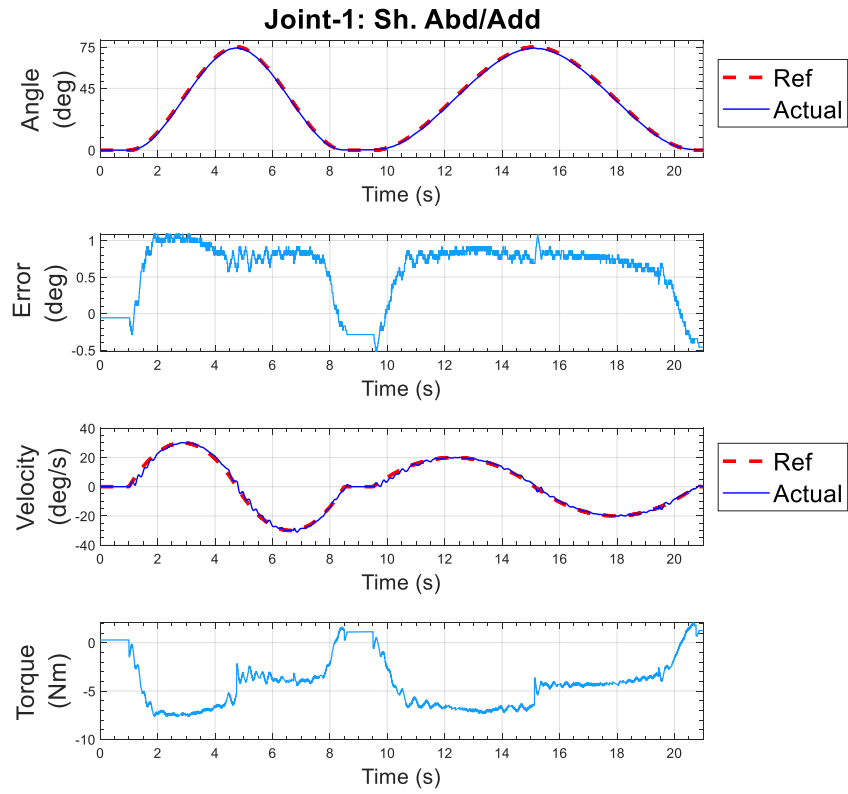
Figure 6.3 Individual joint exercise, shoulder abduction-adduction
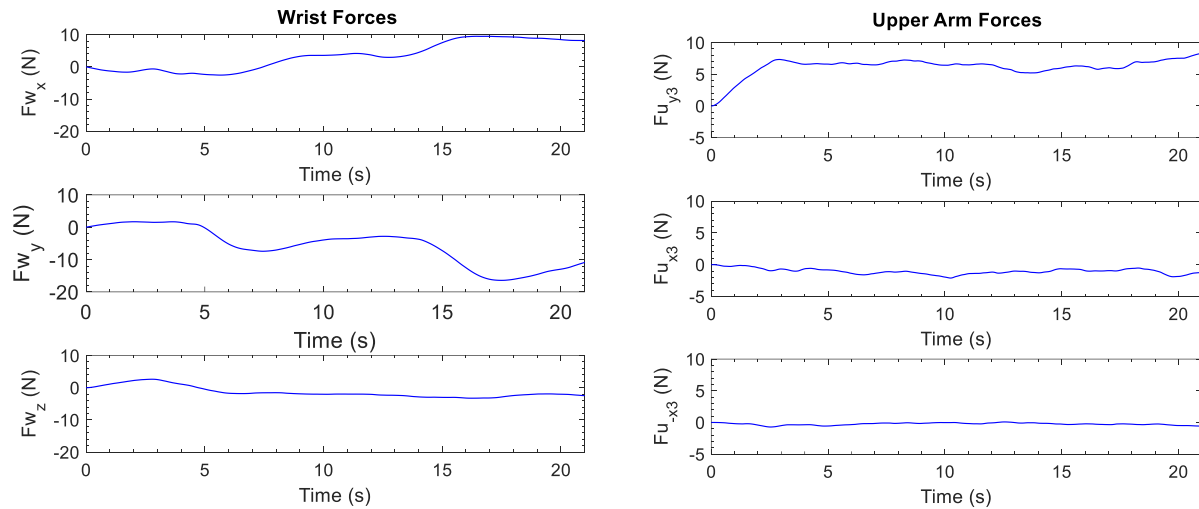
Figure 6.4 Subject's forces during shoulder abduction and adduction

This repetitive exercise was initiated with all joints at zero position, and then the shoulder was abducted to 75º and returned to 0º. After a second, the same movement was repeated with a slower velocity. The result of the experiment is shown in Figure 6.3. From the figure's topmost plot, it is clearly seen that the actual position and reference position is almost overlapped, meaning the proposed exoskeleton robot followed the given (reference) position. The maximum error for position tracking was found 1.09º, which shows the excellent tracking performance of the controller. The maximum velocity during the first and second repetition was 30 deg/s and 20 deg/s, respectively.

The force exerted by the subject at the wrist and upper arm are shown in Figure 6.4. The figure shows that subject interacted mostly at the x and y-axis of the end-effector. At the upper arm, most interactions happened in the positive y8-direction of the end-effector. These results demonstrate the interaction/ resistance between the subject and the proposed exoskeleton robot. This resistance can be quantified and read on an appropriate scale to measure the user's discomfort, stiff arm, and so on.

Shoulder vertical flexion-extension exercise:

This repetitive exercise was initiated with all joints at zero position, and then the shoulder was vertically flexed to 170º and returned to 0º. The exercise was repeated with a slower velocity. The experimental results are shown in Figure 6.5. The maximum error for position tracking was found around 0.91º, which shows the excellent tracking performance of the controller. The maximum velocity during the first and second repetition was 60 deg/s and 45 deg/s, respectively. The force plots are shown in Figure 6.6. It is seen that subject

mostly exerts forces along the x3-axis at the upper arm. During shoulder joint vertical flexion, the force sensor interacts with the subject most.
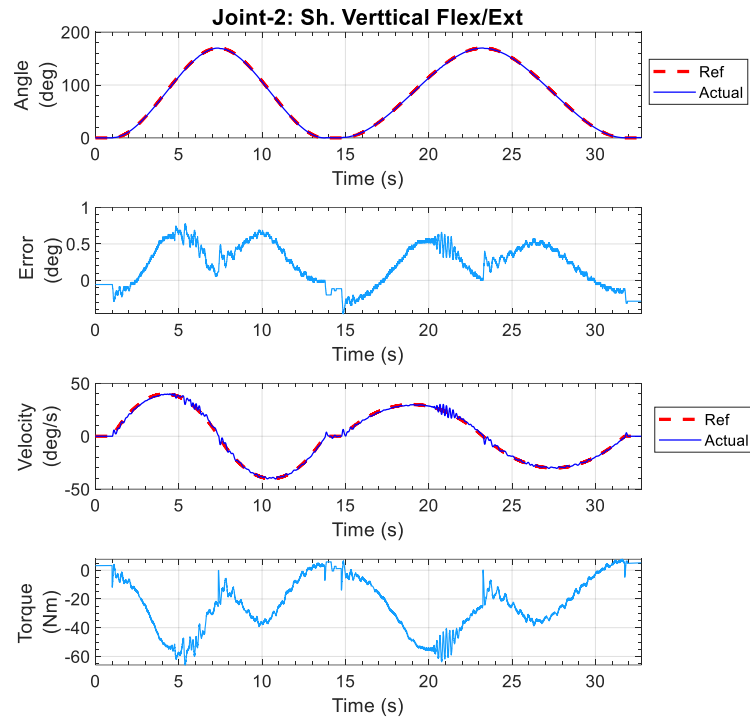
Figure 6.5 Individual joint exercise, shoulder vertical flexion-extension
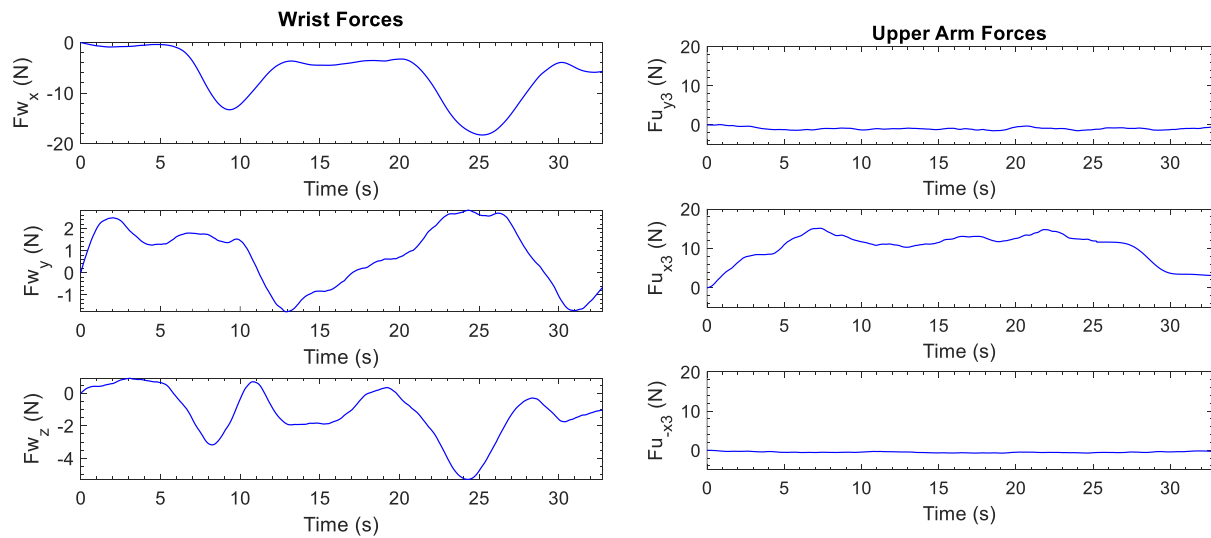
Figure 6.6 Subject's forces during shoulder vertical flexion-extension

169

Upper Arm internal-external rotation exercise:

This exercise was initiated with all joints at zero position except the elbow at 90º. After that, the upper arm is externally rotated to 30º and returned to 0º. After staying at the initial position for two seconds, the upper arm is internally rotated to 60º. The experimental result is shown in Figure 6.7. The maximum error for position tracking was found around 1.05º. The maximum velocity during the exercise was 30 deg/s. The force plots are shown in Figure 6.8.
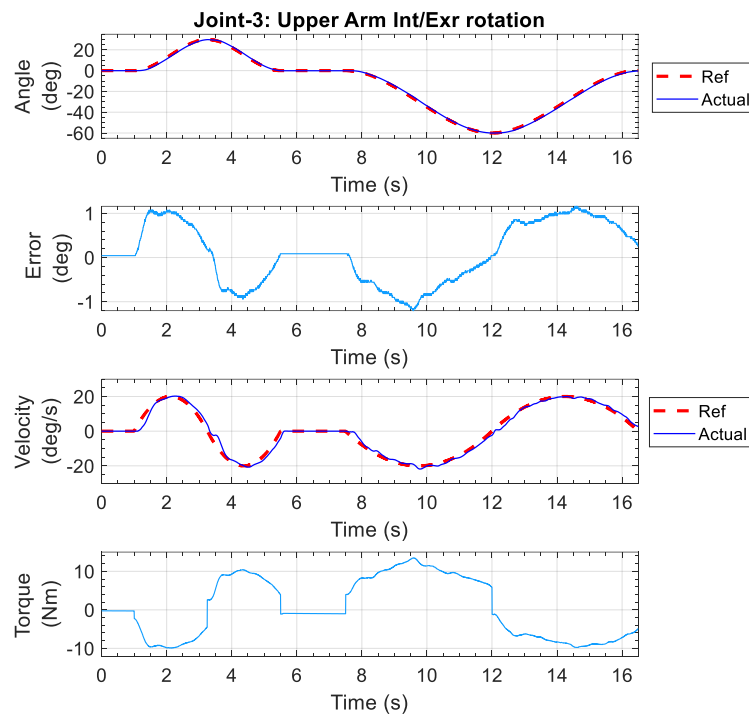
Figure 6.7 Individual joint exercise, upper arm internal-external rotation
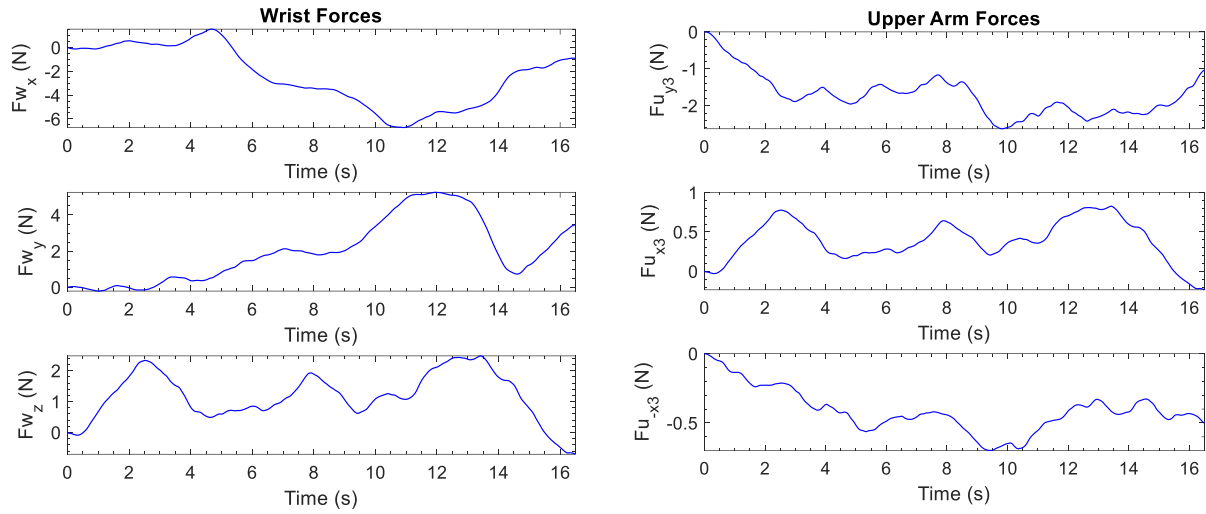
Figure 6.8 Subject's forces during upper arm internal-external rotation

Elbow flexion-extension exercise:

In this experiment, the elbow flexion-extension motion was performed and repeated three times. This exercise was initiated with elbow joint angle at 90º; all other joints remained at zero position. The experimental result is shown in Figure 6.9. The maximum error for position tracking was found around 1.17º. The peak velocities for the repetitions were 60 deg/s, 30 deg/s, and 20 deg/s, respectively. The force plots are shown in Figure 6.10.
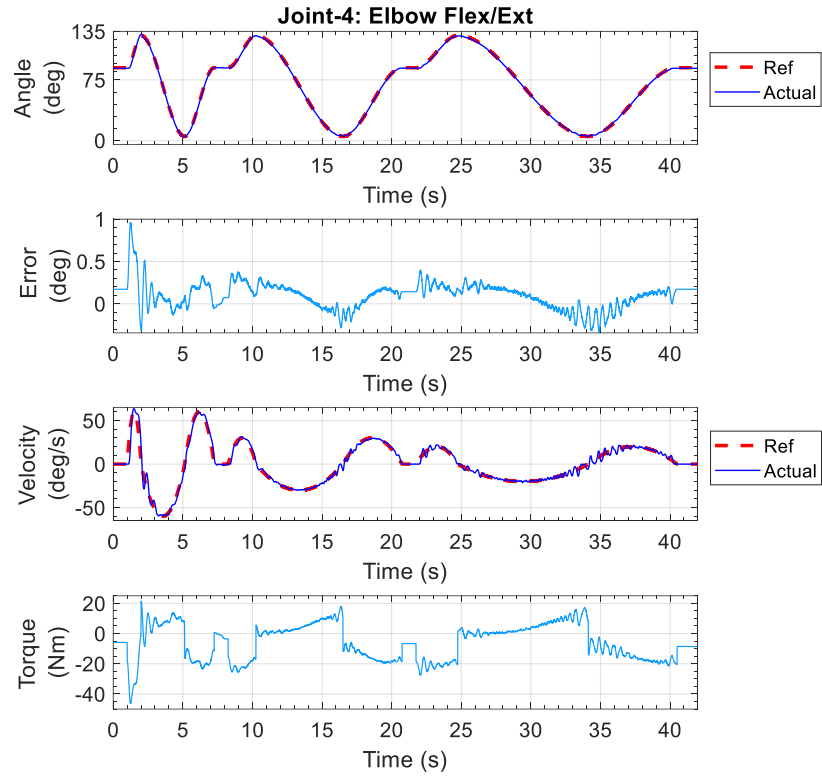
Figure 6.9 Individual joint exercise, elbow flexion-extension.
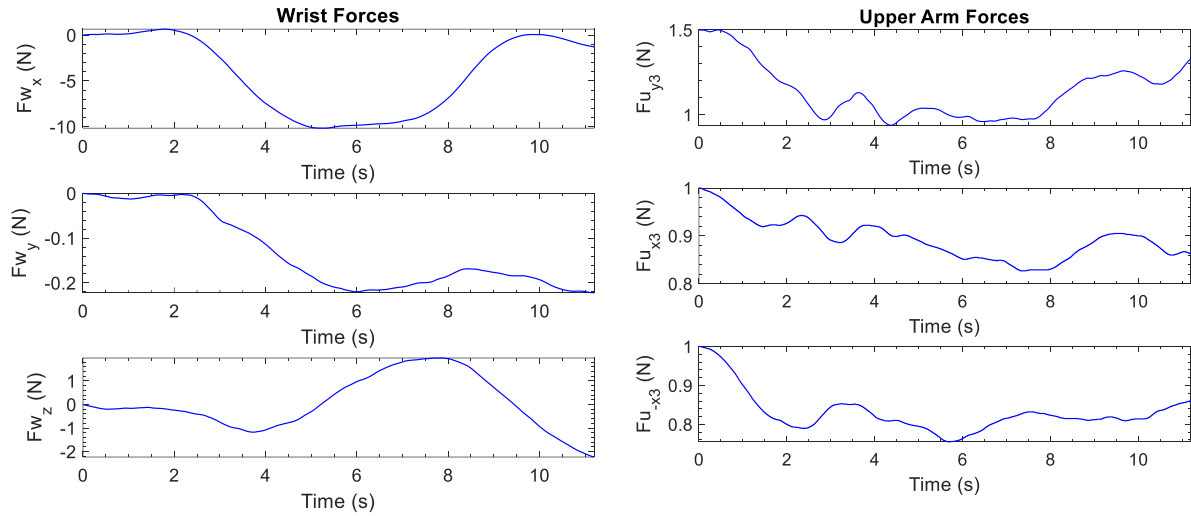
Figure 6.10 Subject's forces during elbow flexion-extension

Forearm pronation-supination exercise:

This exercise was initiated with all joints at zero position except the elbow at 90º. After that, the forearm is pronated to 75º. Then it was supinated to 75º and finally returned to 0º. During this time of the experiment, the elbow joint always stays at 90º and maintains gravity. The experimental result is shown in Figure 6.11. The maximum error for position tracking was found around 1.6º. The maximum velocity during the exercise was 45 deg/s. The force plots are shown in Figure 6.12. It is seen from the figure that subject has negligible interaction with the upper arm cuff.
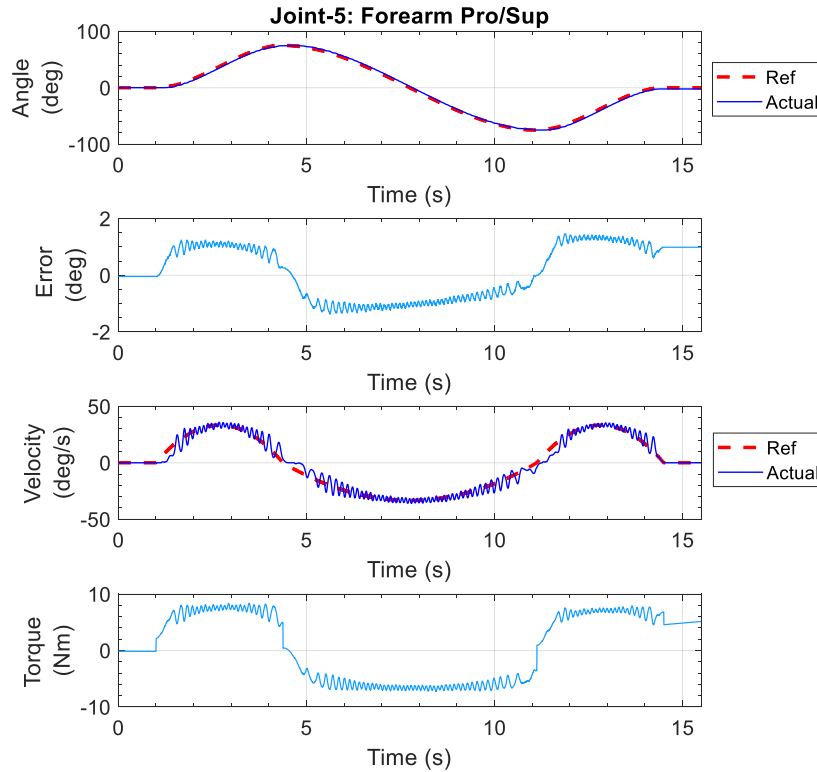
Figure 6.11 Individual joint exercise, forearm pronation-supination.
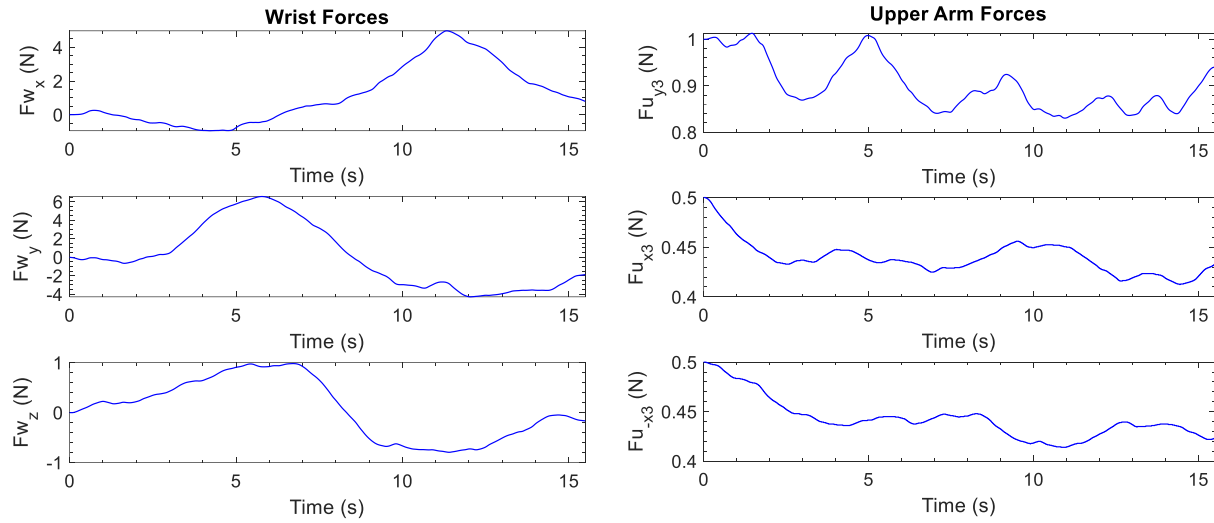
Figure 6.12 Subject's forces during forearm pronation-supination

Wrist Radial-Ulnar deviation exercise:
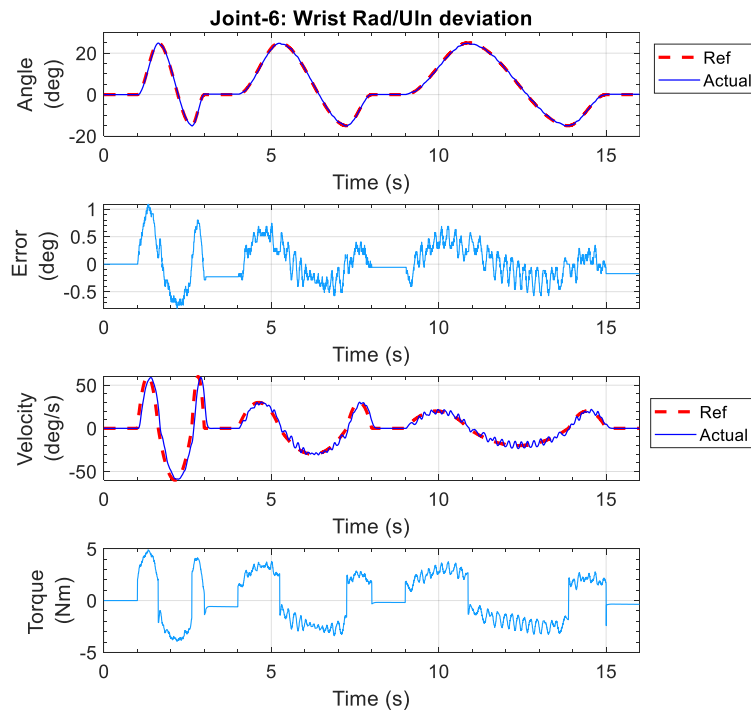
Figure 6.13 Individual joint exercise, wrist radial-ulnar deviation.

In this exercise, the exoskeleton moved subject arms through 20º ulnar deviation and 15º radial deviation. The movement was started from the elbow at 90º and maintained this

position during the experiment. The movement was repeated three times with different velocities. The peak velocities for the repetitions were 60 deg/s, 30 deg/s, and 20 deg/s, respectively. The results are shown in Figure 6.13 the maximum tracking error was observed around 1º. The force plot is shown in Figure 6.14. Only wrist forces are shown as upper arm force is not dominant for this exercise.
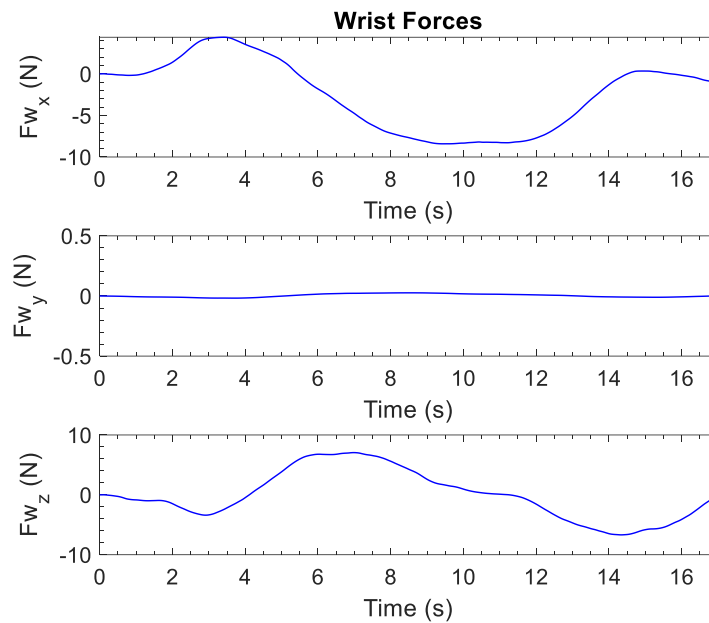
Figure 6.14 Subject's wrist forces during radial-ulnar deviation

Wrist flexion-extension exercise:

This repetitive exercise initiated with elbow joint angle at 90º angle and maintained that position during the experiment. All the other joints remained in zero position. From the initial position, the wrist was extended to 55º and then flexed to 50º. The exercise ended with the wrist returned at the initial position. The trajectory tracking results are shown in Figure 6.15. Once again, the error of position tracking is observed less than 1º. The force plots are shown in Figure 6.16.

175
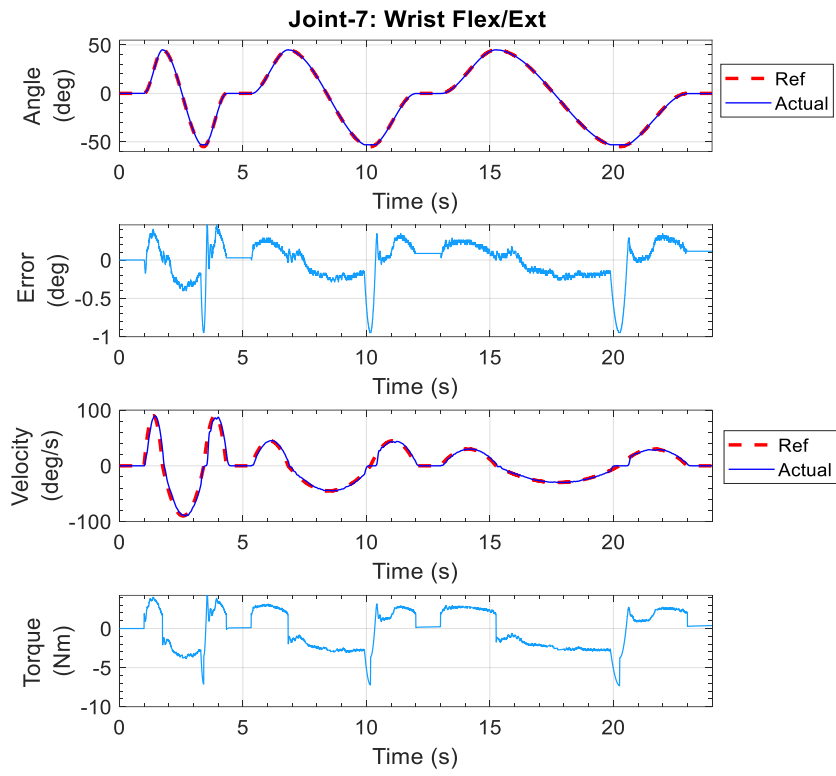
Figure 6.15 Individual joint exercise (Wrist flexion-extension)
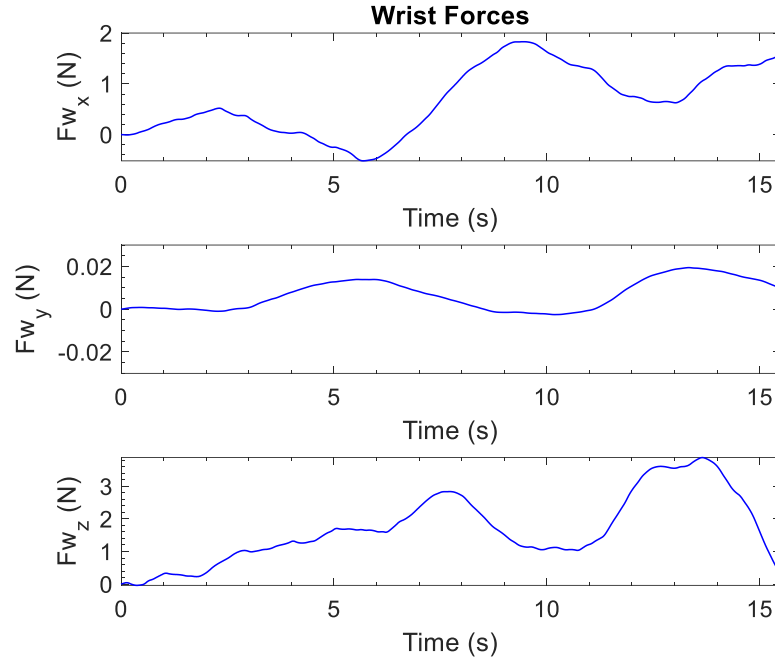
Figure 6.16 Subject's wrist force during wrist flexion-extension

6.4.2 Experimental results for multi-joint movements:

Simultaneous joint movement of shoulder, elbow, and wrist:

This exercise involves simultaneous movement of all joints except the joint-7 (wrist flexion-extension). It replicates a diagonal reaching movement that starts moving from an initial position (all joints are in 0º while the elbow is at 90º position) to the reaching position (abduction 15º, vertical flexion 90º, external rotation 45º, elbow flexion 10º, forearm pronation 45º and wrist ulnar deviation 15º), and then return to the initial position. The exercises are repeated three times, as shown in Figure 6.17. The results show that our developed exoskeleton robot follows the reference trajectory. From the figure, it is seen that the position for all the joints remained below 2º. The maximum error (1.85º) was found for the elbow joint. The force plots are shown in Figure 6.18.
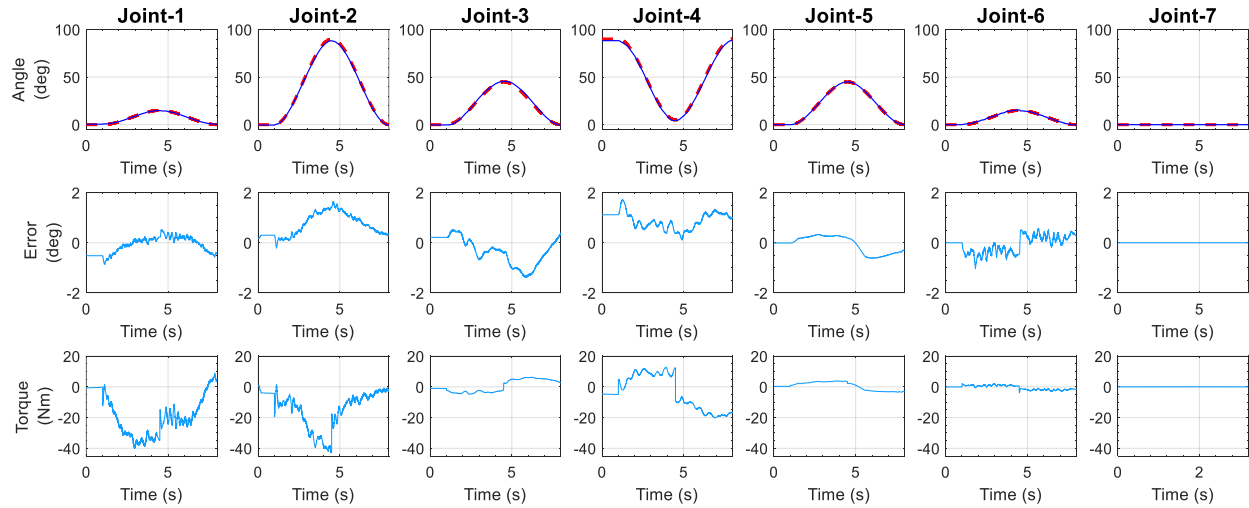
Figure 6.17 Experimental result for the movement (a diagonal reaching) of all joints but joint-7
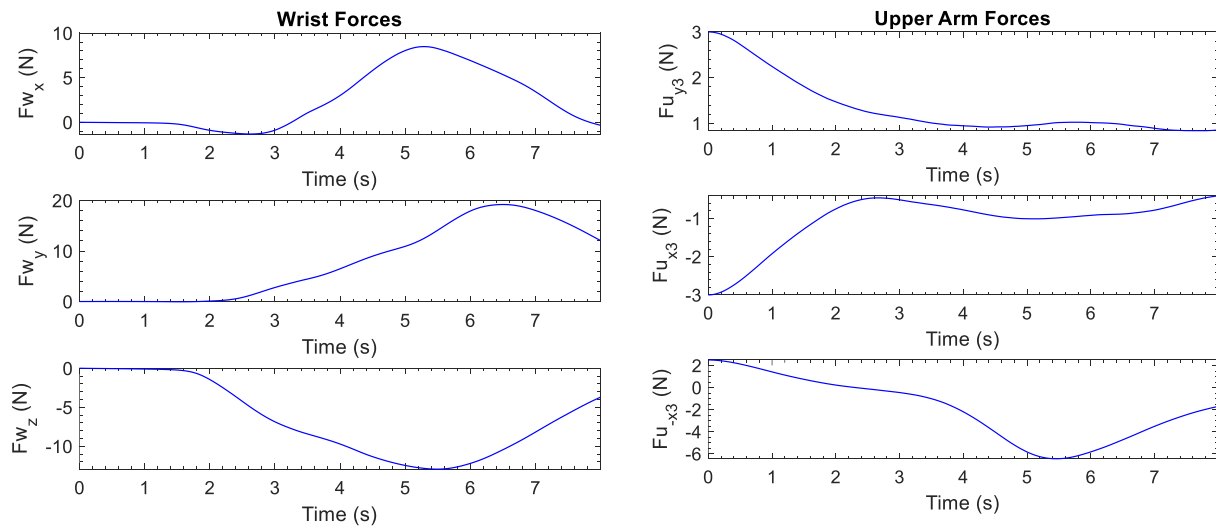
Figure 6.18 Subject's forces during the simultaneous joint movement

Diagonal reaching exercise:

This diagonal reaching exercise comprised of shoulder, elbow, and wrist joints movements. The exercise was initiated with the elbow at 90°. Then, the shoulder joint is abducted from 0° to 45° and adducted back to 0° at the end of the exercise. The shoulder was also vertically flexed from 0° to 90° and extended back to 0° at the end of the training. During

178

the movement of the shoulder, the elbow was extended to zero and returned to 0º. In the meantime, the wrist was extended to 50º and returned to zero. The experimental results are shown in Figure 6.19. The maximum error between the reference and actual position was observed around 1.81º in joint 4.
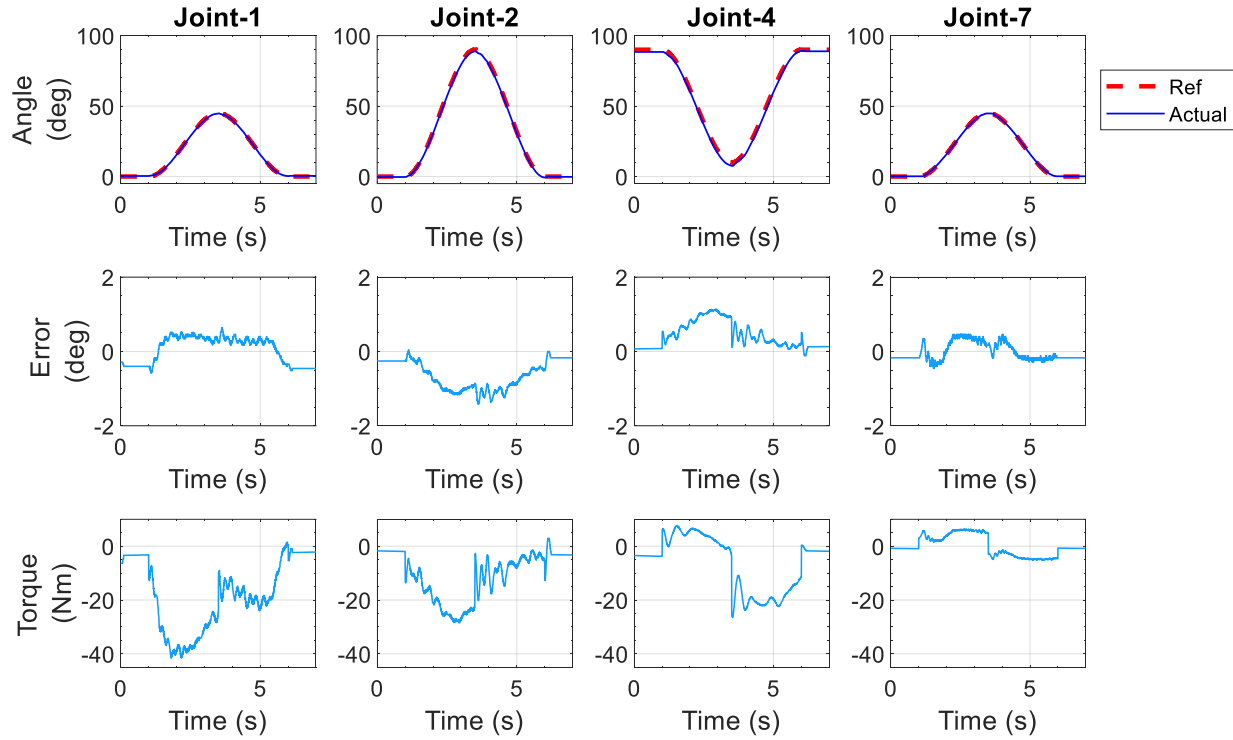
Figure 6.19 Experimental results of diagonal reaching exercise

6.5 Experimental results for cartesian (end-point) exercises:

In cartesian control, the proposed exoskeleton robot was given the positions and orientation of the end-effector. Using cubic polynomial, these positions and orientations were then transformed into end-effector cartesian velocities. The inverse kinematic solution was obtained for the proposed exoskeleton robot with these velocities according to the method described in section 4.5. The control architecture of cartesian control is depicted in Figure 6.20.
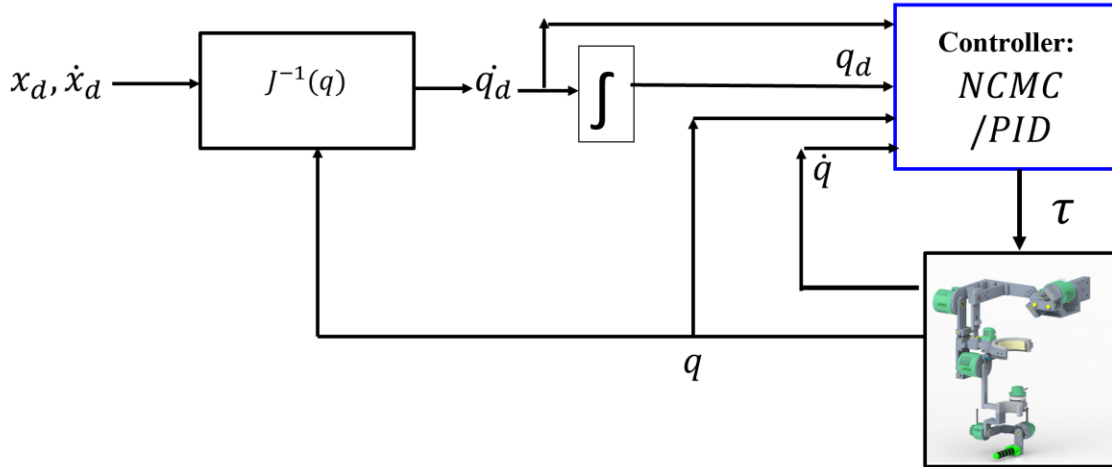
Figure 6.20 Schematic of cartesian control of the proposed exoskeleton robots

Reaching exercise in the transverse plane:

In this exercise, while carrying the subject's limb, the exoskeleton robot moved from a point to another point in the transverse plane, as shown in Figure 6.21. The top plot is position tracking of end-effector in 3D space, whereas the bottom plots show the cartesian trajectory tracking of the exoskeleton in x, y, and z positions and the corresponding tracking errors. This kind of motion resembles tasks like wiping a table. The end-effector position was tracked nicely; the maximum error found was 1 cm that occurred in the y-axis.
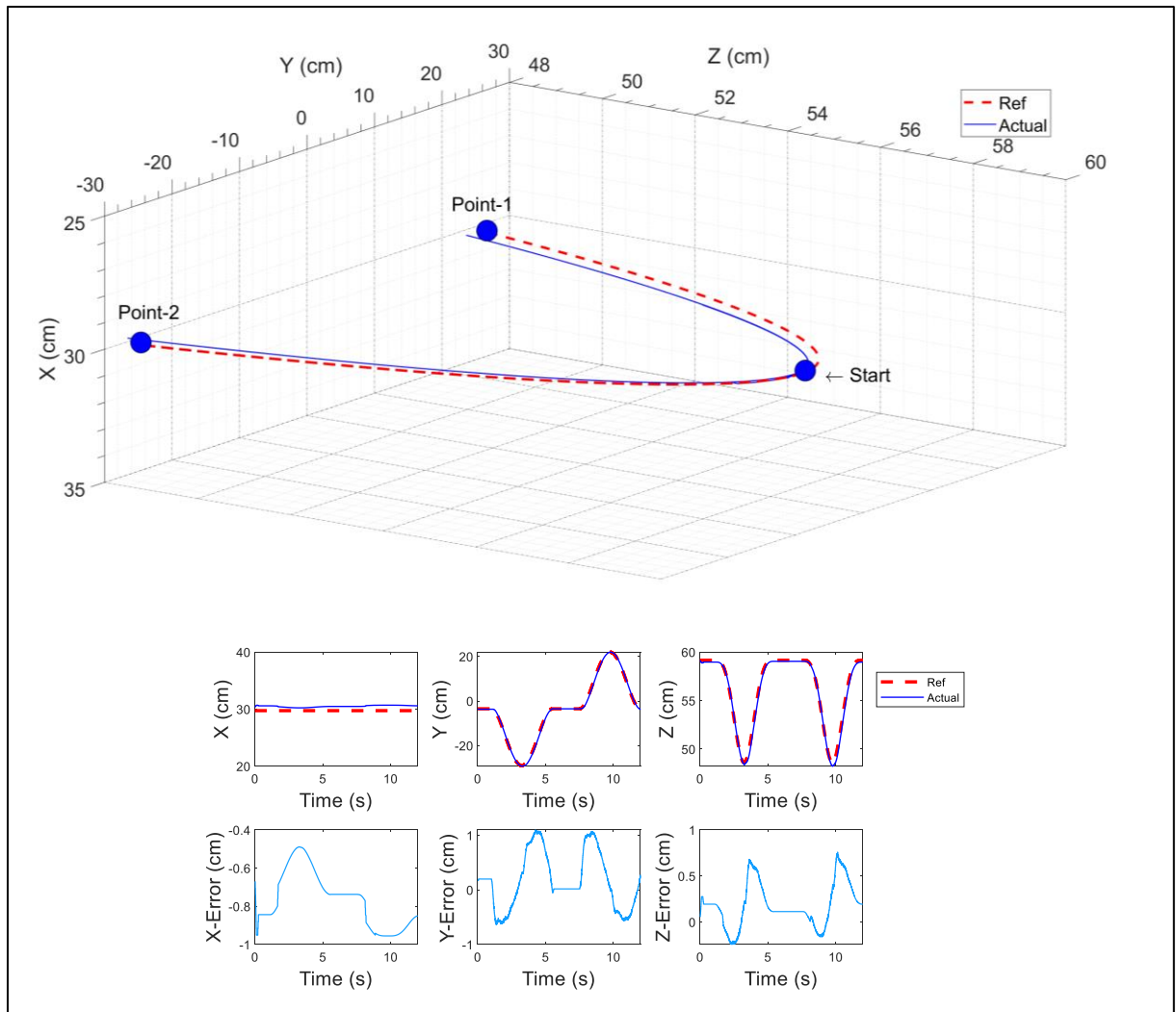
Figure 6.21 Reaching in Transverse plane

Forward reaching in the sagittal plane:

This kind of exercise is similar to pull or push an object (e.g., opening a door). The end-effector reached the target (blue marker) and then returned to the initial position. The experimental results for this exercise are shown in Figure 6.22. The maximum error (2.12 cm) was found in the x8 direction.
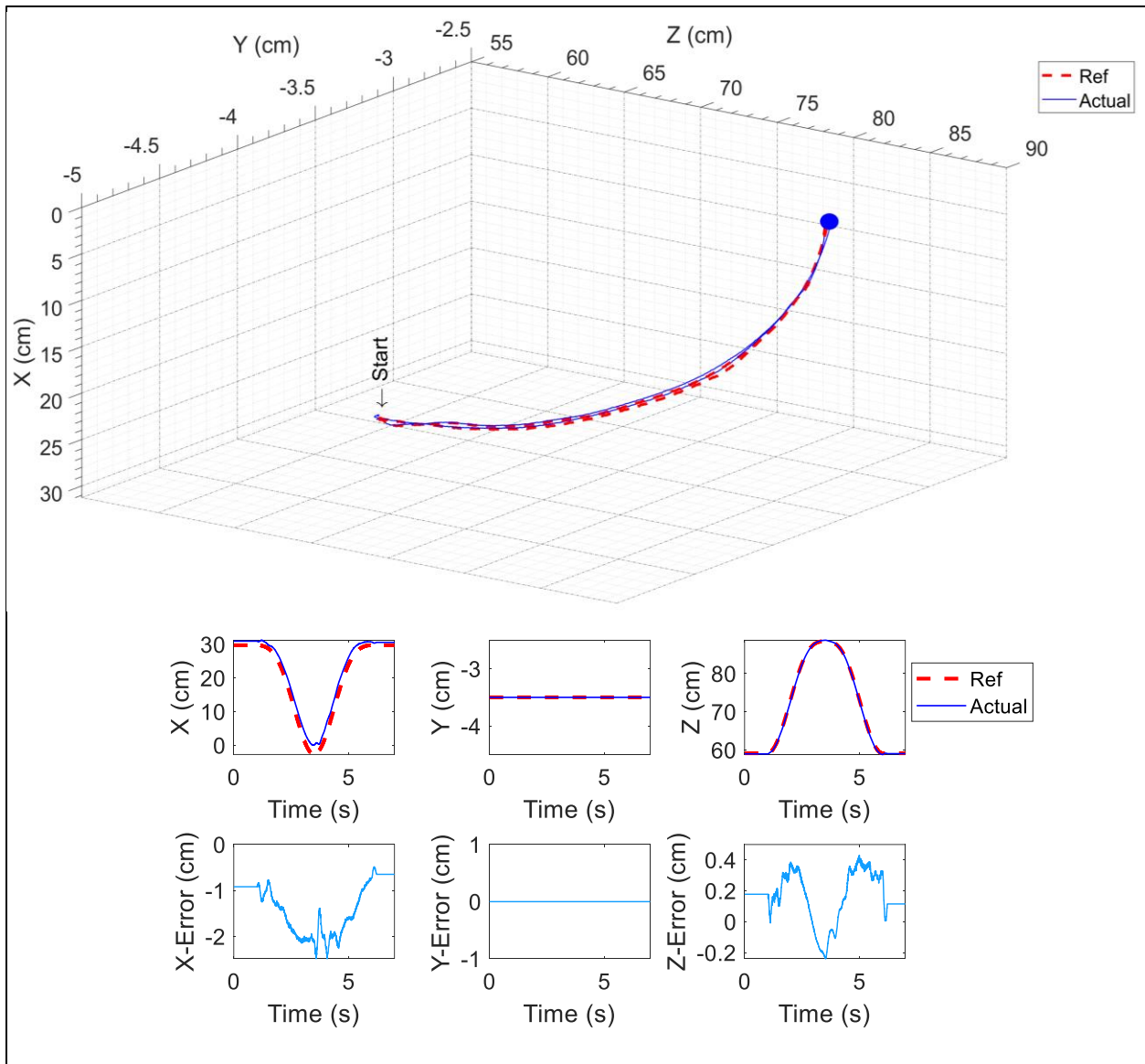
Figure 6.22 Forward reaching in the sagittal plane

3D reaching:

In this exercise, as shown in Figure 6.23, the end-effector reached a point (i.e., point-1) in 3D space from the start position. After that, it went to the point-2. The result shows excellent tracking with an error below 1.5 cm.
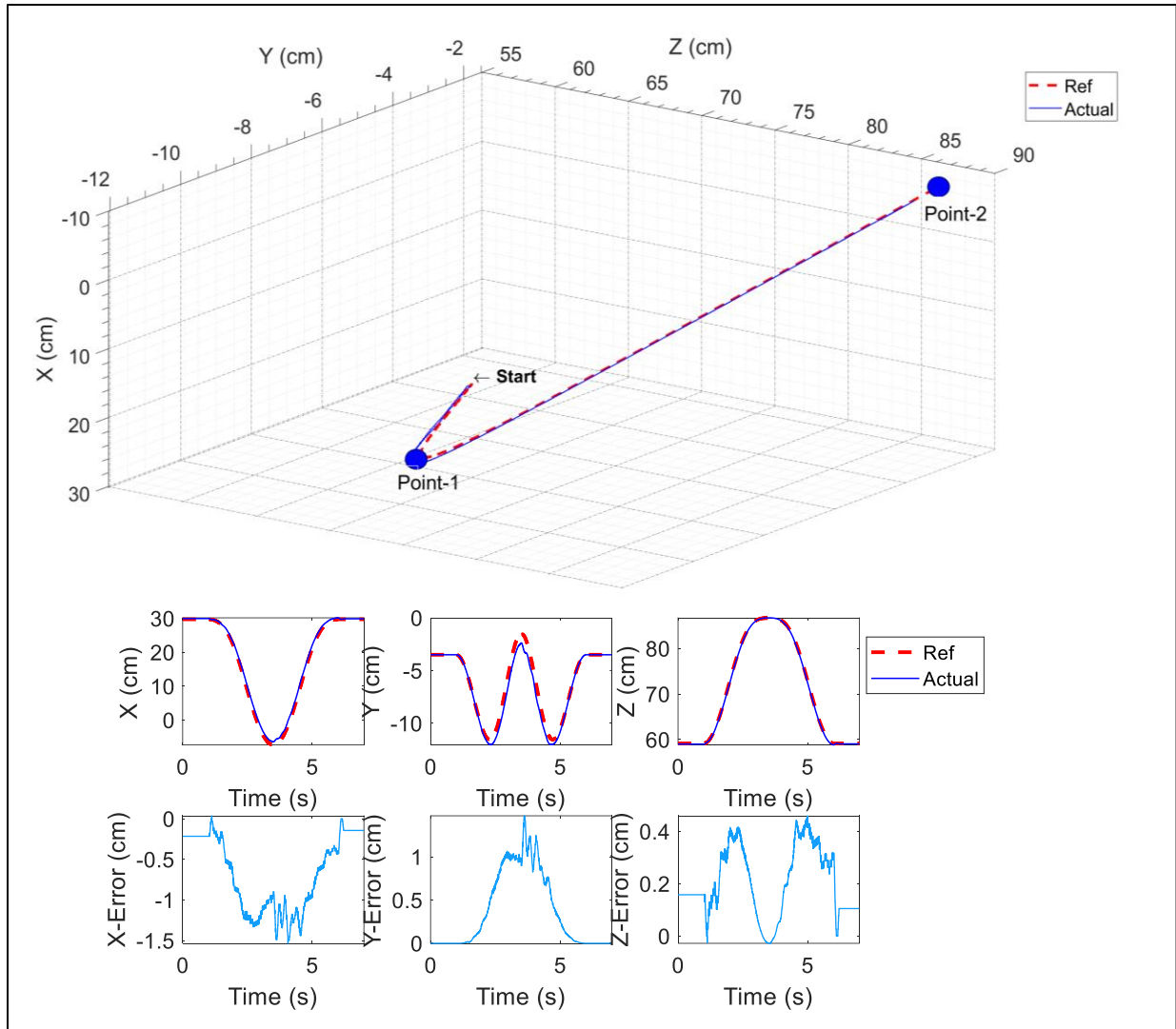
Figure 6.23 3D reaching

6.6 Experiments of active exercises:

The active exercises are suitable for increasing strength. As mentioned earlier, in active rehabilitation therapy, patients contribute to the extent of their ability to perform the given activity. In this research, based on the upper arm and wrist forces, a control algorithm was developed for active rehabilitation, which is described in the next sub-section.

6.6.1   Control approach for active rehabilitation:

The purpose of this control approach is to move the proposed exoskeleton when patients try to move it. Therefore, unlike passive rehabilitation, robot-aided active therapy does not require a predefined trajectory. Instead, the control approach is responsible for making a trajectory based on user input (e.g., force). In this research, a control algorithm was designed that transformed user's force into the trajectory, which eventually was followed by the trajectory-tracking controller (NCMC/PID). The schematic of the proposed control approach in performing active exercises is shown in Figure 6.24.
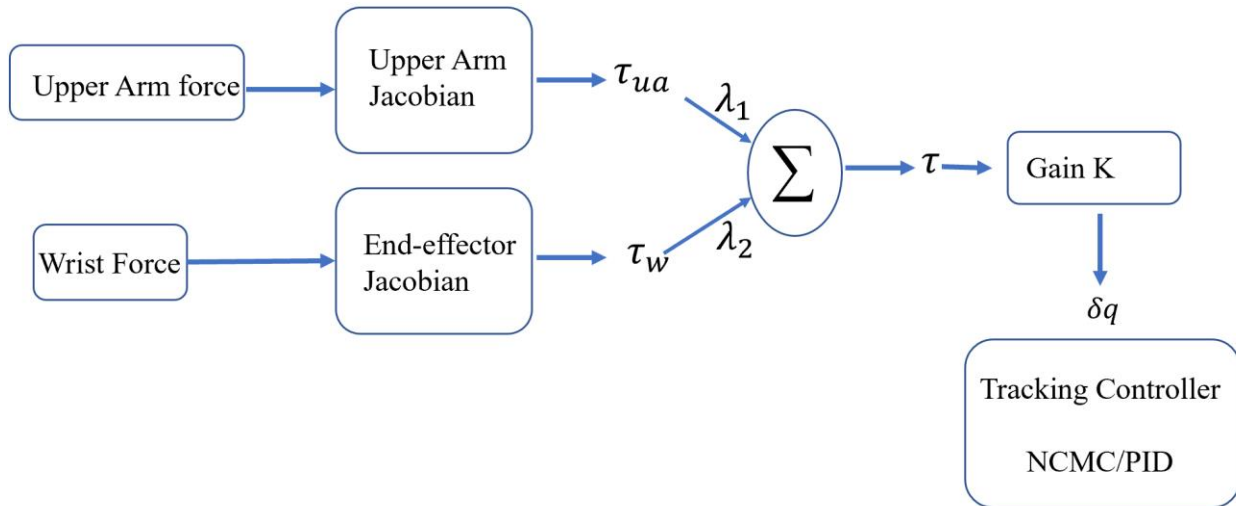
Figure 6.24 Schematic diagram of the proposed active control approach.

As shown in the Figure 6.24, both upper arm and wrist forces are used to estimate torque using their respective Jacobians. Since upper arm force contributes more at the shoulder, the shoulder joints (joint-1 and joint-2) joints' torque are calculated using τ_{ua} and τ_w with weights λ_1 and λ_2. The torques for the rest joints of the developed exoskeleton are the corresponding join torque in the τ_w torque vector. Then, the increment of joint positions was obtained from these

torques and by setting an appropriate gain. Thus, the trajectory for the proposed exoskeleton robot has been obtained and sent to the controller (NCMC/PID).

6.6.2   Reaching movement in (XZ) sagittal plane

In this exercise, the subject seated at elbow 90º was asked to reach a target (goal) in the sagittal plane. The purpose of the experiment was to see if the subjects can initiate the robot movement by applying force at the wrist and upper arm. The results are shown in Figure 6.25. The top graph shows the Virtual Reality (VR) interface, followed by the plot of the end-effector or the subject's hand position. The bottom graphs are a plot of forces exerted by the subject at the wrist (left figure) and upper arm (right figure). From the force plot, it is seen that forces are dominant in the axes that remain in the sagittal plane. So, the control approach produced trajectories, which led the subject's hand to reach the target (goal). The subject can see his/her progress towards reaching the target in the VR environment. The explicit feedback (subject's hand position with respect to the robot base) can also be seen in the GUI of the Game scene.
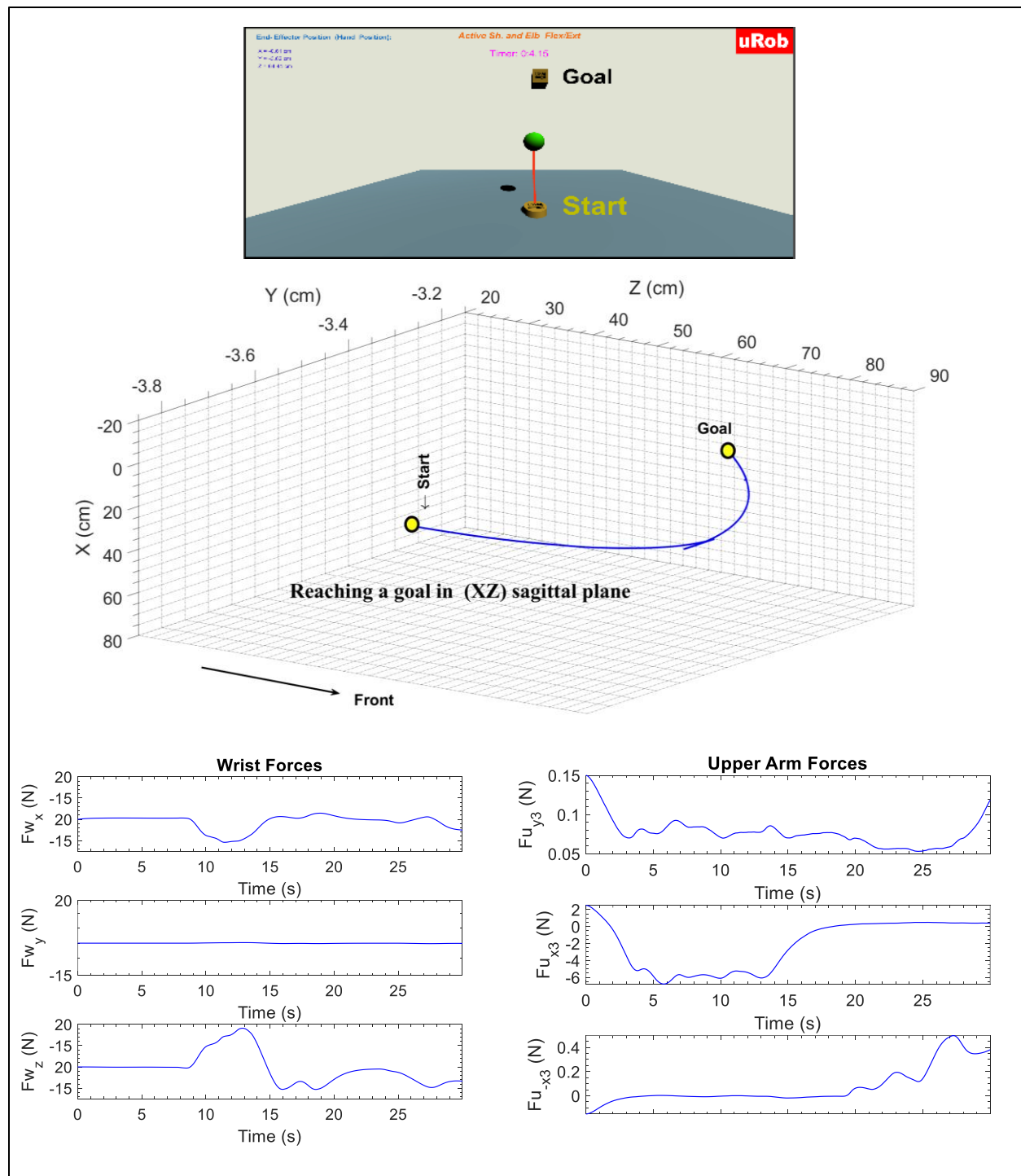
Figure 6.25 Reaching goal in the sagittal (XZ) plane

6.6.3   Reaching movement in the frontal (XY) plane

In this exercise as shown in Figure 6.26, the subject was seated in zero position was asked to reach the target (goal) in the frontal (XY) plane. From the force plot, it is seen that forces are dominant in the axes that remain in the frontal plane. So, the control approach produced trajectories, which led the subject's hand to reach the target (goal). The subject can see his/her progress towards reaching the target in the VR environment. The explicit feedback (subject's hand position with respect to the robot base) can also be seen in the GUI of the Game scene
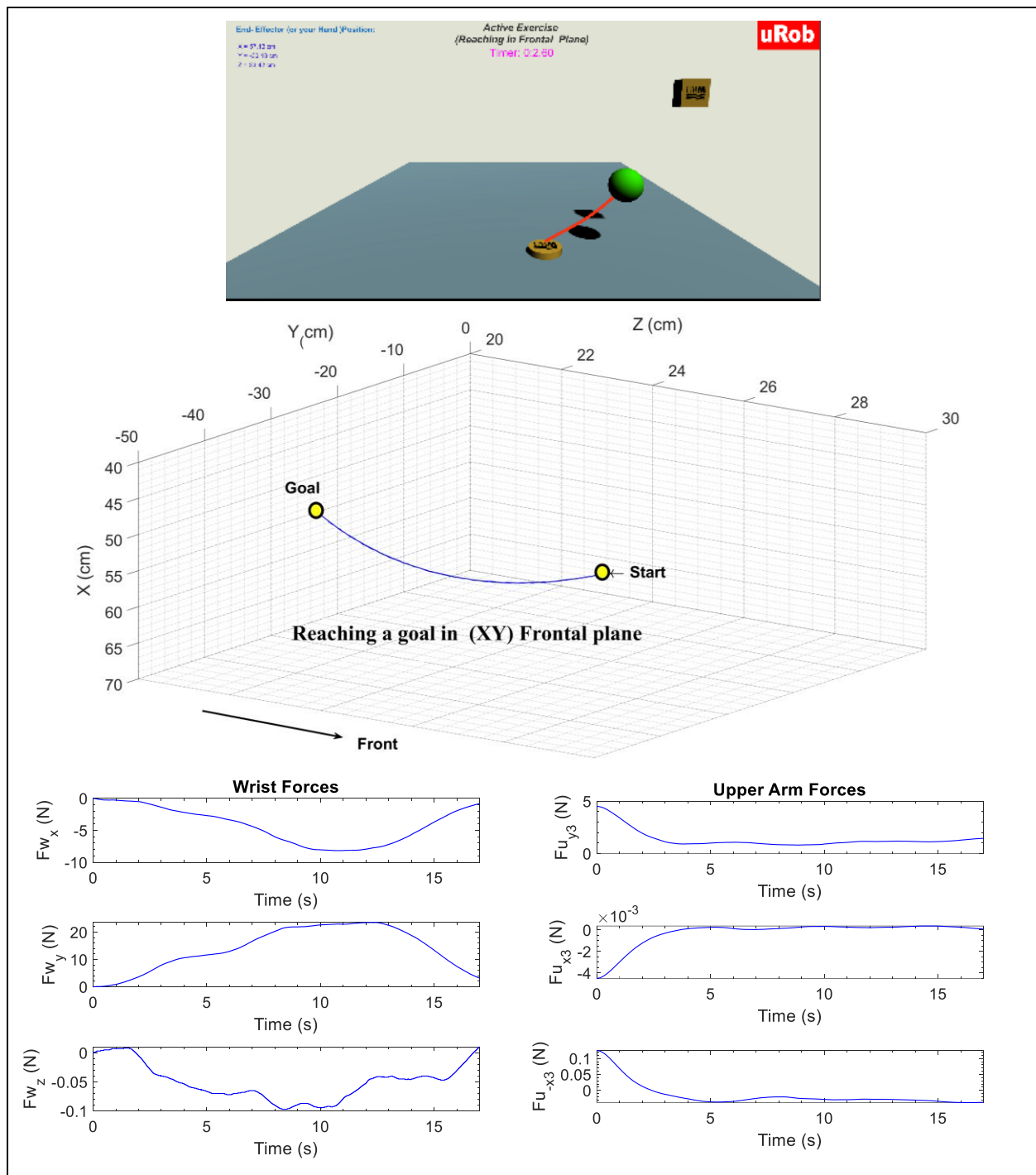
Figure 6.26 Reaching goal in the frontal (XY) plane

6.7 Comparison of NCMC and PID Control:

In this section, experimental results are compared for NCMC and PID Control. Figure 6.27 and Figure 6.28 shows the result for NCMC and PID, respectively. In the experiments, the same exercises were carried out. The results (Figure 6.27 and Figure 6.28) show that the PID control produced a larger tracking error (max error 4.1 deg) than the NCMC (max error 1.19 deg). The proposed new compound model-based control considers tracking errors, robot dynamics, and interaction forces; thus, NCMC shows better position tracking compared to a PID control. Because of better position tracking, all the experiments presented in this chapter were done with the proposed NCMC.
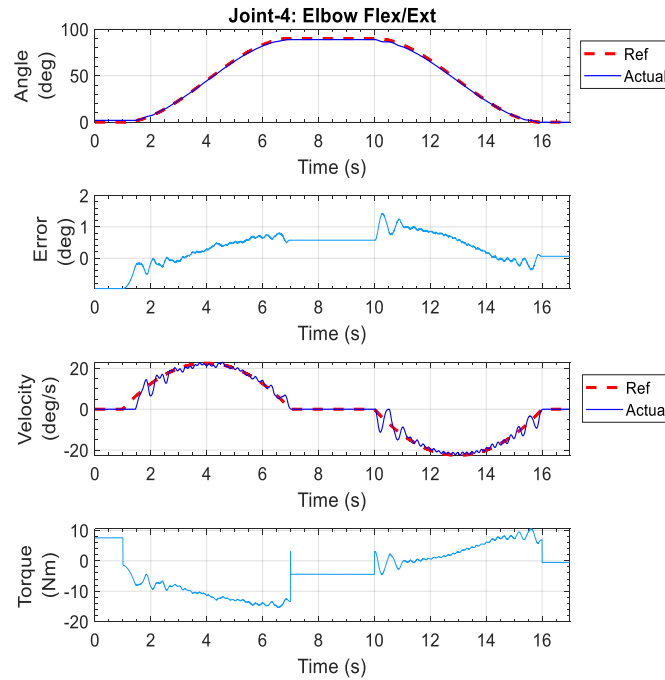
Figure 6.27 Elbow flexion-extension exercise with the NCMC Control
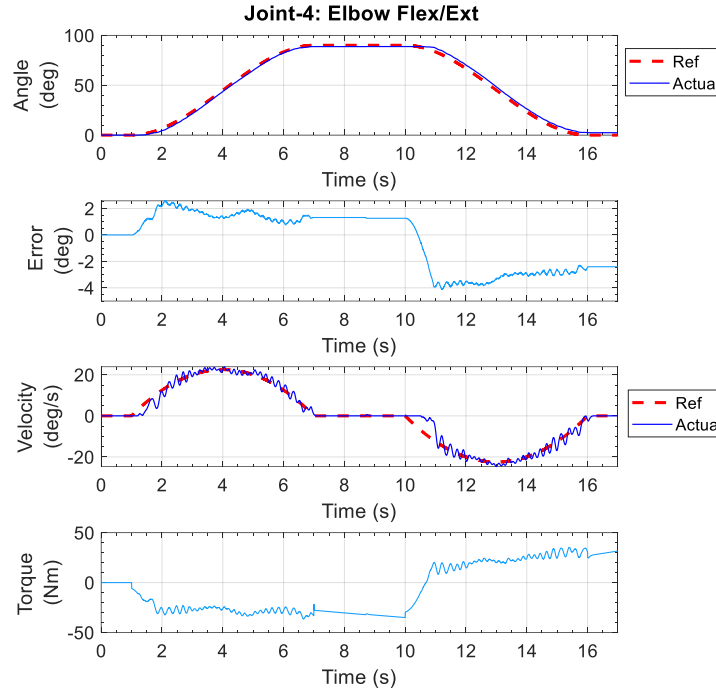
Figure 6.28 Elbow flexion-extension exercise with PID control

6.8 Experimental results to observe muscle activity to compare with the sensed forces:

To validate the use of force and ensure subject's muscles are engaged in active exercises, three exercises were conducted to observe electromyography (EMG) signals. Besides, to provide safe therapy during passive exercises, the forces can be observed. The exercises were passive elbow flexion-extension. Since the controller is robust, no matter how hard the subject applies resistance, the robot would make the subject's limb follow the predefined trajectory. However, subject muscle activity can be observed and compared with the force exerted by the subject at the wrist handle. Therefore, three experiments (no resistance, medium resistance, and high resistance to simulate spasticity in subject's limb) were conducted with three healthy subjects (age: 26 ± 4 years, 2 Male, 1 Female, weight: 137 ± 18 lbs, height: 5 ft 5 inch $\pm$ 2 inch) where EMG of biceps and triceps were recorded. Each experiment was conducted for five trials. All the results are plotted for subject-1

190

as the trends are similar for all three subjects. However, maximum and mean maximal values of forces and root mean square (RMS) values of EMG values for all three subjects are tabulated (Table 11-13). The findings from these experiments are that variation of forces also shows the variation of muscle activity. Moreover, it is possible to get an idea of subject's spasticity during passive rehabilitation by looking at the forces exerted by the subject. This monitoring of forces may be helpful for safe rehabilitation with the developed exoskeleton system.

6.8.1 Experimental setup of electromyography sensors:

During the elbow flexion and extension, biceps and triceps are contracted and relaxed, respectively (Halett et al., 1975). As a result, the biceps are contracted (agonist muscle), and the triceps are relaxed (antagonist muscle), as shown in Figure 6.29. A total of four sensors (Delsys Avanti) were placed on the subject's upper arm for biceps (medial and lateral part) and triceps (medial and lateral part). The sampling rate for EMG signals was 1260 samples/sec, and a total of 31500 samples were taken during the experiments. The experimental setup with the developed exoskeleton robot is depicted in Figure 6.30.
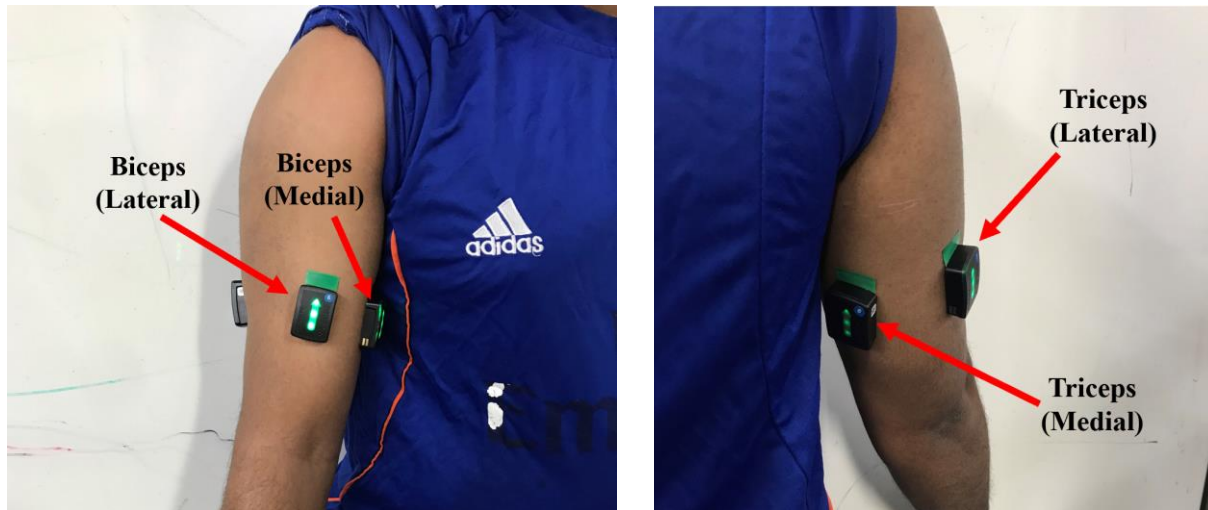
Figure 6.29 Placement of EMG sensors for biceps (left) and triceps (right)
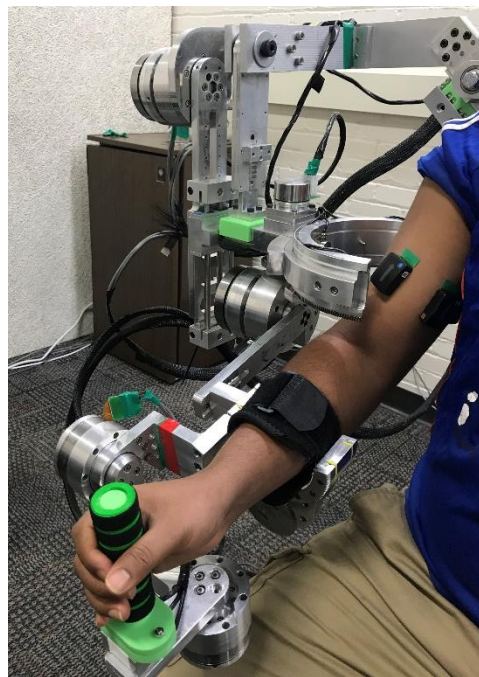
Figure 6.30 Experimental set up of elbow flexion-extension for EMG recording

6.8.2 Results for no resistance, resembling no spasticity:

In this experiment, the subject arm is passively flexed to 115° from the initial position (all joints remained at 0°). During the experiment, the subject offered no resistance to the developed

exoskeleton robot. The force and electromyography (EMG) signals of all four sensors were recorded. The RMS values of raw EMG values were extracted to compare with the force values. The results are plotted in Figure 6.31. To demonstrate the experimental results, plots of joint position vs. time, velocity vs. time, wrist forces vs. Time, root mean square values of EMG of biceps and triceps vs. time, and torque vs. time are presented. The red dotted line stands for reference (desired) value in the position. In the force plot, solid blue, red dash, and black dotted line stand for the force exerted at wrist x-axis, y-axis, and z-axis, respectively. In the electromyography plot, solid blue, red dash, black dotted, and green dash-dot line stand for the root mean square values of biceps medial, biceps lateral, triceps medial and triceps lateral EMG values. As mentioned earlier, the results are plotted in Figure 6.31only for subject-1 as the trends are similar for all the subjects. However, the maximum and mean of maxim values of forces and EMG values for all three subjects are presented in Table 11. The first column in the table depicts the maximum values of wrist forces of all five trials. The second column presents the mean values of all five trails. The third column shows the maximum value of the torque from all five trials, whereas the fourth column shows the mean torque values for all trials. The fifth and sixth column depicts the root mean square values of electromyography of biceps medial and lateral part accordingly. The sixth and seventh column presents the root mean square values of electromyography of triceps medial and lateral part accordingly.

From Figure 6.31, the subject's muscle activities (root mean square of electromyograph signals) for biceps and triceps are not significant as the subject was asked to apply no resistance. However, when the subject applied some forces, corresponding electromyograph signals started to appear. From Table 11, the values of maximum (10 N, 0.5 N, and 2.5 N) and mean forces ($F_x =$

$5.2\ N, F_y = 0.25\ N, F_z = 1.14\ N$) corroborates that subject applied little to no resistance during the exercise. The mean and standard deviation of the electromyography signals of biceps and triceps are also presented in the table.

6.8.3 Results for medium resistance, resembling some level of spasticity:

In this exercise, the subject applied some resistance during elbow flexion-extension to simulate some level of spasticity. The results are plotted in Figure 6.32. The maximum and mean of maxim values of forces and EMG values for all three subjects are presented in Table 12. From the figure, it is seen that applied forces along all three axes are higher than the previous (no resistance) exercise. For these force values, the subject's corresponding muscle activities (please see EMG plots) also appear. For example, when the elbow is flexed, the RMS values of EMG of the biceps medial part is increased.

6.8.4 Results for medium resistance, resembling high spasticity:

In this exercise, the subject applied high resistance during elbow flexion-extension to simulate some level of spasticity. The results are plotted in Figure 6.33. The maximum and mean of maxim values of forces and EMG values for all three subjects are presented in Table 13. From the figure, it is seen that applied forces along all three axes are higher than the previous (medium/some resistance) exercise. For these force values, the subject's corresponding muscle activities (please see EMG plots) have also appeared. The highest muscle activity is seen for this exercise. It can also be observed from the figure that, during the flexion-extension, the change in force and change in EMG signals almost corresponds. Therefore, it can be said that the variation of forces also causes a variation of EMG values.
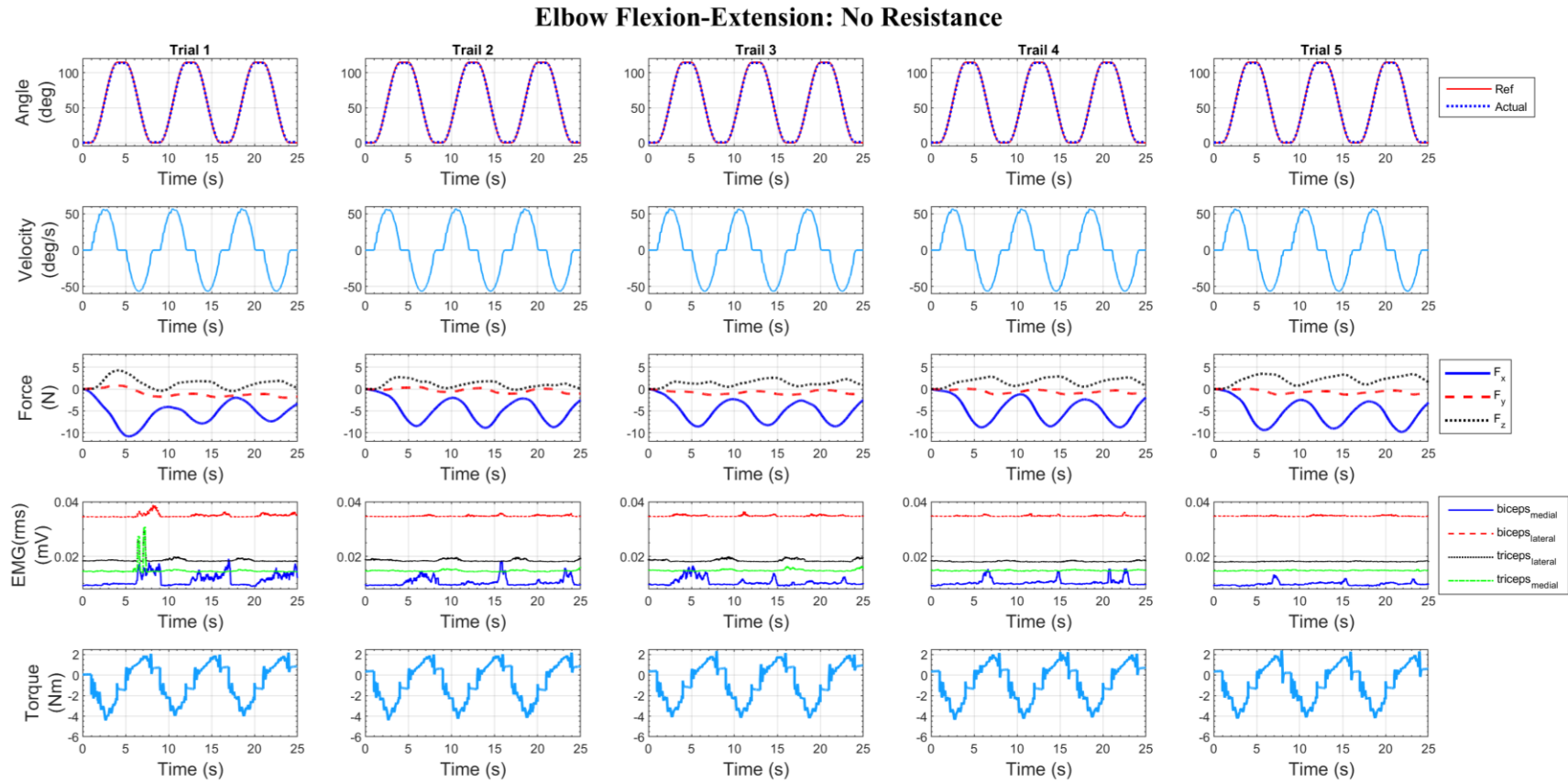
Figure 6.31 Results for the exercise where the subject applied no resistance

Table 11: Results when subject applied no resistance

Subject-1 (Male, 29 years, 145 lb, 5 ft 4 inch)							
Max. Forces (*Fx, Fy, Fz*) (N)	Mean of Max. Forces (*Fx, Fy, Fz*) (N)	Max. Torque (Nm)	Mean of Max. Torques (Nm)	Biceps (Med) *Mean ± SD* (mV)	Biceps (Lat) *Mean ± SD* (mV)	Triceps (Lat) *Mean ± SD* (mV)	Triceps (Med) *Mean ± SD* (mV)
10.1, 0.5, 2.5	5.2, 0.25, 1.14	30	3.28	0.01 ± 0.002	0.03 ± 0.004	0.02 ± 0.002	0.01 ± 0.002
Subject-2 (Male, 30 years, 155 lb, 5 ft 5 inch)							
9.12, 2.5, 2.8	6.4, 1.25, 1.81	4.11	3.24	0.01 ± 0.002	0.03 ± 0.005	0.01 ± 0.005	0.02 ± 0.007
Subject-3 (Female, 23 years, 119 lb, 5 ft 3 inch)							
7.34, 1.2, 4.2	5.4, 0.87, 3.62	4.24	3.28	0.009 ± 0.001	0.03 ± 0.005	0.02 ± 0.002	0.01 ± 0.002
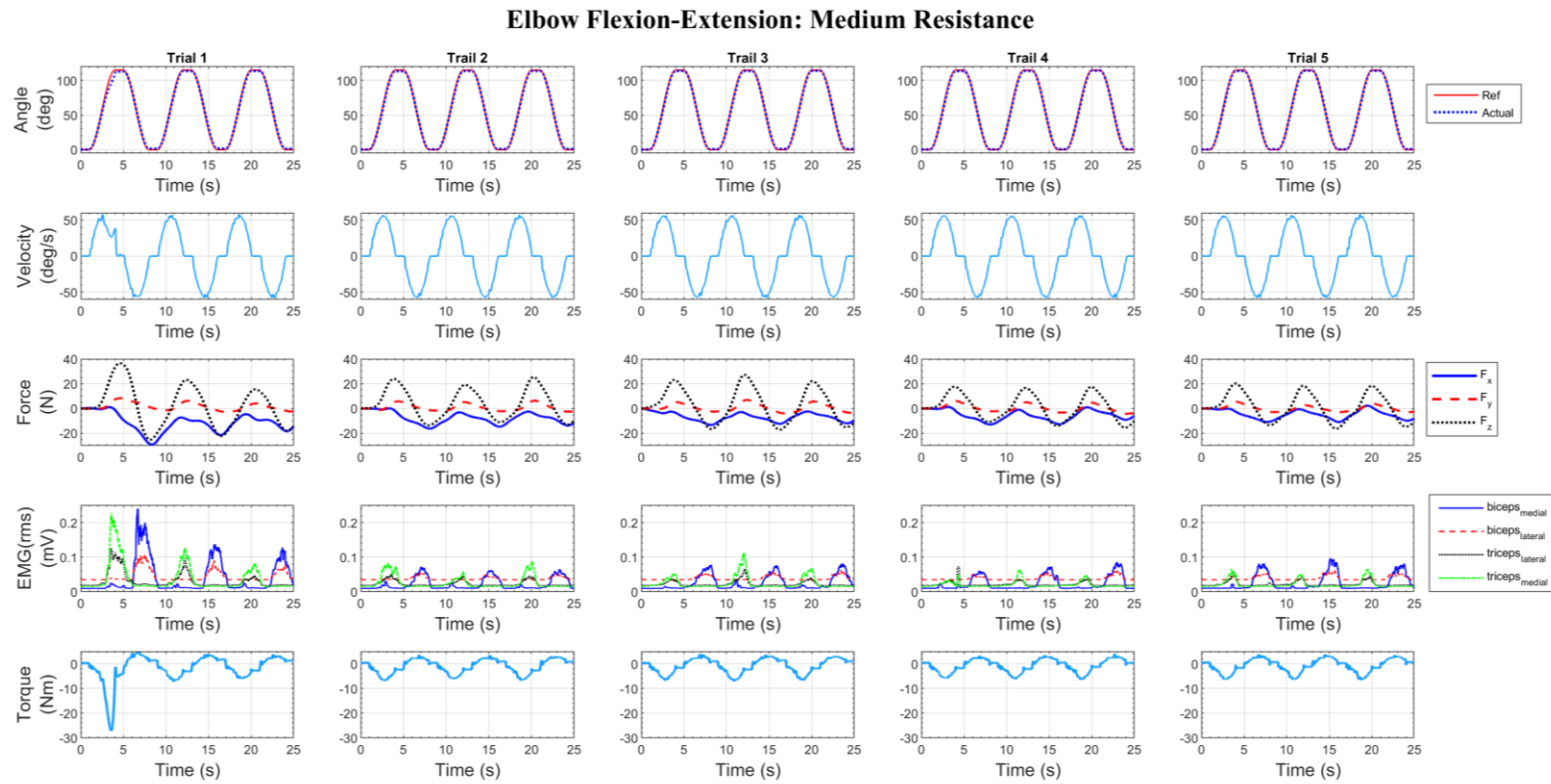
Figure 6.32 Results for the exercise where the subject applied some resistance

Table 12: Results when subject applied some resistance

Subject-1 (Male, 29 years, 145 lb, 5 ft 4 inch)							
Max. Forces (*Fx, Fy, Fz*) (N)	Mean of Max. Forces (*Fx, Fy, Fz*) (N)	Max. Torque (Nm)	Mean of Max. Torques (Nm)	Biceps (Med) *Mean ± SD* (mV)	Biceps (Lat) *Mean ± SD* (mV)	Triceps (Lat) *Mean ±SD* (mV)	Triceps (Med) *Mean ± SD* (mV)
25, 17, 40	18, 14, 34	6.50	4.50	0.02 ± 0.02	0.04 ± 0.01	0.02± 0.01	0.02 ± 0.02
Subject-2 (Male, 30 years, 155 lb, 5 ft 5 inch)							
32, 9, 26	24, 5.9, 21.4	5.62	4.41	0.01 ± 0.003	0.02 ± 0.005	0.03 ± 0.002	0.02 ± 0.007
Subject-3 (Female, 23 years, 119 lb, 5 ft 3 inch)							
35, 5.6, 16	30, 3.4, 14.4	6.74	5.53	0.01 ± 0.008	0.04 ± 0.009	0.02 ± 0.005	0.02 ± 0.005
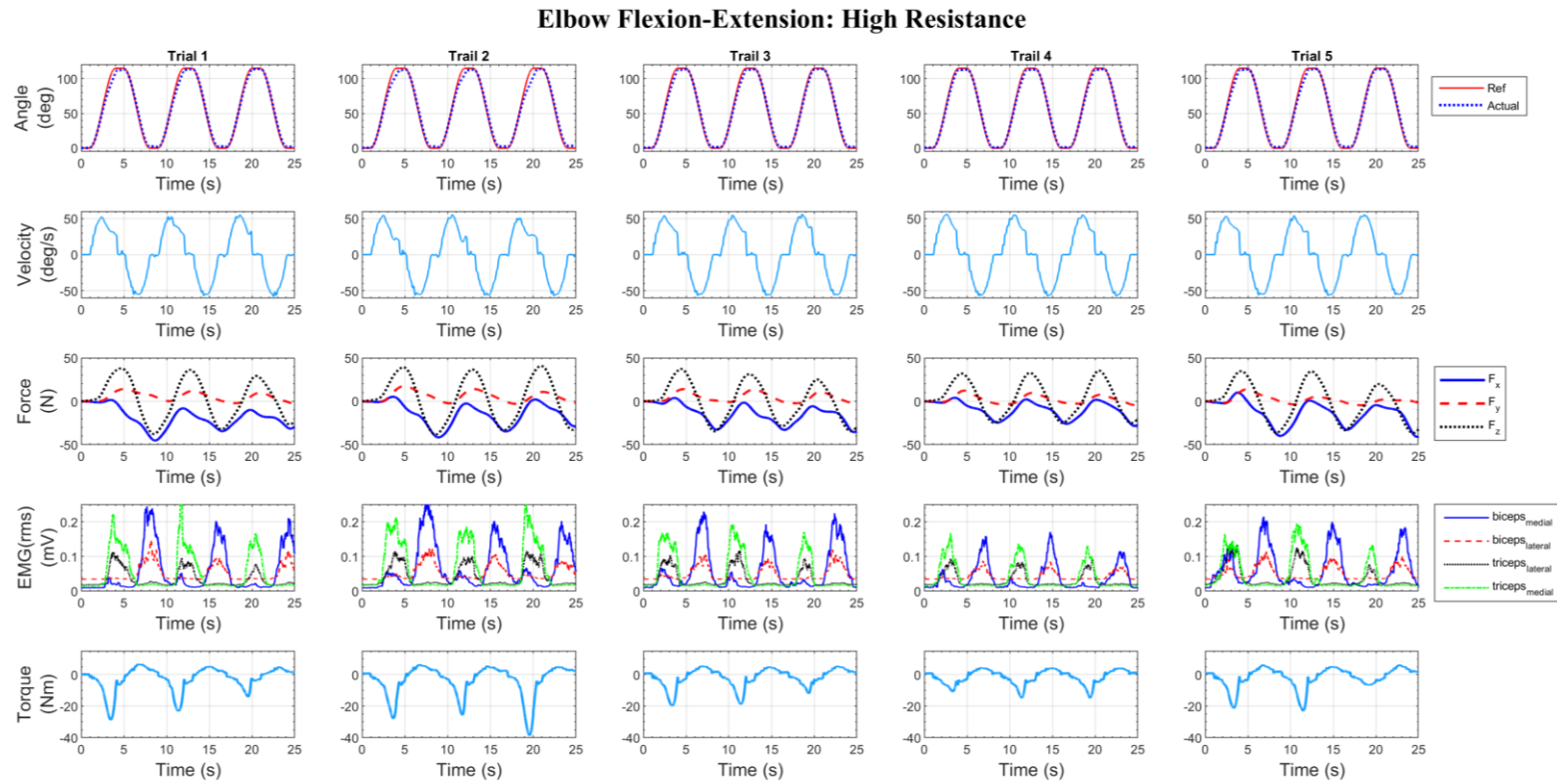
Figure 6.33 Results for the exercise where the subject applied high resistance

Table 13: Results when subject applied high resistance

Subject-1 (Male, 29 years, 145 lb, 5 ft 4 inch)							
Max. Forces (Fx, Fy, Fz) (N)	Mean of Max. Forces (Fx, Fy, Fz) (N)	Max. Torque (Nm)	Mean of Max. Torques (Nm)	Biceps (Med) Mean ± SD (mV)	Biceps (Lat) Mean ± SD (mV)	Triceps (Lat) Mean ± SD (mV)	Triceps (Med) Mean ± SD (mV)
49, 14, 45	45, 12, 39	40	15	0.04 ± 0.05	0.05 ± 0.05	0.03± 0.03	0.04 ± 0.05
Subject-2 (Male, 30 years, 155 lb, 5 ft 5 inch)							
49, 12, 40	48, 11, 34	35	12	0.02 ± 0.009	0.04 ± 0.005	0.04 ± 0.004	0.03 ± 0.001
Subject-3 (Female, 23 years, 119 lb, 5 ft 3 inch)							
46, 17.3, 37	42, 13, 33	25	10	0.03 ± 0.03	0.05 ± 0.01	0.03 ± 0.01	0.02 ± 0.008

6.9 Conclusion:

From the experimental results of passive, active, and Cartesian exercises, the following conclusion can be drawn.

- Results show that the developed robot with the ergonomic shoulder can perform given exercises with very low error. Therefore, it can be used in rehabilitation with real patients.

- The successful completion of cartesian trajectories proves that the developed robot can provide end-point exercises.

- The results also show that new compound model-based control approach can deal with the high non-linearity of the developed robot.

- The results of active exercises that used proposed force-based control are promising.

- The results of recorded electromyography (EMG) signals during exercises show that forces can be used in active exercises, as the variation of forces also caused significant variation of muscle activity (EMG values). Besides, this result may explain spastic behavior during rehabilitation and may act as a basis for patient-tailored therapy.

CONCLUSION

A 7 DOF upper limb rehabilitative exoskeleton robot with an ergonomic shoulder joint is developed to provide effective rehabilitation to people with upper limb impairments.

In this Ph.D. research work, the kinematic and dynamic modeling, design of link and joint mechanisms to allow movement of shoulder joint center of rotation, design of the entire mechanical structure of the robot, development of the physical prototype of the robot, and control strategies (for the passive and active exercise) of the *developed exoskeleton robot* has been conducted.

Since the developed exoskeleton robot comprises both serial linkage and parallel mechanisms, a hybrid approach was applied to find the robot kinematics. The analytical approach was used to find the kinematics of the developed parallel mechanisms (i.e., frontal and sagittal mechanisms). On the other hand, the modified Denavit-Hartenberg convention was applied to obtain the kinematics of the serial part of the exoskeleton robot. Dynamic modeling was obtained using the iterative Newton-Euler formulation.

To deal with the high non-linearity of the developed exoskeleton robot, a non-linear control approach based on the developed exoskeleton's model, tracking error, and interaction forces were proposed.

In experiments, both passive (pre-defined trajectories of recommended rehabilitation exercises) and active exercises were used. Both individual joint and multi-joint movement exercises were used in the experiments. End-point exercises were carried out using Cartesian control. The goal-oriented exercises were conducted using force-based control.

The findings from the experiments are:

1. the developed exoskeleton robot can allow the mobility of shoulder joint's center of rotation,

2. the developed exoskeleton can perform passive and active exercises,

3. Proposed New Compound Model-based Control (NCMC) can deliver good trajectory tracking, and

4. the developed exoskeleton can perform both joint-based and end-point exercises.

FUTURE RECOMMENDATIONS

The developed exoskeleton robot shows promising results in delivering human upper limb rehabilitation. However, the following recommendations may be considered to improve its performance and functionality further.

- A three-axis force sensor may be mounted in the upper arm. This will help the exoskeleton robot sense all three Cartesian forces in the upper arm. Incorporating these forces in the active control approach will allow the robot to function independently of wrist force sensor signals.

- The developed exoskeleton robot was made using Aluminum 6061. However, a lighter material such as carbon fiber will be useful to reduce its weight significantly.

- The range of motion of abduction-adduction may be increased by modifying join-1's links. The mechanical design currently limits shoulder joint abduction-adduction motion to 90 degrees. Remote placement of the actuator and links behind the shoulder joint could potentially increase the range of motion.

- Tele-rehabilitation of developed exoskeleton system can be done so that that therapist can use it remotely for rehabilitation.

- The experiments described in section 6.8 show promising results to understand the spastic behavior of patient limb with the developed exoskeleton robot. An algorithm to find a safe range of motion for each patient may be developed based on this preliminary result.

APPENDIX

ANNEX-I: Motor specifications, maxon EC-90, 90W

EC 90 flat ⌀90 mm, brushless, 90 Watt

		with Hall sensors	323772	429271	244879
Motor Data					
	Values of nominal voltage				
1	Nominal voltage	V	24	36	48
2	No load speed	rpm	3190	3520	2080
3	No load current	mA	544	368	135
4	Nominal speed	rpm	2500	2540	1640
5	Nominal torque (max. continuous torque)	mNm	444	560	533
6	Nominal current (max. continuous current)	A	6.06	4.76	2.27
7	Stall torque	mNm	4940	7480	4570
8	Stall current	A	70	69	21.1
9	Max. efficiency	%	84	87	85
	Characteristics				
10	Terminal resistance phase to phase	Ω	0.343	0.522	2.28
11	Terminal inductance phase to phase	mH	0.284	0.625	2.5
12	Torque constant	mNm/A	70.5	109	217
13	Speed constant	rpm/V	135	88	44
14	Speed/torque gradient	rpm/mNm	0.659	0.473	0.462
15	Mechanical time constant	ms	21.1	13.6	14.8
16	Rotor inertia	gcm²	3060	3060	3060

Specifications

Thermal data
17 Thermal resistance housing-ambient 1.91 K/W
18 Thermal resistance winding-housing 2.6 K/W
19 Thermal time constant winding 46 s
20 Thermal time constant motor 283 s
21 Ambient temperature -40...+100°C
22 Max. winding temperature +125°C

Mechanical data (preloaded ball bearings)
23 Max. speed 5000 rpm
24 Axial play at axial load < 15 N 0 mm
    > 15 N 0.14 mm
25 Radial play preloaded
26 Max. axial load (dynamic) 12 N
27 Max. force for press fits (static) 165 N
    (static, shaft supported) 6000 N
28 Max. radial load, 5 mm from flange 68 N

Other specifications
29 Number of pole pairs 12
30 Number of phases 3
31 Weight of motor 600 g

Values listed in the table are nominal.

Connection
Pin 1 Hall sensor 1
Pin 2 Hall sensor 2
Pin 3 V_cc 4.5 ... 50 VDC
Pin 4 Motor winding 3
Pin 5 Hall sensor 3
Pin 6 GND
Pin 7 Motor winding 1
Pin 8 Motor winding 2
Wiring diagram for Hall sensors see p. 43

Cable
Connection cable Universal, L = 500 mm 339380
Connection cable to EPOS2, L = 500 mm 354045

Operating Range

Comments

Continuous operation
In observation of above listed thermal resistance (lines 17 and 18) the maximum permissible winding temperature will be reached during continuous operation at 25°C ambient.
= Thermal limit.

Short term operation
The motor may be briefly overloaded (recurring).

— Assigned power rating

maxon Modular System Overview on page 26–36

Planetary Gearhead
⌀32 mm
4 - 30 Nm
Page 351

Encoder MILE
512 - 6400 CPT,
2 channels
Page 390

Recommended Electronics:
Notes Page 32
ESCON Mod. 50/4 EC-S 477
ESCON Mod. 50/5 477
ESCON 50/5 428
ESCON 70/10 428
DEC Module 50/5 430
EPOS2 24/5, 50/5, 70/10 435
EPOS2 P 24/5 438
EPOS4 Module/CB 50/5 442
EPOS4 Module 50/8 443
EPOS4 Comp. 50/8 CAN 443
MAXPOS 50/5 447

May 2017 edition / subject to change

maxon EC motor 271

ANNEX-II: Motor specifications, maxon EC-45, 70W

EC 45 flat ∅42.8 mm, brushless, 70 Watt

Connector:
39-28-1003 Molex

M 1:2

maxon flat motor

Stock program
Standard program
Special program (on request)

Part Numbers

Motor Data (provisional)		with Hall sensors	397172	403165	403166	402987			
Values at nominal voltage									
1 Nominal voltage	V		24	30	36	48			
2 No load speed	rpm		6110	6230	6330	3440			
3 No load current	mA		234	194	166	48.1			
4 Nominal speed	rpm		4860	4980	5080	2540			
5 Nominal torque (max. continuous torque)	mNm		128	132	134	134			
6 Nominal current (max. continuous current)	A		3.21	2.36	1.93	0.938			
7 Stall torque	mNm		1460	1570	1590	915			
8 Stall current	A		39.5	25.8	20.7	6.57			
9 Max. efficiency	%		85	84	83	84			
Characteristics									
10 Terminal resistance phase to phase	Ω		0.608	1.16	1.74	6.89			
11 Terminal inductance phase to phase	mH		0.463	0.891	0.966	5.85			
12 Torque constant	mNm / A		36.9	45.1	53.3	131			
13 Speed constant	rpm / V		259	212	179	72.7			
14 Speed / torque gradient	rpm / mNm		4.26	5.44	5.85	3.82			
15 Mechanical time constant	ms		8.07	10.3	11.1	7.24			
16 Rotor inertia	gcm²		181	181	181	181			

Specifications

Thermal data
17 Thermal resistance housing-ambient 3.56 K/W
18 Thermal resistance winding-housing 4.1 K/W
19 Thermal time constant winding 29.6 s
20 Thermal time constant motor 170 s
21 Ambient temperature -40 ... +100°C
22 Max. winding temperature +125°C

Mechanical data (preloaded ball bearings)
23 Max. speed 10000 rpm
24 Axial play at axial load <4.0 N 0.0 mm
  >4.0 N 0.14 mm
25 Radial play preloaded
26 Max. axial load (dynamic) 3.6 N
27 Max. force for press fits (static) 50 N
  (static, shaft supported) 1000 N
28 Max. radial load, 5 mm from flange 21 N

Other specifications
29 Number of pole pairs 8
30 Number of phases 3
31 Weight of motor 141 g

Values listed in the table are nominal.

Connection
Pin 1 Hall sensor 1*
Pin 2 Hall sensor 2*
Pin 3 V$_{cc}$ 4.5 ... 18 VDC
Pin 4 Motor winding 3
Pin 5 Hall sensor 3*
Pin 6 GND
Pin 7 Motor winding 1
Pin 8 Motor winding 2
*Internal pull-up (7 ... 13 kΩ) on pin 3
Wiring diagram for Hall sensors see p. 43

Cable
Connection cable Universal, L = 500 mm 308800
Connection cable to EPOS, L = 500 mm 354045

Operating Range

n [rpm]

70 W

397172

Comments

Continuous operation
In observation of above listed thermal resistance (lines 17 and 18) the maximum permissible winding temperature will be reached during continuous operation at 25°C ambient.
= Thermal limit.

Short term operation
The motor may be briefly overloaded (recurring).

— Assigned power rating

maxon Modular System

Planetary Gearhead
∅42 mm
3 - 15 Nm
Page 347

Spur Gearhead
∅45 mm
0.5 - 2.0 Nm
Page 349

Recommended Electronics:
Notes Page 32
ESCON 36/3 EC 427
ESCON Mod. 50/4 EC-S 427
ESCON Module 50/5 427
ESCON 50/5 428
DEC Module 50/5 430
EPOS2 Module 36/2 434
EPOS2 24/5, 50/5 435
EPOS2 P 24/5 438
EPOS4 Module/CB 50/5 442
MAXPOS 50/5 447

Overview on page 26–36

Encoder MILE
256 - 2048 CPT,
2 channels
Page 388

Option
With Cable and Connector
(Ambient temperature -20 ... +100°C)

May 2017 edition / subject to change

maxon EC motor 267

206

EC 45 flat ∅45 mm, brushless, 30 Watt

maxon flat motor

A with Hall sensors B sensorless

M 1:2

- ■ Stock program
- □ Standard program
- ▢ Special program (on request)

Order Number

| | | with Hall sensors | 200142 | | 339281 | | 339282 | | 339284 |
| | | sensorless | | 200189 | | 339283 | | | |

Motor Data (provisional)

	Values at nominal voltage							
1	Nominal voltage	V	12.0	12.0	24.0	24.0	36.0	36.0
2	No load speed	rpm	4370	4360	4370	4370	4760	4760
3	No load current	mA	151	150	75.3	75.2	56.9	56.9
4	Nominal speed	rpm	2860	2820	2850	2840	3210	3210
5	Nominal torque (max. continuous torque)	mNm	59.0	54.3	58.8	57.5	70.6	69.5
6	Nominal current (max. continuous current)	A	2.14	2.00	1.07	1.05	0.893	0.882
7	Stall torque	mNm	255	219	253	243	380	369
8	Starting current	A	10.0	8.57	4.96	4.77	5.38	5.22
9	Max. efficiency	%	77	76	77	77	81	81
	Characteristics							
10	Terminal resistance phase to phase	Ω	1.20	1.40	4.84	5.04	6.70	6.9
11	Terminal inductance phase to phase	mH	0.560	0.560	2.24	2.24	4.29	4.29
12	Torque constant	mNm / A	25.5	25.5	51.0	51.0	70.6	70.6
13	Speed constant	rpm / V	374	374	187	187	135	135
14	Speed / torque gradient	rpm / mNm	17.6	20.6	17.8	18.5	12.8	13.2
15	Mechanical time constant	ms	17.1	19.9	17.2	17.9	12.4	12.8
16	Rotor inertia	gcm²	92.5	92.5	92.5	92.5	92.5	92.5

Specifications

Thermal data
- 17 Thermal resistance housing-ambient 4.23 K / W
- 18 Thermal resistance winding-housing 4.57 K / W
- 19 Thermal time constant winding 13.2 s
- 20 Thermal time constant motor 186 s
- 21 Ambient temperature -40..+100°C
- 22 Max. permissible winding temperature +125°C

Mechanical data (preloaded ball bearings)
- 23 Max. permissible speed 10000 rpm
- 24 Axial play at axial load < 5.0 N 0 mm
-                            > 5.0 N typ. 1.0 mm
- 25 Radial play preloaded
- 26 Max. axial load (dynamic) 4.8 N
- 27 Max. force for press fits (static) 50 N
-    (static, shaft supported) 1000 N
- 28 Max. radial loading, 7.5 mm from flange 5.5 N

Other specifications
- 29 Number of pole pairs 8
- 30 Number of phases 3
- 31 Weight of motor 88 g
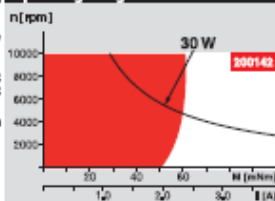
Values listed in the table are nominal.

Connection	with Hall sensors	sensorless
Pin 1	4.5 ... 18 VDC	Motor winding 1
Pin 2	Hall sensor 3*	Motor winding 2
Pin 3	Hall sensor 1*	Motor winding 3
Pin 4	Hall sensor 2*	⊥ neutral point
Pin 5	GND	
Pin 6	Motor winding 3	
Pin 7	Motor winding 2	
Pin 8	Motor winding 1	

*Internal pull-up (7 ... 13 kΩ) on pin 1
Wiring diagram for Hall sensors see page 28

	Order number	Order number
Adapter see p. 283	220300	220310
Connector	Article number	Article number
AMP	1-487951-4	487951-4
MOLEX	52207-1190	52207-0490
MOLEX	52089-1110	52089-0410

Pin for design with Hall sensors:
FPC, 11 pole, pitch 1.0 mm, top contact style

May 2007 edition / subject to change

Operating Range

n [rpm]

30 W

200142

Comments

■ Continuous operation
In observation of above listed thermal resistance (lines 17 and 18) the maximum permissible winding temperature will be reached during continuous operation at 25°C ambient.
= Thermal limit.

□ Short term operation
The motor may be briefly overloaded (recurring).

── Assigned power rating

maxon Modular System

Overview on page 16 - 21

Spur Gearhead
∅45 mm
0.5 -2.0 Nm
Page 237

Recommended Electronics:	
AECS 35.3	Page 276
DEC 24/3	277
DEC 50/5	277
DECV 50/5	278
EPOS 24/1	286
EPOS 24/5	286
EPOS P 24/5	287
Notes	29

maxon EC motor 197

ANNEX-IV: CSF-17-100-2UH & CSF-11-100-2XH-F

CSF Rating Table

Table 1

Size	Ratio	Rated Torque at 2000 Tr rpm		Limit for Repeated Peak Torque Nm		Limit for Average Torque Nm		Limit for Momentary Peak Torque Nm		Maximum Input Speed rpm		Limit for Average Input Speed rpm		Moment of Inertia	
		Nm	in-lb	Nm	in-lb	Nm	in-lb	Nm	in-lb	Oil	Grease	Oil	Grease	x10⁻⁴kg·m²	x10⁻⁵kgf·m·s²
8	30	0.9	8	1.8	16	1.4-	12	3.3	29	14000	8500	6500	3500	0.003	0.0031
	50	1.8	16	3.3	29	2.3-	20	6.6	58						
	100	2.4	18	4.8	42	3.3-	29	9.0	80						
11	30	2.2	19	4.5	40	3.4-	30	8.5	75	14000	8500	6500	3500	0.012	0.012
	50	3.5	31	8.3	73	5.5-	49	17	150						
	100	5.0	44	11	97	8.9-	79	25	221						
14	30	4.0	35	9.0	80	6.8	60	17	150	14000	8500	6500	3500	0.033	0.034
	50	5.4	48	18	159	6.9	61	35	310						
	80	7.8	69	23	204	11	97	47	416						
	100	7.8	69	28	248	11	97	54	478						
17	30	8.8	78	16	142	12	106	30	266	10000	7300	6500	3500	0.079	0.081
	50	16	142	34	301	26	230	70	620						
	80	22	195	43	381	27	239	87	770						
	100	24	212	54	478	39	345	108	956						
	120	24	212	54	478	39	345	86	761						
	30	15	133	27	239	20	177	50	443						

208

LHSG-I series

Parameter Table

Item / Model No	Reduction Ratio	Rated Torque at 2000r/min	Allowable Peak Torque at Start and Stop	Allowable Average Torque	Allowable Maximum Momentary Torque	Maximum Input Speed	Allowable Average Input Speed	Back lash	Weight	Design Life
		Nm	Nm	Nm	Nm	r/min	r/min	Arc sec	Kg	Hour
14	50	6. 6	23	8. 6	43	8000	3500	≤10	0. 38	10000
	80	9. 6	29	13. 5	57			≤10		15000
	100	9. 6	34	13. 5	66			≤10		15000
17	50	19. 8	42	32	86	7000	3500	≤10	0. 56	10000
	80	27. 5	53	33	108			≤10		15000
	100	30	66	49	134			≤10		15000
	120	30	66	49	107			≤10		15000

ANNEX-VI: Body segment lengths

Body segment lengths in terms of body height H, adpated from winter (Winter, 2009):
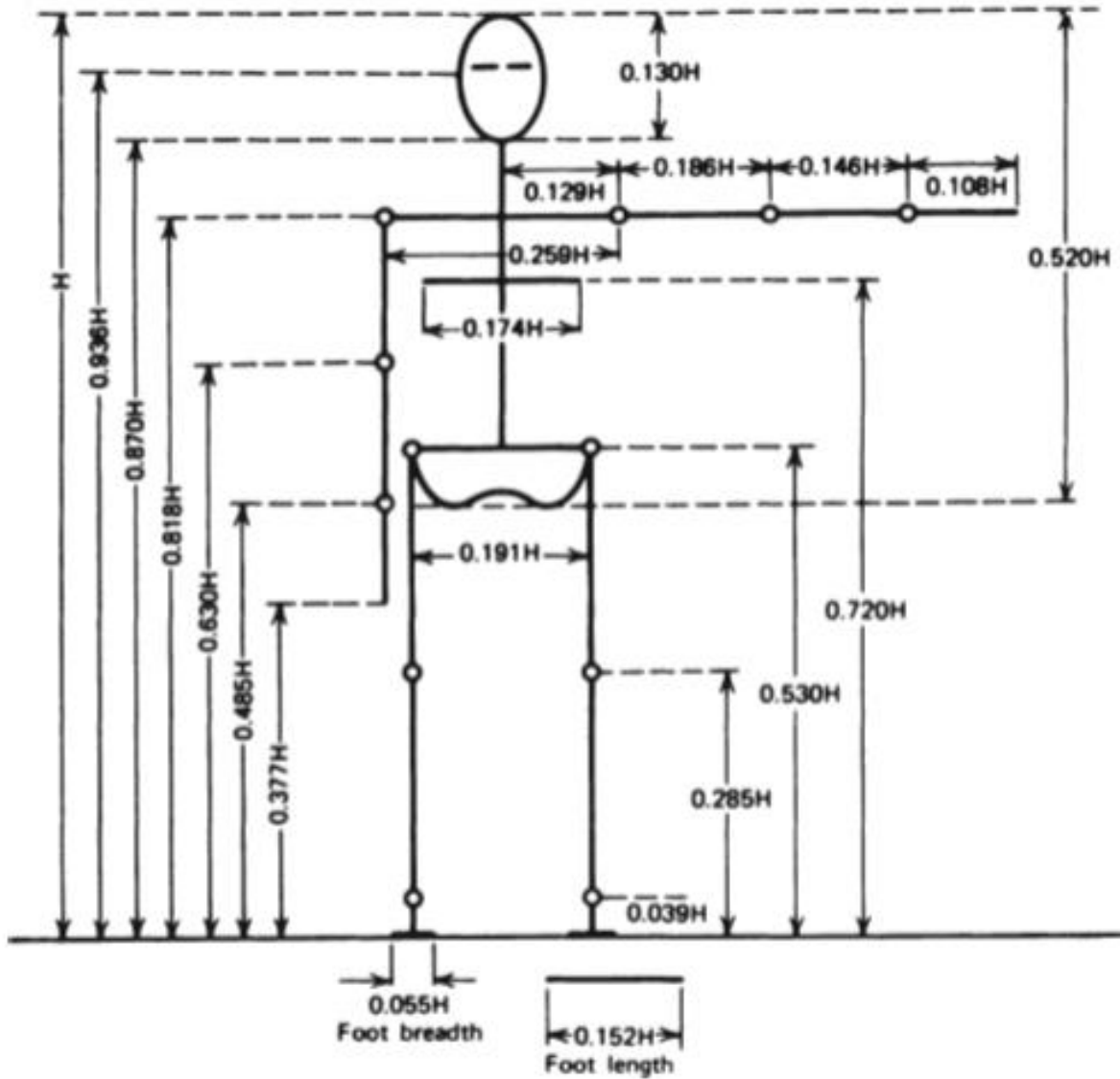
ANNEX-VII: Anthropometric data of human upper limb

Table AV-1: Anthropometric data of human upper limb segments', adapted from (Winter, 2009)

Segments	Segment length/ stature	Segment weight/body weight	Centre of mass/segment length		Radius of Gyration / Segment length		
			Proximal	Distal	C of G	Proximal	Distal
Upper arm	0.186	0.028	0.436	0.564	0.322	0.542	0.645
Forearm	0.146	0.016	0.430	0.570	0.303	0.526	0.647
Hand	0.108	0.006	0.506	0.494	0.297	0.587	0.577
Forearm and Hand	0.254	0.022	0.682	0.318	0.468	0.827	0.565
Total limb	0.44	0.050	0.530	0.470	0.368	0.645	0.569

ANNEX-VIII: Regression coefficients for inertia characteristics of upper limb

Table-A VI-1 Regression coefficients for inertia characteristics of upper limb
Adapted from Zatsiorsky and Seluyanov (1983)

Limb Segment	Constant	Body Weight (kg)	Stature (cm)	R
Moment of Inertia around X axis (kg.cm^2)				
Upper arm	-250.70	1.56	1.512	0.62
Forearm	-64.00	0.95	0.340	0.71
Hand	-19.50	0.17	0.116	0.50
Moment of Inertia around Y axis (kg.cm^2)				
Upper arm	-232.00	1.525	1.343	0.62
Forearm	-67.90	0.855	0.376	0.71
Hand	-13.68	0.088	0.092	0.43
Moment of Inertia around Z axis (kg.cm^2)				
Upper arm	-16.90	0.6620	0.0435	0.44
Forearm	5.66	0.3060	-0.0880	0.66
Hand	-6.26	0.0762	0.0347	0.43

The origin of the coordinate system for each segment is the center of gravity of that segment. The X axis is defined as the frontal plane and +X is the direction from origin towards the front of the body. The Y axis is defined as the saggital plane and +Y is the direction from the origin towards the left of the body. The Z axis is defined as the transverse plane and +Z is the direction from the origin towards the head.

Sample calculation:

$$Moment\ of\ Inertia\ of\ upper\ arm\ around\ Z\ axis\ (kg.cm2) = -16.90 + 0.6620 \times$$

ANNEX-IX: Mass and inertia properties of segment-1
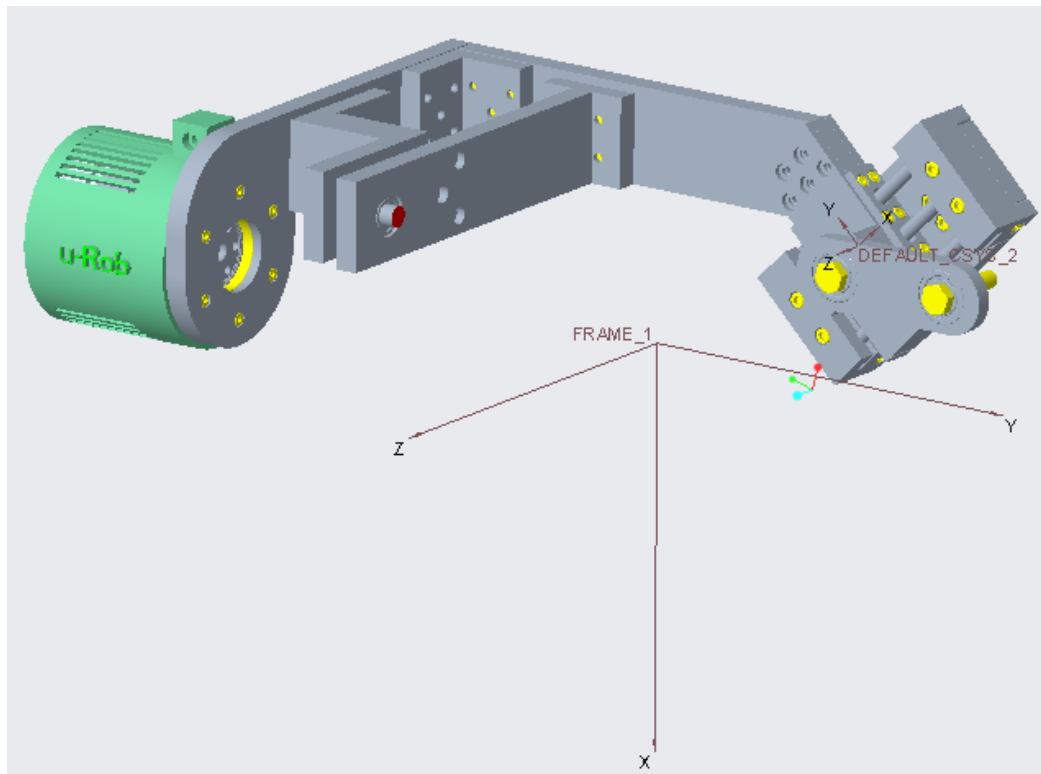
VOLUME = 1.5210317e+06 MM^3
SURFACE AREA = 3.8291479e+05 MM^2
AVERAGE DENSITY = 3.2422788e-06 KILOGRAM / MM^3
MASS = 4.9316090e+00 KILOGRAM

CENTER OF GRAVITY with respect to FRAME1 coordinate frame:
X Y Z   -6.6574741e+00 -2.2155187e+02 -6.3634614e+01 MM

INERTIA with respect to FRAME1 coordinate frame: (KILOGRAM * MM^2)

INERTIA TENSOR:
Ixx Ixy Ixz 3.8059770e+05 -2.1089053e+03 -3.0720038e+03
Iyx Iyy Iyz -2.1089053e+03 5.1678265e+04 -3.3065958e+04
Izx Izy Izz -3.0720038e+03 -3.3065958e+04 3.3673131e+05

INERTIA at CENTER OF GRAVITY with respect to FRAME1 coordinate frame: (KILOGRAM * MM^2)

INERTIA TENSOR:
Ixx Ixy Ixz 1.1855865e+05 5.1650988e+03 -9.8274844e+02
Iyx Iyy Iyz 5.1650988e+03 3.1489807e+04 3.6461679e+04
Izx Izy Izz -9.8274844e+02 3.6461679e+04 9.4443564e+04

PRINCIPAL MOMENTS OF INERTIA: (KILOGRAM * MM^2)
I1 I2 I3   1.4547093e+04 1.1093567e+05 1.1900926e+05

ROTATION MATRIX from FRAME1 orientation to PRINCIPAL AXES:
    -0.04903   -0.15718   0.98635
     0.90842   0.40347   0.10945

213

-0.41517   0.90139   0.12300

ROTATION ANGLES from FRAME1 orientation to PRINCIPAL AXES (degrees):
angles about x y z -41.665   80.523   107.326

RADII OF GYRATION with respect to PRINCIPAL AXES:
R1 R2 R3 5.4311748e+01 1.4998274e+02 1.5534456e+02 MM

ANNEX-X: Mass and inertia properties of segment-2
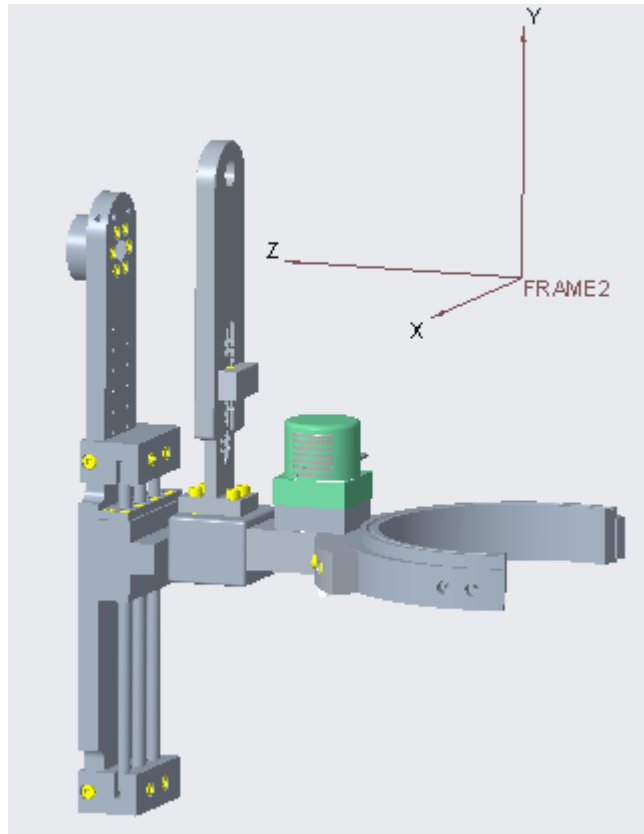
VOLUME = 4.2349922e+05 MM^3
SURFACE AREA = 1.5922355e+05 MM^2
AVERAGE DENSITY = 2.6552223e-06 KILOGRAM / MM^3
MASS = 1.1244846e+00 KILOGRAM

CENTER OF GRAVITY with respect to FRAME2 coordinate frame:
X Y Z   -8.9504485e+00 -1.0954094e+02 1.7296359e+02 MM

INERTIA with respect to FRAME2 coordinate frame: (KILOGRAM * MM^2)

INERTIA TENSOR:
Ixx Ixy Ixz 9.4297056e+04 -3.0367160e+03 -1.6413197e+03
Iyx Iyy Iyz -3.0367160e+03 5.9415830e+04 1.0876395e+04
Izx Izy Izz -1.6413197e+03 1.0876395e+04 3.7917855e+04

INERTIA at CENTER OF GRAVITY with respect to FRAME2 coordinate frame: (KILOGRAM * MM^2)

INERTIA TENSOR:
Ixx Ixy Ixz 4.7163586e+04 -1.9342257e+03 -3.3821362e+03
Iyx Iyy Iyz -1.9342257e+03 2.5685212e+04 -1.0428759e+04
Izx Izy Izz -3.3821362e+03 -1.0428759e+04 2.4334837e+04

PRINCIPAL MOMENTS OF INERTIA: (KILOGRAM * MM^2)
I1 I2 I3   1.4124091e+04 3.5395338e+04 4.7664205e+04

ROTATION MATRIX from FRAME2 orientation to PRINCIPAL AXES:
```
    0.11410    -0.07219    -0.99084
    0.67589     0.73661     0.02416
    0.72812    -0.67246     0.13284
```

ROTATION ANGLES from FRAME2 orientation to PRINCIPAL AXES (degrees):
angles about x y z -10.310   -82.240   32.321

RADII OF GYRATION with respect to PRINCIPAL AXES:
R1 R2 R3 1.1207364e+02 1.7741743e+02 2.0588250e+02 MM

ANNEX-XI: Mass and inertia properties of segment-3
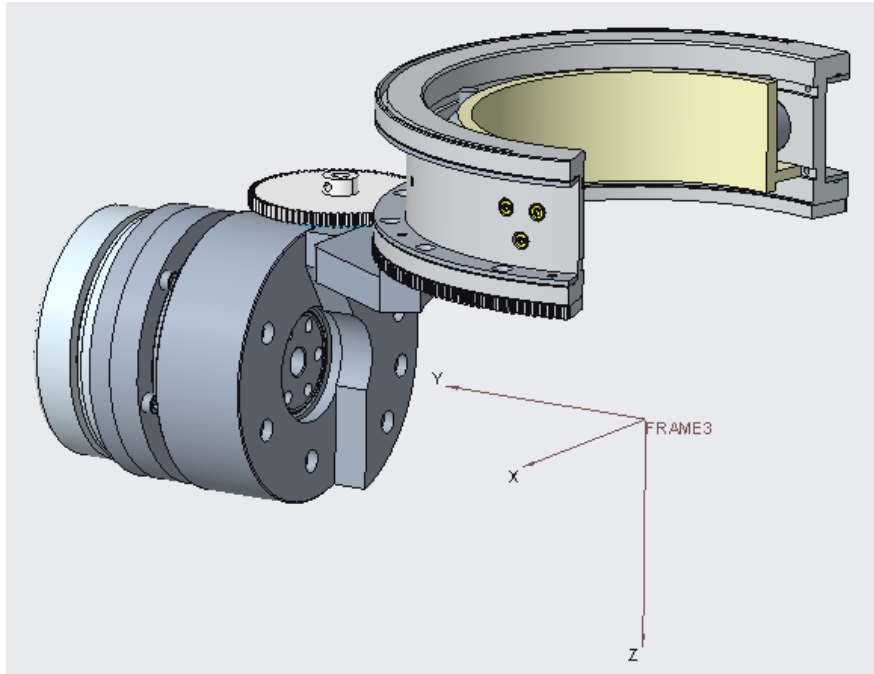
VOLUME = 9.7965792e+05 MM^3
SURFACE AREA = 3.2208701e+05 MM^2
AVERAGE DENSITY = 3.4249822e-06 KILOGRAM / MM^3
MASS = 3.3553110e+00 KILOGRAM

CENTER OF GRAVITY with respect to FRAME3 coordinate frame:
X Y Z   -1.0988248e+01 1.3873613e+02 -2.7719959e+01 MM

INERTIA with respect to FRAME3 coordinate frame: (KILOGRAM * MM^2)

INERTIA TENSOR:
Ixx Ixy Ixz 1.0722475e+05 1.1883512e+03 -3.1155893e+03
Iyx Iyy Iyz 1.1883512e+03 1.7081283e+04 -1.6431594e+03
Izx Izy Izz -3.1155893e+03 -1.6431594e+03 9.7932997e+04

INERTIA at CENTER OF GRAVITY with respect to FRAME3 coordinate frame: (KILOGRAM * MM^2)

INERTIA TENSOR:
Ixx Ixy Ixz 4.0064473e+04 -3.9267097e+03 -2.0935824e+03
Iyx Iyy Iyz -3.9267097e+03 1.4097950e+04 -1.4546880e+04
Izx Izy Izz -2.0935824e+03 -1.4546880e+04 3.2945807e+04

PRINCIPAL MOMENTS OF INERTIA: (KILOGRAM * MM^2)
I1 I2 I3   5.6144189e+03 4.0633396e+04 4.0860415e+04

ROTATION MATRIX from FRAME3 orientation to PRINCIPAL AXES:
     0.12810   -0.97891   0.15916
     0.87138   0.03446   -0.48940
     0.47359   0.20139   0.85741

ROTATION ANGLES from FRAME3 orientation to PRINCIPAL AXES (degrees):

angles about x y z 29.717   9.158   82.544

RADII OF GYRATION with respect to PRINCIPAL AXES:
R1 R2 R3 4.0905906e+01 1.1004623e+02 1.1035322e+02 MM

ANNEX-XII: Mass and inertia properties of segment-4
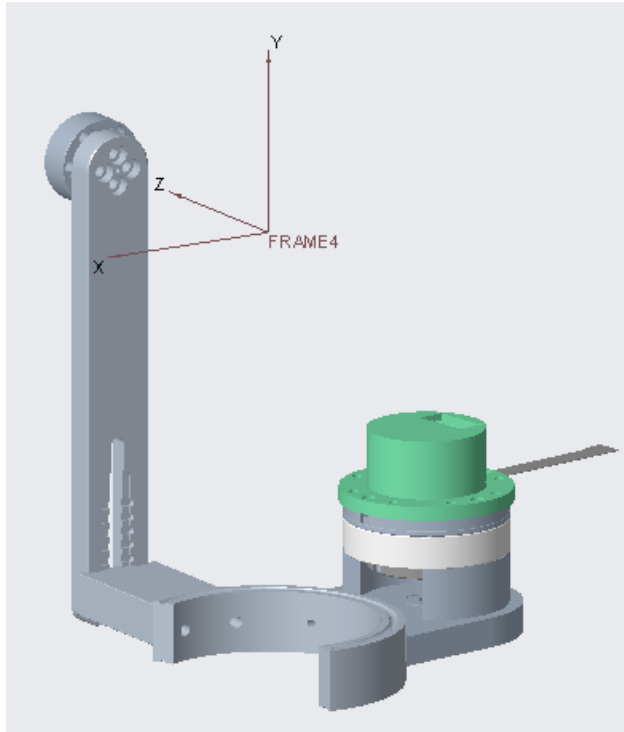
VOLUME = 3.4347806e+05 MM^3
SURFACE AREA = 1.4910371e+05 MM^2
AVERAGE DENSITY = 3.6340632e-06 KILOGRAM / MM^3
MASS = 1.2482210e+00 KILOGRAM

CENTER OF GRAVITY with respect to FRAME4 coordinate frame:
X Y Z -5.7671125e+01 -1.4231862e+02 4.0644131e+01 MM

INERTIA with respect to FRAME4 coordinate frame: (KILOGRAM * MM^2)

INERTIA TENSOR:
Ixx Ixy Ixz 3.1623516e+04 -1.0604081e+04 1.3856520e+03
Iyx Iyy Iyz -1.0604081e+04 1.0862245e+04 6.3120916e+03
Izx Izy Izz 1.3856520e+03 6.3120916e+03 3.3181087e+04

INERTIA at CENTER OF GRAVITY with respect to FRAME4 coordinate frame: (KILOGRAM * MM^2)

INERTIA TENSOR:
Ixx Ixy Ixz 4.2793176e+03 -3.5908805e+02 -1.5401690e+03
Iyx Iyy Iyz -3.5908805e+02 4.6487202e+03 -9.0813903e+02
Izx Izy Izz -1.5401690e+03 -9.0813903e+02 3.7473494e+03

PRINCIPAL MOMENTS OF INERTIA: (KILOGRAM * MM^2)
I1 I2 I3 2.1090406e+03 4.8675676e+03 5.6987791e+03

ROTATION MATRIX from FRAME4 orientation to PRINCIPAL AXES:
     0.58043   -0.50275   -0.64058
     0.34571   0.86438   -0.36515
     0.73729   -0.00951   0.67551

ROTATION ANGLES from FRAME4 orientation to PRINCIPAL AXES (degrees):
angles about x y z 28.394   -39.835   40.898

RADII OF GYRATION with respect to PRINCIPAL AXES:
R1 R2 R3 4.1105197e+01 6.2446809e+01 6.7568638e+01 MM

ANNEX-XIII: Mass and inertia properties of segment-5
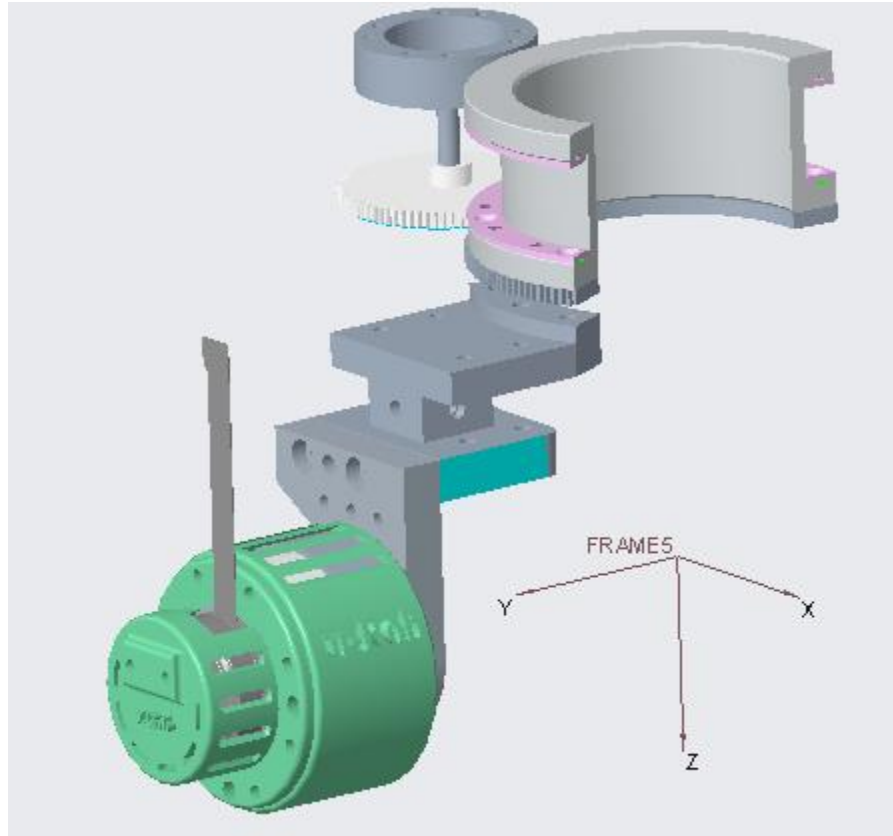
VOLUME = 3.4529351e+05 MM^3
SURFACE AREA = 1.6865978e+05 MM^2
AVERAGE DENSITY = 3.9090396e-06 KILOGRAM / MM^3
MASS = 1.3497660e+00 KILOGRAM

CENTER OF GRAVITY with respect to FRAME5 coordinate frame:
X Y Z -1.8249914e+01 8.3247523e+01 -4.8602695e+01 MM

INERTIA with respect to FRAME5 coordinate frame: (KILOGRAM * MM^2)

INERTIA TENSOR:
Ixx Ixy Ixz 2.2001861e+04 -2.0489979e+01 -2.5652750e+03
Iyx Iyy Iyz -2.0489979e+01 8.7588220e+03 1.4394807e+03
Izx Izy Izz -2.5652750e+03 1.4394807e+03 1.7485454e+04

INERTIA at CENTER OF GRAVITY with respect to FRAME5 coordinate frame: (KILOGRAM * MM^2)

INERTIA TENSOR:
Ixx Ixy Ixz 9.4593327e+03 -2.0711357e+03 -1.3680393e+03
Iyx Iyy Iyz -2.0711357e+03 5.1208229e+03 -4.0217454e+03
Izx Izy Izz -1.3680393e+03 -4.0217454e+03 7.6818208e+03

PRINCIPAL MOMENTS OF INERTIA: (KILOGRAM * MM^2)
I1 I2 I3 1.4162175e+03 1.0193958e+04 1.0651801e+04

ROTATION MATRIX from FRAME5 orientation to PRINCIPAL AXES:

221

```
     0.29463      -0.92384      0.24435
     0.77366       0.08051     -0.62846
     0.56093       0.37420      0.73847
```

ROTATION ANGLES from FRAME5 orientation to PRINCIPAL AXES (degrees):
angles about x y z 40.399   14.143   72.312

RADII OF GYRATION with respect to PRINCIPAL AXES:
R1 R2 R3 3.2391849e+01 8.6904483e+01 8.8834626e+01 MM

ANNEX-XIV: Mass and inertia properties of segment-6
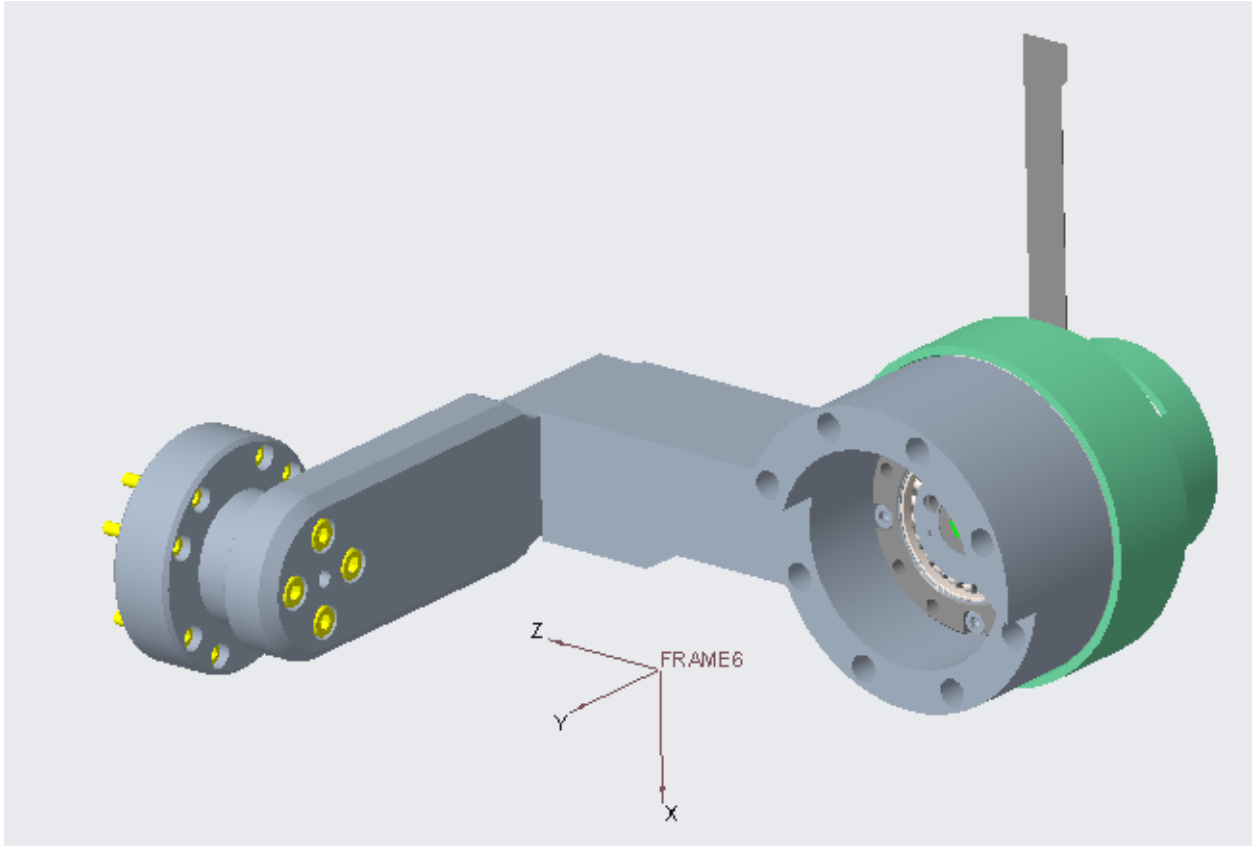
VOLUME = 2.9277946e+05 MM^3
SURFACE AREA = 1.2688631e+05 MM^2
AVERAGE DENSITY = 3.7058610e-06 KILOGRAM / MM^3
MASS = 1.0850000e+00 KILOGRAM

CENTER OF GRAVITY with respect to FRAME6 coordinate frame:
X Y Z   -5.5555846e-01 -9.2656899e+01 3.3806189e+01 MM

INERTIA with respect to FRAME6 coordinate frame: (KILOGRAM * MM^2)

INERTIA TENSOR:
Ixx Ixy Ixz 1.5104176e+04 -5.1066445e+01 2.5583190e+00
Iyx Iyy Iyz -5.1066445e+01 4.1759477e+03 1.6380040e+03
Izx Izy Izz 2.5583190e+00 1.6380040e+03 1.1558849e+04

INERTIA at CENTER OF GRAVITY with respect to FRAME6 coordinate frame: (KILOGRAM * MM^2)

INERTIA TENSOR:
Ixx Ixy Ixz 4.5491237e+03 4.7853672e+00 -1.7819407e+01
Iyx Iyy Iyz 4.7853672e+00 2.9356115e+03 -1.7606246e+03
Izx Izy Izz -1.7819407e+01 -1.7606246e+03 2.2434622e+03

PRINCIPAL MOMENTS OF INERTIA: (KILOGRAM * MM^2)
I1 I2 I3 7.9519107e+02 4.3824990e+03 4.5505072e+03

223

ROTATION MATRIX from FRAME6 orientation to PRINCIPAL AXES:
```
   0.00286    -0.08974    -0.99596
   0.63525     0.76935    -0.06750
   0.77230    -0.63250     0.05920
```

ROTATION ANGLES from FRAME6 orientation to PRINCIPAL AXES (degrees):
angles about x y z 48.745   -84.849   88.177

RADII OF GYRATION with respect to PRINCIPAL AXES:
R1 R2 R3 2.7072033e+01 6.3554462e+01 6.4761222e+01 MM

ANNEX-XV: Mass and inertia properties of segment-7
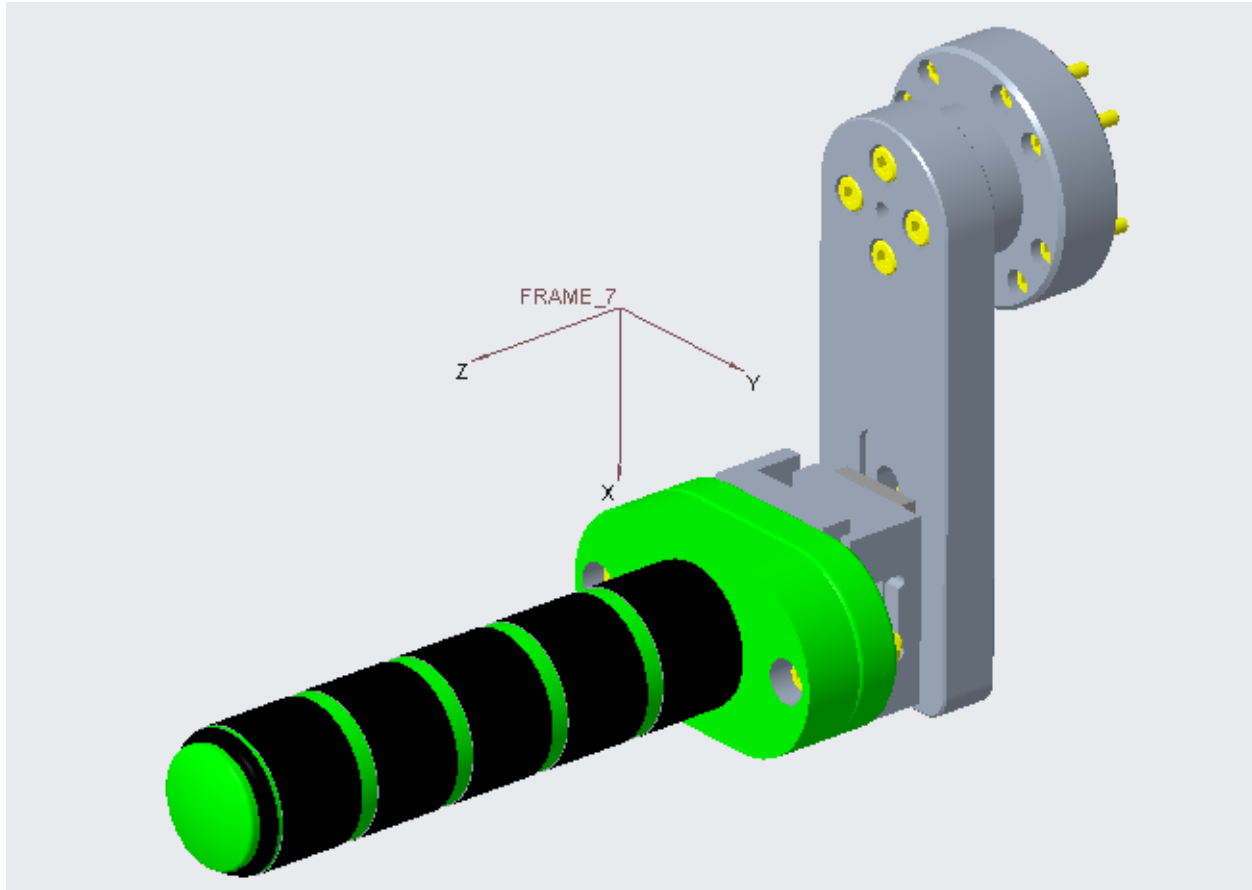
VOLUME = 8.0471311e+04 MM^3
SURFACE AREA = 2.8794220e+04 MM^2
AVERAGE DENSITY = 2.7338936e-06 KILOGRAM / MM^3
MASS = 2.2000000e-01 KILOGRAM

CENTER OF GRAVITY with respect to FRAME7 coordinate frame:
X   Y   Z   2.3881007e+01 0.0000000e+00 -8.0984229e+01 MM

INERTIA with respect to FRAME7 coordinate frame: (KILOGRAM * MM^2)

INERTIA TENSOR:
Ixx Ixy Ixz 1.5112017e+03 0.0000000e+00 3.7544666e+02
Iyx Iyy Iyz 0.0000000e+00 1.8750544e+03 0.0000000e+00
Izx Izy Izz 3.7544666e+02 0.0000000e+00 4.3264167e+02

INERTIA at CENTER OF GRAVITY with respect to FRAME7 coordinate frame: (KILOGRAM * MM^2)

INERTIA TENSOR:
Ixx Ixy Ixz 6.8343705e+01 0.0000000e+00 -5.0030031e+01
Iyx Iyy Iyz 0.0000000e+00 3.0672986e+02 0.0000000e+00
Izx Izy Izz -5.0030031e+01 0.0000000e+00 3.0717512e+02

PRINCIPAL MOMENTS OF INERTIA: (KILOGRAM * MM^2)
I1 I2 I3   5.8286963e+01 3.0672986e+02 3.1723186e+02

ROTATION MATRIX from FRAME7 orientation to PRINCIPAL AXES:
       0.98039   0.00000   -0.19707
       0.00000   1.00000   0.00000
       0.19707   0.00000   0.98039

ROTATION ANGLES from FRAME7 orientation to PRINCIPAL AXES (degrees):
angles about x y z 0.000   -11.366   0.000

RADII OF GYRATION with respect to PRINCIPAL AXES:
R1 R2 R3 1.6277000e+01 3.7339345e+01 3.7973188e+01 MM

REFERENCES

Healthcare Robot market size (2020). [Online]. Global Market Inshights. Available: https://www.grandviewresearch.com/press-release/global-exoskeleton-market [Accessed November 12 2020].

Industry analysis for eoskleton market (2020b). [Online]. Grand View Research. Available: https://www.grandviewresearch.com/press-release/global-exoskeleton-market [Accessed November 13 2020].

2020c. *Physical Therapy Standards of Care and Protocol* [Online]. Department of Rehabilitation Services, Brigham and Women's Hospital. Available: https://www.brighamandwomens.org/patients-and-families/rehabilitation-services/physical-therapy-standards [Accessed May 12 2018].

ACCOGLI, A., GRAZI, L., CREA, S., PANARESE, A., CARPANETO, J., VITIELLO, N. & MICERA, S. EMG-Based Detection of User's Intentions for Human-Machine Shared Control of an Assistive Upper-Limb Exoskeleton. *In:* GONZÁLEZ-VARGAS, J., IBÁÑEZ, J., CONTRERAS-VIDAL, J. L., VAN DER KOOIJ, H. & PONS, J. L., eds. Wearable Robotics: Challenges and Trends, 2017// 2017 Cham. Springer International Publishing, 181-185.

ADAMS, M. M. & HICKS, A. L. 2005. Spasticity after spinal cord injury. *Spinal Cord,* 43**,** 577.

AMIRABDOLLAHIAN, F., LOUREIRO, R., GRADWELL, E., COLLIN, C., HARWIN, W. & JOHNSON, G. 2007. Multivariate analysis of the Fugl-Meyer outcome measures assessing the effectiveness of GENTLE/S robot-mediated stroke therapy. *Journal of NeuroEngineering and Rehabilitation,* 4**,** 4.

BADESA, F. J., MORALES, R., GARCIA-ARACIL, N., SABATER, J. M., CASALS, A. & ZOLLO, L. 2014. Auto-adaptive robot-aided therapy using machine learning techniques. *Computer Methods and Programs in Biomedicine,* 116**,** 123-130.

BADESA, F. J., MORALES, R., GARCIA-ARACIL, N., SABATER, J. M., PEREZ-VIDAL, C. & FERNANDEZ, E. 2012. Multimodal Interfaces to Improve Therapeutic Outcomes in Robot-Assisted Rehabilitation. *IEEE Transactions on Systems, Man, and Cybernetics, Part C (Applications and Reviews),* 42**,** 1152-1158.

BAI, S., CHRISTENSEN, S. & ISLAM, M. R. U. An upper-body exoskeleton with a novel shoulder mechanism for assistive applications. 2017 IEEE International Conference on Advanced Intelligent Mechatronics (AIM), 3-7 July 2017 2017. 1041-1046.

BALASUBRAMANIAN, S. & HE, J. 2012. Adaptive Control of a Wearable Exoskeleton for Upper-Extremity Neurorehabilitation. *Applied Bionics and Biomechanics,* 9.

BALASUBRAMANIAN, S., RUIHUA, W., PEREZ, M., SHEPARD, B., KOENEMAN, E., KOENEMAN, J. & JIPING, H. RUPERT: An exoskeleton robot for assisting rehabilitation of arm functions. 2008 Virtual Rehabilitation, 25-27 Aug. 2008 2008. 163-167.

BASSO, D. M. & LANG, C. E. 2017. Consideration of Dose and Timing When Applying Interventions After Stroke and Spinal Cord Injury. *J Neurol Phys Ther,* 41 Suppl 3**,** S24-s31.

BAYONA, N. A., BITENSKY, J., SALTER, K. & TEASELL, R. 2005. The Role of Task-Specific Training in Rehabilitation Therapies. *Topics in Stroke Rehabilitation,* 12**,** 58-65.

BEIGZADEH, B., ILAMI, M. & NAJAFIAN, S. Design and development of one degree of freedom upper limb exoskeleton. 2015 3rd RSI International Conference on Robotics and Mechatronics (ICROM), 7-9 Oct. 2015 2015. 223-228.

BENJAMIN, E. J., BLAHA, M. J., CHIUVE, S. E., CUSHMAN, M., DAS, S. R., DEO, R., DE FERRANTI, S. D., FLOYD, J., FORNAGE, M., GILLESPIE, C., ISASI, C. R., JIMENEZ, M. C., JORDAN, L. C., JUDD, S. E., LACKLAND, D., LICHTMAN, J. H., LISABETH, L., LIU, S., LONGENECKER, C. T., MACKEY, R. H., MATSUSHITA, K., MOZAFFARIAN, D., MUSSOLINO, M. E., NASIR, K., NEUMAR, R. W., PALANIAPPAN, L., PANDEY, D. K., THIAGARAJAN, R. R., REEVES, M. J., RITCHEY, M., RODRIGUEZ, C. J., ROTH, G. A., ROSAMOND, W. D., SASSON, C., TOWFIGHI, A., TSAO, C. W., TURNER, M. B., VIRANI, S. S., VOEKS, J. H., WILLEY, J. Z., WILKINS, J. T., WU, J. H., ALGER, H. M., WONG, S. S., MUNTNER, P., AMERICAN HEART ASSOCIATION STATISTICS, C. & STROKE STATISTICS, S. 2017. Heart Disease and Stroke Statistics-2017 Update: A Report From the American Heart Association. *Circulation,* 135**,** e146-e603.

BENJAMIN, E. J., MUNTNER, P., ALONSO, A., BITTENCOURT, M. S., CALLAWAY, C. W., CARSON, A. P., CHAMBERLAIN, A. M., CHANG, A. R., CHENG, S., DAS, S. R., DELLING, F. N., DJOUSSE, L., ELKIND, M. S. V., FERGUSON, J. F., FORNAGE, M., JORDAN, L. C., KHAN, S. S., KISSELA, B. M., KNUTSON, K. L., KWAN, T. W., LACKLAND, D. T., LEWIS, T. T., LICHTMAN, J. H., LONGENECKER, C. T., LOOP, M. S., LUTSEY, P. L., MARTIN, S. S., MATSUSHITA, K., MORAN, A. E., MUSSOLINO, M. E., O'FLAHERTY, M., PANDEY, A., PERAK, A. M., ROSAMOND, W. D., ROTH, G. A., SAMPSON, U. K. A., SATOU, G. M., SCHROEDER, E. B., SHAH, S. H., SPARTANO, N. L., STOKES, A., TIRSCHWELL, D. L., TSAO, C. W., TURAKHIA, M. P., VANWAGNER, L. B., WILKINS, J. T., WONG, S. S. & VIRANI,

S. S. 2019. Heart Disease and Stroke Statistics—2019 Update: A Report From the American Heart Association. *Circulation,* 139**,** e56-e528.

BHAGAT, N. A., VENKATAKRISHNAN, A., ABIBULLAEV, B., ARTZ, E. J., YOZBATIRAN, N., BLANK, A. A., FRENCH, J., KARMONIK, C., GROSSMAN, R. G., O'MALLEY, M. K., FRANCISCO, G. E. & CONTRERAS-VIDAL, J. L. 2016. Design and Optimization of an EEG-Based Brain Machine Interface (BMI) to an Upper-Limb Exoskeleton for Stroke Survivors. *Frontiers in Neuroscience,* 10.

BLENNERHASSETT, J. & DITE, W. 2004. Additional task-related practice improves mobility and upper limb function early after stroke: A randomised controlled trial. *Australian Journal of Physiotherapy,* 50**,** 219-224.

BOISSONEAULT, C., GRIMES, T., ROSE, D. K., WATERS, M. F., KHANNA, A., DATTA, S. & DALY, J. J. 2020. Innovative Long-Dose Neurorehabilitation for Balance and Mobility in Chronic Stroke: A Preliminary Case Series. *Brain Sci,* 10.

BRACKBILL, E. A., MAO, Y., AGRAWAL, S. K., ANNAPRAGADA, M. & DUBEY, V. N. Dynamics and control of a 4-dof wearable cable-driven upper arm exoskeleton. 2009 IEEE International Conference on Robotics and Automation, 12-17 May 2009 2009. 2300-2305.

BRAHIM, B., RAHMAN, M., SAAD, M., OCHOA LUNA, C. & ISLAM, M. R. 2016. Sliding mode-backstepping control for upper-limb rehabilitation with the ets-marse exoskeleton robot. *RESNA 2016.* Arlington, VA.

BRAHMI, B., SAAD, M., BRAHMI, A., LUNA, C. O. & RAHMAN, M. H. 2018. Compliant control for wearable exoskeleton robot based on human inverse kinematics. *International Journal of Advanced Robotic Systems,* 15**,** 1729881418812133.

BUDYNAS., R. G. & NISBETT, J. K. 2015. *SHIGLEY'S Mechanical engineering design,* New York, McGraw-Hill Publishing Company.

BURGAR, C. G., LUM, P.S., SHOR, P.C., DER LOOS, H F M V 2000. Development of robots for rehabilitation therapy: the Palo Alto VA/Stanford experience. *J Rehabil Res Dev,* 37**,** 663–673.

BURGAR, G. C., LUM, P., A SCREMIN, M., GARBER, S., VAN DER LOOS, M., KENNEY, D. & C SHOR, P. 2011. Robot-assisted upper-limb therapy in acute rehabilitation setting following stroke: Department of Veterans Affairs multisite clinical trial. *J Rehabil Res Dev,* 48**,** 445-458.

CAMPOLO, D., TOMMASINO, P., GAMAGE, K., KLEIN, J., HUGHES, C. M. L. & MASIA, L. 2014. H-Man: A planar, H-shape cabled differential robotic manipulandum for experiments on human motor control. *Journal of Neuroscience Methods,* 235**,** 285-297.

CARIGNAN, C., TANG, J., RODERICK, S. & NAYLOR, M. A Configuration-Space Approach to Controlling a Rehabilitation Arm Exoskeleton. 2007 IEEE 10th International Conference on Rehabilitation Robotics, 13-15 June 2007 2007. 179-187.

CEPEDA, N. J., PASHLER, H., VUL, E., WIXTED, J. T. & ROHRER, D. 2006. Distributed practice in verbal recall tasks: A review and quantitative synthesis. *Psychol Bull,* 132**,** 354-80.

CHANG, J.-J., TUNG, W.-L., WU, W.-L., HUANG, M.-H. & SU, F.-C. 2007. Effects of Robot-Aided Bilateral Force-Induced Isokinetic Arm Training Combined With Conventional Rehabilitation on Arm Motor Function in Patients With Chronic Stroke. *Archives of Physical Medicine and Rehabilitation,* 88**,** 1332-1338.

CHEN, Y., FAN, J., ZHU, Y., ZHAO, J. & CAI, H. 2015. A passively safe cable driven upper limb rehabilitation exoskeleton. *Technology and Health Care,* 23**,** S197–S202

CHEN, Y., LI, G., ZHU, Y., ZHAO, J. & CAI, H. 2014. Design of a 6-DOF upper limb rehabilitation exoskeleton with parallel actuated joints. *Bio-medical materials and engineering,* 24**,** 2527-2535.

CHENG, H.-S., JU, M.-S. & LIN, C.-C. K. 2004. Improving Elbow Torque Output of Stroke Patients with Assistive Torque Controlled by EMG Signals. *Journal of Biomechanical Engineering,* 125**,** 881-886.

CHRISTENSEN, S. & BAI, S. A Novel Shoulder Mechanism with a Double Parallelogram Linkage for Upper-Body Exoskeletons. 2017 Cham. Springer International Publishing, 51-56.

COLOMBO, R., PISANO, F., MICERA, S., MAZZONE, A., DELCONTE, C., CARROZZA, M. C., DARIO, P. & MINUCO, G. 2007. Assessing Mechanisms of Recovery During Robot-Aided Neurorehabilitation of the Upper Limb. *Neurorehabilitation and Neural Repair,* 22**,** 50-63.

COOTE, S., MURPHY, B., HARWIN, W. & STOKES, E. 2008. The effect of the GENTLE/s robot-mediated therapy system on arm function after stroke. *Clinical Rehabilitation,* 22**,** 395-405.

CRABOLU, M., PANI, D., RAFFO, L., CONTI, M., CRIVELLI, P. & CEREATTI, A. 2017. In vivo estimation of the shoulder joint center of rotation using magneto-inertial sensors: MRI-based accuracy and repeatability assessment. *Biomedical engineering online,* 16**,** 34-34.

CRAIG, J. J. 2017. *Introduction to Robotics: Mechanics and Control,* Upper saddle river, New Jersy, Pearson, 448 pages.

CREA, S., CEMPINI, M., MOISÈ, M., BALDONI, A., TRIGILI, E., MARCONI, D., CORTESE, M., GIOVACCHINI, F., POSTERARO, F. & VITIELLO, N. A novel shoulder-elbow exoskeleton with series elastic actuators. 2016 6th IEEE International Conference on Biomedical Robotics and Biomechatronics (BioRob), 26-29 June 2016 2016. 1248-1253.

CUI, X., CHEN, W., JIN, X. & AGRAWAL, S. K. 2017. Design of a 7-DOF Cable-Driven Arm Exoskeleton (CAREX-7) and a Controller for Dexterous Motion Training or Assistance. *IEEE/ASME Transactions on Mechatronics,* 22**,** 161-172.

DALY, J. J. & RUFF, R. L. 2007. Construction of efficacious gait and upper limb functional interventions based on brain plasticity evidence and model-based measures for stroke patients. *ScientificWorldJournal,* 7**,** 2031-45.

DENAVIT, J. & HARTENBERG, R. S. 1955. A kinematic notation for lower-pair mechanisms based on matrices. *Trans. of the ASME. Journal of Applied Mechanics,* 22**,** 215-221.

DI RIENZO, F., DEBARNOT, U., DALIGAULT, S., SARUCO, E., DELPUECH, C., DOYON, J., COLLET, C. & GUILLOT, A. 2016. Online and Offline Performance Gains Following Motor Imagery Practice: A Comprehensive Review of Behavioral and Neuroimaging Studies. *Frontiers in human neuroscience,* 10**,** 315-315.

DODSON, C. C., CORDASCO,F.A. 2008. Anterior glenohumeral joint dislocations. *Orthop Clin North Am* 39**,** 507-518, vii.

DROMERICK, A. W., LANG, C. E., BIRKENMEIER, R. L., WAGNER, J. M., MILLER, J. P., VIDEEN, T. O., POWERS, W. J., WOLF, S. L. & EDWARDS, D. F. 2009. Very Early Constraint-Induced Movement during Stroke Rehabilitation (VECTORS): A single-center RCT. *Neurology,* 73**,** 195-201.

DVIR, Z. & BERME, N. 1978. The shoulder complex in elevation of the arm: A mechanism approach. *Journal of Biomechanics,* 11**,** 219-225.

FAZEKAS, G., HORVATH, M., TROZNAI, T. & TOTH, A. 2007. Robot-mediated upper limb physiotherapy for patients with spastic hemiparesis: A preliminary study. *Journal of Rehabilitation Medicine,* 39**,** 580-582.

FITLE, K. D., PEHLIVAN, A. U. & MALLEY, M. K. O. A robotic exoskeleton for rehabilitation and assessment of the upper limb following incomplete spinal cord injury. 2015 IEEE International Conference on Robotics and Automation (ICRA), 26-30 May 2015 2015. 4960-4966.

FLINTREHAB. 2020. *Arm Exercises for Stroke Patients* [Online]. [Accessed May 2020].

FRAILE, J. C., PÉREZ-TURIEL, J., BAEYENS, E., VIÑAS, P., ALONSO, R., CUADRADO, A., FRANCO-MARTÍN, M., PARRA, E., AYUSO, L., GARCÍA-BRAVO, F., NIETO, F. & LAURENTIU, L. 2016. E2Rebot: A robotic platform for upper limb rehabilitation in patients with neuromotor disability. *Advances in Mechanical Engineering,* 8**,** 1687814016659050.

FREEMAN, C. T., HUGHES, A. M., BURRIDGE, J. H., CHAPPELL, P. H., LEWIN, P. L. & ROGERS, E. 2009. A robotic workstation for stroke rehabilitation of the upper extremity using FES. *Medical Engineering and Physics,* 31**,** 364-373.

FRENCH, J. A., ROSE, C. G. & O'MALLEY, M. K. 2014. System Characterization of MAHI Exo-II: A Robotic Exoskeleton for Upper Extremity Rehabilitation. V003T43A006.

FRISOLI, A., SALSEDO, F., BERGAMASCO, M., ROSSI, B. & CARBONCINI, M. C. 2009. A Force-Feedback Exoskeleton for Upper-Limb Rehabilitation in Virtual Reality. *Applied Bionics and Biomechanics,* 6.

GAMS, A. & LENARCIC, J. Humanoid arm kinematic modeling and trajectory generation. The First IEEE/RAS-EMBS International Conference on Biomedical Robotics and Biomechatronics, 2006. BioRob 2006., 20-22 Feb. 2006 2006. 301-305.

GANDOLFI, M., FORMAGGIO, E., GEROIN, C., STORTI, S. F., BOSCOLO GALAZZO, I., BORTOLAMI, M., SALTUARI, L., PICELLI, A., WALDNER, A., MANGANOTTI, P. & SMANIA, N. 2018. Quantification of Upper Limb Motor Recovery and EEG Power Changes after Robot-Assisted Bilateral Arm Training in Chronic Stroke Patients: A Prospective Pilot Study. *Neural Plasticity,* 2018**,** 15.

GARREC, P., FRICONNEAU, J. P., MEASSON, Y. & PERROT, Y. ABLE, an innovative transparent exoskeleton for the upper-limb. 2008 IEEE/RSJ International Conference on Intelligent Robots and Systems, 22-26 Sept. 2008 2008. 1483-1488.

GARRIDO, J., YU, W. & LI, X. 2016. Modular design and control of an upper limb exoskeleton. *Journal of Mechanical Science and Technology,* 30**,** 2265-2271.

GATES, D. H., WALTERS, L. S., COWLEY, J., WILKEN, J. M. & RESNIK, L. 2015. Range of Motion Requirements for Upper-Limb Activities of Daily Living. *American Journal of Occupational Therapy,* 70**,** 7001350010p1-7001350010p10.

GOPURA, R. A. R. C., BANDARA, D. S. V., KIGUCHI, K. & MANN, G. K. I. 2016. Developments in hardware systems of active upper-limb exoskeleton robots: A review. *Robotics and Autonomous Systems,* 75**,** 203-220.

GOPURA, R. A. R. C., KIGUCHI, K. & LI, Y. SUEFUL-7: A 7DOF upper-limb exoskeleton robot with muscle-model-oriented EMG-based control. 2009 IEEE/RSJ International Conference on Intelligent Robots and Systems, 10-15 Oct. 2009 2009. 1126-1131.

GRAY, H. & CLEMENTE, C. D. 1985. *Anatomy of the human body*, Philadelphia (Pa.) : Lea & Febiger.

GRESHAM, G. E., ALEXANDER, D., BISHOP, D. S., GIULIANI, C., GOLDBERG, G., HOLLAND, A., KELLY-HAYES, M., LINN, R. T., ROTH, E. J., STASON, W. B. & TROMBLY, C. A. 1997. Rehabilitation. *Stroke,* 28**,** 1522-1526.

GUADAGNOLI, M. A. & LEE, T. D. 2004. Challenge point: a framework for conceptualizing the effects of various practice conditions in motor learning. *J Mot Behav,* 36**,** 212-24.

GUIDALI, M., DUSCHAU-WICKE, A., BROGGI, S., KLAMROTH-MARGANSKA, V., NEF, T. & RIENER, R. 2011. A robotic system to train activities of daily living in a virtual environment. *Medical & Biological Engineering & Computing,* 49**,** 1213.

GUNASEKARA, M., GOPURA, R. & JAYAWARDENA, S. 2015. 6-REXOS: Upper Limb Exoskeleton Robot with Improved pHRI. *International Journal of Advanced Robotic Systems,* 12**,** 47.

GUPTA, A. & MALLEY, M. K. O. 2006. Design of a haptic arm exoskeleton for training and rehabilitation. *IEEE/ASME Transactions on Mechatronics,* 11**,** 280-289.

HALDER, A. M., ITOI, E. & AN, K.-N. 2000. ANATOMY AND BIOMECHANICS OF THE SHOULDER. *Orthopedic Clinics,* 31**,** 159-176.

HALLETT, M., SHAHANI, B. T. & YOUNG, R. R. 1975. EMG analysis of stereotyped voluntary movements in man. *Journal of Neurology, Neurosurgery &amp; Psychiatry,* 38**,** 1154.

HAMILTON, N., WEIMAR, W. & LUTTGENS, K. 2012. *Kinesiology: Scientific Basis of Human Motion, 12th,* New York, NY, McGraw-Hill, XV, 622p.

HEIDENREICH, P. A., TROGDON, J. G., KHAVJOU, O. A., BUTLER, J., DRACUP, K., EZEKOWITZ, M. D., FINKELSTEIN, E. A., HONG, Y., JOHNSTON, S. C., KHERA, A., LLOYD-JONES, D. M., NELSON, S. A., NICHOL, G., ORENSTEIN, D., WILSON, P. W. F. & WOO, Y. J. 2011. Forecasting the Future of Cardiovascular Disease in the United States. *Circulation*.

HESSE, S., SCHULTE-TIGGES, G., KONRAD, M., BARDELEBEN, A. & WERNER, C. 2003. *Robot-assisted arm trainer for the passive and active practice of bilateral forearm and wrist movements in hemiparetic subjects 1 1 An organization with which 1 or more of the authors is associated has received or will receive financial benefits from a commercial party having a direct financial interest in the results of the research supporting this article*.

HOGAN, N. & I KREBS, H. 2004. *Interactive robots for neuro-rehabilitation*.

HOGAN, N., KREBS, H. I., CHARNNARONG, J., SRIKRISHNA, P. & SHARON, A. MIT-MANUS: a workstation for manual therapy and training. I. [1992] Proceedings IEEE International Workshop on Robot and Human Communication, 1-3 Sep 1992 1992. 161-165.

HOLDEN, M. K. 2005. Virtual environments for motor rehabilitation: review. *Cyberpsychol Behav,* 8**,** 187-211; discussion 212-9.

HOLZBAUR, K. R. S., MURRAY, W. M. & DELP, S. L. 2005. A Model of the Upper Extremity for Simulating Musculoskeletal Surgery and Analyzing Neuromuscular Control. *Annals of Biomedical Engineering,* 33**,** 829-840.

HOU, Y. & KIGUCHI, K. Virtual Tunnel Generation Algorithm for Perception-Assist with an Upper-Limb Exoskeleton Robot. 2018 IEEE International Conference on Cyborg and Bionic Systems (CBS), 25-27 Oct. 2018 2018. 204-209.

HU, X. L., TONG, K. Y., SONG, R., ZHENG, X. J., LUI, K. H., LEUNG, W. W. F., NG, S. & AU-YEUNG, S. S. Y. 2009. Quantitative evaluation of motor functional recovery process in chronic stroke patients during robot-assisted wrist training. *Journal of Electromyography and Kinesiology,* 19**,** 639-650.

HUSSAIN, A., BUDHOTA, A., HUGHES, C. M. L., DAILEY, W. D., VISHWANATH, D. A., KUAH, C. W. K., YAM, L. H. L., LOH, Y. J., XIANG, L., CHUA, K. S. G., BURDET, E. & CAMPOLO, D. 2016. Self-Paced Reaching after Stroke: A Quantitative Assessment

of Longitudinal and Directional Sensitivity Using the H-Man Planar Robot for Upper Limb Neurorehabilitation. *Frontiers in Neuroscience,* 10.

HUSSAIN, A., DAILEY, W., HUGHES, C., BUDHOTA, A., GAMAGE, W. G. K. C., VISHWANATH, D. A., KUAH, C., CHUA, K., BURDET, E. & CAMPOLO, D. Quantitative motor assessment of upperlimb after unilateral stroke: A preliminary feasibility study with H-Man, a planar robot. 2015 IEEE International Conference on Rehabilitation Robotics (ICORR), 11-14 Aug. 2015 2015. 654-659.

ISLAM, M. R., ASSAD-UZ-ZAMAN, M., AL ZUBAYER SWAPNIL, A., AHMED, T. & RAHMAN, M. H. 2020a. An ergonomic shoulder for robot-aided rehabilitation with hybrid control. *Microsystem Technologies*.

ISLAM, M. R., ASSAD-UZ-ZAMAN, M. & RAHMAN, M. H. 2020b. Design and control of an ergonomic robotic shoulder for wearable exoskeleton robot for rehabilitation. *International Journal of Dynamics and Control,* 8**,** 312-325.

ISLAM, M. R., ASSAD-UZ-ZAMAN, M., SPIEWAK, C. & RAHMAN, M. H. Motion control of a robotic device for passive rehabilitation of human shoulder and elbow joint movement. 2017 IEEE Great Lakes Biomedical Conference (GLBC), 6-7 April 2017 2017. 1-1.

ISLAM, M. R., RAHMANI, M. & RAHMAN, M. H. 2020c. A Novel Exoskeleton with Fractional Sliding Mode Control for Upper Limb Rehabilitation. *Robotica***,** 1-22.

J REINKENSMEYER, D., E KAHN, L., AVERBUCH, M., MCKENNA-COLE, A. N., SCHMIT, B. & RYMER, W. 2000. Understanding and treating arm movement impairment after chronic brain injury: Progress with the ARM Guide. *The Journal of Rehabilitation Research and Development,* 37**,** 653-62.

JANNE, M. V., ANNELI, C. L.-A., ERWIN, E. H. V. W., CAREL, G. M. M. & GERT, K. 2016. Effects of Robot-Assisted Therapy for the Upper Limb After Stroke: A Systematic Review and Meta-analysis. *Neurorehabilitation and Neural Repair,* 31**,** 107-121.

JARRETT, C. & MCDAID, A. J. 2017. Robust Control of a Cable-Driven Soft Exoskeleton Joint for Intrinsic Human-Robot Interaction. *IEEE Transactions on Neural Systems and Rehabilitation Engineering,* 25**,** 976-986.

JIANG, L., DOU, Z.-L., WANG, Q., WANG, Q.-Y., DAI, M., WANG, Z., WEI, X.-M. & CHEN, Y.-B. 2015. Evaluation of clinical outcomes of patients with post-stroke wrist and finger spasticity after ultrasonography-guided BTX-A injection and rehabilitation training. *Frontiers in Human Neuroscience,* 9**,** 485.

JOHNSON, G. R., CARUS, D. A., PARRINI, G., MARCHESE, S. & VALEGGI, R. 2001. The design of a five-degree-of-freedom powered orthosis for the upper limb. *Proceedings of the Institution of Mechanical Engineers, Part H: Journal of Engineering in Medicine,* 215**,** 275-284.

KANG, H.-B. & WANG, J.-H. 2015. Adaptive robust control of 5 DOF Upper-limb exoskeleton robot. *International Journal of Control, Automation and Systems,* 13**,** 733-741.

KIGUCHI, K., ESAKI, R., TSURUTA, T., WATANABE, K. & FUKUDA, T. An exoskeleton system for elbow joint motion rehabilitation. Proceedings 2003 IEEE/ASME International Conference on Advanced Intelligent Mechatronics (AIM 2003), 20-24 July 2003 2003. 1228-1233 vol.2.

KIGUCHI, K. & HAYASHI, Y. 2012. An EMG-Based Control for an Upper-Limb Power-Assist Exoskeleton Robot. *IEEE Transactions on Systems, Man, and Cybernetics, Part B (Cybernetics),* 42**,** 1064-1071.

KIGUCHI, K., RAHMAN, M. H., SASAKI, M. & TERAMOTO, K. 2008. Development of a 3DOF mobile exoskeleton robot for human upper-limb motion assist. *Robot. Auton. Syst.,* 56**,** 678-691.

KIM, B. & DESHPANDE, A. D. Controls for the shoulder mechanism of an upper-body exoskeleton for promoting scapulohumeral rhythm. 2015 IEEE International Conference on Rehabilitation Robotics (ICORR), 11-14 Aug. 2015 2015. 538-542.

KIM, B. & DESHPANDE, A. D. 2017. An upper-body rehabilitation exoskeleton Harmony with an anatomical shoulder mechanism: Design, modeling, control, and performance evaluation. *The International Journal of Robotics Research,* 36**,** 414-435.

KIM, G., LIM, S., KIM, H., LEE, B., SEO, S., CHO, K. & LEE, W. 2017. Is robot-assisted therapy effective in upper extremity recovery in early stage stroke? —a systematic literature review. *Journal of Physical Therapy Science,* 29**,** 1108-1112.

KIM, H. & KIM, J. 2017. Control of the seven-degree-of-freedom upper limb exoskeleton for an improved human-robot interface. *Journal of the Korean Physical Society,* 70**,** 726-734.

KIM, K., PARK, D. S., KO, B. W., LEE, J., YANG, S. N., KIM, J. & SONG, W. K. Arm motion analysis of stroke patients in activities of daily living tasks: A preliminary study. 2011 Annual International Conference of the IEEE Engineering in Medicine and Biology Society, Aug. 30 2011-Sept. 3 2011 2011. 1287-1291.

KLEIM, J. A. & JONES, T. A. 2008. Principles of experience-dependent neural plasticity: implications for rehabilitation after brain damage. *J Speech Lang Hear Res,* 51**,** S225-39.

KLEIN, J., SPENCER, S., ALLINGTON, J., BOBROW, J. E. & REINKENSMEYER, D. J. 2010. Optimization of a Parallel Shoulder Mechanism to Achieve a High-Force, Low-Mass, Robotic-Arm Exoskeleton. *IEEE Transactions on Robotics,* 26**,** 710-715.

KNILL, D. C. & POUGET, A. 2004. The Bayesian brain: the role of uncertainty in neural coding and computation. *Trends in Neurosciences,* 27**,** 712-719.

KOMMU S S 2007. *Rehabilitation Robotics,* Vienna, Austria, Itech Education and Publishing.

KREBS, H. I., EDWARDS, D. & HOGAN, N. 2016. Forging Mens et Manus: The MIT Experience in Upper Extremity Robotic Therapy. *In:* REINKENSMEYER, D. J. & DIETZ, V. (eds.) *Neurorehabilitation Technology.* Cham: Springer International Publishing.

KREBS, H. I., VOLPE, B. T., WILLIAMS, D., CELESTINO, J., CHARLES, S. K., LYNCH, D. & HOGAN, N. 2007. Robot-Aided Neurorehabilitation: A Robot for Wrist Rehabilitation. *IEEE Transactions on Neural Systems and Rehabilitation Engineering,* 15**,** 327-335.

KUCERA, E., HAFFNER, O. & LESKOVSKÝ, R. Interactive and virtual/mixed reality applications for mechatronics education developed in unity engine. 2018 Cybernetics & Informatics (K&I), 31 Jan.-3 Feb. 2018 2018. 1-5.

KUNG, P. C., JU, M. S. & LIN, C. C. K. Design of a forearm rehabilitation robot. 2007 IEEE 10th International Conference on Rehabilitation Robotics, 13-15 June 2007 2007. 228-233.

KWAKKEL, G. Intensity of practice after stroke: More is better. 2009.

KWAKKEL, G., KOLLEN, B. & TWISK, J. 2006. Impact of time on improvement of outcome after stroke. *Stroke,* 37**,** 2348-53.

KWAKKEL, G., KOLLEN, B. J., VAN DER GROND, J. & PREVO, A. J. H. 2003. Probability of Regaining Dexterity in the Flaccid Upper Limb. *Stroke,* 34**,** 2181.

KWAKKEL, G., VEERBEEK, J. M., VAN WEGEN, E. E. H. & WOLF, S. L. 2015. Constraint-induced movement therapy after stroke. *The Lancet. Neurology,* 14**,** 224-234.

LAKHAL, O., MELINGUI, A. & MERZOUKI, R. 2016. Hybrid Approach for Modeling and Solving of Kinematics of a Compact Bionic Handling Assistant Manipulator. *IEEE/ASME Transactions on Mechatronics,* 21**,** 1326-1335.

LANGHORNE, P., BERNHARDT, J. & KWAKKEL, G. 2011. Stroke rehabilitation. *Lancet,* 377**,** 1693-702.

LAVER, K. E., LANGE, B., GEORGE, S., DEUTSCH, J. E., SAPOSNIK, G. & CROTTY, M. 2017. Virtual reality for stroke rehabilitation. *Cochrane Database of Systematic Reviews*.

LEE, K. W., KIM, S. B., LEE, J. H., LEE, S. J. & KIM, J. W. 2017. Effect of Robot-Assisted Game Training on Upper Extremity Function in Stroke Patients. *Annals of Rehabilitation Medicine,* 41**,** 539-546.

LENAR, J., #269, #269, KLOP, N., #269 & AR 2006. Positional kinematics of humanoid arms. *Robotica,* 24**,** 105-112.

LI, Z., HUANG, Z., HE, W. & SU, C. Y. 2017. Adaptive Impedance Control for an Upper Limb Robotic Exoskeleton Using Biological Signals. *IEEE Transactions on Industrial Electronics,* 64**,** 1664-1674.

LI, Z., SU, C., LI, G. & SU, H. 2015. Fuzzy Approximation-Based Adaptive Backstepping Control of an Exoskeleton for Human Upper Limbs. *IEEE Transactions on Fuzzy Systems,* 23**,** 555-566.

LIU, L., SHI, Y.-Y. & XIE, L. 2016. A NOVEL MULTI-DOF EXOSKELETON ROBOT FOR UPPER LIMB REHABILITATION. *Journal of Mechanics in Medicine and Biology,* 16**,** 1640023.

LOHSE, K. R., LANG, C. E. & BOYD, L. A. 2014. Is More Better? Using Metadata to Explore Dose–Response Relationships in Stroke Rehabilitation. *Stroke,* 45**,** 2053-2058.

LUM, P., G BURGAR, C., VAN DER LOOS, M., C SHOR, P., MAJMUNDAR, M. & YAP, R. 2006. *MIME robotic device for upper-limb neurorehabilitation in subacute stroke subjects: A follow-up study*.

LUM, P. S., BURGAR, C. G., SHOR, P. C., MAJMUNDAR, M. & VAN DER LOOS, M. 2002. Robot-assisted movement training compared with conventional therapy techniques for the rehabilitation of upper-limb motor function after stroke. *Archives of Physical Medicine and Rehabilitation,* 83**,** 952-959.

MADANI, T., DAACHI, B. & DJOUANI, K. 2017. Modular-Controller-Design-Based Fast Terminal Sliding Mode for Articulated Exoskeleton Systems. *IEEE Transactions on Control Systems Technology,* 25**,** 1133-1140.

MAHDAVIAN, M., TOUDESHKI, A. G. & YOUSEFI-KOMA, A. Design and fabrication of a 3DoF upper limb exoskeleton. 2015 3rd RSI International Conference on Robotics and Mechatronics (ICROM), 7-9 Oct. 2015 2015. 342-346.

MAIER, M., BALLESTER, B. R. & VERSCHURE, P. F. M. J. 2019. Principles of Neurorehabilitation After Stroke Based on Motor Learning and Brain Plasticity Mechanisms. *Frontiers in Systems Neuroscience,* 13.

MALOSIO, M., PEDROCCHI, N., VICENTINI, F. & TOSATTI, L. M. Analysis of elbow-joints misalignment in upper-limb exoskeleton. 2011 IEEE International Conference on Rehabilitation Robotics, June 29 2011-July 1 2011 2011. 1-6.

MASIA, L., KREBS, H. I., CAPPA, P. & HOGAN, N. 2007. Design and Characterization of Hand Module for Whole-Arm Rehabilitation Following Stroke. *IEEE/ASME Transactions on Mechatronics,* 12**,** 399-407.

MEHTA, J. A., BAIN, G.I 2004. Elbow dislocations in adults and children. *Clin Sports Med 23* 23**,** 609-627.

MIHELJ, M., NEF, T. & RIENER, R. ARMin II - 7 DoF rehabilitation robot: mechanics and kinematics. Proceedings 2007 IEEE International Conference on Robotics and Automation, 10-14 April 2007 2007. 4120-4125.

MOESLUND, T. B., MADSEN, C. B. & GRANUM, E. 2005. Modelling the 3D pose of a human arm and the shoulder complex utilising only two parameters. *Integr. Comput.-Aided Eng.,* 12**,** 159-175.

MOZAFFARIAN, D., BENJAMIN, E. J., GO, A. S., ARNETT, D. K., BLAHA, M. J., CUSHMAN, M., DE FERRANTI, S., DESPRES, J. P., FULLERTON, H. J., HOWARD, V. J., HUFFMAN, M. D., JUDD, S. E., KISSELA, B. M., LACKLAND, D. T., LICHTMAN, J. H., LISABETH, L. D., LIU, S., MACKEY, R. H., MATCHAR, D. B., MCGUIRE, D. K., MOHLER, E. R., 3RD, MOY, C. S., MUNTNER, P., MUSSOLINO, M. E., NASIR, K., NEUMAR, R. W., NICHOL, G., PALANIAPPAN, L., PANDEY, D. K., REEVES, M. J., RODRIGUEZ, C. J., SORLIE, P. D., STEIN, J., TOWFIGHI, A., TURAN, T. N., VIRANI, S. S., WILLEY, J. Z., WOO, D., YEH, R. W., TURNER, M. B., AMERICAN HEART ASSOCIATION STATISTICS, C. & STROKE STATISTICS, S. 2015. Heart disease and stroke statistics--2015 update: a report from the American Heart Association. *Circulation,* 131**,** e29-322.

MULDER, T. 2007. Motor imagery and action observation: cognitive tools for rehabilitation. *Journal of neural transmission (Vienna, Austria : 1996),* 114**,** 1265-1278.

MUSHAGE, B. O., CHEDJOU, J. C. & KYAMAKYA, K. 2017. Fuzzy neural network and observer-based fault-tolerant adaptive nonlinear control of uncertain 5-DOF upper-limb exoskeleton robot for passive rehabilitation. *Nonlinear Dynamics,* 87**,** 2021-2037.

NAHUM, M., LEE, H. & MERZENICH, M. M. 2013. Chapter 6 - Principles of Neuroplasticity-Based Rehabilitation. *In:* MERZENICH, M. M., NAHUM, M. & VAN VLEET, T. M. (eds.) *Progress in Brain Research.* Elsevier.

NAMDARI, S., YAGNIK, G., EBAUGH, D. D., NAGDA, S., RAMSEY, M. L., WILLIAMS, G. R. & MEHTA, S. 2012. Defining functional shoulder range of motion for activities of daily living. *Journal of Shoulder and Elbow Surgery,* 21**,** 1177-1183.

NARAYAN ARYA, K., VERMA, R., GARG, R. K., SHARMA, V. P., AGARWAL, M. & AGGARWAL, G. G. 2012. Meaningful Task-Specific Training (MTST) for Stroke Rehabilitation: A Randomized Controlled Trial. *Topics in Stroke Rehabilitation,* 19**,** 193-211.

NATHAN, D. E., PROST, R. W., GUASTELLO, S. J., JEUTTER, DC & REYNOLDS, N. C. 2012. Investigating the neural correlates of goal-oriented upper extremity movements. *NeuroRehabilitation,* 31**,** 421-8.

NEF, T., GUIDALI, M., KLAMROTH-MARGANSKA, V. & RIENER, R. ARMin - Exoskeleton Robot for Stroke Rehabilitation. *In:* DÖSSEL, O. & SCHLEGEL, W. C., eds. World Congress on Medical Physics and Biomedical Engineering, September 7 - 12, 2009, Munich, Germany, 2009// 2009a Berlin, Heidelberg. Springer Berlin Heidelberg, 127-130.

NEF, T., GUIDALI, M. & RIENER, R. 2009b. ARMin III – Arm Therapy Exoskeleton with an Ergonomic Shoulder Actuation. *Applied Bionics and Biomechanics,* 6.

NEF, T., MIHELJ, M., KIEFER, G., PERNDL, C., MULLER, R. & RIENER, R. ARMin - Exoskeleton for Arm Therapy in Stroke Patients. 2007 IEEE 10th International Conference on Rehabilitation Robotics, 13-15 June 2007 2007a. 68-74.

NEF, T., MIHELJ, M. & RIENER, R. 2007b. ARMin: a robot for patient-cooperative arm therapy. *Medical & Biological Engineering & Computing,* 45**,** 887-900.

NEF, T. & RIENER, R. Shoulder actuation mechanisms for arm rehabilitation exoskeletons. 2008 2nd IEEE RAS & EMBS International Conference on Biomedical Robotics and Biomechatronics, 19-22 Oct. 2008 2008. 862-868.

NGUYEN, V. T. & DANG, T. Setting up Virtual Reality and Augmented Reality Learning Environment in Unity. 2017 IEEE International Symposium on Mixed and Augmented Reality (ISMAR-Adjunct), 9-13 Oct. 2017 2017. 315-320.

OTTEN, A., VOORT, C., STIENEN, A., AARTS, R., ASSELDONK, E. V. & KOOIJ, H. V. D. 2015. LIMPACT:A Hydraulically Powered Self-Aligning Upper Limb Exoskeleton. *IEEE/ASME Transactions on Mechatronics,* 20**,** 2285-2298.

PAPADOPOULOS, E., PATSIANIS,G. Design of an Exoskeleton Mechanism for the Shoulder Joint. Twelfth World Congr. In Mechanism and Machine Sci, 2007 Besancon, France. 1-6.

PAPALEO, E., ZOLLO, L., SPEDALIERE, L. & GUGLIELMELLI, E. Patient-tailored adaptive robotic system for upper-limb rehabilitation. 2013 IEEE International Conference on Robotics and Automation, 6-10 May 2013 2013. 3860-3865.

PARK, H., KIM, S., WINSTEIN, C. J., GORDON, J. & SCHWEIGHOFER, N. 2016. Short-Duration and Intensive Training Improves Long-Term Reaching Performance in Individuals With Chronic Stroke. *Neurorehabilitation and Neural Repair,* 30**,** 551-561.

PEREIRA, J., OFNER, P., SCHWARZ, A., SBURLEA, A. I. & MÜLLER-PUTZ, G. R. 2017. EEG neural correlates of goal-directed movement intention. *NeuroImage,* 149**,** 129-140.

PERRY, J. C., ROSEN, J. & BURNS, S. 2007. Upper-Limb Powered Exoskeleton Design. *IEEE/ASME Transactions on Mechatronics,* 12**,** 408-417.

PIGNOLO, L. 2009. Robotics in neuro-rehabilitation. *J Rehabil Med,* 41**,** 955-60.

PIGNOLO, L., DOLCE, G., BASTA, G., LUCCA, L. F., SERRA, S. & SANNITA, W. G. Upper limb rehabilitation after stroke: ARAMIS a "robo-mechatronic" innovative approach and prototype. 2012 4th IEEE RAS & EMBS International Conference on Biomedical Robotics and Biomechatronics (BioRob), 24-27 June 2012 2012. 1410-1414.

PIÑA-MARTÍNEZ, E., ROBERTS, R., RODRIGUEZ-LEAL, E., FLORES-ARREDONDO, J. H. & SOTO, R. 2017. A Novel Exoskeleton for Continuous Monitoring of the Upper-Limb During Gross Motor Rehabilitation. *In:* IBÁÑEZ, J., GONZÁLEZ-VARGAS, J., AZORÍN, J. M., AKAY, M. & PONS, J. L. (eds.) *Converging Clinical and Engineering Research on Neurorehabilitation II: Proceedings of the 3rd International Conference on NeuroRehabilitation (ICNR2016), October 18-21, 2016, Segovia, Spain.* Cham: Springer International Publishing.

PIRONDINI, E., COSCIA, M., MARCHESCHI, S., ROAS, G., SALSEDO, F., FRISOLI, A., BERGAMASCO, M. & MICERA, S. 2014. Evaluation of a New Exoskeleton for Upper Limb Post-stroke Neuro-rehabilitation: Preliminary Results. *In:* JENSEN, W., ANDERSEN, O. K. & AKAY, M. (eds.) *Replace, Repair, Restore, Relieve – Bridging Clinical and Engineering Solutions in Neurorehabilitation: Proceedings of the 2nd International Conference on NeuroRehabilitation (ICNR2014), Aalborg, 24-26 June, 2014.* Cham: Springer International Publishing.

POLI, P., MORONE, G., ROSATI, G. & MASIERO, S. 2013. Robotic Technologies and Rehabilitation: New Tools for Stroke Patients’ Therapy. *BioMed Research International,* 2013**,** 8.

PYLATIUK, C., KARGOV, A., GAISER, I., WERNER, T., SCHULZ, S. & BRETTHAUER, G. Design of a flexible fluidic actuation system for a hybrid elbow orthosis. 2009 IEEE International Conference on Rehabilitation Robotics, 23-26 June 2009 2009. 167-171.

RAHMAN, M. H. 2018a. Customer Discovery: Powered Hand Rehab Glove. I Corps Milwaukee Site: NSF.

RAHMAN, M. H. 2018b. Wheelchair Mounted Robotic Assistive Arm. I Corps Milwaukee Site: NSF.

RAHMAN, M. H., KITTEL-OUIMET, T., SAAD, M., KENN, #XE9, , J.-P. & ARCHAMBAULT, P. S. 2012. Development and Control of a Robotic Exoskeleton for Shoulder, Elbow and Forearm Movement Assistance. *Applied Bionics and Biomechanics,* 9.

RAHMAN, M. H., OUIMET, T. K., SAAD, M., KENNÉ, J. P. & ARCHAMBAULT, P. S. Development and control of a wearable robot for rehabilitation of elbow and shoulder joint movements. IECON 2010 - 36th Annual Conference on IEEE Industrial Electronics Society, 7-10 Nov. 2010 2010. 1506-1511.

RAHMAN, M. H., RAHMAN, M. J., CRISTOBAL, O. L., SAAD, M., KENNÉ, J. P. & ARCHAMBAULT, P. S. 2014. Development of a whole arm wearable robotic exoskeleton for rehabilitation and to assist upper limb movements. *Robotica,* 33**,** 19-39.

RAHMAN, M. H., SAAD, M., KENNÉ, J.-P. & ARCHAMBAULT, P. S. 2013. Control of an exoskeleton robot arm with sliding mode exponential reaching law. *International Journal of Control, Automation and Systems,* 11**,** 92-104.

REID, D. C. 1992. *Sports Injury Assessment and Rehabilitation,* New York, NY: , Churchill Livingstone.

ROCON, E., BELDA-LOIS, J. M., RUIZ, A. F., MANTO, M., MORENO, J. C. & PONS, J. L. 2007. Design and Validation of a Rehabilitation Robotic Exoskeleton for Tremor Assessment and Suppression. *IEEE Transactions on Neural Systems and Rehabilitation Engineering,* 15**,** 367-378.

ROSALES, Y., LOPEZ, R., ROSALES, I., SALAZAR, S. & LOZANO, R. Design and modeling of an upper limb exoskeleton. 2015 19th International Conference on System Theory, Control and Computing (ICSTCC), 14-16 Oct. 2015 2015. 266-272.

ROSATI, G., GALLINA, P. & MASIERO, S. 2007. Design, Implementation and Clinical Tests of a Wire-Based Robot for Neurorehabilitation. *IEEE Transactions on Neural Systems and Rehabilitation Engineering,* 15**,** 560-569.

ROSEN, J., BRAND, M., FUCHS, M. B. & ARCAN, M. 2001. A myosignal-based powered exoskeleton system. *IEEE Transactions on Systems, Man, and Cybernetics - Part A: Systems and Humans,* 31**,** 210-222.

RUIZ, A. F., ROCON, E. & FORNER-CORDERO, A. 2009. Exoskeleton-Based Robotic Platform Applied in Biomechanical Modelling of the Human Upper Limb. *Applied Bionics and Biomechanics,* 6.

SALE, P., FRANCESCHINI, M., MAZZOLENI, S., PALMA, E., AGOSTI, M. & POSTERARO, F. 2014. Effects of upper limb robot-assisted therapy on motor recovery in subacute stroke patients. *Journal of NeuroEngineering and Rehabilitation,* 11**,** 104.

SANCHEZ, R., REINKENSMEYER, D., SHAH, P., LIU, J., RAO, S., SMITH, R., CRAMER, S., RAHMAN, T. & BOBROW, J. Monitoring functional arm movement for home-based therapy after stroke. The 26th Annual International Conference of the IEEE Engineering in Medicine and Biology Society, 1-5 Sept. 2004 2004. 4787-4790.

SASAKI, D., NORITSUGU, T. & TAKAIWA, M. Development of Active Support Splint driven by Pneumatic Soft Actuator (ASSIST). Proceedings of the 2005 IEEE International Conference on Robotics and Automation, 18-22 April 2005 2005. 520-525.

SAVION-LEMIEUX, T. & PENHUNE, V. B. 2005. The effects of practice and delay on motor skill learning and retention. *Experimental Brain Research,* 161**,** 423-431.

SCHENKMAN, M. & RUGO DE CARTAYA, V. 1987. Kinesiology of the shoulder complex. *The Journal of orthopaedic and sports physical therapy,* 8**,** 438-450.

SCHIELE, A. & HELM, F. C. T. V. D. 2006. Kinematic Design to Improve Ergonomics in Human Machine Interaction. *IEEE Transactions on Neural Systems and Rehabilitation Engineering,* 14**,** 456-469.

SCHMIDT, R. A., LEE, T. D., CAROLEE, J. W., GABRIELE, W. & HOWARD, N. Z. 2019. *Motor control and learning-A behavioral emphasis,* Champaign, IL, Human Kinetics.

SHARMA, M. K. & ORDONEZ, R. Design and fabrication of an intention based upper-limb exoskeleton. 2016 IEEE International Symposium on Intelligent Control (ISIC), 19-22 Sept. 2016 2016. 1-6.

SHEA, J. B. & MORGAN, R. L. 1979. Contextual interference effects on the acquisition, retention, and transfer of a motor skill. *Journal of Experimental Psychology: Human Learning and Memory,* 5**,** 179-187.

SHIN, J.-H., KIM, M.-Y., LEE, J.-Y., JEON, Y.-J., KIM, S., LEE, S., SEO, B. & CHOI, Y. 2016. Effects of virtual reality-based rehabilitation on distal upper extremity function and health-related quality of life: a single-blinded, randomized controlled trial. *Journal of NeuroEngineering and Rehabilitation,* 13**,** 17.

SICILIANO, B., SCIAVICCO, L., VILLANI, L. & ORIOLO, G. 2009. *Robotics* London, Springer-Verlag

SOLTANI-ZARRIN, R., ZEIAEE, A., LANGARI, R. & TAFRESHI, R. 2017. A computational approach for human-like motion generation in upper limb exoskeletons supporting scapulohumeral rhythms. *IEEE International Symposium on Wearable & Rehabilitation Robotics (WeRob2017).* Houston, Texas, USA.

SONG, R., TONG, K. Y., HU, X. L. & ZHENG, X. J. Myoelectrically Controlled Robotic System That Provide Voluntary Mechanical Help for Persons after Stroke. 2007 IEEE 10th International Conference on Rehabilitation Robotics, 13-15 June 2007 2007. 246-249.

SOSLOWSKY, L. J., FLATOW, E. L., BIGLIANI, L. U. & MOW, V. C. 1992. Articular Geometry of the Glenohumeral Joint. *Clinical orthopaedics and related research,* 285**,** 181-90.

SPENCER, S. J., KLEIN, J., MINAKATA, K., LE, V., BOBROW, J. E. & REINKENSMEYER, D. J. A low cost parallel robot and trajectory optimization method for wrist and forearm rehabilitation using the Wii. 2008 2nd IEEE RAS & EMBS International Conference on Biomedical Robotics and Biomechatronics, 19-22 Oct. 2008 2008. 869-874.

STEFANO, M., PATRIZIA, P., MARIO, A., FERLINI, G., RIZZELLO, R. & ROSATI, G. 2014. Robotic Upper Limb Rehabilitation after Acute Stroke by NeReBot: Evaluation of Treatment Costs. *BioMed Research International,* 2014**,** 5.

STIENEN, A. H. A., HEKMAN, E. E. G., HELM, F. C. T. V. D. & KOOIJ, H. V. D. 2009. Self-Aligning Exoskeleton Axes Through Decoupling of Joint Rotations and Translations. *IEEE Transactions on Robotics,* 25**,** 628-633.

STROPPA, F., LOCONSOLE, C., MARCHESCHI, S. & FRISOLI, A. A Robot-Assisted Neuro-Rehabilitation System for Post-Stroke Patients' Motor Skill Evaluation with ALEx Exoskeleton. *In:* IBÁÑEZ, J., GONZÁLEZ-VARGAS, J., AZORÍN, J. M., AKAY, M. & PONS, J. L., eds. Converging Clinical and Engineering Research on Neurorehabilitation II, 2017// 2017 Cham. Springer International Publishing, 501-505.

SUGAR, T. G., HE, J., KOENEMAN, E. J., KOENEMAN, J. B., HERMAN, R., HUANG, H., SCHULTZ, R. S., HERRING, D. E., WANBERG, J., BALASUBRAMANIAN, S., SWENSON, P. & WARD, J. A. 2007. Design and Control of RUPERT: A Device for Robotic Upper Extremity Repetitive Therapy. *IEEE Transactions on Neural Systems and Rehabilitation Engineering,* 15**,** 336-346.

SUTAPUN, A. & SANGVERAPHUNSIRI, V. 2015. A 4-DOF Upper Limb Exoskeleton for Stroke Rehabilitation: Kinematics Mechanics and Control. *International Journal of Mechanical Engineering and Robotics Research,* 4**,** 269-272.

TAKAIWA, M. & NORITSUGU, T. Development of wrist rehabilitation equipment using pneumatic parallel manipulator -Acquisition of P.T.'s motion and its execution for patient. 2009 IEEE International Conference on Rehabilitation Robotics, 23-26 June 2009 2009. 34-39.

TAKAIWA, M. & NORITSUGU, T. Wrist rehabilitaion equipment using pneumatic parallel manipulator. 2010 World Automation Congress, 19-23 Sept. 2010 2010. 1-6.

TANG, Z., ZHANG, K., SUN, S., GAO, Z., ZHANG, L. & YANG, Z. 2014. An Upper-Limb Power-Assist Exoskeleton Using Proportional Myoelectric Control. *Sensors (Basel, Switzerland),* 14**,** 6677-6694.

TAUB, E., USWATTE, G., MARK, V. W. & MORRIS, D. M. 2006. The learned nonuse phenomenon: implications for rehabilitation. *Eura Medicophys,* 42**,** 241-56.

TAUB, E., USWATTE, G. & PIDIKITI, R. 1999. Constraint-Induced Movement Therapy: a new family of techniques with broad application to physical rehabilitation--a clinical review. *J Rehabil Res Dev,* 36**,** 237-51.

TEASELL, R. W. & KALRA, L. 2004. What's New in Stroke Rehabilitation. *Stroke,* 35**,** 383-385.

TOTH, A., FAZEKAS, G., ARZ, G., JURAK, M. & HORVATH, M. Passive robotic movement therapy of the spastic hemiparetic arm with REHAROB: report of the first clinical test and the follow-up system improvement. 9th International Conference on Rehabilitation Robotics, 2005. ICORR 2005., 28 June-1 July 2005 2005. 127-130.

TRIWIYANTO, WAHYUNGGORO, O., NUGROHO, H. A. & HERIANTO. String actuated upper limb exoskeleton based on surface electromyography control. 2016 6th International Annual Engineering Seminar (InAES), 1-3 Aug. 2016 2016. 176-181.

TSAGARAKIS, N. G. & CALDWELL, D. G. 2003. Development and Control of a 'Soft-Actuated' Exoskeleton for Use in Physiotherapy and Training. *Autonomous Robots,* 15**,** 21-33.

UMEMURA, A., SAITO, Y. & FUJISAKI, K. A study on power-assisted rehabilitation robot arms operated by patient with upper limb disabilities. 2009 IEEE International Conference on Rehabilitation Robotics, 23-26 June 2009 2009. 451-456.

VACA BENITEZ, L. M., TABIE, M., WILL, N., SCHMIDT, S., JORDAN, M. & KIRCHNER, E. A. 2013. Exoskeleton Technology in Rehabilitation: Towards an EMG-Based Orthosis System for Upper Limb Neuromotor Rehabilitation. *Journal of Robotics,* 2013**,** 13.

VAN COTT, H. P. & KINKADE, R. G. 1972. *Human engineering guide to equipment design,* [Washington], [Dept. of Defense; for sale by the Supt. of Docs., U.S. Govt. Print. Off.].

VOSS, P., THOMAS, M. E., CISNEROS-FRANCO, J. M. & DE VILLERS-SIDANI, É. 2017. Dynamic Brains and the Changing Rules of Neuroplasticity: Implications for Learning and Recovery. *Frontiers in Psychology,* 8.

WADE, D. T., LANGTON-HEWER, R., WOOD, V. A., SKILBECK, C. E. & ISMAIL, H. M. 1983. The hemiplegic arm after stroke: measurement and recovery. *J Neurol Neurosurg Psychiatry,* 46**,** 521-4.

WANG, S., MAO, Z., ZENG, C., GONG, H., LI, S. & CHEN, B. A new method of virtual reality based on Unity3D. 2010 18th International Conference on Geoinformatics, 18-20 June 2010 2010. 1-5.

WEBMD. 2020. *Stroke Rehab to Regain Arm Movement* [Online]. [Accessed January 12 2020].

WHO. 2020. *Rehabilitation* [Online]. World Health Organization. Available: https://www.who.int/news-room/fact-sheets/detail/rehabilitation [Accessed Oct 1 2020].

WINTER, D. A. 2009. Anthropometry. *Biomechanics and Motor Control of Human Movement.* New York: John Wiley & Sons.

WISNESKI, K. J. & JOHNSON, M. J. 2007. Quantifying kinematics of purposeful movements to real, imagined, or absent functional objects: implications for modelling trajectories for robot-assisted ADL tasks. *J Neuroeng Rehabil,* 4**,** 7.

WU, C., TROMBLY, C. A., LIN, K. & TICKLE-DEGNEN, L. 2000. A kinematic study of contextual effects on reaching performance in persons with and without stroke: influences of object availability. *Arch Phys Med Rehabil,* 81**,** 95-101.

XIAO, F., GAO, Y., WANG, Y., ZHU, Y. & ZHAO, J. 2017. Design of a wearable cable-driven upper limb exoskeleton based on epicyclic gear trains structure. *Technol Health Care,* 25**,** 3-11.

XIAO, F., GAO, Y., WANG, Y., ZHU, Y. & ZHAO, J. 2018. Design and evaluation of a 7-DOF cable-driven upper limb exoskeleton. *Journal of Mechanical Science and Technology,* 32**,** 855-864.

YOO, D. H. & KIM, S. Y. 2015. Effects of upper limb robot-assisted therapy in the rehabilitation of stroke patients. *Journal of Physical Therapy Science,* 27**,** 677-679.

ZEIAEE, A., SOLTANI-ZARRIN, R., LANGARI, R. & TAFRESHI, R. Design and kinematic analysis of a novel upper limb exoskeleton for rehabilitation of stroke patients. 2017 International Conference on Rehabilitation Robotics (ICORR), 17-20 July 2017 2017. 759-764.

CURRICULUM VITAE

Md Rasedul Islam

Place of birth: Bhola, Bangladesh

Education
   B.Sc in Engineering, Khulna University of Engineering & Technology, July 2012
   Major: Mechanical Engineering

Dissertation Title: Design and Development of a 7 DOF Robot with Ergonomic Shoulder for Upper Limb Rehabilitation

Teaching Experineces:
   Assistant professor, University of Wisconsin-Green Bay, January 2020 – Present
   Department: Resch School of Engineering

   Teaching Assistant, University of Wisconsin-Milwaukee, August 2019 – January 2020
   Department: Mechnaical Engineering

   Teaching Assistant, University of Wisconsin-Milwaukee, January 2016 – May 2017
   Department: Mechnaical Engineering

   Lecturer, Khulna University of Engineering & Technology, September 2012 – August 2015
   Department: Mechnaical Engineering

Research Experineces:
   Research Assistant, Bio-Robotics Lab, University of Wisconsin-Milwaukee, August 2015 – May 2016

   Research Assistant, Bio-Robotics Lab, University of Wisconsin-Milwaukee, June 2017 – August 2019

   Researcher, Consultancy Research and Testing Services, Khulna University of Engineering & Technology September 2012 – August 2015

Award/Honors:
   Chancellor Graduate Student Award, University of Wisconsin-Milwaukee, Spring 2020

   Distinguished Dissertation Fellowship, University of Wisconsin-Milwaukee, Fall 2018

Chancellor Graduate Student Award, University of Wisconsin-Milwaukee, Spring 2018

Distinguished Graduate Student Fellowship, University of Wisconsin-Milwaukee, Fall 2017

Chancellor Graduate Student Award, University of Wisconsin-Milwaukee, Spring 2017

Chancellor Graduate Student Award, University of Wisconsin-Milwaukee, Spring 2016

Prime Minister Gold Medal, People's Republic of Bangladesh, 2012

University Gold Medal, Khulna University of Engineering & Technology, 2012

Publications:
  Book Chapters:
    Islam MR, Brahimi B, Ahmed T, Assad-Uz-Zaman M, Rahman MH (2020) "Chapter 9 - Exoskeletons in upper limb rehabilitation: A review to find key challenges to improve functionality". In: BOUBAKER, O. (ed.) Control Theory in Biomedical Engineering. Academic Press, Elsevier June 2020.

    Brahimi B, Saad M, Rahman MH, Ochoa-Luna C, Islam MR (2019) , "Design Development and Control of an Upper extremity Exoskeleton Robot for Rehabilitation", Wearable robotics, Ed Jacob Rosen, Elsevier November 2019

  Journals:

    Islam, M.R., Assad-Uz-Zaman, M., Al Zubayer Swapnil, A. *et al.* An ergonomic shoulder for robot-aided rehabilitation with hybrid control. *Microsyst Technol* (2020). https://doi.org/10.1007/s00542-020-04934-2

    Islam, M. R., Rahman, Mehrani., & Rahman, M.H. (2020) "A Novel Exoskeleton with Fractional Sliding Mode Control for Upper Limb Rehabilitation" Robotica, https://doi.org/10.1017/S0263574719001851, Cambridge University press.

    Islam, M. R., Assad-Uz-Zaman, M. & Rahman, M.H. (2020) "Design and Control of an Ergonomic Robotic shoulder for Wearable exoskeleton robot for Rehabilitation" Int. J. Dynam. Control, Vol:8, Issue:1, Page 312–325. https://doi.org/10.1007/s40435-019-00548-3

    Assad Uz Zaman, M., Islam, M.R., Rahman, M.H. et al. (2020), "Robot sensor system for supervised rehabilitation with real-time feedback". Multimedia Tools Appl 79, 26643–26660 (2020). https://doi.org/10.1007/s11042-020-09266-x

Assad-Uz-Zaman, Md, Islam, M., Rahman, M., Wang, Y., & McGonigle, E. (2020). "Kinect Controlled NAO Robot for Telerehabilitation", *Journal of Intelligent Systems*, Vol: *30* Issue:1, Page 224-239. doi: https://doi.org/10.1515/jisys-2019-0126

Jin, Min., Islam, M. R., Li, Liu., & Rahman, M.H. (2019) "Contact stress and bending stress calculation model of spur face gear drive based on orthogonal test" Microsystem Technologies, https://doi.org/10.1007/s00542-019-04630-w , Springer.

Assad-Uz-Zaman, M., Islam, M.R, Miah, S., & Rahman, M. H. (2019). NAO robot for cooperative rehabilitation training. Journal of Rehabilitation and Assistive Technologies engineering, 6, 2055668319862151. doi:10.1177/2055668319862151.

Spiewak, C., Islam, M.R., Assad-Uz-Zaman, M., and MH. Rahman (2018), "A Comprehensive Study on EMG Feature Extraction and Classifiers ", Op Acc J Bio Eng & App 1(1)- 2018. OAJBEA.MS.ID.000104.

Islam, M. R., Spiewak, C., Rahman, M.H., & Fareh, R. (2017) A Brief Review on Robotic Exoskeletons for Upper Extremity Rehabilitation to Find the Gap between Research Prototype and Commercial Type. Adv Robot Autom, Vol:6, Issue:3, Page 1-11.

Christopher Spiewak, M. R. Islam, Mohammad Arifur Rahaman, Mohammad H. Rahman, Roger Smith, Maarouf Saad (2016), "Modeling and Control of a 4DoF Robotic Assistive Device for Hand Rehabilitation", International Journal of Mechanical, Aerospace, Industrial, Mechatronic and Manufacturing Engineering Vol:10, No:8.

Conferences:
Islam, M. R., Rahman, M.A., Assad-Uz-Zaman, M., & Rahman, M.H., (2019) "Cartesian Trajectory Based Control of Dobot Robot", Fourth North American on Industrial Engineering and Operations Management (IEOM Toronto'19), Toronto, Canada, October 23 -25, 2019.

Ahmed, T., Rulink, I., Swapnil, A.A.Z., Assad-Uz-Zaman, M., Islam, M. R.,& Rahman, M.H., (2019) "Cartesian Trajectory Based Control of Dobot Robot", Fourth North American on Industrial Engineering and Operations Management (IEOM Toronto'19), Toronto, Canada, October 23 -25, 2019.

Brahim, B, Laraki, M.H, Islam, M. R., Assad-Uz-Zaman, M., & Rahman, M.H., (2019) "Combined Model Predictive Controller technique with Zero Moment Point Algorithm for Enhancing Nao gait Stabilization", International Conference on Electronics, Circuits, Control and Robotics, New York, USA, Aug, 2019.

Assad-Uz-Zaman, M., Islam, M. R., & Rahman, M.H., (2018) "Upper-Extremity Rehabilitation with NAO Robot", Proceedings of 5th International Conference of

Control, Dynamic Systems, and Robotics (CDSR'18), Niagara Falls, Canada, June 7 - 9, 2018.

Islam, M. R., Assad-Uz-Zaman, M., Spiewak,C., & Rahman, M.H., (2017), "Motion Control of a Robotic Device for Passive Rehabilitation of Human Shoulder and Elbow Joint Movement ", Great Lakes Biomedical Conference 2017, Milwaukee, WI, USA.

Brahim, B., Luna, C.O., Saad, M., Assad-Uz-Zaman, M., Islam, M. R., Rahman, M.H., (2017)"A new Adaptive Super-Twisting Control for an Exoskeleton Robot with Dynamic Uncertainties" Great Lakes Biomedical Conference 2017, Milwaukee, WI, USA.

Hossain, M.S., Haque, M.E., Islam, M.R., & Mashud, M., (2015) "Design and Development of Ducted VTOL UAV", International Conference on Mechanical Engineering and Renewable Energy 2015, Chittagong, Bangladesh, ICMERE2015-PI-228.

Hasan, M.R., Islam, M.R., Shahariar, G.M.H., & Mashud, M., (2014) "Numerical Analysis of Vertical Axis Wind Turbine", 9th International forum on strategic Technology, (IFOST), Paper ID S2-P130, October 2014, Cox's Bazar, Bangladesh.

Presentation:
Research talk on "An Upperlimb Robotic Exoskeleton (u-Rob) with Ergonomic Shoulder for Joint based and end-point exercises" in BME seminar series, University of Wisconsin-Milwaukee, October 23, 2020

Memberships
Member, Institute of Electrical and Electronics Engineers (IEEE)
Member, IEEE Robotics and Automation Society (RAS)
Member, American Society of Mechanical Engineers (ASME)
Member, Institution of Engineers (IEB), Bangladesh
Member, Bangladesh Society of Mechanical Engineers (BSME)